DISSERTATION

ADVANCING POINT-OF-NEED BACTERIA DETECTION USING MICROFLUIDIC PAPER-BASED ANALYTICAL DEVICES

Submitted by

Katherine Elizabeth Boehle

Department of Chemistry

In partial fulfillment of the requirements

For the Degree of Doctor of Philosophy

Colorado State University

Fort Collins, Colorado

Summer 2018

Doctoral Committee:

Advisor: Charles S. Henry

Amber T. Krummel
Christopher J. Ackerson
Brian J. Geiss

ABSTRACT

ADVANCING POINT-OF-NEED BACTERIA DETECTION USING MICROFLUIDIC PAPER-BASED ANALYTICAL DEVICES

Bacteria are responsible for more hospitalizations and deaths than any other foodborne contaminant, making the detection of these pathogens of utmost importance. To further complicate bacteria detection, the overuse of antibiotics and genetic plasticity of bacteria has caused antimicrobial resistant (AMR) bacteria to become a more prevalent issue that threatens to be the number one cause of death worldwide by 2050 unless significant innovations are made. Although bacteria detection in the field is ideal, the current gold standards for detection require trained personnel and a central laboratory. The primary work in this dissertation acts to improve upon current bacteria detection methods by designing, developing, and optimizing inexpensive user-friendly tests that detect bacteria at the point-of-need without trained personnel or expensive equipment. These goals are accomplished using microfluidic paper-based analytical devices (μPADs), a growing field for point-of-need detection that have been used for a variety of analytes and applications. Using paper as a platform has allowed for the simple development of user-friendly devices because of their easily designed and modifiable material that typically costs <$0.01 USD per device and allows for multiple tests to be completed from one sample addition.

Devices that will be described include colorimetric spot tests that detect common fecal indicator bacteria (FIB) species *Escherichia coli* and *Enterococci spp.* based on

enzymes that are naturally produced by the bacteria. Utilizing these enzymes, a test was developed that turns from clear to yellow as an indication of live bacteria. These tests were successfully used in the detection of bacteria in food and water samples to demonstrate its efficacy in food safety applications. To improve specificity and sensitivity of bacteria detection, a second spot test was developed that utilizes immunomagnetic separation (IMS) and an enzymatic sandwich immunoassay in the detection of another common foodborne pathogen, *Salmonella typhimurium*. This assay was developed specifically for detecting pathogens in complex matrices, such as one of the most common causes of pathogen contamination: animal feces.

Because AMR bacteria are becoming a more prevalent problem, devices were developed to specifically detect bacteria resistant to β-lactam antibiotics, the most common case of antimicrobial resistance observed in bacteria. The first generation of devices were developed to detect β-lactamase activity, an enzyme that facilitates resistance against β-lactam antibiotics. These devices were successful in detecting AMR in different species of bacteria isolated from environmental samples, and in the detection of AMR in sewage water. The second generation of devices enables detection of resistance against specific antibiotics through hydrolysis of the antibiotic and detecting a change in pH. Although not yet demonstrated, these devices will eventually be used to determine if bacteria are resistant against specific classes of β-lactam antibiotics, including a commonly used class of last resort antibiotics, carbapenems.

Beyond bacteria detection, this dissertation also explores developing a field-ready device to identify falsified and substandard antibiotics. Because antibiotics are most commonly counterfeited in resource-limited settings, it is imperative to develop

user-friendly point-of-need devices that can quantify the amount of active pharmaceutical ingredient in antibiotics. This was accomplished using enzyme competition, a method that had not been demonstrated paper-based devices.

Finally, all devices that have been developed and optimized in this dissertation utilized colorimetric detection. While a user-friendly and easily implemented method of detection, it does suffer from drawbacks such as sensitivity and user subjectivity when using the devices. To eliminate subjectivity, a portable system using a Raspberry Pi computer and 3D-printed light box and device holder have been optimized. Although the system has been demonstrated by automatically analyzing images and calculating Michaelis-Menten enzyme kinetic values, this system has limitless possibilities in automatically analyzing colorimetric paper-based devices for truly objective colorimetric readouts and quantitative infield detection of pathogens or other analytes.

ACKNOWLEDGEMENTS

I would like to first and foremost thank my advisor, Dr. Chuck Henry, for all his mentoring and support throughout grad school. You are truly an inspiration in everything you do, all while having a family and being Chair of the Chemistry Department. Without your constant work, we would not keep breaking records in the number of papers we publish each year (we will achieve 40 publications in 2018!). Thank you for not only encouraging better science, but better communication. I have become a much better writer and presenter because of you, and I will always value your advice. Dr. Brian Geiss, thank you for teaching me everything I know about bacteria and biosafety. Without your knowledge, we would probably still be stuck on some bacteria detection projects. Thanks to you and Chuck, I am leaving CSU with a far more rounded education than I could have asked for going into graduate school.

Also, a huge thank you goes to all Henry Group members and collaborators, past and present. Especially Dr. Jaclyn Adkins who was always there for my silly questions while I adjusted to doing lab work and taking over her bacteria detection projects. Thanks for making the long drives to Laramie, Wyoming, and sometimes 12+ hour days, more entertaining with great conversation and audiobooks. Cody Carrell, thank you for all your help and second opinions with my projects. You are destined to do great things in and after graduate school. Dr. Robert Channon, although we never worked on projects together, you have been a great friend, running partner, and volleyball team member. Thanks for being there for any science or non-science-related rants, and I will always value our great conversations. A few collaborators to thank include Sadie Henry,

Erin Doan, Dr. Elizabeth Ryan, Jake Gilliland, and Amethyst Holder, who were all incremental in the work completed in this document, and would not have been completed without them.

Lastly, I would like to thank my supportive family and friends. My loving parents and sister for helping whenever I needed it, and my amazing fiancé for doing extra work around the house, and for our needy fur-child, when I worked 60-70 hours a week. I could not ask for a more supportive partner in life. I will always treasure all the fun lunches and outings with the amazing people I have met at Colorado State University. I will always treasure my time in graduate school and Fort Collins, and will miss everyone and the city greatly.

TABLE OF CONTENTS

CHAPTER 1. INTRODUCTION

Most bacteria present in the environment coexist with humans and animals without harm. However, certain strains of bacteria are pathogenic and result in serious illness or death, making the detection of bacteria of significant importance.[1] While studying bacteria pathology and evolution is central, diagnostics is a underrepresented and important field. A recent study found that 2% of healthcare spending is used in diagnostics, yet account for up to 70% of clinical decisions.[2] Bacterial diagnostics are especially underrepresented as demonstrated by the medical field still employing the same diagnostic procedure as 80 years ago: bacteria culture.[3] While a reliable and accurate method, the assay is time-consuming, taking up to 2-3 days for results. Therefore, doctors are more likely to employ empirical diagnostics, where treatment is prescribed based on assumptions and previous experience.[4] The primary pitfall of empirical diagnostics is the unnecessary prescription of antibiotics when the patient could have a viral or fungal infection instead of bacterial infection. It was recently estimated that two-thirds of antibiotic prescriptions are unnecessary (Figure 1.1A).[3] Due to unnecessary use of antibiotics and the genetic plasticity of bacteria, more pathogens have developed the ability to resist antimicrobials, giving rise to antimicrobial resistant (AMR) bacteria.[5] At present, AMR infections cause 700,000 annual deaths worldwide and cost the United States upwards of $34 billion in additional healthcare costs.[6] Unless significant innovations are made in the field, it is currently estimated that AMR infections will surpass cancer and heart disease as the global leading cause of death by 2050.[3] AMR bacteria add an additional hurdle for diagnosing bacterial infections because even

if bacteria are causing the infection, the physician will not know what antibiotics to prescribe without additional diagnostic tests. Therefore, it is not only imperative that tests are developed to distinguish between bacteria and other pathogens, but to determine what antibiotics can treat a bacterial infection. In addition to new diagnostic methods being rapid, devices that are inexpensive, portable, and user-friendly also need to be developed for point-of-care (POC) diagnostics.[7] Most of the world's morbidity and mortality is occurring in resource-poor countries, where sending patient samples to a central laboratory is not an option.[8] By developing and employing rapid diagnostic tests instead of empirical diagnosis, this can reduce unnecessary use of antibiotics, prescribing the correct treatment to patients as soon as possible, whether that patient is in a hospital or needing treatment at the POC (Figure 1.1).

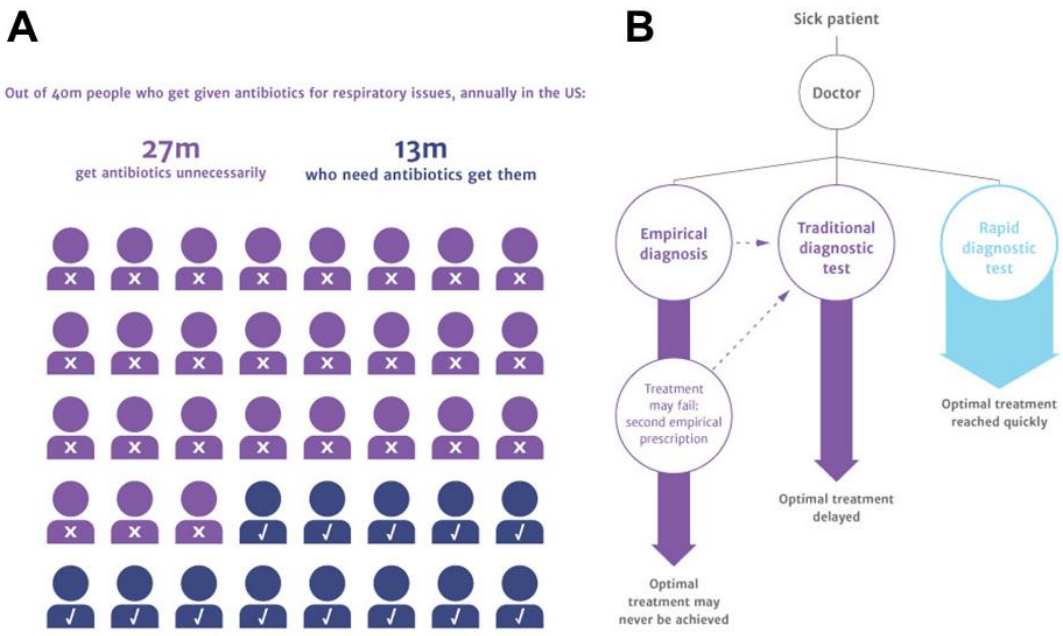

Figure 1.1 | Approximately two-thirds of antibiotic prescriptions for respiratory issues alone are unnecessary prescriptions **(A)**, which can be prevented through the development and use of rapid diagnostics tests instead traditional or empirical diagnostics **(B)**.[3]

Foodborne Bacteria in the United States. Although bacteria detection needs are most commonly associated with diagnosing bacterial infections in patients, a review found the most popular application was for food safety purposes, followed by clinical use, then environmental monitoring (Figure 1.2A).[9] Bacteria detection is applicable in the United States food industry because foodborne illness outbreaks caused by bacteria results in 36,000 hospitalizations and over 800 deaths per year, more than any other foodborne contaminant.[10] By implementing field-ready bacteria detection, outbreaks could be prevented by detecting bacteria before food is distributed, decreasing the approximate $36 billion USD lost to foodborne illnesses every year.[11] Of these foodborne pathogens, *Salmonella* and *Escherichia coli* are estimated to cost over $4 billion USD per year in the US alone, contributing to their popularity as the most reported species for bacteria detection (Figure 1.2B).[9,12] Foodborne outbreaks are most commonly caused by animal fecal contamination of either the food directly or irrigation water.[13-15] Therefore, it is not only important to detect bacteria in the food directly, but also in animal feces and water.[16,17]

Detecting Bacteria in the Field. Even though bacteria are most commonly found in the environment, detecting bacteria currently requires samples to be transported to a central laboratory for laborious, time-consuming, and expensive diagnostic tests. Upon verbal correspondence with our funding agency, the National Wildlife Research Center, a division of the United States Department of Agriculture, around 200,000 wildlife and environmental samples are sent to their central laboratory for testing every year. Of these samples, approximately 90-95% are negative results. By developing inexpensive field-ready tests for bacteria detection, the number of samples

sent to the laboratory for comprehensive testing can be cut to 10,000-20,000 samples. At their reported $10 USD for the materials for each laboratory test, not including labor, this could result in at least $1.8 million USD in savings for this government agency alone. In addition to using field-ready bacteria tests for monitoring bacteria in wildlife samples, these developed portable biosensors would also be applicable to in-field testing of other environmental samples, food samples, and POC diagnostic testing for bacterial infections.

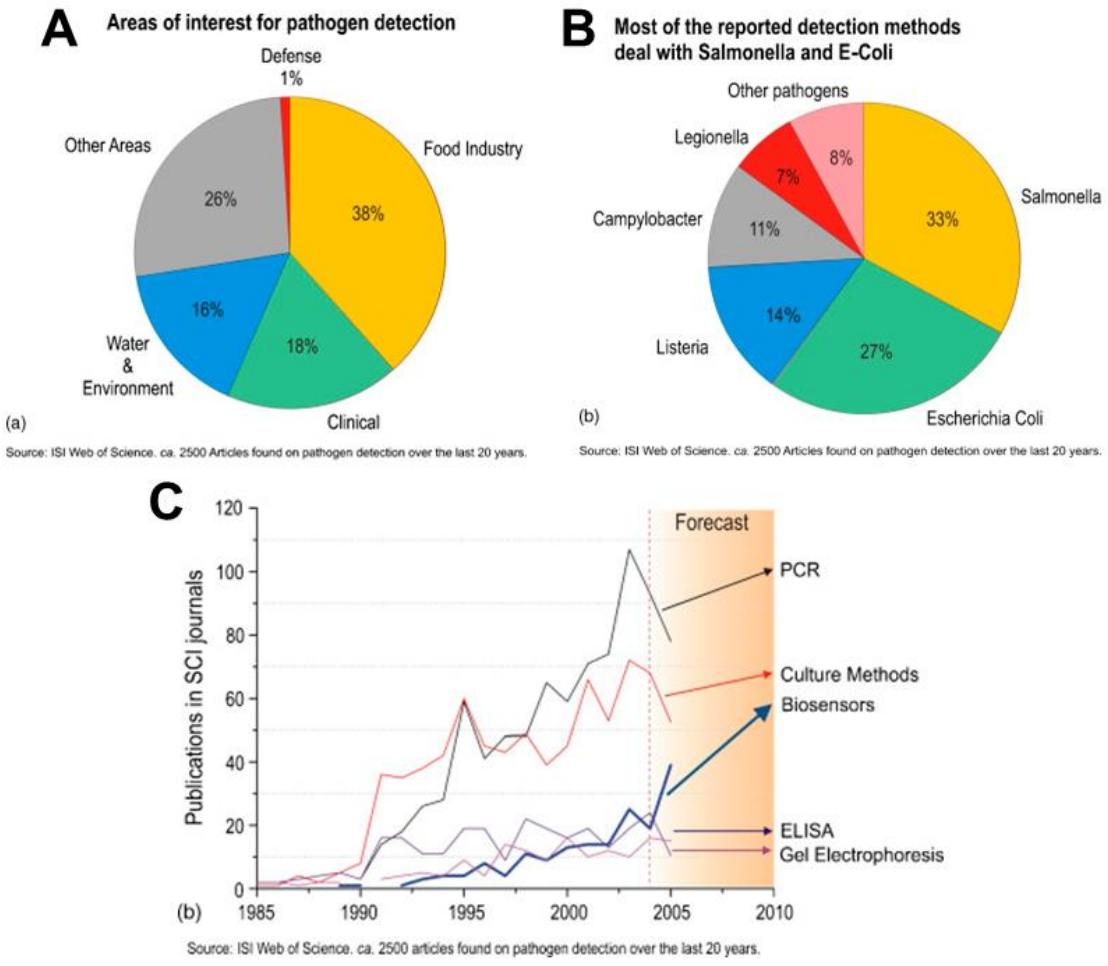

Figure 1.2 | Trends in bacterial detection. **(A)** Academic papers over the last 20 years show food industry is the most popular application. **(B)** *Salmonella* and *E. coli* are the most commonly detected pathogen. **(C)** PCR is the most popular detection motif.[9]

Laboratory Methods for Bacteria Detection. Three of the most popular methods for bacteria detection are culturing, polymerase chain reaction (PCR), and the enzyme-linked immunosorbent assay (ELISA). Although culturing has been the gold standard for bacteria detection for decades, PCR has surpassed the method in popularity in more recent scientific literature (Figure 1.2C).[9] Traditional culturing is an ideal method because it detects viable bacteria, and selective culture can identify specific species, but the assay is time-consuming and can take up to several days to obtain a result.[18] When detecting AMR bacteria, an additional step is required to test for susceptibility against certain antibiotics by growing the bacteria in the presence of the drugs.[19] This method is still the gold standard for AMR bacteria diagnostics because it can quantify susceptibility against specific antibiotics, but the procedure can take several days. PCR is based on amplifying specific genes in the bacteria genome by denaturing the DNA and using a DNA polymerase to extend the genes using DNA primers and additional nucleotides in the solution (Figure 1.3A).[20] The assay has gained traction because it is faster and more specific when compared to culturing. Depending on the assay, PCR can give results in as little as a few hours, and specific genes can be detected that are associated with pathogen strains or antimicrobial resistance.[21,22] Although the results are fast and specific, PCR can suffer from inhibition effects and detects genes only, and it is therefore unknown whether the bacteria are dead or alive.[23] ELISAs, which are based on specific antibodies adhering to the pathogen, have also been used in bacteria detection, but are less commonly used as compared to PCR and culturing.[24] The assay is most commonly completed in a 96-well polystyrene plate and read with a plate reader. Although there are many different ELISA models, the sandwich

ELISA is one of the most popular motifs. The assay starts with a primary antibody, followed by the blocking agent (used to prevent nonspecific binding), bacteria sample, then completed with either biotinylated or enzyme-conjugated antibody (Figure 1.3B).[25] Using a biotinylated antibody allows the user to implement any enzyme that has been conjugated to streptavidin, which forms a stable noncovalent bond with biotin.[26]

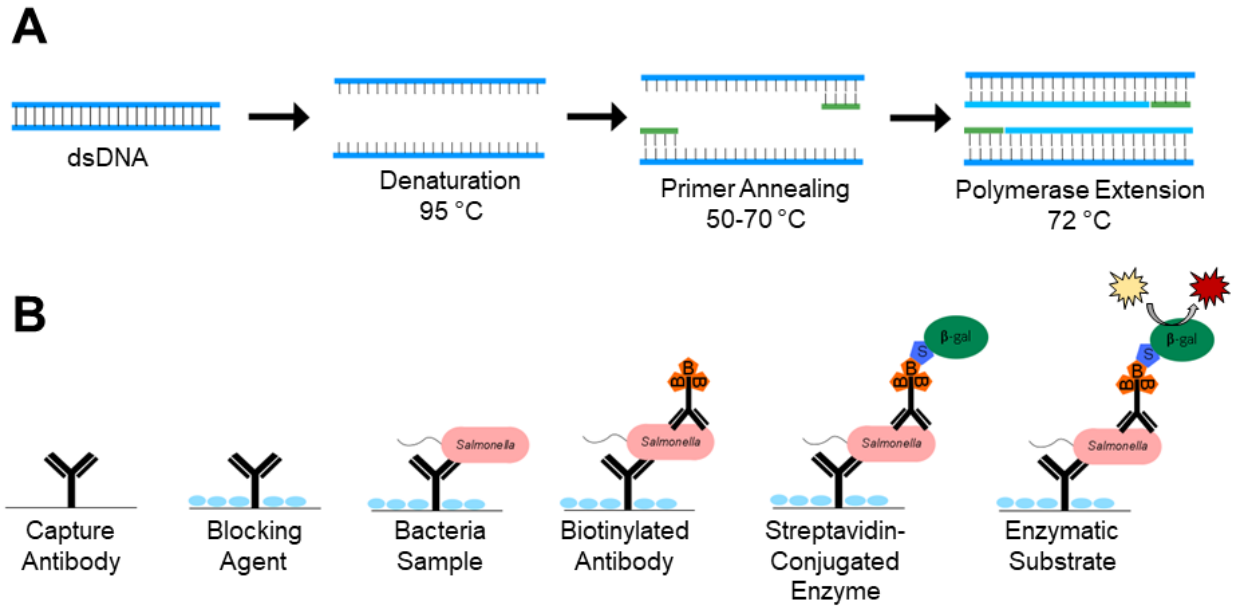

Figure 1.3 | Two common detection motifs used in bacteria detection include **(A)** the polymerase chain reaction (PCR) based on amplifying bacterial DNA associated with specific species or AMR mechanisms and **(B)** the enzyme-linked immunosorbent assay (ELISA) which is based on detection through antibodies specific to a certain bacteria species.

Between each step of the ELISA procedure, the sample is washed with buffer containing Tween 20 to remove unbound substrates and prevent signal background. Antibodies are widely available biological substrates, making them easy to implement into new assays and optimize. However, aptamers and bacteriophages have also been suggested for specific detection of bacteria in a similar fashion to immunoassays.[27,28] Although these biomolecules are not as widely available as antibodies, their ease to

mass produce and higher stability makes them a promising alternative for future applications. PCR and ELISA have also been combined for sensitive and specific detection of various pathogens in food and clinical samples.[29-32] All presented laboratory methods are reliable and accurate, but these procedures require trained personnel, expensive instrumentation, and are hence not favorable for field settings.

Developing Biosensors for Bacteria Detection. As seen in Figure 1.2C, biosensors are a growing alternative to traditional bacteria detection and are predicted to surpass PCR and culturing in popularity.[33] Biosensors can use different detection methods including optical and electrochemical measurements, and have incorporated three main classes of recognition elements: enzymes, antibodies, and nucleic acids. In addition to detection and diagnostics, biosensors have been developed for bacteria enumeration beyond the traditional and time-consuming culturing technique for more sensitive in-field detection.[34] Nucleic acid amplification techniques have been applied to biosensors to decrease cost and increase user-friendliness to make the techniques more favorable for a point-of-care setting.[35] For example, isothermal amplification techniques have been used as a replacement for PCR for amplifying genetic material in biosensors.[36] PCR requires fluctuating temperatures throughout the assay, necessitating an expensive thermocycler. Isothermal amplification, however, requires the solution to be heated to a set temperature, without fluctuation, to complete the assay. Another popular motif in biosensors for bacteria detection is electrochemical impedance spectroscopy (EIS), which is an electrochemical technique based on electrical resistance. When the electrode surface becomes more crowded, for example, capturing more and more pathogens through antibodies covalently attached to the

electrode, decreasing electron transfer, and thereby increasing resistance. This method has been demonstrated in bacteria detection for a variety of applications and species including *Salmonella*, *E. coli*, and *S. aureus*, to name a few.[37-41]

Biosensors for specifically detecting AMR bacteria have also been developed. Card et al. introduced the use of expanded microarrays for accurately and simultaneously testing gram-negative bacteria against 75 different antibiotics.[42] Although this method tests for a breadth of antibiotic susceptibility, it requires an extensive procedure, including overnight culturing, cell lysing, and DNA extraction, which increases both detection time and assay costs. Microfluidic devices fabricated with polydimethysiloxane (PDMS) have also been developed for determining the minimum inhibitory concentration (MIC) of different antibiotics against a specific bacteria isolate.[43] One of these established PDMS devices can determine MIC within 3-4 hr by monitoring a single bacterium via microscopy.[44] Another microfluidic device was recently developed for susceptibility testing that decreased total assay time to 1 hr by using a droplet generator and a fluorescent resazurin-based assay.[45] Using a droplet generator effectively increased the concentration of bacteria without culture enrichment and fluorescence provided greater sensitivity compared to colorimetry. Many resazurin-based sensors have been optimized for detecting AMR bacteria as the assay is based on detecting live vs. dead bacteria and can determine whether a certain antibiotic is effective against the bacteria.[46-48] While these are all accurate and promising systems that provide alternatives to traditional methods, they require expensive equipment and trained personnel, making these assays more suitable for laboratory settings. To monitor bacteria in the field and diagnose bacterial infections at the point-of-care, rapid,

portable, and inexpensive devices that do not require instrumentation or trained laboratory personnel for analysis still need to be developed.

Microfluidic Paper-Based Analytical Devices. While using paper in chemical assays was established over 200 years ago,[49] it was reintroduced as a microfluidic platform in 2007 for portable and inexpensive analytical assays.[50] This reintroduction of paper was groundbreaking because Whitesides and coworkers incorporated hydrophobic barriers into the paper to direct fluid flow to several channels and separate detection zones.[50] Each zone was responsible for a different analytical test, enabling the detection of multiple analytes (glucose and protein in this device) from a single addition of sample (Figure 1.4A). Although this initial device had higher limits of detection and low sensitivity compared to conventional methods, this enabled the thousands of paper-based devices that followed this article and created the field known as microfluidic paper-based analytical devices (μPADs). Paper has gained significant popularity as a platform for analytical devices because of their inexpensive material (often <$0.01 per device), ability to store and stabilize chemical and biological reagents, natural fluid-wicking properties, and device disposability.[51] Because of these properties, μPADs are specifically being developed as point-of-need analytical tests that enable the detection of analytes without trained personnel or a central laboratory.[52] While the first device used qualitative detection based on color change, user-friendly quantitative detection has since been implemented using a “chemometer” design with readout similar to a common analog thermometer (Figure 1.4B).[53] Instead of a simple yes or no answer, chemometers have been designed for the user to quantify an analyte by measuring the distance of color and relating that distance to a specific analyte concentration.

In addition to their ease of use, µPADs are also easy to design and fabricate and are practical for large-scale development and implementation.[54] Paper-based devices are most often fabricated with Whatman chromatography paper, but almost any paper substrate can be used. To make µPADs, the user simply needs to develop a hydrophobic barrier that directs sample flow. The hydrophobic barrier can be many different materials including photo resist, or even scholar glue that is not vulnerable to potent chemicals like other barriers.[55] One of the most popular hydrophobic barriers is wax, which can be deposited onto the paper using a common office wax printer[56] or screen printing.[57] Using a wax printer or screen printing allows for the user to create device designs using a common computer vector program such as Adobe Illustrator™ or Corel Draw™. Following wax application, the paper needs to be heated to melt the wax through the paper pores, creating a hydrophobic barrier, which can be completed using an oven or hotplates (Figure 1.4C). Once the hydrophobic barrier has been established, the user can modify the paper with chemicals to complete the desired analytical test. The back of the devices then need to be taped to prevent sample leakage.

Since the first device, µPADs have been developed for environmental and biological applications for the detection of metals, organic compounds, biomarkers, bacteria, and viruses, to name a few.[58] While this first device used simple and user-friendly colorimetric detection, additional detection motifs have been established including electrochemical,[59,60] fluorescence,[61] and chemiluminescence,[62] which were implemented into µPADs to lower limits-of-detection and increase sensitivity. As previously mentioned, paper has many different properties that are advantageous for

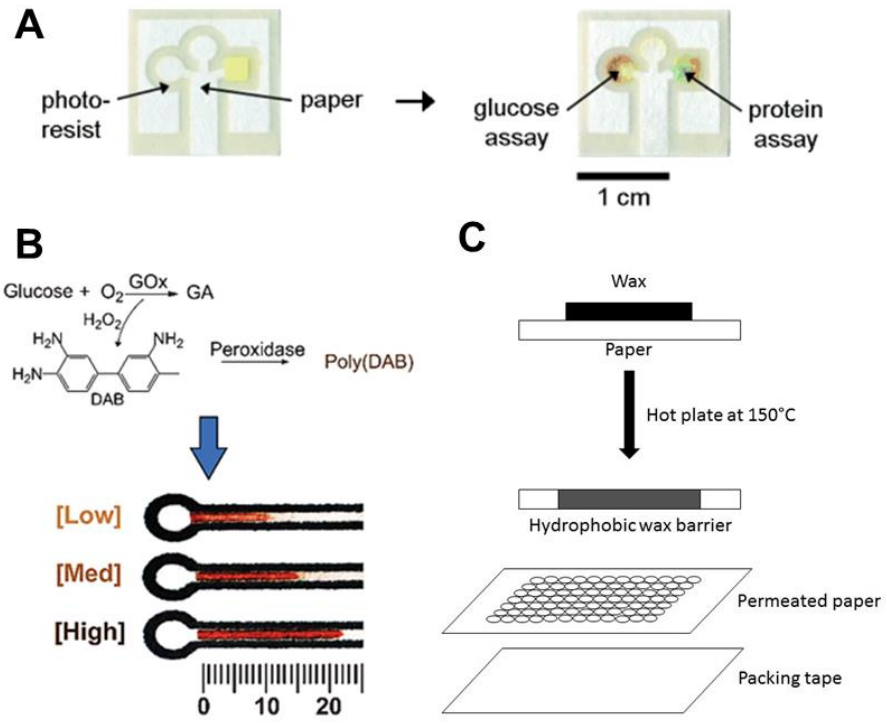

Figure 1.4 | Microfluidic paper-based analytical devices (µPADs). **(A)** The first µPAD for the detection of glucose and protein using qualitative colorimetric detection.[50] **(B)** Distance-based colorimetric detection of glucose for user-friendly quantification of analytes.[53] **(C)** Fabricating paper-based devices by making a hydrophobic barrier with wax and taping the back of the device sheet.

point-of-need detection, but one of the most critical properties is its ability to store and stabilize chemical reagents. This allows for reactions to take place on the paper substrate without additional solutions beyond the sample, facilitating user-friendly detection of countless analytes in a field-setting, including bacteria.

Biological Assays on Paper-Based Devices. While PCR is the most popular method in recent years for bacteria detection outside of µPADs, PCR has not been directly applied to paper-based devices. This is likely because PCR requires a thermocycler, an expensive and complex piece of equipment that makes the assay not ideal for point-of-need settings. A thermocycler is necessary because PCR requires the

solution to shift between several different specific temperatures to complete the assay.[20] Instead, isothermal amplification techniques including loop-mediated isothermal amplification (LAMP) and recombinase polymerase amplification (RPA) has been applied to μPADs for sensitive and point-of-need detection of bacteria[63] and viruses.[64-66] While isothermal systems still require a heating element, LAMP only requires to be heated to a set temperature of 60 °C, and RPA requires a set temperature of 40 °C for amplification. To further establish isothermal amplification for field settings, an inexpensive incubator was developed using a Styrofoam cup and chemical hand warmers,[67] and it has been reported that polyethersulfone is the best paper substrate to use for LAMP-based μPADs.[68] While isothermal amplification has been demonstrated in paper-based devices as a conducive alternative to PCR for field settings, the underlying issue with nucleic-acid based techniques is the lack of live/dead verification. Furthermore, in the application of AMR bacteria detection, it is unknown whether the AMR gene is expressed or simply present in the genome.

Enzymes are one of the most popular detection motifs associated with paper-based devices due to their catalytic abilities to accelerate a chemical reaction and amplify a detectable product. Enzymes can be used to detect an analyte of interest, including one of the most popular proof-of-concept reactions used in paper-based devices: glucose.[69] Other enzymatic reactions that have been used in μPADs include the detection of other biomolecules such as uric acid, urine creatine, phenylalanine, and lactate.[70-74] In addition to using enzymes to detect analytes, substrates can be used to detect enzyme activity in a sample. Detecting the activity of specific enzymes can indicate certain pathogens or health ailments. For example, assessing human health

based on enzyme detection has been established for many diseases that are associated with the expression or lack of function of specific enzymes, including liver function,[75] organ failure,[76] male fertility,[77] and even organophosphate poisoning.[78] Using this concept, µPADs can be developed for bacteria detection based on unique enzymes the bacteria produce. Detecting bacteria based on enzymatic activity is an attractive platform because it detects healthy and viable bacteria, like traditional culturing or the resazurin assay. Additionally, it is not as specific as PCR and immunoassays, enabling pan-bacteria detection, which is advantageous for applications such as food safety monitoring. Using enzymes as a detection motif has been described previously for colorimetric detection of *E. coli*, *Listeria*, and *Salmonella* in food and water samples.[79-81]

When the user does desire species-specific and sensitive detection, immunoassays provide an attractive and robust platform that can easily be adapted to µPADs. Antibodies are naturally very specific to the analyte with little cross-reactivity, and can be manufactured to be specific to almost any analyte. One of the most recognizable forms of paper-based devices is the pregnancy test, which is a lateral flow assay (LFA). Pregnancy tests are based on nanoparticle-conjugated antibodies specific to human chorionic gonadotropin (hCG), a protein women express when pregnant.[82] A similar device was developed for detecting pathogenic bacteria where bacteria are captured by antibodies resulting in the nanoparticles aggregating resulting in the formation of colored line.[83] Another popular application of antibodies in µPADs is through ELISAs where enzymes are covalently attached to antibodies instead of nanoparticles. Enzymes provide an advantage over nanoparticles because enzymes can continually amplify a substrate, providing a lower limit-of-detection. As previously

mentioned, ELISAs are traditionally completed in 96-well polystyrene plates, but ELISA was first introduced into paper-based devices in 2010.[84] By moving the assay to paper, there was decreased reagent consumption, waste, and total assay time. Since its introduction to paper, ELISA has been demonstrated in the detection of biomarkers,[62,85,86] and pathogens including viruses[87,88] and bacteria.[89] To further advance analyte detection in complex samples, antibodies are also used in the process of immunomagnetic separation (IMS), where antibodies are covalently attached to the surface of a magnetic bead.[90] The immunomagnetic beads are added to a complex sample to adhere to the analyte before separating the beads from the sample using a magnet and reconstituting the beads in fresh buffer. Reconstituting the sample in fresh buffer also allows for the user to concentrate the sample by resuspending the beads in a smaller volume of buffer than the original sample. IMS has been demonstrated for efficiently separating target analytes and cells from complex mixtures such as blood,[91] milk,[92] meat,[93] cheese and yogurt,[94] and bovine feces,[95,96] making the technique relevant to food safety applications.

Paper-Based Devices for Foodborne Pathogen Detection. The work presented in this document revolve around improving bacteria detection at the point-of-need using paper-based devices, including both spot tests and microfluidic devices. The first set of devices that will be discussed are spot tests that detect common fecal indicator bacteria, *E. coli* and *Enterococci*, and the most common foodborne pathogen, *Salmonella typhimurium*, for the application of food safety monitoring. The first device detects *E. coli* and *Enterococci* based on enzymes the bacteria produce: β-galactosidase and β-glucuronidase[97] for *E. coli* detection and β-glucosidase for

Enterococci detection.[98] This method was successfully demonstrated in detecting bacteria in irrigation water and alfalfa sprouts, which are a common source of food poisoning. While this method provided accurate and user-friendly results, the limits of detection were rather high at 10^8 CFU mL^{-1} of bacteria, necessitating a culture enrichment step. By sampling the culture enrichment every four hours, we cut the analysis time to 8 hours for low bacteria concentrations compared to upwards of two days for traditional methods. However, the ideal bacterial detection system will have a low LOD without needing culture enrichment.

To meet these needs, another paper-based spot test was developed to specifically detect *S. typhimurium* using antibodies. Implementing IMS as the first step of the procedure enabled us to isolate and concentrate the pathogen for detection in complex samples. Because IMS is a sample preparation step, not a detection method, an enzymatic sandwich immunoassay, similar to an ELISA, was added for sensitive and rapid analysis without expensive instrumentation. Using these two techniques for isolation, concentration, and detection of the pathogen, our LOD was decreased to 10^2 CFU mL^{-1} in culture media. By using antibodies as our detection method, not only did we increase sensitivity of the assay, eliminating the need for culture enrichment, the assay is also very specific to *S. typhimurium* and showed no cross reactivity with *E. coli* bacteria. The final assay was demonstrated with bird feces and whole milk for food safety applications.

Detecting AMR Bacteria using µPADs. The next set of devices that will be discussed are also based on enzymes the bacteria produce, but instead of identifying bacteria species, these devices detect enzymes that indicate AMR properties. There are

many different classes of antibiotics, therefore many different classes of antimicrobial resistance, and many of these resistance mechanisms are based off enzyme activity.[99] Using this idea, we developed a paper-based spot test to detect β-lactamase, an enzyme that facilitates resistance against the most commonly prescribed antibiotics, penicillins and cephalosporins.[100] β-lactamase enables resistance by hydrolyzing the β-lactam ring in β-lactam antibiotics, deactivating the compound. Taking advantage of this mechanism, we can use nitrocefin, a chromogenic cephalosporin, that turns from yellow to red upon enzyme hydrolysis (Figure 1.5).[101] Using nitrocefin and paper-based devices, a spot test was developed to detect the enzyme activity at a fraction of the cost and time as traditional methods. Contaminated water is a significant source of infection and outlet for the spread of AMR bacteria and is therefore a popular area of study for environmental scientists.[102-105] To study AMR bacteria epidemiology, scientists currently must transport samples to a central laboratory for testing. Hence, it is not only important to use AMR tests in the application of point-of-care diagnostics, but also in environmental monitoring. The test was demonstrated in environmental applications by detecting AMR bacteria in sewage water samples and 46 different environmental bacterial isolates. There was only one false result as verified by traditional methods, indicating 98% accuracy.

To further expand upon this idea of detecting AMR bacteria based on enzyme expression, another μPAD was developed to detect bacteria that produce carbapenemase. This enzyme facilitates resistance against carbapenem antibiotics, a commonly used class of last resort antibiotics used in clinical cases.[106] Carbapenem-resistant bacteria are becoming a prevalent problem and is recognized as one of the top

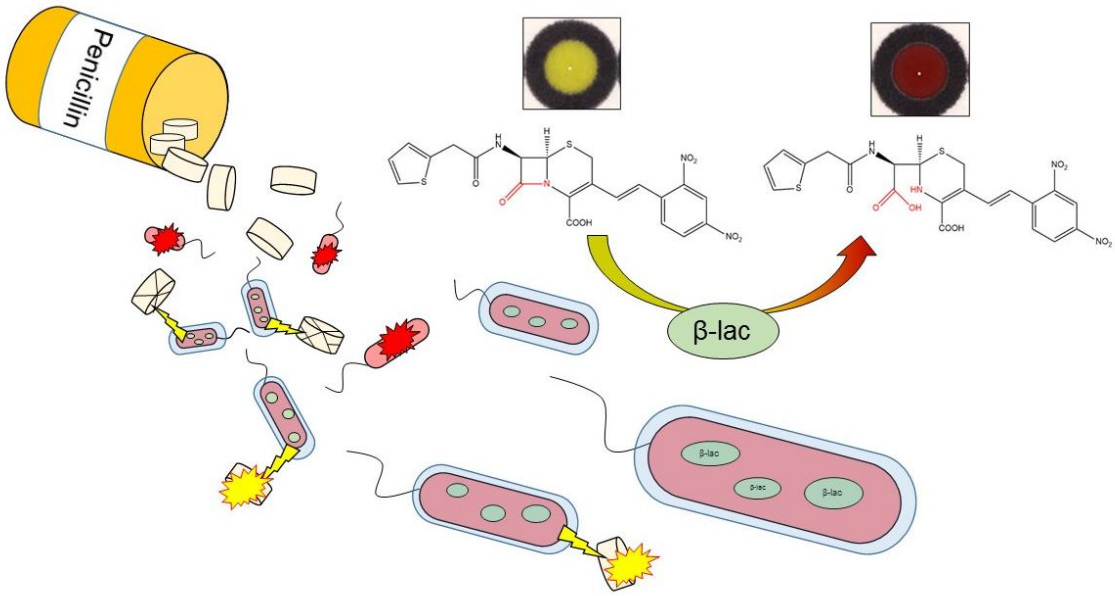

Figure 1.5 | Using nitrocefin, a chromogenic substrate, to detect antimicrobial resistant bacteria based on bacterial enzymes that facilitate resistance against antibiotics through deactivation.

three most urgent threats of AMR in the US by the CDC.[107,108] Although there is no chromogenic substrate for carbapenemase as there is for β-lactamase, the hydrolysis the enzyme facilitates results in a decrease in pH. Using paper-based microfluidics, we developed a device that allows the bacteria sample to react with imipenem, a carbapenem antibiotic, then the sample flows to another section of the device with pH indicators. If the antibiotic is hydrolyzed, the user will observe a corresponding decrease in pH as compared to a sample of bacteria that does not express carbapenemase. This device has not been demonstrated in detecting carbapenem-resistant bacteria specifically, but has been developed and optimized for detecting specific penicillin antibiotics such as penicillin V and amoxicillin.

In-Field Devices for Counterfeit Antibiotic Screening. In addition to the use of enzymes in detecting an analyte based on color change, or using an analyte to detect

enzymes, analytes can be detected through enzyme inhibition, resulting in a lack of color change. This concept has been demonstrated in the detection of organophosphate pesticides that inhibit the reaction of acetylcholinesterase with a colorimetric substrate, resulting in less color change as the pesticide concentration increases.[109,110] Using a similar concept, we have developed a μPAD to test for the authenticity of β-lactam antibiotics using β-lactamase and nitrocefin, but using enzyme competition, not direct inhibition. Counterfeit antibiotics is a prevalent problem in developing countries and it is estimated that up to 5% of global antibiotics are counterfeit.[111,112] Of all counterfeit antibiotics, β-lactam antibiotics are the most counterfeited, accounting for over half of counterfeit antibiotics.[113] To help combat this problem and monitor counterfeit antibiotics in the field, a μPAD was developed to detect the purity of β-lactam antibiotics using the same system that was used to detect β-lactam-resistant bacteria. The device operates through adding an antibiotic sample to the sample inlet where it travels down a channel, rehydrates nitrocefin, then travels to a detection zone where β-lactamase is stored. If the antibiotics are genuine, β-lactamase will statistically react more often with the concentrated β-lactam antibiotic compared to the dilute nitrocefin. If the antibiotics are counterfeit, β-lactamase will react with nitrocefin, turning the device red, indicating no or little active ingredient. Calibration curves for four different β-lactam antibiotics were generated and the device was tested with six common counterfeit ingredients, demonstrating its potential for in-field use of antibiotic screening.

Developing a Raspberry Pi for Automating Color Analysis. All devices presented in this work use colorimetric readout for detection. While colorimetry is a user-friendly method that does not require external instrumentation, such as a

potentiostat in electrochemical detection, there is the underlying issue of subjectivity when reading the results. Currently, to quantify the color intensity in devices, an image is captured using either a Smart Phone camera and a light box, or a common desktop scanner. The image is then sent to a computer for analysis by an image software program such as NIH ImageJ or Adobe Photoshop. While this method works for laboratory research, it is not conducive to field settings. Consequently, smart phone applications have been developed to automatically analyze the device color following image capture.[114,115] Although these applications are much more appropriate for field settings, the caveat of smart phone applications is the need to update the application for new and expensive phones and software. To enhance colorimetric detection capabilities in the field, we have chosen the Raspberry Pi format for developing a program where the user simply needs to input a command and the Raspberry Pi will automatically capture and analyze the images. A 3D-printed lightbox with a battery-powered light source was designed to hold the raspberry pi computer and camera and house the paper-based devices. The entire system costs <$100, which is cheaper than the average Smart Phone, and the system is portable and can be used in resource-limited settings. As a proof-of-concept, we have developed a program that automatically calculates Michaelis-Menten enzyme kinetics based on images captured by the Raspberry Pi™. This would enable the user to use the system for time-dependent reactions and calculate kinetics for enzyme-based detection methods.

Summary. The work in this dissertation advances in-field bacteria detection through expanding biological assays to complex samples, such as food, milk, and animal feces. It also presents the first work on detecting antimicrobial resistant bacteria

using paper-based devices, both generally and to specific antibiotics. Although not directly related to bacteria detection, the first μPAD based on enzymatic substrate competition is used to develop the first quantitative μPAD for identifying substandard antibiotics. Finally, we describe the first Raspberry Pi system to use flood-fill in quantifying color change in the application of calculating Michaelis-Menten enzyme kinetic parameters.

REFERENCES

(1) Stephens, C.; Murray, W. *Curr. Biol.* **2001**, *11*, R53-R56.
(2) Rohr, U. P.; Binder, C.; Dieterle, T.; Giusti, F.; Messina, C. G.; Toerien, E.; Moch, H.; Schafer, H. H. *PLoS One* **2016**, *11*, e0149856.
(3) Tackling Drug-Resistant Infections Globally: Final Report and Recommendations Welcome Trust, UK Government, **2016**.
(4) Morrell, M.; Fraser, V. J.; Kollef, M. H. *Antimicrob. Agents Chemother.* **2005**, *49*, 3640-3645.
(5) Levy, S. B.; Marshall, B. *Nat. Med.* **2004**, *10*, S122-129.
(6) Global Action Plan on Antimicrobial Resistance, World Health Organization, **2015**.
(7) Chin, C. D.; Linder, V.; Sia, S. K. *Lab Chip* **2012**, *12*, 2118-2134.
(8) Chin, C. D.; Laksanasopin, T.; Cheung, Y. K.; Steinmiller, D.; Linder, V.; Parsa, H.; Wang, J.; Moore, H.; Rouse, R.; Umviligihozo, G.; Karita, E.; Mwambarangwe, L.; Braunstein, S. L.; van de Wijgert, J.; Sahabo, R.; Justman, J. E.; El-Sadr, W.; Sia, S. K. *Nat. Med.* **2011**, *17*, 1015-1019.
(9) Lazcka, O.; Del Campo, F. J.; Munoz, F. X. *Biosens. Bioelectron.* **2007**, *22*, 1205-1217.
(10) Painter, J. A.; Hoekstra, R. M.; Ayers, T.; Tauxe, R. V.; Braden, C. R.; Angulo, F. J.; Griffin, P. M. *Emerg. Infect. Dis.* **2013**, *19*, 407-415.
(11) Minor, T.; Lasher, A.; Klontz, K.; Brown, B.; Nardinelli, C.; Zorn, D. *Risk Anal.* **2015**, *35*, 1125-1139.
(12) Hoffman, S.; Batz, M.; Morris, J. G. *J. Food Prot.* **2012**, *75*, 1291-1302.
(13) Laidler, M. R.; Tourdjman, M.; Buser, G. L.; Hostetler, T.; Repp, K. K.; Leman, R.; Samadpour, M.; Keene, W. E. *Clin. Infect. Dis.* **2013**, *57*, 1129-1134.
(14) Steele, M.; Odumeru, J. *J. Food Prot.* **2004**, *67*, 2839-2849.
(15) Uyttendaele, M.; Jaykus, L.-A.; Amoah, P.; Chiodini, A.; Cunliffe, D.; Jacxsens, L.; Holvoet, K.; Korsten, L.; Lau, M.; McClure, P.; Medema, G.; Sampers, I.; Rao Jasti, P. *Compr. Rev. Food Sci. Food Saf.* **2015**, *14*, 336-356.
(16) Sayah, R. S.; Kaneene, J. B.; Johnson, Y.; Miller, R. *Appl. Environ. Microbiol.* **2005**, *71*, 1394-1404.
(17) Renter, D. G.; Gnad, D. P.; Sargeant, J. M.; Hygnstrom, S. E. *J. Wildl. Dis.* **2006**, *42*, 699-703.
(18) Wang, Y.; Salazar, J. K. *Compr. Rev. Food Sci. Food Saf.* **2016**, *15*, 183-205.
(19) Bauer, A. W.; Kirby, W. M.; Sherris, J. C.; Turck, M. *Am. J. Clin. Pathol*.**1966**, *45*, 493-496.
(20) Schochetman, G.; Ou, C.; Jones, W. K. *J. Infect. Dis.* **1988**, *158*, 1154-1157.
(21) Jamali, H.; Paydar, M.; Radmehr, B.; Ismail, S.; Dadrasnia, A. *Food Control* **2015**, *54*, 383-388.
(22) Clerc, O.; Prod'hom, G.; Senn, L.; Jaton, K.; Zanetti, G.; Calandra, T.; Greub, G. *Clin. Microbiol. Infect.* **2014**, *20*, 355-360.
(23) Gonzalez, R. A.; Noble, R. T. *Water Res.* **2014**, *48*, 296-305.
(24) Magliulo, M.; Simoni, P.; Guardigli, M.; Michelini, E.; Luciani, M.; Lelli, R.; Roda, A. *J. Agric. Food Chem.* **2007**, *55*, 4933-4939.

(25) Drijvers, J. M.; Awan, I. M.; Perugino, C. A.; Rosenberg, I. M.; Pillai, S. **2017**, In *Basic Science Methods for Clinical Researchers*, Jalali, M.; Saldanha, F. Y. L.; Jalali, M., Eds.; Elsevier, 2017, pp 119-133.
(26) Taninaka, A.; Takeuchi, O.; Shigekawa, H. *Int. J. Mol. Sci.* **2010**, *11*, 2134-2151.
(27) Toh, S. Y.; Citartan, M.; Gopinath, S. C.; Tang, T. H. *Biosens. Bioelectron.* **2015**, *64*, 392-403.
(28) Singh, A.; Arutyunov, D.; Szymanski, C. M.; Evoy, S. *Analyst* **2012**, *137*, 3405-3421.
(29) Perelle, S.; Dilasser, F.; Malorny, B.; Grout, J.; Hoorfar, J.; Fach, P. *Mol. Cell. Probes* **2004**, *18*, 409-420.
(30) Tamminen, M.; Joutsjoki, T.; Sjoblom, M.; Joutsen, M.; Palva, A.; Ryhanen, E. L.; Joutsjoki, V. *Lett. Appl. Microbiol.* **2004**, *39*, 439-444.
(31) Ge, B.; Zhao, S.; Hall, R.; Meng, J. *Microbes Infect.* **2002**, *4*, 285-290.
(32) Daly, P.; Collier, T.; Doyle, S. *Lett. Appl. Microbiol.* **2002**, *34*, 222-226.
(33) Velusamy, V.; Arshak, K.; Korostynska, O.; Oliwa, K.; Adley, C. *Biotechnol. Adv.* **2010**, *28*, 232-254.
(34) Zhang, J. Y.; Do, J.; Premasiri, W. R.; Ziegler, L. D.; Klapperich, C. M. *Lab Chip* **2010**, *10*, 3265-3270.
(35) Niemz, A.; Ferguson, T. M.; Boyle, D. S. *Trends Biotechnol.* **2011**, *29*, 240-250.
(36) Safavieh, M.; Ahmed, M. U.; Sokullu, E.; Ng, A.; Braescu, L.; Zourob, M. *Analyst* **2014**, *139*, 482-487.
(37) Muhammad-Tahir, Z.; Alocilja, E. C. *Biosens. Bioelectron.* **2003**, *18*, 813-819.
(38) Yang, L.; Bashir, R. *Biotechnol. Adv.* **2008**, *26*, 135-150.
(39) Tan, F.; Leung, P. H. M.; Liu, Z.; Zhang, Y.; Xiao, L.; Ye, W.; Zhang, X.; Yi, L.; Yang, M. *Sens. Actuators B Chem.* **2011**, *159*, 328-335.
(40) Wang, Y.; Ping, J.; Ye, Z.; Wu, J.; Ying, Y. *Biosens. Bioelectron.* **2013**, *49*, 492-498.
(41) Wang, Y.; Ye, Z.; Ying, Y. *Sensors* **2012**, *12*, 3449-3471.
(42) Card, R.; Zhang, J.; Das, P.; Cook, C.; Woodford, N.; Anjum, M. F. *Antimicrob. Agents Chemother.* **2013**, *57*, 458-465.
(43) Kim, K. P.; Kim, Y. G.; Choi, C. H.; Kim, H. E.; Lee, S. H.; Chang, W. S.; Lee, C. S. *Lab Chip* **2010**, *10*, 3296-3299.
(44) Choi, J.; Jung, Y. G.; Kim, J.; Kim, S.; Jung, Y.; Na, H.; Kwon, S. *Lab Chip* **2013**, *13*, 280-287.
(45) Kaushik, A. M.; Hsieh, K.; Chen, L.; Shin, D. J.; Liao, J. C.; Wang, T. H. *Biosens. Bioelectron.* **2017**, *97*, 260-266.
(46) Elavarasan, T.; Chhina, S. K.; Parameswaran, M.; Sankaran, K. *Sens. Actuators B Chem.* **2013**, *176*, 174-180.
(47) Boedicker, J. Q.; Li, L.; Kline, T. R.; Ismagilov, R. F. *Lab Chip* **2008**, *8*, 1265-1272.
(48) Deiss, F.; Funes-Huacca, M. E.; Bal, J.; Tjhung, K. F.; Derda, R. *Lab Chip* **2014**, *14*, 167-171.
(49) Davy, J. *Phil. Trans. R. Soc. Lond.* **1812**, *102*, 144-151.
(50) Martinez, A. W.; Phillips, S. T.; Butte, M. J.; Whitesides, G. M. *Angew. Chem. Int. Ed. Engl*. **2007**, *46*, 1318-1320.
(51) Cate, D. M.; Adkins, J. A.; Mettakoonpitak, J.; Henry, C. S. *Anal. Chem.* **2015**, *87*, 19-41.

(52) Yetisen, A. K.; Akram, M. S.; Lowe, C. R. *Lab Chip* **2013**, *13*, 2210.
(53) Cate, D. M.; Dungchai, W.; Cunningham, J. C.; Volckens, J.; Henry, C. S. *Lab Chip* **2013**, *13*, 2397-2404.
(54) Akram, M. S.; Daly, R.; da Cruz Vasconcellos, F.; Yetisen, A. K.; Hutchings, I.; Hall, E. A. H. In *Lab-on-a-Chip Devices and Micro-Total Analysis Systems*, Castillo-Leon, J.; Svendson, W. E., Eds.; Springer International Publishing Switzerland, 2015, pp 161-195.
(55) Cardoso, T. M. G.; de Souza, F. R.; Garcia, P. T.; Rabelo, D.; Henry, C. S.; Coltro, W. K. T. *Anal. Chim. Acta* **2017**, *974*, 63-68.
(56) Carrilho, E.; Martinez, A. W.; Whitesides, G. M. *Anal. Chem.* **2009**, *81*, 7091-7095.
(57) Dungchai, W.; Chailapakul, O.; Henry, C. S. *Analyst* **2011**, *136*, 77-82.
(58) Yang, Y.; Noviana, E.; Nguyen, M. P.; Geiss, B. J.; Dandy, D. S.; Henry, C. S. *Anal. Chem.* **2017**, *89*, 71-91.
(59) Adkins, J.; Boehle, K.; Henry, C. *Electrophoresis* **2015**, *36*, 1811-1824.
(60) Mettakoonpitak, J.; Boehle, K.; Nantaphol, S.; Teengam, P.; Adkins, J. A.; Srisa-Art, M.; Henry, C. S. *Electroanalysis* **2016**, *28*, 1420-1436.
(61) Noor, M. O.; Krull, U. J. *Anal. Chem.* **2014**, *86*, 10331-10339.
(62) Wang, S.; Ge, L.; Song, X.; Yu, J.; Ge, S.; Huang, J.; Zeng, F. *Biosens. Bioelectron.* **2012**, *31*, 212-218.
(63) Lafleur, L. K.; Bishop, J. D.; Heiniger, E. K.; Gallagher, R. P.; Wheeler, M. D.; Kauffman, P.; Zhang, X.; Kline, E. C.; Buser, J. R.; Kumar, S.; Byrnes, S. A.; Vermeulen, N. M.; Scarr, N. K.; Belousov, Y.; Mahoney, W.; Toley, B. J.; Ladd, P. D.; Lutz, B. R.; Yager, P. *Lab Chip* **2016**, *16*, 3777-3787.
(64) Rodriguez, N. M.; Linnes, J. C.; Fan, A.; Ellenson, C. K.; Pollock, N. R.; Klapperich, C. M. *Anal. Chem.* **2015**, *87*, 7872-7879.
(65) Rodriguez, N. M.; Wong, W. S.; Liu, L.; Dewar, R.; Klapperich, C. M. *Lab Chip* **2016**, *16*, 753-763.
(66) Rohrman, B. A.; Richards-Kortum, R. R. *Lab Chip* **2012**, *12*, 3082-3088.
(67) Huang, S.; Do, J.; Mahalanabis, M.; Fan, A.; Zhao, L.; Jepeal, L.; Singh, S. K.; Klapperich, C. M. *PLoS One* **2013**, *8*, e60059.
(68) Linnes, J. C.; Rodriguez, N. M.; Liu, L.; Klapperich, C. M. *Biomed. Microdevices* **2016**, *18*, 30.
(69) Liu, S.; Su, W.; Ding, X. *Sensors* **2016**, *16*.
(70) Gabriel, E. F.; Garcia, P. T.; Cardoso, T. M.; Lopes, F. M.; Martins, F. T.; Coltro, W. K. *Analyst* **2016**, *141*, 4749-4756.
(71) Chen, X.; Chen, J.; Wang, F.; Xiang, X.; Luo, M.; Ji, X.; He, Z. *Biosens. Bioelectron.* **2012**, *35*, 363-368.
(72) Talalak, K.; Noiphung, J.; Songjaroen, T.; Chailapakul, O.; Laiwattanapaisal, W. *Talanta* **2015**, *144*, 915-921.
(73) Robinson, R.; Wong, L.; Monnat, R.; Fu, E. *Micromachines* **2016**, *7*, 28.
(74) Dungchai, W.; Chailapakul, O.; Henry, C. S. *Anal. Chim. Acta* **2010**, *674*, 227-233.
(75) Pollock, N. R.; Rolland, J. P.; Kumar, S.; Beattie, P. D.; Jain, S.; Noubary, F.; Wong, V. L.; Pohlmann, R. A.; Ryan, U. S.; Whitesides, G. M. *Sci. Transl. Med.* **2012**, *4*.
(76) Kannan, B.; Jahanshahi-Anbuhi, S.; Pelton, R. H.; Li, Y.; Filipe, C. D.; Brennan, J. D. *Anal. Chem.* **2015**, *87*, 9288-9293.

(77) Nosrati, R.; Gong, M. M.; San Gabriel, M. C.; Pedraza, C. E.; Zini, A.; Sinton, D. *Clin. Chem.* **2016**, *62*, 458-465.
(78) Yen, T. H.; Chen, K. H.; Hsu, M. Y.; Fan, S. T.; Huang, Y. F.; Chang, C. L.; Wang, Y. P.; Cheng, C. M. *Talanta* **2015**, *145*, 66-72.
(79) Jokerst, J. C.; Adkins, J. A.; Bisha, B.; Mentele, M. M.; Goodridge, L. D.; Henry, C. S. *Anal. Chem.* **2012**, *84*, 2900-2907.
(80) Bisha, B.; Adkins, J. A.; Jokerst, J. C.; Chandler, J. C.; Perez-Mendez, A.; Coleman, S. M.; Sbodio, A. O.; Suslow, T. V.; Danyluk, M. D.; Henry, C. S.; Goodridge, L. D. *J. Vis. Exp.* **2014**, *88*.
(81) Zakir Hossain, S. M.; Ozimok, C.; Sicard, C.; Aguirre, S. D.; Monsur Ali, M.; Li, Y.; Brennan, J. D. *Anal. Bioanal. Chem.* **2012**, *403*, 1567-1576.
(82) Posthuma-Trumpie, G. A.; Korf, J.; van Amerongen, A. *Anal. Bioanal. Chem.* **2009**, *393*, 569-582.
(83) Li, C.; Vandenberg, K.; Prabhulkar, S.; Zhu, X.; Schneper, L.; Methee, K.; Rosser, C. J.; Almeide, E. *Biosens. Bioelect.* **2011**, *26*, 4342-4348.
(84) Cheng, C. M.; Martinez, A. W.; Gong, J.; Mace, C. R.; Phillips, S. T.; Carrilho, E.; Mirica, K. A.; Whitesides, G. M. *Angew. Chem. Int. Ed. Engl.* **2010**, *49*, 4771-4774.
(85) Murdock, R. C.; Shen, L.; Griffin, D. K.; Kelley-Loughnane, N.; Papautsky, I.; Hagen, J. A. *Anal. Chem.* **2013**, *85*, 11634-11642.
(86) Sun, X.; Li, B.; Tian, C.; Yu, F.; Zhou, N.; Zhan, Y.; Chen, L. *Anal. Chim. Acta* **2018**, *1007*, 33-39.
(87) Mu, X.; Zhang, L.; Chang, S.; Cui, W.; Zheng, Z. *Anal Chem* **2014**, *86*, 5338-5344.
(88) Khan, M. S.; Pande, T.; van de Ven, T. G. *Colloids Surf. B Biointerfaces* **2015**, *132*, 264-270.
(89) Shih, C. M.; Chang, C. L.; Hsu, M. Y.; Lin, J. Y.; Kuan, C. M.; Wang, H. K.; Huang, C. T.; Chung, M. C.; Huang, K. C.; Hsu, C. E.; Wang, C. Y.; Shen, Y. C.; Cheng, C. M. *Talanta* **2015**, *145*, 2-5.
(90) He, J.; Huang, M.; Wang, D.; Zhang, Z.; Li, G. *J. Pharm. Biomed. Anal.* **2014**, *101*, 84-101.
(91) Cohen, S. J.; Punt, C. J.; Iannotti, N.; Saidman, B. H.; Sabbath, K. D.; Gabrail, N. Y.; Picus, J.; Morse, M.; Mitchell, E.; Miller, M. C.; Doyle, G. V.; Tissing, H.; Terstappen, L. W.; Meropol, N. J. *J. Clin. Oncol.* **2008**, *26*, 3213-3221.
(92) Brandao, D.; Liebana, S.; Campoy, S.; Alegret, S.; Isabel Pividori, M. *Talanta* **2015**, *143*, 198-204.
(93) Skjerve, E.; Rorvik, L. M.; Olsvik, O. *Appl. Environ. Microbiol.* **1990**, *56*, 3478-3481.
(94) Skjerve, E.; Olsvik, O. *Int. J. Food Microbiol.* **1991**, *14*, 11-18.
(95) Chapman, P. A.; Wright, D. J.; Siddons, C. A. *J. Med. Microbiol.* **1994**, *40*, 424-427.
(96) LeJeune, J. T.; Hancock, D. D.; Besser, T. E. *J. Clin. Microbiol.* **2006**, *44*, 872-875.
(97) Wu, J.; Stewart, J. R.; Sobsey, M. D.; Cormency, C.; Fisher, M. B.; Bartram, J. K. *Curr. Microbiol.* **2018**.
(98) Perry, J. D.; Morris, K. A.; James, A. L.; Oliver, M.; Gould, F. K. *J. Appl. Microbiol.* **2007**, *102*, 410-415.
(99) Poole, K. *J. Pharm. Pharmacol.* **2001**, *53*, 283-294.
(100) Murray, B. E.; Mederski-Samaroj, B. *J. Clin. Invest.* **1983**, *72*, 1168-1171.
(101) O'Callaghan, C. H.; Morris, A.; Kirby, S. M.; Chingler, A. H. *Antimicrob. Agents Chemother.* **1972**, *1*, 283-288.

(102) Lupo, A.; Coyne, S.; Berendonk, T. U. *Front. Microbiol.* **2012**, *3*, 116-128.
(103) Jiang, L.; Hu, X.; Xu, T.; Zhang, H.; Sheng, D.; Yin, D. *Sci.Total Environ.* **2013**, *458-460*, 267-272.
(104) Holvoet, K.; Sampers, I.; Callens, B.; Dewulf, J.; Uyttendaele, M. *Appl. Environ. Microbiol.* **2013**, *79*, 6677-6683.
(105) Baquero, F.; Martinez, J. L.; Canton, R. *Curr. Opin. Biotechnol.* **2008**, *19*, 260-265.
(106) Nordmann, P.; Poirel, L.; Dortet, L. *Emerg. Infect. Dis.* **2012**, *18*, 1503-1507.
(107) Nordmann, P.; Naas, T.; Poirel, L. *Emerg. Infect. Dis.* **2011**, *17*, 1791-1798.
(108) Antibiotic Resistance Threats in the United States, Center for Disease Control and Prevention, **2013**.
(109) Zakir Hossain, S. M.; Luckham, R. E.; McFadden, M. J.; Brennan, J. D. *Anal. Chem.* **2009**, *81*, 9055-9064.
(110) Sicard, C.; Glen, C.; Aubie, B.; Wallace, D.; Jahanshahi-Anbuhi, S.; Pennings, K.; Daigger, G. T.; Pelton, R.; Brennan, J. D.; Filipe, C. D. *Water. Res.* **2015**, *70*, 360-369.
(111) Delepierre, A.; Gayot, A.; Carpentier, A. *Med. Mal. Infect.* **2012**, *42*, 247-255.
(112) Global Surveillance and Monitoring System for Substandard and Falsified Medical, World Health Organization, **2017**.
(113) Kelesidis, T.; Falagas, M. E. *Clin. Microbiol. Rev.* **2015**, *28*, 443-464.
(114) Vashist, S. K.; Mudanyali, O.; Schneider, E. M.; Zengerle, R.; Ozcan, A. *Anal. Bioanal. Chem*. **2014**, *406*, 3263-3277.
(115) Grushnikov, A.; Kikuchi, K.; Matsumoto, Y.; Kanade, T.; Yagi, Y. *Adv. Biomed. Eng.* **2017**, *6*, 76-82.

CHAPTER 2. DEVELOPING PAPER-BASED SPOT TESTS FOR DETECTING BACTERIA IN FOOD SAFETY APPLICATIONS

Foodborne illnesses caused by bacteria account for the highest number of hospitalizations and deaths compared to any other foodborne contaminant. Preventing foodborne illness outbreaks begs for faster and portable bacterial sensors that can be taken into the field to detect bacteria before food is distributed, cutting back on the approximate billions of dollars lost to outbreaks every year. Most commonly, contamination occurs through fecal contamination of the food directly or the irrigation water. Hence, not only do these sensors necessitate the capability to detect bacteria on food, but also fecal and water samples. In this chapter, two different sets of bacteria devices are presented based on two different detection motifs.

The first set of devices are paper-based spot tests that detect *Escherichia coli* and *Enterococcus* species, as indicators of fecal contamination. These fecal indicator bacteria (FIB) were detected using substrates specific to enzymes produced by each species. β-galactosidase (β-gal) and β-glucuronidase (β-glucur) are both produced by *E. coli*, while β-glucosidase (β-gluco) is produced by *Enterococcus spp*. Substrates used produced either p-nitrophenol (PNP) or o-nitrophenol (ONP) as colorimetric products (from clear to yellow). Low concentrations (10^1 CFU mL^{-1}) of pathogenic and nonpathogenic *E. coli* isolates and (10^0 CFU mL^{-1}) *E. faecalis* and *E. faecium* strains were detected within 4 and 8 h of pre-enrichment. Alfalfa sprout and lagoon water samples served as model food and water samples, and while water samples did not test positive, sprout samples did test positive within 4 h of pre-enrichment. Positive detection

of inoculated (2.3×10^2 and 3.1×10^1 CFU mL^{-1} or g^{-1} of *E. coli* and *E. faecium*, respectively) sprout and water samples tested positive within 4 and 12 h, respectively.

The second set of devices presents another colorimetric paper-based device that was combined with immunomagnetic separation (IMS) for detecting *Salmonella typhimurium*. IMS was completed with anti-*Salmonella* coated magnetic beads that were applied to capture and separate bacteria from the sample matrix and preconcentrate it into small volumes before testing on paper. To directly detect *S. typhimurium* after IMS, a sandwich immunoassay was used in the procedure with β-gal as the detection enzyme. Using the antibody/enzyme complex, we performed a colorimetric assay with chlorophenol red-β-D-galactopyranoside (CPRG) for bacteria quantification, which has a noticeable color change from yellow to red. Using this system, the limit of detection of *S. typhimurium* was found to be 10^2 CFU mL^{-1} in culturing solution without any pre-enrichment or cross-reaction with other common bacteria species. Finally, the proposed platform was applied for detection of *S. typhimurium* in inoculated bird fecal samples and whole milk with detection limits of 10^5 CFU g^{-1} and 10^3 CFU mL^{-1}, respectively, without any cultural enumeration.

Because each set of devices has their advantages and disadvantages, this chapter will conclude with comparing the two different methods and their applications. This chapter is a compilation of my personal contribution to two different projects which were both accepted for publication in *Analytical Chemistry*.[1,2]

Introduction

Of all contaminants found in food and water (bacterial, viral, chemical, etc.), bacterial contamination causes the highest number of hospitalizations and deaths within

the United States annually.[3,4] Whereas drinking polluted water can lead to illness, the use of unsafe water for irrigation can also contaminate agricultural products causing foodborne illness.[5,6] Leafy greens, for example, are responsible for 46% of foodborne outbreaks within the United States and, because alfalfa sprouts are cultivated in a moist humid growth environment that facilitates bacterial growth, they are one of the leading sources of multi-state foodborne outbreaks.[7,8] Human and animal excreta (primarily feces) are major sources of food and waterborne diseases, but it is impossible to test for all possible transferable pathogens in a comprehensive manner.[9] Instead, general indicators for bacterial contamination are commonly detected, and both *E. coli* and *Enterococcus* spp. are used as standard fecal indicator bacteria (FIB).[10-13] *E. coli* and enterococci are found in high concentrations, 10^9 and $>10^4$ colony forming units (CFU) per wet gram of stool respectively, predominantly in the gut of warm-blooded animals. Their presence is an indication of not only fecal contamination but also if conditions are amenable for the presence of other pathogens.[13,14] FDA guidance and compliance regulations for both the agricultural production and industrial processing of food and beverages now call for the frequent testing of FIB species, necessitating portable, inexpensive, and user-friendly methods of testing.[15]

Of these other foodborne pathogens that can be present as indicated by FIB, *Salmonella* is widely known as one of the most prevalent pathogens causing foodborne illness outbreaks.[16] Per the Center for Disease Control and Prevention (CDC), *Salmonella* causes an estimated one million illnesses in the United States resulting in 19,000 hospitalizations and 380 deaths, more than any other pathogenic bacteria.[17] *Salmonella* contaminates food products, like eggs, fruits, vegetables, meat, poultry, and

milk[18] also through animal fecal contamination.[19] This is because, like *E. coli* and enterococci, *Salmonella* live and replicate in the intestinal tracts of humans and animals, and therefore present in their feces.[20] Studies have shown a strong correlation between skin and meat contamination of *Salmonella*, and prevalence in the animal's feces, making feces an important sample matrix to detect the pathogen's presence.[21] Conventional methods are not practical for on-site detection of bacteria and the need for expensive equipment and trained lab personnel increases testing costs, making large scale studies of *Salmonella* and other pathogen epidemiology difficult.[22]

Due to the harmful role bacterial infections can play in human health, numerous bacteria detection methods have been developed. Common methods for bacterial detection include immunoassays, DNA amplification/detection methods such as polymerase chain reaction (PCR), and traditional culture methods.[23,24] While DNA and immunoassays have advantages such as selectivity and sensitivity, both can suffer from inhibition effects from sample components that lead to false positives or negatives as well as high instrumentation and/or test costs.[25,26] As a result, the gold standard for bacterial detection has remained culture-based methods.[27] Culturing microorganisms allows for sensitive isolation and confirmation of live target bacteria. Non-selective and selective media are used sequentially in conjunction with biochemical testing and microscopy, making this method time-consuming and material intensive. Accordingly, a rapid, user-friendly, cost-effective, and reliable approach for FIB and *Salmonella* detection is required to overcome the drawbacks of conventional methods. The need for improved bacteria detection methods has led to the development of biosensors and analytical methods, including the use of paper-based analytical devices (PADs). PADs

provide a simple, easily modifiable and mass produced alternative platform, and can be incorporated with several different detection motifs.[28,29]

Other advantages of PADs include small sample and reagent consumption, rapid analysis, simple operation, disposability, and portability.[30,31] PADs hold great promise for use as analytical tools in remote areas or areas where minimal instrumentation is available due to their natural fluid wicking properties and ability to store and stabilize reagents. This renders PADs to be attractive and simple platforms for analysis in fields such as environmental monitoring, medical diagnostics, point-of-care testing, and food safety control.[28,30] However, there have been only a few reports on using PADs for rapid detection of bacteria, including *Pseudomonas aeruginosa*,[32] *Staphylococcus aureus*,[32,33] *Escherichia coli,*[34-38] *Salmonella typhimurium*,[35,39] *and Listeria monocytogenes*.[35] Our lab has previously demonstrated bacteria detection in food and water samples based on bacterial enzyme expression.[40,41] While detecting bacteria based on naturally expressed enzymes is a reliable method to detect viable bacteria, it does suffer from low limits-of-detection, necessitating a culture enrichment step. Although the entire process was still shorter than traditional methods, the ideal bacteria detection system will not necessitate culture enrichment.

Immunomagnetic separation (IMS) is an analytical method that was developed to separate targets of interest from complex sample matrices, and can also be used as an alternative to culture enumeration as a pre-enrichment step for pathogens. IMS is a procedure where antibodies specific to an analyte or cell are covalently attached to magnetic particles. These magnetic particles are added to the sample matrix to adhere to the target and are separated from the matrix with a magnet and re-suspended in

buffer. After separation from the sample matrix, many detection methods have been used including microscopy, broth enrichment, immunoassays, and PCR.[42] IMS does not require bulky and expensive equipment to complete the procedure, making it ideal for in-field measurements. IMS has been demonstrated for efficiently separating target analytes and cells from complex mixtures such as blood,[43] milk,[44] meat,[45] cheese and yogurt,[46] and even bovine feces.[47] With IMS, the antibodies attached to the beads can be specific to any analyte or cell of interest. Because of this, IMS has been demonstrated for detecting many biomarkers,[43,48] along with various bacteria[45-47] and viruses.[49-51] Combining IMS with paper-based devices has been previously described for the detection of *E. coli* in contaminated water.[34] In this work, the authors describe the use of IMS to pre-concentrate samples from contaminated water before lysing the bacteria and detecting bacterial enzymes β-galactosidase and β-glucuronidase. To the best of our knowledge, there has not been a paper-based device that is coupled with IMS for the detection of bacteria in more complicated sample matrices, such as animal feces and whole milk. Furthermore, despite the prevalence of *Salmonella* in bird feces, to the best of our knowledge, there has not been a proposed alternative detection method to traditional culture enrichment.

Herein, two different colorimetric paper-based spot tests for bacteria detection are reported. The first is to detect FIB bacteria, *E. coli* and *Enterococcus* spp., *via* their production of species-indicative enzymes. Both β-galactosidase and β-glucuronidase were used for *E. coli* detection and β-glucosidase for *Enterococcus* spp. detection. Due to their association with coliforms and FIB, these enzymatic reactions are also used as indicators of microbial safety.[52] Substrates for each enzyme produced either ONP or

PNP, initiating a color change from clear to yellow. PNP and ONP can also be detected electrochemically (Figure 2.1), but this will not be discussed in depth. Pathogenic and non-pathogenic strains of *E. coli*, as well as *Enterococcus faecalis* and *E. faecium* were detected in pure culture as well as model surface irrigation water (uninoculated and inoculated lagoon water) and model food samples (uninoculated and inoculated alfalfa sprouts).

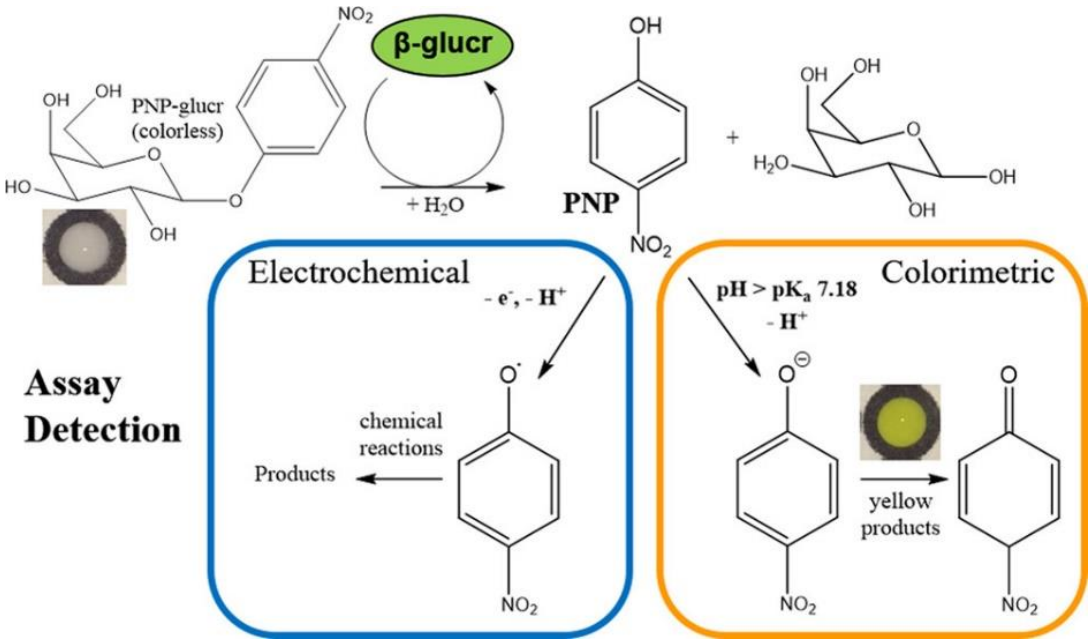

Figure 2.1 | Reaction scheme showing the dual electrochemical and colorimetric detection of formed PNP from reacting with bacterially produced β-glucr with PNP-glucr.

To improve the limit-of-detection and eliminate culturing that was used in the first set of devices, another method was developed by coupling PADs with IMS for specific colorimetric detection of *S. typhimurium*. IMS was applied to capture and separate target bacteria from the sample matrix, then preconcentrated into small volumes for further assays. By separating the pathogen from feces, this allowed us to complete a sandwich immunoassay to detect the presence of *S. typhimurium* in the sample (Figure

2.2A) without the concern of inhibition effects from the sample matrix. A second anti-*Salmonella* antibody was conjugated with biotin, which was bound to streptavidin linked to β-galactosidase (β-gal) to perform a colorimetric assay with chlorophenol red-β-D-galactopyranoside (CPRG) (Figure 2.2B). The PAD coupled with IMS demonstrated sensitive detection of *S. typhimurium* in media, and was also demonstrated in detecting *S. typhimurium* in inoculated bird feces samples. To show the PAD's promise for onsite detection of contaminated food products, this method was also demonstrated in detecting *S. typhimurium* in inoculated whole milk.

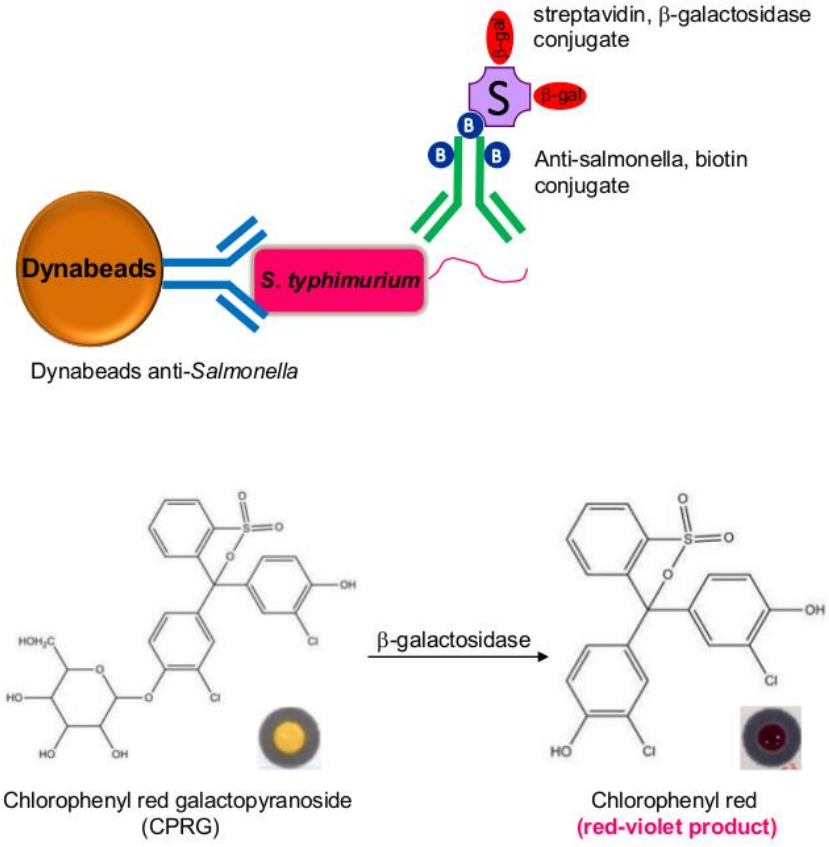

Figure 2.2 | System for detecting *S. typhimurium*. **(A)** Schematic of selected approach for *S. typhimurium*. **(B)** S. typhimurium detection based on an enzymatic assay between β-gal and CPRG, resulting in chlorophenol red as a red-violet product.

Materials and Methods

Materials and Reagents. Potassium chloride (KCl), potassium ferricyanide ($K_3Fe(CN)_6$), and Whatman #1 filter paper were purchased from Fisher Scientific (Fairlawn, NJ). Potassium ferrocyanide ($K_4Fe(CN)_6$) was purchased from Mallinckrodt Chemical Works (St. Louis, MO). Carbon ink and Graphite (<20-μm diameter) were purchased from Ercon (Warham, MA) and Sigma (St. Louis, MO) respectively. High-purity silver ink was purchased from SPI Supplies (West Chester, PA). *p*-Aminophenol (PAP) was purchased from EMD Millipore (VWR, Billerica, MA). Sodium chloride (KCl), potassium phosphate monobasic (KH_2PO_4), potassium phosphate dibasic (K_2HPO_4), β-galactosidase (β-gal), β-glucosidase, β-glucuronidase (β-glucr), *p*-nitrophenyl-β-D-glucopyranoside (PNP-Gluco), and *p*-nitrophenyl-β-D-glucuronide (PNP-glucr) were purchased from Sigma. *p*-Nitrophenol (PNP) and *p*-nitrophenyl-β-D-galactopyranoside (PNP-gal) were purchased from TCI America (VWR, Portland, OR). *o*-Nitrophenol (ONP) and *o*-nitrophenyl-β-D-galactopyranoside (ONP-gal) were purchased from ACROS Organics™ (Thermo Fisher Scientific, Waltham, MA). *p*-Aminophenyl-β-D-galactopyranoside (PAP-gal) was purchased from Biosynth (Itasca, IL). *o*-Nitrophenyl-β-D-glucopyranoside (ONP-Gluco) was purchased from Alfa Aesar (VWR, Haverhill, MA).

For the *S. typhimurium* assay, Dynabeads® M-280 Tosylactivated (Product no. 14203, Invitrogen) were purchased from Thermo Fisher Scientific Inc. (Waltham, MA, USA). Anti-*Salmonella typhimurium* 0-4 antibody (mouse monoclonal [1E6] against lipopolysaccharides, Product no. ab 8274) was obtained from Abcam (Cambridge, MA, USA). *Salmonella* antibody, biotin conjugate (4-5 mg mL^{-1}, Product no. PA1-73022, Invitrogen) and Streptavidin, β -galactosidase conjugate (Product no. S931, Life

Technologies) were purchased from Thermo Fisher Scientific Inc. (Waltham, MA, USA). The streptavidin, β -galactosidase conjugate was reconstituted in Milli Q water to a concentration of 2 mg mL^{-1} upon arrival. Chlorophenol Red- β -D-galactopyranoside (CPRG, Product no 59767) was obtained from Sigma-Aldrich (St. Louis, MO, USA).

Device Fabrication. CorelDRAW software was used to design geometries for wax barriers. A wax printer was used to print wax designs onto the copy paper surface that was then melted through the paper using a hotplate at (150°C) for 60 s to form hydrophobic wax barriers (Figure 2.3). Packing tape was used to seal the back of the printed circles to form wells. Paper-based well plates consisted of 7 columns and 12 rows for a total of 84 wells that were each 6-mm in diameter (inner) after melting and held 50 µL of total solution volume (Figure 2.3).

For the devices to detect *S. typhimurium*, two formats of paper devices were employed: well-array[35] and distance-based (referred to as “chemometer”)[53] patterns. Both configurations were designed using CorelDRAW and fabricated on Whatman No. 4 filter paper (GE Healthcare Life Sciences, NY, USA) using wax printing as described below.

The design of well-array paper-based devices followed the layout from the previous work.[35] These well arrays were 7-mm diameter circular wells with 4-pt line thickness. After printing the design using a wax printer (Xerox Colorqube 8870), devices were heated on a hot plate at 175 °C for 50 s to melt the wax through the paper (Figure 2.3), creating a hydrophobic barrier. Finally, the backs of the paper devices were taped with Scotch® packing tape to control fluid flow and prevent leaking during the assay. Application of reagents and samples were performed on the front (wax-printed) side.

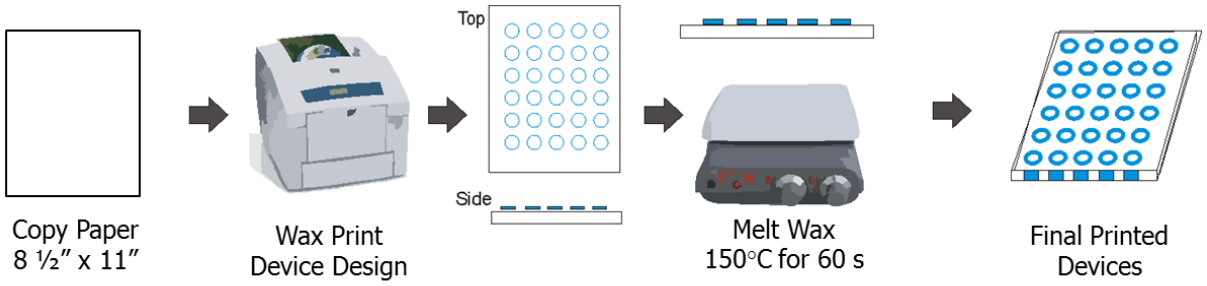

Figure 2.3 | Fabrication schemes for wax printed paper-based well devices.

The design and fabrication of distance-based paper devices or chemometers followed the process described previously.[53] Device features containing a circular reservoir (6 mm diameter) and a straight channel (4 mm wide and 5.5 cm long) with 4-pt line thickness were generated using CorelDRAW software. A ruler was added parallel to the channel for easy reading of the distance of color development along the channel. The ruler design was first ink printed on the Whatman No. 4 filter paper to generate rulers for the chemometers, then wax printing was performed as above to create the remaining chemometer features. The ink-printed rulers are not affected by heating the devices on a hotplate. To prevent leaking and evaporation of reagents, the paper chemometers were thermally laminated at 110 °C by passing the chemometers enveloped in Scotch®thermal laminating pouches through an Apache AL13P thermal laminator. A 4 mm (internal diameter) hole was punched through the reservoir using a 4 mm diameter disposable biopsy punch (Robbins Instruments, Inc., Chatham, NJ, USA). The back of the laminated chemometer was then taped with the Scotch® shipping packing tape to allow reagent addition to the reservoir.

Colorimetric Assay Detection. For quantification of colorimetric products, a "light box" and the camera of an iPhone 5S were used to capture images (Figure 2.4A).

The light box was fabricated by lining a square cardboard box (16 cm x 16 cm x 16 cm) with white copy paper and cutting a small opening (2 x 5 cm) at the top to accommodate the camera phone and flash. For each experiment, three samples of each reaction (replicate measurements) were placed in every other column (Figure 2.4B). The columns on each side of the samples contained DI water, which acted as lighting controls. Due to the inconsistent flash intensity across the device, the light controls were used to normalize the brightness to give more precise results. A white paper lining was used in the box to reflect and distribute light from the camera flash more evenly, and decrease the appearance of low lighting regions. Blank spot rows were further used to normalize lighting conditions.

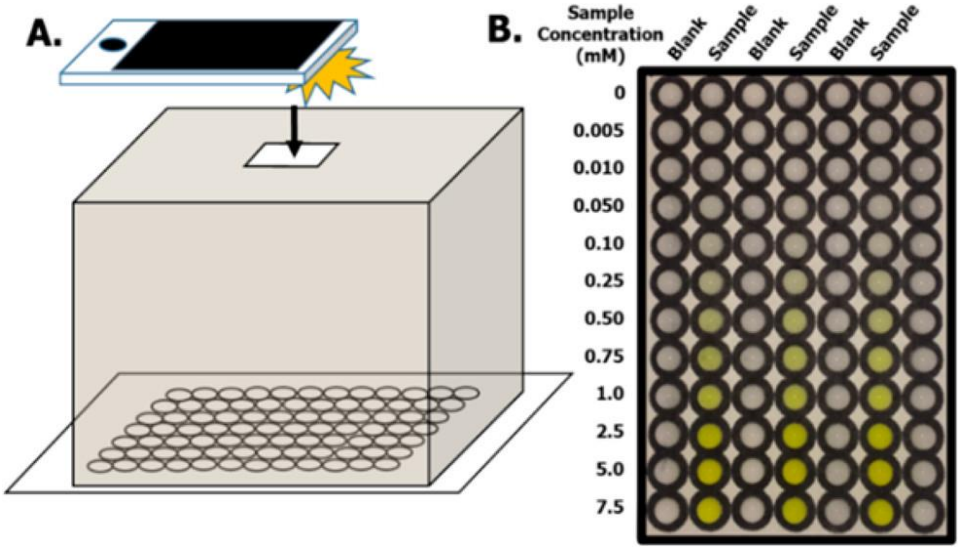

Figure 2.4 | Scheme showing **(A)** the image capture process using a cellphone for the "light box" plate reading method and resulting **(B)** PNP calibration image labeled with blank and sample regions.

Figure 2.5 shows the process of image analysis using NIH ImageJ software. First, the image was split into RGB color channels and the blue color channel was selected for optimal analysis of the yellow formed products. The channel was then

inverted, so that as color intensity due to product formation increased so did the measured mean grey intensity. The mean intensity of each spot test was measured, and normalized to a background lighting condition by subtracting the average mean intensity of the water spots on each side of the sample as shown in Figure 2.5.

Colorimetric analysis for the devices to detect *S. typhimurium* was also carried out using NIH ImageJ, but instead of the blue channel, the green channel was selected and inverted before the grey color intensity was obtained. Light normalization was not used for *S. typhimurium* detection. For the assay on chemometers, the red-violet product (chlorophenol red) was wicked through the channel of the chemometer. Color development along the channel was proportional to the number of bacteria. For biosafety consideration, all assays on paper devices were carried out in covered petri dishes at BSL-2 containment.

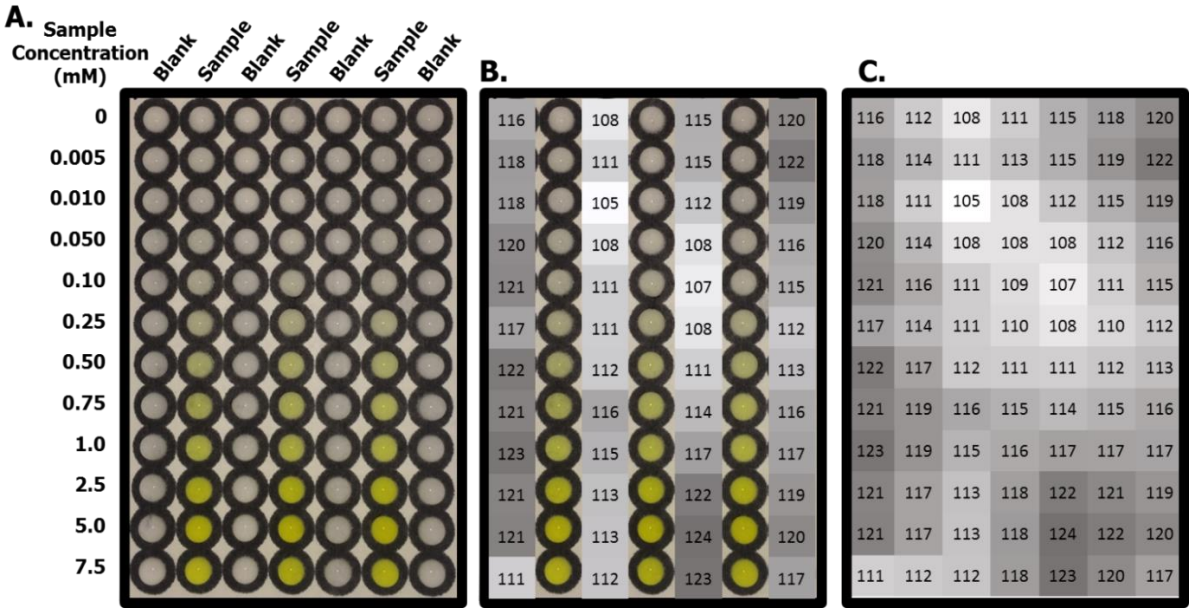

Figure 2.5 | Background normalization process for **(A)** an example PNP calibration image, where **(B)** the blank spots are converted to an intensity unit and are shown shaded dark to light from highest to lowest intensity respectively. **(C)** The spots surrounding a sample spot are averaged to form an average background lighting condition for that sample to be subtracted from the measured sample intensity.

Preparation of Dynabeads® anti-*Salmonella*. The anti-*Salmonella typhimurium* 0-4 antibody was covalently conjugated onto M-280 tosylactivated Dynabeads® using the standard protocol from Invitrogen.[54] Before antibody immobilization, the beads were washed using pre-washing buffer. Beads were vortexed for approximately 30 s or until a homogeneous suspension was obtained. A volume of 165 µL (5 mg) of the beads was pipetted into a 1.5 mL Eppendorf tube followed by adding 165 µL of pre-washing buffer. Beads were thoroughly mixed, then separated from solution using a magnet (DynaMag™-2 Magnet, product no. 12321D, Thermo Fisher Scientific Inc., Waltham, MA, USA) for 1 min and the supernatant was discarded. The washing process was repeated once with the pre-washing buffer before immobilization.

To covalently immobilize antibody onto the beads, 100 µg of antibody (for 5 mg beads) was recommended by the beads' manufacturer. 50 µL of anti-*Salmonella typhimurium* 0-4 antibody (2 mg mL^{-1}, 250 µg) was added to re-suspend the washed beads. Pre-washing buffer was also added to give a total volume of 150 µL, and 100 µL of coupling buffer was added to the beads mixture and thoroughly mixed on a rotator (RotoFlex, product no. R2000, Argos Technologies, Elgin, IL, USA) at 37 °C for 12-18 h. The bead-antibody mixture was placed on the magnet for 1 min and the supernatant was discarded. 1 mL of washing buffer was added into the beads and the tube was incubated on the rotator at 37 °C for 1 h, then the wash buffer was removed using the magnet as above. The beads were washed using 1 mL of storage buffer, vortexed for 5-10 s, and the tube placed on the magnet to remove the supernatant. The washing step was performed twice. Finally, the beads immobilized with anti-*Salmonella* antibody were

re-suspended in storage buffer to a final bead concentration of 20 mg mL^{-1}. The anti-*Salmonella* magnetic beads were stored at 4 °C for further use.

FIB Enzymatic Assay Optimization. Enzymatic assay optimization was performed spectrophotometrically for ONP and PNP-producing reactions within 96-well plates and read using a microtiter plate reader (BioTek Synergy 2 Plate Reader). Each well contained a total reaction volume of 200 µL, and reactions were quenched by adding 0.5 M NaOH to the sample (0.25 M NaOH final concentration). Detection was completed under alkaline conditions to inactivate the enzyme, and ensure the product was in its anionic form for colorimetric detection. PNP and ONP are colorless below and yellow above their pK_a values (pH 7.18 and 7.23 respectively). ONP and PNP production was detected at 400 nm. β-gal activity was detected using PNP-gal and ONP-gal. β-glucr activity was detected using PNP-glucr. β-gluco was detected using PNP-Gluco and ONP-Gluco. With each of these substrates, the carbohydrate moiety is cleaved off by the enzyme leaving either PNP or ONP as the product. The optimal reaction pH/buffer of each enzyme was determined using PCS buffer of pH 3 to 7.5 for β-gluco or PBS of pH 5.5 to 9 for both β-glucr and β-gal. Optimal pH for β-gal, β-glucr, and β-gluco were determined to be pH 7.5 PBS, pH 6.5 PBS, pH 5.5 PCS buffers respectively.

Immunomagnetic Separation and Incubation. Immunomagnetic separation (IMS) was employed to isolate *S. typhimurium* from culture media, bird feces, or whole milk. The IMS process was performed using anti-*Salmonella* Dynabeads® that had been previously prepared. Subsequently, the bead-bacteria complex was conjugated to

β-gal through a biotin-streptavidin linkage. Both processes are schematically illustrated in Fig. 2.

For IMS of bacteria, the anti-*Salmonella* magnetic beads were vortexed until a homogeneous suspension was obtained. Subsequently, 5 µL of the magnetic beads were pipetted into a 1.5 mL Eppendorf tube and 1 mL of bacteria suspension was added into the tube and mixed thoroughly by pipetting. The mixture was incubated on the rotator at room temperature for 15 min. Next, the tube was placed in the magnet for 1 min before carefully removing the supernatant without disturbing the pellet of IMS beads attached on the side wall of the tube.

Anti-*Salmonella* biotin conjugated antibody (Ab-biotin) was diluted to 0.02 mg mL^{-1} in phosphate buffered saline (PBS) pH 7.4. 100 µL of the diluted Ab-biotin (~2.0 µg) was added to the bead-bacteria complex from the IMS process and incubated on the rotator at room temperature for 20 min. The tube was then placed onto the magnet to remove the supernatant and washed twice using washing buffer (PBS Tween). 100 µL of streptavidin/ β-galactosidase conjugate (strep-β-gal), diluted at 1:1,000 v/v in PBS, was then pipetted into the bead-bacteria complex. This corresponded to a concentration of approximately 0.2 µg for strep-β-gal. The mixture was incubated on the rotator at room temperature for 10 min, placed onto the magnet to remove the supernatant, washed twice to remove unbound strep-β-gal, and re-suspended in 100 µL PBS. The β-gal-labeled bacteria were detected with CPRG on paper devices as described below.

Determining Capture and Retention Efficiency. The capture efficiency of the anti-*Salmonella* magnetic beads for *Salmonella* was considered using initial bacteria concentrations of 10^2, 10^3, 10^4 and 10^5 CFU mL^{-1}. After the IMS process the bead-

bacteria complex pellet was re-suspended in 100 µL PBS. High-concentration samples were diluted to have final concentrations of approximately 10^1 and 10^2 CFU mL^{-1} before using 10 µL of the final suspension to spread onto Difco™ nutrient broth agar plates. Colonies on the plates were counted after incubation for 24 h at 37 °C. The number of colonies before ($n_{\text{before IMS}}$) and after ($n_{\text{after IMS}}$) IMS were compared to calculate the capture efficiency using the equation below;

$$\text{Capture efficiency (\%)} = \frac{n_{\text{after IMS}}}{n_{\text{before IMS}}} \times 100$$

The number of bacteria before the IMS ($n_{\text{before IMS}}$) was obtained from plating 100 µL of 10^1, 10^2, and 10^3 CFU mL^{-1} bacteria suspension on the agar plates before starting the IMS process. The number of colonies on each plate was averaged to determine an estimate of the initial bacteria concentration.

The same bacteria concentrations used to investigate the capture efficiency were used to evaluate retention efficiency. After bacteria capture using the IMS procedure, the coupling process was performed as previously described. The suspension of the bead-bacteria-β-gal complex was diluted in PBS to final concentrations of 10^1 and 10^2 CFU mL^{-1} before using 10 µL for plating on the nutrient broth agar plates. After 24 h incubation at 37 °C, colonies on the plates were counted as the number of bacteria after the coupling process ($n_{\text{after coupling}}$) which was compared with before the coupling step ($n_{\text{before coupling}}$ which was equal to the number of bacteria after the IMS, $n_{\text{after IMS}}$). The retention efficiency was determined using the equation below;

$$\text{Retention efficiency (\%)} = \frac{n_{\text{after coupling}}}{n_{\text{before coupling}}} \times 100$$

FIC Bacteria Detection. The bacterial strains included; pathogenic *Escherichia coli* O157:H7 PTVS016 (lettuce-associated outbreak isolate obtained from human feces) and *E. coli* O157:H7 PTVS087 (lettuce isolate possibly linked to an outbreak); *Enterococcus faecalis* BB1172 and *E. faecium* BB498 (wild-type strains isolated from concentrated animal feeding operations); as well as nonpathogenic *E. coli* P14 (ATCC BA-1430) and *E. coli* P68 (ATCC BA-1431) originating from cattle hides. Probe sonication was compared to chemical lysing using an optimal 20 s for cell lysing and a 50:50 solution of 10% chloroform and 0.005% SDS for chemical lysing prior to performing enzymatic assays. Detection of low concentrations of pure bacterial cultures was conducted using dilutions of pure cultures at stationary phase (18-24 h old) incubated in media with 1 mL aliquots taken for enzymatic assay testing.

Salmonella Strains and Culture Conditions. The bacterial strains used in this work were *Salmonella enterica* serovar Typhimurium (ATCC® 14028™, product no. 0363P) purchased from Microbiologics (St. Cloud, MN, USA) and *DH5a Escherichia coli* were purchased from Thermo Fisher Scientific. Both strains were grown in Difco™ Nutrient Broth (Product no. 234000, BD, Sparks, MD, USA) at 37 °C with gently shaking at 125 RPM for 16 h. Serial dilutions of bacteria suspension were prepared in the range from 10^2 to 10^8 CFU mL^{-1} in nutrient broth. The exact bacteria concentration was quantified by plating 100 µL of 10^2 and 10^3 CFU mL^{-1} dilutions onto Difco™ Nutrient agar plates (Product no. 213000, BD, Sparks, MD, USA). The plates were incubated at

37 °C for 24 h before counting the colonies. All experiments with bacteria in this work were performed in a biosafety level 2 (BSL-2) laboratory.

Detecting FIB in Food and Water Samples. Alfalfa sprouts were purchased from Whole Foods and unfiltered water was obtained from Colorado State University's Lagoon (Latitude: 40.57566, Longitude: -105.08631, Elevation: 1523 meters, Date: 02/08/2016, Outdoor temperature: -1.7°C) and both were stored in the refrigerator at 4°C overnight (10 h) prior to testing. Inoculated water and sprout samples contained 2.3 x 10^2 and 3.1 x 10^1 CFU g^{-1} of *E. coli* and *E. faecalis*, respectively. For food samples and water samples, 10 g or 10 mL of sample (inoculated or uninoculated control) alfalfa sprouts or lagoon water, respectively, were mixed with 90 mL of BHI media. Sprout-media mixtures were placed in a stomacher mixer for 1 min to mix/wash the sprouts. Water-media solutions were hand mixed to ensure a homogeneity. All samples were incubated in a 37°C shaker incubator with shaking at 100 RPM, sampled at set time intervals, and then sonicated (1 mL for 30 s at 5 W). Assays were reacted in centrifuge tubes with 250 µL of sonicated sample, and 250 µL of substrate and buffer. After 1 h, 250 µL of 0.5 M NaOH in 0.4 M KCl was added to stop the reaction and the final solution was analyzed for both colorimetric and electrochemical measurements. Spread plating following serial dilutions was performed to determine inoculum levels in CFU/mL.

***S. typhimurium* Detection in Bird Fecal Samples.** Bird fecal samples were obtained from captive Starling birds maintained by the National Wildlife Research Center, a division of the United States Department of Agriculture located in Fort Collins, Colorado, United States. Samples were collected and kept on ice or in a 4 °C refrigerator until testing. To perform IMS on bird feces samples, ~0.10 g fecal samples

were weighed in Eppendorf tubes and 1 mL of Difco™ nutrient broth was added to the samples. The sample suspensions were vortexed for 30 s to break up the sample matrix and allow for separation of bacteria from the particulates. For inoculated fecal samples, at this point in the procedure, 10 µL of bacteria concentrations ranging from 10^2 CFU mL^{-1} to 10^8 CFU mL^{-1} were added to the suspensions and vortexed for an additional 15 s. For fecal samples without inoculation, this step was omitted. To observe the microorganism load in the fecal samples before immunomagnetic separation of *Salmonella*, 10 µL of each sample suspension was plated onto BBL™xylose lysine deoxycholate (XLD) agar plates (BD, Sparks, MD, USA) and labeled as “before IMS”. 5 µL of the anti-*Salmonella* magnetic beads was added into the samples, vortexed for 5-10 s, and then immediately placed on the rotator to avoid fecal matter settling. After incubation for 15 min on the rotator, the samples were vortexed immediately before placing on the magnet to separate the bead-bacteria complex from the matrix. After placing the tubes on the magnet for 2 min, unbound particulate matter was removed using 1 mL pipette tips with the first 5 mm cut off to allow the pipette to remove fecal matter from the tubes without clogging the pipette tip. The beads were washed twice with 500 µL of 1x PBS pH 7.4 before re-suspending the beads in 100 µL of Ab-biotin (0.02 mg mL^{-1}). The remainder of the IMS procedure was completed using the steps and incubation times optimized for detecting *Salmonella* in media. At the end of the IMS procedure, 10 µL was plated on XLD agar and labeled as “after IMS” to compare to the “before IMS” plates. Finally, 10 µL of re-suspended beads was used to perform the assay with CPRG as previously described. For quantitative determination of *Salmonella*

in the sample, the color intensity of the sample spots was compared with that of standard solutions of known amounts of bacteria.

Assessment of Beads Lost to Sample Matrix. To determine if beads were lost in the sample matrix, Ab-biotin was directly conjugated to tosyl-activated Dynabeads®. The coupling process was the same as previously described. The antibody-conjugated beads were added directly to either media or bird fecal samples. Samples were incubated with the beads for 15 min on a rotator to replicate the first steps of the IMS procedure. After media or fecal matter was removed from the beads and washed, the beads were incubated with strep-β-gal for 10 min. After incubation, the beads were washed twice with washing buffer (PBS Tween®), re-suspended in PBS, followed by the enzymatic assay with CPRG on paper devices as previously described.

Analysis of Milk Samples. King Soopers City Market branded organic whole pasteurized milk was purchased from King Soopers in Fort Collins, Colorado, United States, on 05/31/2017. Milk was warmed to room temperature before diluting *S. typhimurium* in the sample matrix in 10-fold dilutions resulting in concentrations ranging from 10^1-10^7 CFU mL^{-1}. The IMS procedure and sandwich immunoassay was carried out as previously described for media. After re-suspending the beads in 100 µL of 1x PBS, 10 µL of the beads was reacted with 10 µL of CPRG for 30 min before analyzing as previously described.

Results and Discussion

Colorimetric Detection Optimization. Similar to previously described work that used a flat-bed scanner for reading 96-well plates,[55] we developed a simple and

inexpensive detection scheme to take the place of a plate reader for paper-based detection. A cell phone camera was used to both image and wirelessly send results for analysis, which allowed for measurements to be taken as a function of time (Figure 2.4). The method is an improvement to our previously described method for bacteria detection, where results were only acquired using a desktop scanner once the device dried.[41,56,57] We also studied the use of standards on either side of each spot test to normalize the background lighting and solution conditions. Figures 2.4 and 2.5 show the process of image analysis and normalization. Using the light box and background normalization method, the detection limit for ONP was decreased from 151 μM to 81 μM for ONP (Figure 2.6) and from 260 μM to 119 μM for PNP detection. Figure 2.6 shows the decrease in average relative standard deviations with normalization from 28% to 9.2% over the linear range (0.1-1 mM). While the detection limit is higher than that of a plate reader (4.4 μM and 9.6 μM for ONP and PNP, respectively), the portability is improved and cost is significantly reduced. Part of the increase in detection limit is due to the decrease in path length on paper when compared to the plate reader. While the electrochemical detection of PNP has been reported using ePADs,[58] to the best of our knowledge only the colorimetric detection of PNP and not ONP has been reported with PADs.[59] Murdock *et al* used alkaline phosphatase as a tag in enzyme-linked immunosorbent assays (ELISAs) in paper-based wells to react with p-nitrophenyl phosphate (PNPP) and form PNP. While similar, this method only calibrated a dried, end-point color intensity with respect to antigen concentration.

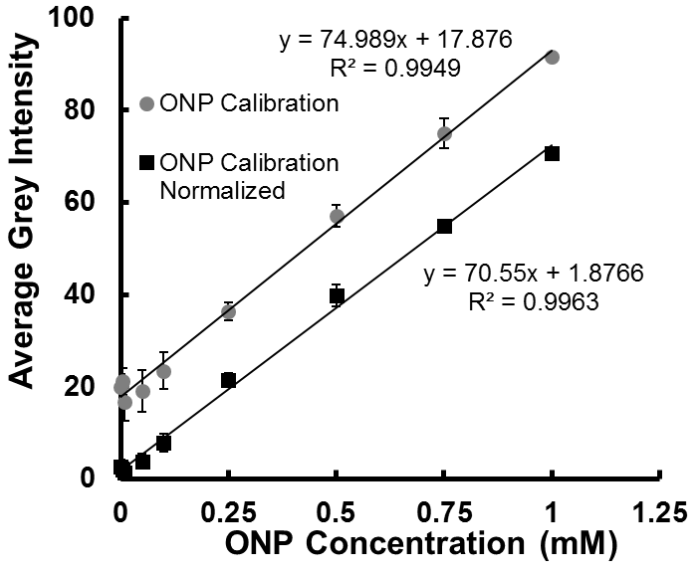

Figure 2.6 | Measured average grey intensity for ONP calibration in paper-based wells with and without background lighting normalization. (n=3)

Enzyme Detection Optimization. Once optimal electrochemical and colorimetric parameters were established for each reaction, enzymatic conditions were optimized. Each enzymatic reaction was optimized using pure enzyme dilutions. Optimal pH conditions for the highest activity were achieved for β-gluco in pH 5.5 Phosphate-citrate buffer (Figure 2.7A) β-gal in pH 7.5 PBS (Figure 2.7B), β-glucr in pH 6.5 PBS. Optimal substrate concentrations for 1 U/mL of enzyme (representative of a high concentration of bacteria) were determined by varying substrate concentrations. With *E. coli* enzymes, peak signal response was reached for β-gal at 2.5 mM for ONP-gal and PNP-gal substrates, while β-glucr peaked at 2 mM PNP-glucr (Figure 2.8A). *Enterococcus* spp. enzyme β-gluco provided a maximum signal at 7.5 mM for PNP-gluco and 10 mM for ONP-gluco (Figure 2.8B). All reactions developed the highest color change after 1 hr with the exception of ONP-gal and ONP-gluco both of which peak in signal within 10

min (Figure 2.8B). Beyond 1 hr, evaporation from the paper-based wells began to significantly change signal response.

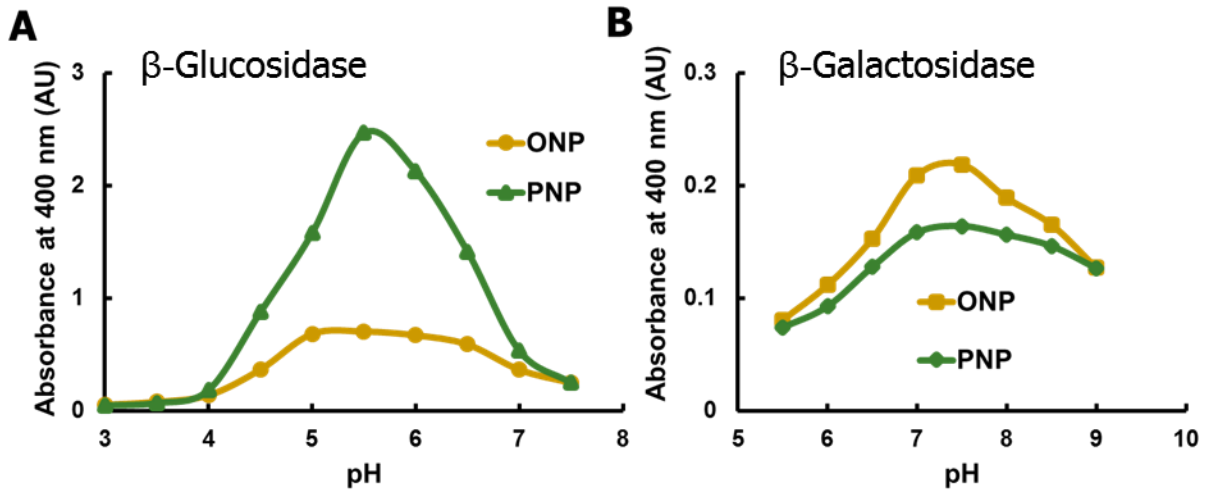

Figure 2.7 | Optimal pH measurements for **(A)** ONP-gluco and PNP-gluco reacted with β-gluco in PCS buffer, and **(B)** ONP-gal and PNP-gal reacted with β-gal in PBS buffer. (n=3)

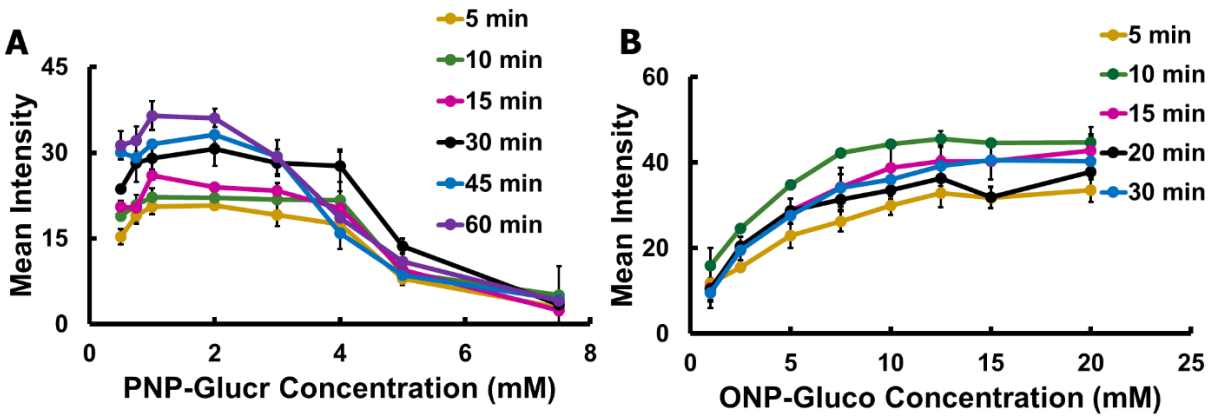

Figure 2.8 | Measured average grey intensity results of enzymatically formed product **(A)** PNP and **(B)** ONP from varying concentrations of substrate PNP-Glucr and ONP-Gluco respectively. Enzymes for ONP-Gluco and PNP-Glucr are β-gluco and β-glucr respectively. (n=3)

Detection limits for each enzyme/substrate pair were conducted using optimal substrate concentrations. Enzyme LODs obtained for PNP-gluco (0.2 µg/mL), ONP-

gluco (2 µg/mL), PNP-glucr (7 µg/mL), PNP-gal and ONP-gal were both 1.5 µg/mL. Differences in LOD and optimal substrate concentrations for the same enzyme but different substrates are a result of substrate affinity and possible feedback inhibition effects.[60] The high relative detection limit for PNP-glucr is probably due to substrate inhibition, which occurs in approximately 20% of enzymes.[61] While most substrate optimization curves were logarithmic, the signal for PNP-glucr (Figure 2.8A) decreased above 2 mM until almost no activity measured at 10 mM. When testing PNP-glucr with bacteria, it also gave the lowest signal, which could also be indicative of substrate inhibition or lower β-glucr expression.

PNP *vs.* ONP Substrates. A comparison between the use of PNP and ONP substrates for β-gluco found that PNP-gluco produced a significantly higher signal than ONP-gluco (Figure 2.8). As such, ONP-gluco was not used in the final experiments involving *Enterococcus* spp. For β-gal, ONP-gal reacted faster than PNP-gal, however, over longer reaction times, PNP-gal provided a higher signal on the plate reader and paper. Because ONP and PNP demonstrate similar molar absorptivity, this is likely due to increased reaction efficiency with β-gal and PNP-gal compared with ONP-gal.

An interesting phenomenon occurred when ONP assays reacted in the paper-based wells for more than 10 min. A noticeable decrease in signal occurred within the sample wells, while simultaneously the light control spots and surrounding paper began to turn yellow. This phenomenon was not observed within the deeper wells of the plate reader or for PNP assays on paper. This was determined to be due to the higher vapor pressure of ONP (12 Pa) relative to the vapor pressure of PNP (0.32 Pa) resulting in gas phase transfer between spots.[62] The higher vapor pressure is in part due to the

ortho- position of the hydroxyl group, which causes ONP to form intramolecular hydrogen bonding, and decreases intermolecular hydrogen bonding, contributing to its volatility. Because of ONP's comparatively high volatility, it would not be practical to react ONP in open PAD devices. When detecting bacteria, therefore, the reactions were completed in microfuge tubes before being quantified on paper so ONP could be used to detect bacteria.

Bacterial Detection. Given the need to enrich bacteria after sampling to verify cell viability, we next considered the impact of growth media on both colorimetric and electrochemical signals. We first studied removing culture media and resuspending cells in buffer to remove the colored background and potential electrochemical interferences as well as provide a simple preconcentration step. Figure 2.9A shows the colorimetric detection of PNP-gluco with resuspension of cells after media removal. It was found, however that keeping the cells in their original media gave higher colorimetric signals than centrifuging and re-suspending cells in buffer (Figure 2.9B). This is due to either loss of secreted enzymes during centrifuging, or possibly the natural release and buildup of enzyme within the media due to cell death and apoptosis over time before centrifuging. Therefore, when removing the media, enzymes were removed as well, decreasing enzymatic activity and product turnover. In an attempt to regain enzymatic activity, we explored chemical and probe sonication-based lysing methods that we have previously shown enhanced detection.[41] 20 s of probe sonication provided the highest intensity signal over no lysing for the majority of bacteria species detected (Figure 2.9C). Chemical lysing, however, resulted in no assay response, likely due to the enzyme denaturation by the chloroform or SDS. While sonication with media removal is

a viable option for measuring enzyme activity within cells, the current study utilized the direct sonication and detection of bacteria within media due to its simpler preparation and higher signal.

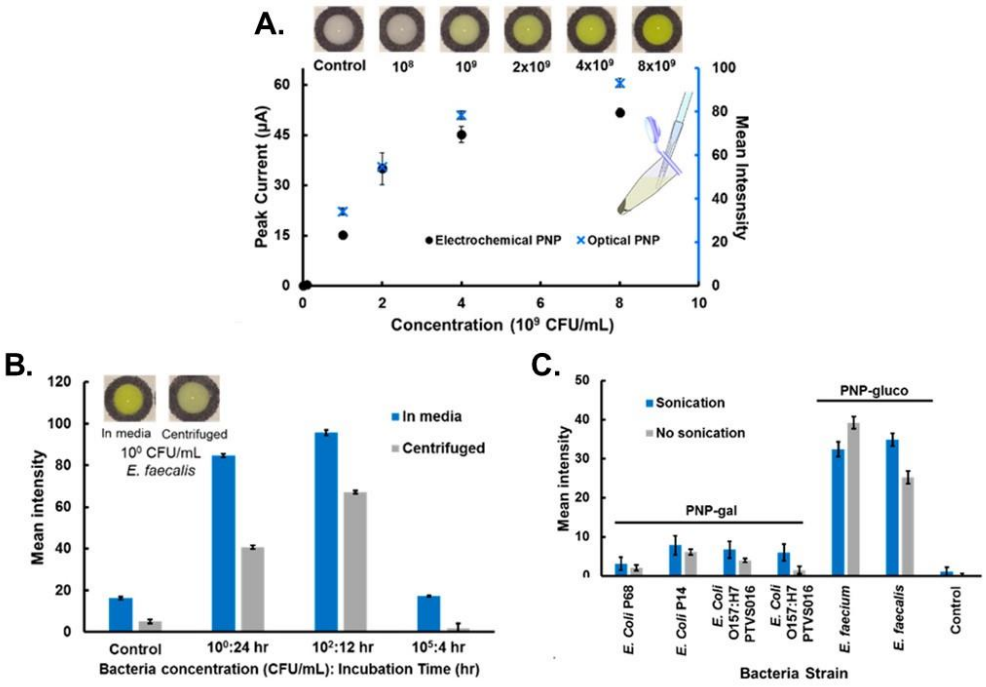

Figure 2.9 | Showing **(A)** electrochemical and colorimetric response of centrifuged and resuspending E. faecalis incubated for 2 hr with PNP-gluco substrate and **(B)** comparison of the same strain and reaction in media vs. centrifuged with increasing concentrations and decreasing assay time. **(C)** Comparison of 20 s of sonication for all tested bacteria strains with their corresponding PNP cubstrates for β-gal for E. coli and β-gluco for enterococci (n=3). Controls include reaction well without bacteria present.

Bacterial strains used as indicators of fecal contamination in food and water, *E. coli* and *Enterococcus* spp. were tested from pure cultures to assess assay performance and time to detection for low concentrations. For colorimetric detection, none of the bacterial strains tested developed signals at 4 h, which is not surprising given the low starting concentrations of bacteria, but all 10^1 CFU mL^{-1} dilutions produced signals by 8 h (Figure 2.10). By 12 h, a maximum signal had been obtained

for all bacterial strains and dilutions, except for detection of PNP-gluco for *E. faecium* and *E. coli* PTVS087, both of which generated maximum signal at 18 h. However, as discussed below, a decrease was seen in the colorimetric *Enterococcus* spp. assays at 24 h. The assay results for PNP-glucr detection were omitted, because these pathogenic strains are negative for β-glucr production and all time points were negative. Because of these results, using this assay has been demonstrated as an option to identify pathogenic strains of *E. coli* O157:H7. It was determined that ONP substrates provided higher signals than PNP substrates for colorimetric detection.

A. Colorimetric (Mean Intensity)

		CFU/mL	Time (hr) 4	8	12	18	24
E. coli P14	PNP-gal	10^1	-	67.93	84.21	83.11	63.71
		10^2	-	64.38	102.25	86.88	90.30
		10^3	-	71.13	103.17	85.18	89.13
	ONP-gal	10^1	-	51.04	113.10	98.91	103.89
		10^2	-	49.00	114.35	99.94	107.28
		10^3	-	67.47	112.28	99.14	107.69
	PNP-Glucr	10^1	-	73.32	76.45	65.65	72.48
		10^2	-	67.80	78.28	67.18	71.58
		10^3	-	70.05	77.86	65.31	72.79
E. coli O157:H7	PNP-gal	10^1	-	27.34	79.93	106.45	106.94
		10^2	-	72.76	82.42	108.13	109.31
		10^3	-	73.13	81.61	109.63	109.28
	ONP-gal	10^1	-	21.37	84.79	116.11	117.41
		10^2	-	63.05	85.16	116.16	118.37
		10^3	-	75.45	85.70	116.90	117.53
E. faecalis	PNP-gluco	10^0	-	-	106.04	104.37	84.37
		10^1	-	6.67	108.70	102.83	85.75
		10^2	-	44.00	96.92	90.76	77.28
E. faecium	PNP-gluco	10^0	-	-	20.72	14.35	66.24
		10^1	-	6.47	38.04	91.97	70.16
		10^2	-	42.17	41.96	90.18	75.42

Figure 2.10 | Heat map showing average (n = 3) measured colorimetric normalized mean intensity detection of PNP and ONP production from enzymatic assays measured after 1 hr of reaction. Each strain was tested for three dilutions at low concentrations (CFU mL^{-1}), cultured, and measured with pre-enrichment culture time (– indicates signals below the detection limit).

Food and water sample testing. Detection of foodborne pathogens requires a sampling and culture technique appropriate for the manner of contamination that might occur. Our lab's previous studies used a swabbing technique to detect surface contamination on ready-to-eat and butcher meats.[63,64] However, for large surface area foods such as leafy greens, a washing/mixing technique is preferable, as was previously demonstrated for bacterial detection from spinach leaves.[63] Raw sprouts were inoculated with a generic *E.coli* species (P14) and *Enterococcus faecalis* to simulate contaminated food, and sampled using a washing/mixing approach. Figure 2.11 shows the resulting colorimetric detection of cultured sprouts as a function of time. For both detection methods there was not a significant difference between raw and inoculated sprouts except for colorimetric detection of β-gal activity at 4, 18 and 24 h in which there is a slightly higher intensity signal for the inoculated sprout samples. Without inoculation, the sprouts contained 1.5×10^9 CFU g^{-1} of bacteria, as verified by culture methods (spread plating). The lack of differences between control and inoculated sprout samples is probably due to the very high initial concentration of bacteria, where, except at initial time points, the enzyme assays quickly reached a saturation point. Our device did not find β-glucr activity in the raw or inoculated sprouts. This high initial concentration could also have inhibited enzyme production or cell growth of the inoculated β-glucr expressing bacteria, which can occur with mixed bacterial growth due to competitive behavior and cellular signaling responses.[65] While β-glucr was negative, all β-gal assays achieved positive signal within 4 h, emphasizing the need for multiple assays when determining FIB contamination.

For model irrigation water sample detection, no signal was obtained with lagoon water samples without inoculation (Figure 2.11). The lagoon water had a significantly lower bacterial concentration at 2.9 x 10^2 CFU mL^{-1} when compared to sprouts. In this case, the species of bacteria present probably did not express the target enzymes employed, and were therefore probably not FIB as concentrations were low enough that inhibition effects are significantly less likely. Inoculated bacteria were detected by all assays within 8 h. Due to the low concentrations of bacteria found in water (<10^2 CFU mL^{-1}), filtration steps are usually taken to reduce analysis and culture time while improving detection limits.[66]

B. Colorimetric (Mean Intensity)

			Time (hr)				
		C/I	4	8	12	18	24
Sprouts	PNP-gal	C	16.59	78.82	82.36	88.68	73.28
		I	27.6	80.81	82.24	108.35	103.37
	ONP-gal	C	20.14	95.78	102.37	88.88	79.55
		I	35.64	95.99	99.87	107.36	102.79
	PNP-Gluco	C	63.00	76.30	69.96	75.25	75.56
		I	65.13	76.87	80.79	78.78	75.30
Water	PNP-gal	C	-	-	-	-	-
		I	-	69.06	111.79	111.33	101.87
	ONP-gal	C	-	-	-	-	-
		I	-	62.09	117.30	120.78	111.25
	PNP-Glucr	C	-	-	-	-	-
		I	-	43.64	81.81	83.91	84.27
	PNP-Gluco	C	-	-	-	-	-
		I	-	75.13	104.11	88.37	78.55

Figure 2.11 | Colorimetric measured mean gray intensity for inoculated (I) and control (C) sprout and water samples measured with increasing pre-enrichment culture time. Assay time 1 hr. (– indicates signals below the detection limit (n = 3)).

Starting at 12 h, the colorimetric signal for all sprout sample assays decreased. This behavior was also seen in inoculated water samples, where a decrease in all

assays except ONP-gal, starting at 18 h for PNP-gal, and 12 h for both PNP-gluco and PNP-glucr. This decrease in signal was also measured at 24 h for all assays except PNP-glucr, which occurred at 18 h. We have two hypotheses to why this is occurring. The first could be associated with changes in pH of the media or other interfering metabolites being produced by the bacteria over time. Measured changes in cell culture for all strains grown from ~10^5 CFU mL^{-1} went from pH 7.5 to 5.5 after 12 h While both *Enterococcus* strains remained relatively low at ~pH 6, the *E. coli* strains increased back up to ~pH 7. This could affect enzymatic reaction rates and possibly measured assay intensities. The second hypothesis could be that the phenomenon is associated with cell growth and the expression of enzymes.

Using IMS and an Immunoassay for *S. typhimurium* Detection. While the above method is excellent for pan-detection of FIB, the method does suffer from the necessity to culture the bacteria in order to reach detectable concentrations. Therefore, we also demonstrated specific and sensitive detection of *S. typhimurium* using IMS coupled with a sandwich immunoassay for faster results. Detection of *S. typhimurium* was also based on an enzymatic assay using β-gal as the reporter enzyme and chlorophenol red-β-d-galactopyranoside (CPRG) as a substrate, which turns from yellow to red upon enzyme cleavage instead of clear to yellow. It was reported previously that β-gal has a relatively low limit of detection of 0.01 ± 0.01 μg mL^{-1} when reacting with CPRG,[35] making it ideal for detection of *S. typhimurium*. Because *S. typhimurium* bacteria do not naturally produce β-gal like *E. coli*, we developed a two-step assay to detect bacteria that consists of (i) incubating bacteria with a biotinylated anti-*Salmonella* antibody (Ab-biotin) and (ii) incubating bacteria with β-gal conjugated

streptavidin (strep-β-gal) and colorimetric detection of β-gal retention with CPRG. A schematic of the *S. typhimurium* detection approach is presented in Figure 2.2 and the step-by-step IMS process is in Figure 2.12.

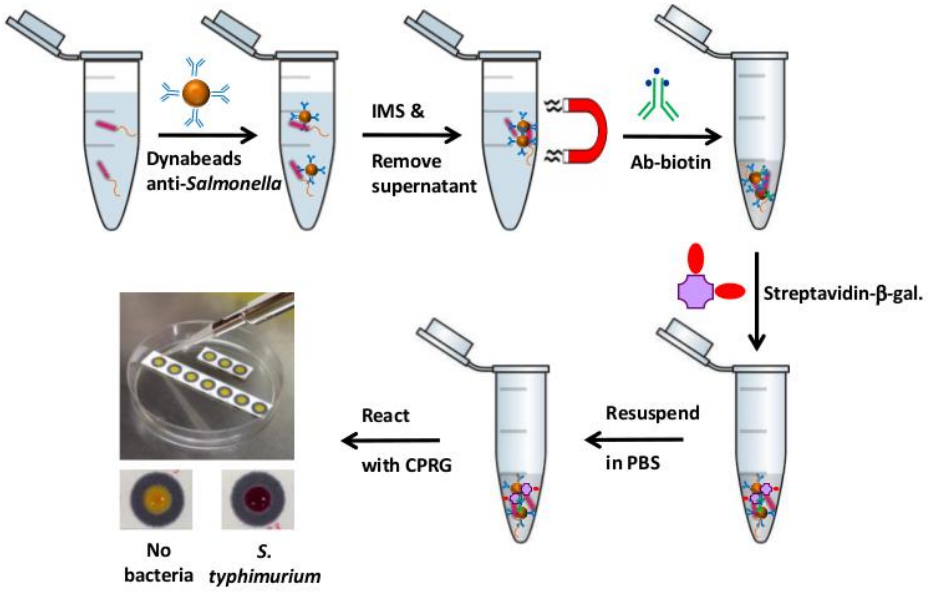

Figure 2.12 | Schematic diagram illustrating the process for detection of *S. typhimurium*, which is based on immunomagnetic separation (15 min), enzyme conjugation (20 min for Ab-biotin and 10 min for strep-β-gal), and the enzymatic assay between β-gal and CPRG (30 min).

Before the incubation with Ab-biotin and strep-β-gal, IMS was performed to isolate *S. typhimurium* from the sample matrix. A *S. typhimurium* antibody, directed against lipopolysaccharides (LPS) on the exterior of the bacteria, was immobilized onto the magnetic bead surface to capture intact *S. typhimurium* bacteria from the samples. In addition to separation from the sample matrix, the IMS process was used for pre-concentrating the bacteria to enhance sensitivity of the assay. A second *S. typhimurium* antibody against “O” and “H” antigens of *S. typhimurium* conjugated with biotin was incubated with the bead-bacteria complex. For the final step of the assay, the bead-

bacteria complex with biotinylated antibody was incubated with the strep-β-gal conjugate. Finally, β-gal labeled bacteria were detected with CPRG on paper devices. The β-gal on the bacteria complex catalyzed the hydrolysis of CPRG into chlorophenol red (Figure 2.2B), which is a red-violet product. Development of a red color in the assay indicated the presence of *S. typhimurium*. If *S. typhimurium* was not present in the sample, then biotinylated antibody and strep-β-gal will have been removed during washing steps and the assay would stay yellow.

Optimized Assay and Sensor LOD. The limit of detection for this approach was determined, as shown in Figure 2.13A. The proposed system detected *S. typhimurium* at concentrations as low as 100 CFU mL^{-1}, a full six orders of magnitude lower than our approach to detect FIB. *E*. *coli* was also applied to investigate the selectivity of the proposed approach. As seen in Figure 2.13A, *E*. *coli* only showed a positive result at a relatively high concentration of 10^7 CFU mL^{-1} with signal intensity equal to the intensity of only 100 CFU mL^{-1} of *S. typhimurium*. Normally, *E*. *coli* can produce intracellular β-gal; however, the result showing a relatively low signal of 10^7 CFU mL^{-1} *E. coli* implied that the enzyme is not secreted and is not detectable with CPRG in intact organisms. The slightly positive result from 10^7 CFU mL^{-1} of *E*. *coli* could be due to non-specific binding of the anti-*Salmonella* antibody. However, non-specific signals only occurred at an extremely high concentration of *E*. *coli*, therefore should not be a concern for real-world samples.

Chemometers were implemented for detection of *S. typhimurium*, as shown in Figure 2.13B, to provide instrument-free CPRG signal quantification. At a high concentration of bacteria (10^4-10^6 CFU mL^{-1}), color development was not significantly

different, likely due to assay saturation. However, for 10^2-10^4 *S. typhimurium*, the distances that color developed along the channels were proportional to the bacteria concentration. The chemometer also showed a detection limit of 100 CFU mL^{-1} for *S. typhimurium* detection. Compared with spot tests on the well-array paper devices, performing the assay on chemometers is more convenient for users because the signal can be read directly on the device without image capture and computer analysis. However, well-array paper devices are slightly easier, faster, and more convenient for fabrication and preliminary testing.

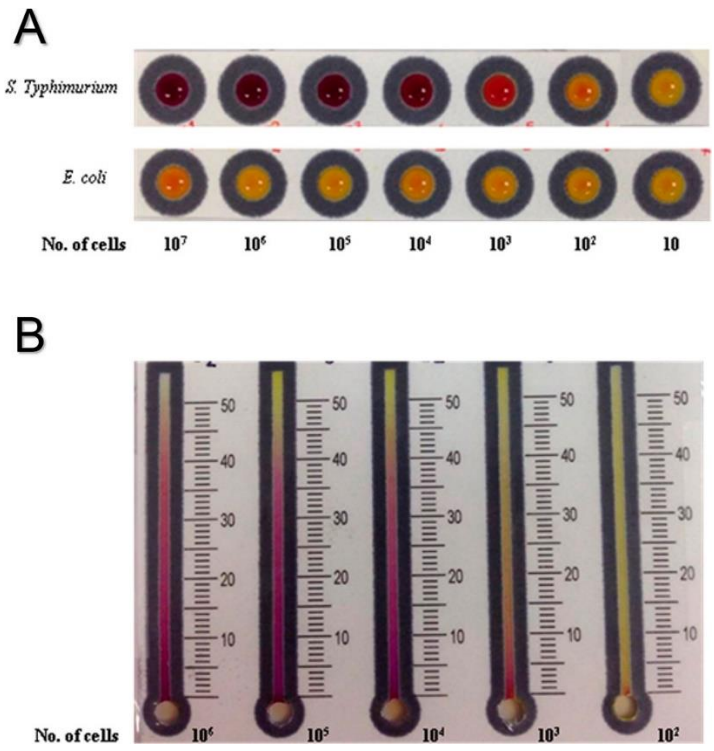

Figure 2.13 | Assay detection limit and specificity using the optimized incubation times and demonstrated on two different PADs: **(A)** well-array devices and **(B)** chemometers.

Results obtained from both formats of paper devices confirmed that detection of *S. typhimurium* using the proposed system was achieved at as low as 100 CFU mL^{-1}, with analysis time of 75 min and an additional 10-15 min for washing steps. The

analysis time for the entire procedure should be within 90 min without any requirement for complex instruments and culture enrichment steps for bacteria incubation. Therefore, the proposed approach has shown its ability as an alternative to culturing to be a sensitive, easy, rapid, instrument-free, reliable, and portable method for detection of *S. typhimurium* and could be an ideal platform for on-site analysis, especially in chemometer format.

Capture and Retention Efficiencies. To determine how efficient the anti-*Salmonella* magnetic beads captured bacteria in solution, the capture efficiencies were calculated. This was determined by comparing the *S. typhimurium* concentration pulled down with anti-*Salmonella* magnetic beads with the original concentrations of *S. typhimurium* (ranging from 10^2-10^5 CFU mL^{-1}). The calculated capture efficiencies ranged from 8.84-21.3%, decreasing as bacteria concentration increased (Table 2.1). This is likely due to bead concentration remaining constant as bacteria concentration increases, therefore fewer bacteria are captured by beads. Because the magnetic beads are smaller than the bacteria, more bacteria in the solution could also lead to steric hindrance, making it harder for bacteria to bind to the antibodies.

Table 2.1 | Determining the anti-*Salmonella* conjugated Dynabeads efficiency to capture *S. typhimurium* in solution and retain the captured bacteria throughout the IMS process.

Bacteria Concentration (CFU mL^{-1})	**Capture Efficiency**	**Retention Efficiency**
2.3×10^5	8.84% ± 5.1%	114 ± 57.4%
2.3×10^4	11.1% ± 4.9%	196% ± 130%
2.3×10^3	20.2% ± 10.8%	115% ± 70.5%
2.3×10^2	21.3% ± 10.3%	12% ± 23.1%

These capture efficiencies are lower than expected as literature citing the use of polyclonal antibodies conjugated to tosyl-activated Dynabeads® for immunomagnetic separation reports ~40% capture efficiency for 10^3 CFU mL^{-1} of *Mycobacterium avium* subsp. *Paratuberculosis*.[67] However, different antibodies will have different binding affinities, which can impact capture efficiencies, and the authors reported using a higher volume of beads. In addition, mycobacteria are much smaller than *Salmonella* bacteria, so more could potentially bind to the beads. The large standard deviations are likely due to the error associated with plating lower concentrations of bacteria. Moreover, pipetting variability could also be an issue because bacteria are not necessarily evenly distributed throughout the media. This caused variation in the number of bacteria pipetted and rendered quantification of small concentrations of bacteria inaccurate. This error could also explain why retention efficiencies were on average >100% with one of the values at 13% and the other three concentrations resulting in well over 100% efficiency. This mostly consistent >100% efficiency could also be due to possible bacteria enumeration during the IMS procedure. Although the capture efficiencies can likely be improved, retention efficiencies are high which indicates that few bacteria are lost throughout the IMS procedure after initial capture. Increasing the capture efficiency using demonstrated techniques will be the subject of future studies. One possible factor could be further studied to improve the capture efficiency is the volume of beads used for bacteria capture. However, this should be compromised between the capture efficiency and the background signal possibly arising from non-specific binding of the reagents used for the sandwich assay and due to Dynabeads® color being similar to chlorophenol red, our detectable product. Grant and coworkers also investigated how different antibodies and

magnetic beads increase capture efficiency of their final IMS assay,[67] something that can be done as future work to ultimately achieve a more sensitive assay.

***S. typhimurium* Detection in Bird Feces.** After optimizing the IMS procedure in media, the method was used with bird feces to demonstrate this assay could be used to accurately detect *S. typhimurium* in animal samples. Fecal samples were collected from Starling birds maintained by the National Wildlife Research Center, a division of the United States Department of Agriculture located in Fort Collins, Colorado, United States. First, it was determined whether the same sensitive LOD would transfer from media to fecal samples despite a complex matrix. 0.1 g of fecal sample was inoculated with different concentrations of *S. typhimurium* before completing the IMS procedure as optimized in media. Final bacteria concentrations in the fecal matrix ranged from 10^1-10^7 CFU g^{-1}. To compare bacteria composition of the sample from before the IMS procedure to after, 10 µL of sample was plated on an XLD agar plate before and after the IMS procedure for comparison. The LOD of *S. typhimurium* in bird fecal samples was significantly higher than in media at 10^5 CFU g^{-1} (Figure 2.14A). This higher LOD could be due to several factors. Because bird feces are a complex matrix, there could be numerous components that affect specificity of antibodies, reducing bacteria binding. For example, high acidic levels in bird feces could decrease binding efficiency of the antibody to the antigen.[68] Solid matter in the solution could also affect the beads' ability to access bacteria in the sample. Lastly, it was observed that the number of beads retrieved from fecal samples varied qualitatively, indicating that beads were likely getting caught in matrix and not adequately recovered by the magnet. When using IMS on fecal samples that had not been inoculated, one slightly positive result was obtained

(Figure 2.14B). However, this result was not confirmed on XLD agar plates. All other fecal samples showed a negative result, and these negatives were confirmed on XLD agar plates. Therefore, of the 10 non-inoculated fecal samples, there was one possible false positive, and no false negatives.

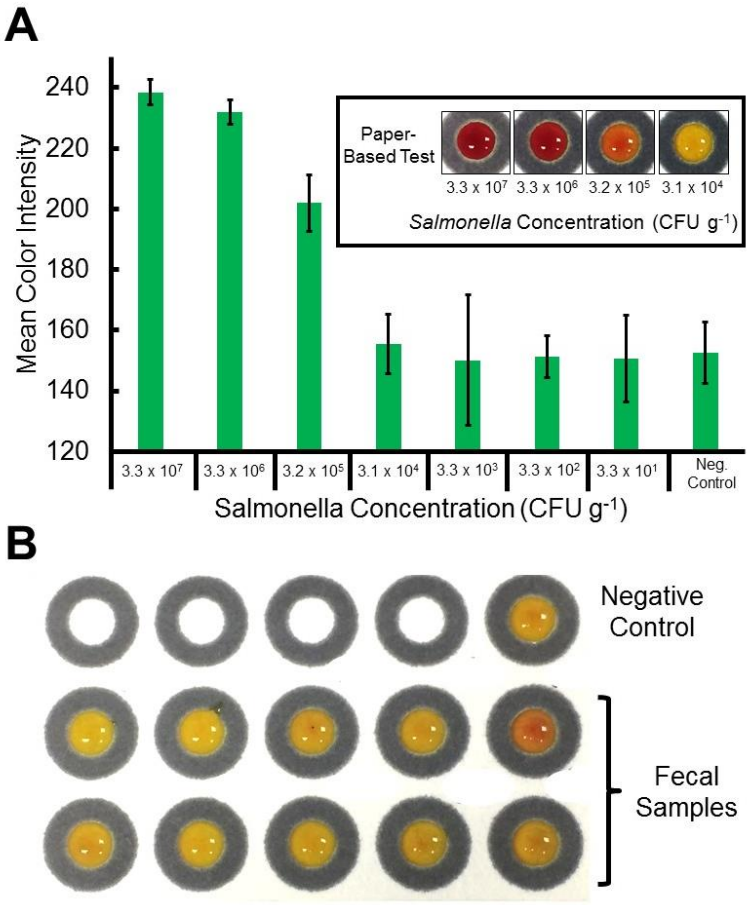

Figure 2.14 | Detecting S. typhimurium in bird fecal samples **(A)** The LOD of S. typhimurium in inoculated bird fecal samples is 10^5 CFU g^{-1}, compared to 100 CFU mL^{-1} in solution. **(B)** Detecting S. typhimurium in noninoculated bird feces samples yielded one slightly false positive that was not confirmed via traditional plating methods.

To confirm whether beads were lost in the sample matrix, Ab-biotin modified beads were added to fecal samples and allowed to incubate on the rotator like traditional IMS. After removing all fecal matter from the solution, Strep-β-gal was

conjugated to the biotin and then reconstituted in PBS before reacting with CPRG. Therefore, unlike traditional IMS, regardless of bacteria present in the sample, the beads should react with CPRG if present in the final solution. Fecal samples were placed on the magnet for 1, 3, and 5 min to determine whether extended time would result in improved bead recovery (Figure 2.15). Extended time on the magnet does not appear to assist with bead recovery, and as observed, significant variation was observed in beads lost in the sample matrix when compared to beads in media. There is still the possibility of sample matrix conditions affecting the antibodies conjugated to Dynabeads®, and this will be the subject of future research.

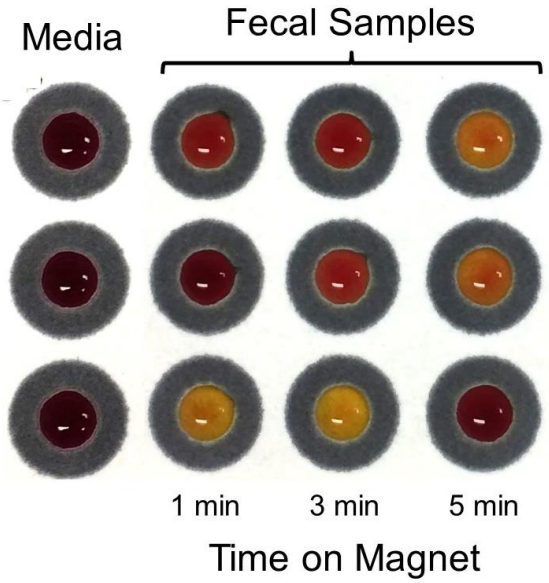

Figure 2.15 | Determining beads lost in fecal sample matrix. While separating beads from sample matrix, different samples were left on the magnet for 1, 3, and 5 min to determine whether extended times on magnet extracted more beads.

While the LOD is not as low in fecal samples, IMS has demonstrated in inoculated bird fecal samples the ability to selectively purify *S. typhimurium* from other bacteria species present in the sample (Figure 2.16). *S. typhimurium* presence is

indicated on XLD plates by black colonies while other bacteria species are yellow. Although no *S. typhimurium* was detected in fecal samples without inoculation, no other bacterial species grew on the “after IMS” agar plates. This indicates that the beads were specific to *S. typhimurium* and would not adhere to other bacterial species, resulting in no bacteria after the IMS procedure if *S. typhimurium* is not present.

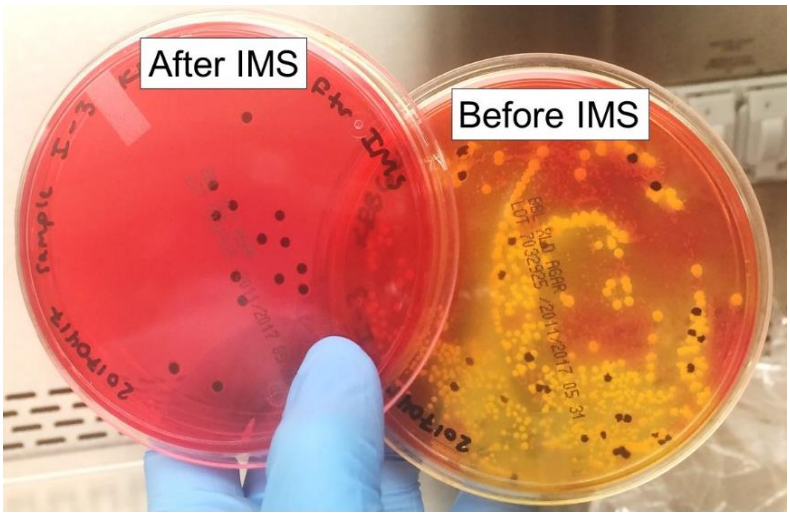

Figure 2.16 | Purifying *S. typhimurium* from other bacteria. *S. typhimurium* presence is indicated by black colonies while other bacteria species are yellow.

***S. typhimurium* Detection in Milk.** To demonstrate the onsite food safety potential of this method, *S. typhimurium* detection was verified in pasteurized whole milk. Utilizing the optimized incubation times and concentrations demonstrated in media, the detection limit of *S. typhimurium* in whole milk was 10^3 CFU mL^{-1} (Figure 2.17). While lower than bird feces, this detection limit is still an order of magnitude higher than media. Although not as complex as feces, milk is still a very complex matrix with solids comprising over 10% of the matrix composition, including numerous proteins, fat globules, and lactose.[69] Any of these solids could affect the specificity of the antibodies during capture, thus raising the detection limit. A capture efficiency study was

not conducted in any other sample matrix other than media, but will be the subject of future research to determine how different sample conditions affect antibody capture. This detection limit should still be efficient in determining whether whole milk has been contaminated by bacteria, and shows promise as a quick and accurate detection method for infield food safety measurements.

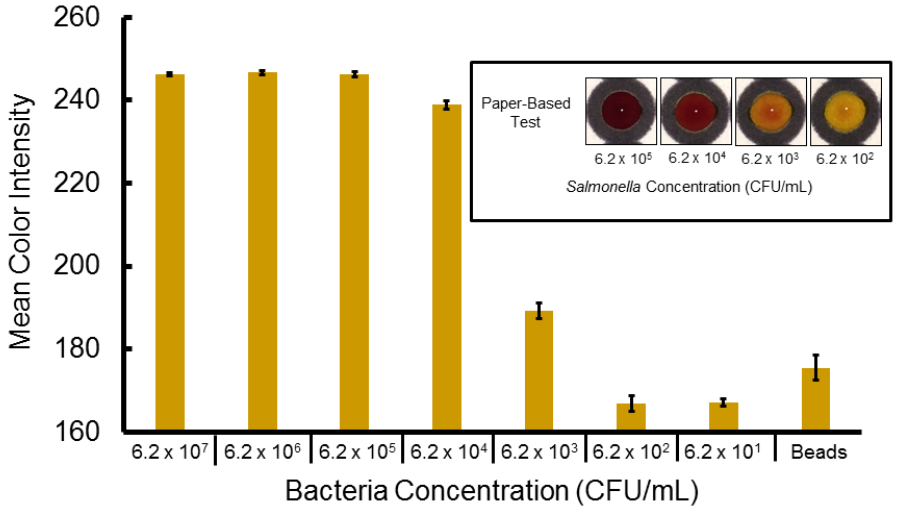

Figure 2.17 | Detecting *S. typhimurium* was demonstrated in whole milk for food safety applications where the detection limit was 10^3 CFU mL^{-1}.

Conclusions

Herein, we have developed procedures for the detection of FIB bacteria and *S. typhimurium* using colorimetric detection within paper-based devices. The first devices successfully measured the presence of FIB using enzyme activity in sprouts and water samples. Although the method still required culture for bacteria enumeration, we could detect low concentrations (10^0 or 10^1 CFU mL^{-1}) of FIB within 8 hr, compared to several days for traditional methods. One way to improve detection limits for this assay is to use inducers to increase enzyme expression in cultured cells.[52] Isopropyl-β-D-thiogalactopranoside (IPTG) and methyl-β-D-glucuronide (MetGlu) have been used to

induce β-Gal and β-glucr expression respectively. Further optimization of colorimetric assays and their detection platforms would provide improved detection of food and water bacterial contamination.

Combining PADs with IMS has also been demonstrated for simple, rapid and sensitive detection of *S. typhimurium* without the culture enumeration required for the first set of devices. A sandwich immunoassay was applied to directly detect *S. typhimurium* in the sample, with the retention of β-gal on the beads and colorimetric conversion of CPRG to chlorophenyl red as a sensitive detection modality. The detectable level of *S. typhimurium* was found to be 10^2 CFU mL^{-1} in pure culturing solution within 90 min. In addition, the proposed approach was confirmed to be highly selective with *S. typhimurium* without any interference from *E. coli*. Chemometers were also used for detection of *S. typhimurium* and showed the same detection limit as the well-array paper devices, providing a more user-friendly device where image processing was not required. IMS was also demonstrated for the first time in the positive detection of inoculated *S. typhimurium* in bird fecal samples and whole milk samples with detection limits of 10^5 CFU g^{-1} and 10^3 CFU mL^{-1}, respectively. Low sensitivity of the developed system for detection of *S. typhimurium* in fecal samples could be due to the matrix effect in feces. However, this method is the first demonstration of an alternative to traditional culture methods, and has shown its potential for onsite detection of *S. typhimurium* in complex sample matrices.

The presented methods are different but each has their individual advantages for in-field bacteria detection. Although the IMS/immunoassay was faster and achieved lower detection limits, the assay would not be sufficient for less specific bacteria

detection or in distinguishing between pathogenic and non-pathogenic bacteria as the FIB tests demonstrated. Additionally, antibodies adhere to bacterial cell wall components and it is therefore unknown whether the bacteria are dead or alive, while the FIB tests detected active enzymes indicating viable bacteria. These tests would work well in conjunction as someone could use the first set of tests to indicate whether there are viable FIB present in their food and water sample, which as mentioned in the introduction, indicates a growth environment where other more pathogenic bacteria can be present. The user can then implement the IMS/immunoassay test for specific detection of concerning pathogens, such as *S. typhimurium.* While this assay was specifically demonstrated for *S. typhimurium* detection, by exchanging the antibodies used in the assay, one can develop an analytical test for not only other bacteria, but other pathogens including viruses and fungi. Detecting bacteria based on enzyme expression can also be applied to other pathogenic bacterial species, and even antimicrobial resistant bacteria, which will be described in the next two chapters. Hence, both tests have demonstrated their potential for in-field use for detecting potentially harmful bacteria in a variety of matrices for food safety applications. Additionally, these paper-based devices are customizable and more tests could be established for more comprehensive pathogen testing to prevent more foodborne illness outbreaks.

REFERENCES

(1) Adkins, J. A.; Boehle, K.; Friend, C.; Chamberlain, B.; Bisha, B.; Henry, C. S. *Anal. Chem.* **2017**, *89*, 3613-3621.
(2) Srisa-Art, M.; Boehle, K. E.; Geiss, B. J.; Henry, C. S. *Anal. Chem.* **2018**, *90*, 1035-1043.
(3) Surveillance for Foodborne Disease Outbreaks-United States, 2009-2010, Center for Disease Control and Prevention **2013**.
(4) Surveillance for Waterborne Disaease Outbreaks Associated with Drinking Water-United States, 2011-2012, Center for Disease Control and Prevention, **2015**.
(5) Uyttendaele, M.; Jaykus, L.-A.; Amoah, P.; Chiodini, A.; Cunliffe, D.; Jacxsens, L.; Holvoet, K.; Korsten, L.; Lau, M.; McClure, P.; Medema, G.; Sampers, I.; Rao Jasti, P. *Compr. Rev. Food Sci. Food Saf.* **2015**, *14*, 336-356.
(6) Steele, M.; Odumeru, J. *J. Food Prot.* **2004**, *67*, 2839-2849.
(7) Painter, J. A.; Hoekstra, R. M.; Ayers, T.; Tauxe, R. V.; Braden, C. R.; Angulo, F. J.; Griffin, P. M. *Emerg. Infect. Dis.* **2013**, *19*, 407-415.
(8) Crowe, S. J.; Mahon, B. E.; Vieira, A. R.; Gould, L. H. *MMWR. Morbid. Mortal. Wkly. Rep.* **2015**, *64*, 1221.
(9) Harwood, V. J.; Staley, C.; Badgley, B. D.; Borges, K.; Korajkic, A. *FEMS Microbiol. Rev.* **2014**, *38*, 1-40.
(10) Silva, N.; Igrejas, G.; Gonçalves, A.; Poeta, P. *Ann. Microbiol.* **2012**, *62*, 449-459.
(11) Odonkor, S. T.; Ampofo, J. K. *Microbiol. Res.* **2013**, *4*, 2.
(12) Scott, T. M.; Jenkins, T. M.; Lukasik, J.; Rose, J. B. *Environ. Sci. Tech.* **2005**, *39*, 283-287.
(13) Boehm, A. B.; Sassoubre, L. M. *Enterococci as indicators of environmental fecal contamination*; Massachusetts Eye and Ear Infirmary: Boston, 2014.
(14) Gorbach, S. L. *Microbiology of the Gastrointestinal Tract.*, 4 ed.: Galveston (TX): University of Texas Medical Branch at Galveston, 1996, p Chapter 95.
(15) FSMA Final Rule on Produce Safety: Standards for the Growing, Harvesting, Packing, and Holding of Produce for Human Consumption, Food and Drug Administration, FDA, **2015**.
(16) Newell, D. G.; Koopmans, M.; Verhoef, L.; Duizer, E.; Aidara-Kane, A.; Sprong, H.; Opsteegh, M.; Langelaar, M.; Threfall, J.; Scheutz, F.; van der Giessen, J.; Kruse, H. *Int. J. Food Microbiol.* **2010**, *139*, S3-S15.
(17) Scallan, E.; Hoekstra, R. M.; Angulo, F. J.; Tauxe, R. V.; Widdowson, M. A.; Roy, S. L.; Jones, J. L.; Griffin, P. M. *Emerg. Infect. Dis.* **2011**, *17*, 7-15.
(18) Glisson, J. R. *Poult. Sci.* **1998**, *77*, 1139-1142.
(19) Narvaez-Bravo, C.; Rodas-Gonzalez, A.; Fuenmayor, Y.; Flores-Rondon, C.; Carruyo, G.; Moreno, M.; Perozo-Mena, A.; Hoet, A. E. *Int. J. Food Microbiol.* **2013**, *166*, 226-230.
(20) Renter, D. G.; Gnad, D. P.; Sargeant, J. M.; Hygnstrom, S. E. *J. Wildl. Dis.* **2006**, *42*, 699-703.
(21) Dione, M. M.; Ieven, M.; Garin, B.; Marcotty, T.; Geerts, S. *J. Food Prot.* **2009**, *72*, 2423-2427.

(22) Singer, R. S.; Cooke, C. L.; Maddox, C. W.; Isaacson, R. E.; Wallace, R. L. *J. Vet. Diagn. Invest.* **2006**, *18*, 319-325.
(23) Lazcka, O.; Campo, F. J. D.; Muñoz, F. X. *Biosens. Bioelectron.* **2007**, *22*, 1205-1217.
(24) Wang, Y.; Salazar, J. K. *Compr. Rev. Food Sci. Food Saf.* **2016**, *15*, 183-205.
(25) Banada, P. P.; Bhunia, A. K. In *Principles of Bacterial Detection: Biosensors, Recognition Receptors and Microsystems*, Zourob, M.; Elwary, S.; Turner, A., Eds.; Springer New York: New York, NY, 2008, pp 567-602.
(26) Gonzalez, R. A.; Noble, R. T. *Water Res.* **2014**, *48*, 296-305.
(27) Rhoads, D. D.; Wolcott, R. D.; Sun, Y.; Dowd, S. E. *Int. J. Mol. Sci.* **2012**, *13*, 2535-2550.
(28) Cate, D. M.; Adkins, J. A.; Mettakoonpitak, J.; Henry, C. S. *Anal.Chem.* **2015**, *87*, 19-41.
(29) Yetisen, A. K.; Akram, M. S.; Lowe, C. R. *Lab Chip* **2013**, *13*, 2210.
(30) Mettakoonpitak, J.; Boehle, K.; Nantaphol, S.; Teengam, P.; Adkins, J. A.; Srisa-Art, M.; Henry, C. S. *Electroanalysis* **2016**, *28*, 1420-1436.
(31) Yang, Y. Y.; Noviana, E.; Nguyen, M. P.; Geiss, B. J.; Dandy, D. S.; Henry, C. S. *Anal. Chem.* **2017**, *89*, 71-91.
(32) Li, C.-z.; Vandenberg, K.; Prabhulkar, S.; Zhu, X.; Schneper, L.; Methee, K.; Rosser, C. J.; Almeide, E. *Biosens. Bioelectron.* **2011**, *26*, 4342-4348.
(33) Wang, Y.; Ping, J.; Ye, Z.; Wu, J.; Ying, Y. *Biosens. Bioelectron.* **2013**, *49*, 492-498.
(34) Hossain, S. M. Z.; Ozimok, C.; Sicard, C.; Aguirre, S. D.; Ali, M. M.; Li, Y. F.; Brennan, J. D. *Anal. Bioanal. Chem.* **2012**, *403*, 1567-1576.
(35) Jokerst, J. C.; Adkins, J. A.; Bisha, B.; Mentele, M. M.; Goodridge, L. D.; Henry, C. S. *Anal. Chem.* **2012**, *84*, 2900-2907.
(36) Adkins, J. A.; Boehle, K.; Friend, C.; Chamberlain, B.; Bisha, B.; Henry, C. S. *Anal. Chem.* **2017**, *89*, 3613-3621.
(37) Hossain, S. M.; Ozimok, C.; Sicard, C.; Aguirre, S. D.; Ali, M. M.; Li, Y.; Brennan, J. D. *Anal. Bioanal. Chem.* **2012**, *403*, 1567-1576.
(38) Wang, Y.; Ping, J.; Ye, Z.; Wu, J.; Ying, Y. *Biosens. Bioelectron.* **2013**, *49*, 492-498.
(39) Park, T. S.; Li, W.; McCracken, K. E.; Yoon, J.-Y. *Lab Chip* **2013**, *13*, 4832-4840.
(40) Bisha, B.; Adkins, J. A.; Jokerst, J. C.; Chandler, J. C.; Perez-Mendez, A.; Coleman, S. M.; Sbodio, A. O.; Suslow, T. V.; Danyluk, M. D.; Henry, C. S.; Goodridge, L. D. *J. Vis. Exp.* **2014**, *88*, e51414.
(41) Jokerst, J. C.; Adkins, J. A.; Bisha, B.; Mentele, M. M.; Goodridge, L. D.; Henry, C. S. *Anal. Chem.* **2012**, *84*, 2900-2907.
(42) Olsvik, O.; Popovic, T.; Skjerve, E.; Cudjoe, K. S.; Hornes, E.; Ugelstad, J.; Uhlen, M. *Clin. Microbiol. Rev.* **1994**, *7*, 43-54.
(43) Cohen, S. J.; Punt, C. J.; Iannotti, N.; Saidman, B. H.; Sabbath, K. D.; Gabrail, N. Y.; Picus, J.; Morse, M.; Mitchell, E.; Miller, M. C.; Doyle, G. V.; Tissing, H.; Terstappen, L. W.; Meropol, N. J. *J. Clin. Oncol.* **2008**, *26*, 3213-3221.
(44) Brandao, D.; Liebana, S.; Campoy, S.; Alegret, S.; Isabel Pividori, M. *Talanta* **2015**, *143*, 198-204.
(45) Skjerve, E.; Rorvik, L. M.; Olsvik, O. *Appl. Environ. Microbiol.* **1990**, *56*, 3478-3481.

(46) Skjerve, E.; Olsvik, O. *Int. J. Food Microbiol.* **1991**, *14*, 11-18.
(47) Chapman, P. A.; Wright, D. J.; Siddons, C. A. *J. Med. Microbiol.* **1994**, *40*, 424-427.
(48) Hyun, K.-A.; Kim, J.; Gwak, H.; Jung, H.-I. *Analyst* **2016**, *141*, 382-392.
(49) Bakkali Kassimi, L.; Gonzague, M.; Boutrouille, A.; Cruciere, C. *J. Virol. Methods* **2002**, *101*, 197-206.
(50) Monceyron, C.; Grinde, B. *J. Virol. Methods* **1994**, *46*, 157-166.
(51) Park, Y.; Cho, Y. H.; Jee, Y.; Ko, G. *Appl. Environ. Microbiol.* **2008**, *74*, 4226-4230.
(52) Tryland, I.; Fiksdal, L. *Appl. Environ. Microbiol.* **1998**, *64*, 1018-1023.
(53) Cate, D. M.; Dungchai, W.; Cunningham, J. C.; Volckens, J.; Henry, C. S. *Lab Chip* **2013**, *13*, 2397-2404.
(54) Arun, R. K.; Halder, S.; Chanda, N.; Chakraborty, S. *Lab Chip* **2014**, *14*, 1661-1664.
(55) Christodouleas, D. C.; Nemiroski, A.; Kumar, A. A.; Whitesides, G. M. *Anal. Chem.* **2015**, *87*, 9170-9178.
(56) Bisha, B.; Adkins, J. A.; Jokerst, J. C.; Chandler, J. C.; Perez-Mendez, A.; Coleman, S. M.; Sbodio, A. O.; Suslow, T. V.; Danyluk, M. D.; Henry, C. S.; Goodridge, L. D. *J. Vis. Exp.* **2014**, 88, e51414.
(57) Mentele, M. M.; Cunningham, J.; Koehler, K.; Volckens, J.; Henry, C. S. *Anal. Chem.* **2012**, *84*, 4474-4480.
(58) Santhiago, M.; Henry, C. S.; Kubota, L. T. *Electrochim. Acta* **2014**, *130*, 771-777.
(59) Murdock, R. C.; Shen, L.; Griffin, D. K.; Kelley-Loughnane, N.; Papautsky, I.; Hagen, J. A. *Anal. Chem.* **2013**, *85*, 11634-11642.
(60) Gerhart, J. C.; Pardee, A. B. *J. Biol. Chem.* **1962**, *237*, 891-896.
(61) Reed, M. C.; Lieb, A.; Nijhout, H. F. *Bioessays* **2010**, *32*, 422-429.
(62) Sabbah, R.; Gouali, M. *Aust. J. Chem.* **1994**, *47*, 1651-1660.
(63) Willford, J. D.; Bisha, B.; Bolenbaugh, K. E.; Goodridge, L. D. *Bacteriophage* **2011**, *1*, 101-110.
(64) Jokerst, J. C.; Adkins, J. A.; Bisha, B.; Mentele, M. M.; Goodridge, L. D.; Henry, C. S. *Anal. Chem.* **2012**.
(65) Hibbing, M. E.; Fuqua, C.; Parsek, M. R.; Peterson, S. B. *Nat. Rev. Microbiol.* **2010**, *8*, 15-25.
(66) Assessing Microbial Safety of Drinking Water Improving Approaches and Methods: Improving Approaches and Methods, World Health Organization, **2003**.
(67) Foddai, A.; Elliott, C. T.; Grant, I. R. *Appl. Environ. Microbiol.* **2010**, *76*, 7550-7558.
(68) Devanaboyina, S. C.; Lynch, S. M.; Ober, R. J.; Ram, S.; Kim, D.; Puig-Canto, A.; Breen, S.; Kasturirangan, S.; Fowler, S.; Peng, L.; Zhong, H. H.; Jermutus, L.; Wu, H.; Webster, C.; Ward, E. S.; Gao, C. S. *Mabs* **2013**, *5*, 851-859.
(69) Ceballos, L. S.; Morales, E. R.; Adarve, G. T.; Castro, J. D.; Martinez, L. P.; Sampelayo, M. R. S. *J. Food Compos. Anal.* **2009**, *22*, 322-329.

CHAPTER 3. UTILIZING PAPER-BASED DEVICES FOR β-LACTAM RESISTANT BACTERIA DETECTION

Antimicrobial resistance (AMR), the ability of a bacterial species to resist the action of an antimicrobial drug, has been on the rise due to the widespread use of antimicrobial agents. Per the World Health Organization, AMR has a current estimated annual cost of $21B to $34B in the United States alone, and is predicted to be the number one cause of death worldwide by 2050. One of the many ways AMR bacteria can spread, and where individuals can contract AMR bacterial infections, is through contaminated water sources. Monitoring AMR bacteria in the environment currently requires samples to be transported off-site to a central laboratory for slow, relatively expensive, and labor-intensive tests. We have developed an inexpensive, fast assay using a paper-based analytical device (PAD) that can test for the presence of β-lactamase-mediated resistance as one major form of AMR. To demonstrate viability, the device reliably and rapidly detected β-lactam resistance in sewage and wastewater samples and identified resistance in individual bacteria species isolated from environmental samples.

This work was accepted for publication in Angewandte Chemie.[1]

Introduction

The introduction of antimicrobial agents in the early 20th century revolutionized medicine, significantly decreasing morbidity and mortality. However, due to the widespread use of antimicrobial agents and the genetic plasticity of bacteria, more

pathogens have developed the ability to resist these drugs, giving rise to antimicrobial resistant (AMR) bacteria.[2] According to the World Health Organization (WHO), AMR is responsible for around 8 million hospital days, and costs approximately $21B to $34B annually within the United States alone. Additionally, AMR infections are predicted to surpass heart disease as the number one cause of death worldwide by 2050.[3] Contaminated water is a significant source of infection and outlet for the spread of AMR bacteria. AMR propagation in water is further advanced through contamination by antimicrobial agents, which results in the selective proliferation of AMR bacteria, and the horizontal gene transfer of resistance from AMR bacteria to non-AMR bacteria.[4] Due to its significant role, many bodies of water have also been studied for the presence of AMR bacteria including urban wastewater,[5] irrigation water,[6] and drinking water in China,[7] to name a few.[8]

The gold standard for detecting AMR bacteria is through antimicrobial susceptibility testing. This is a broad family of tests that include broth dilution, antimicrobial gradients, disk diffusion, and automated systems.[9] While these methods provide reliable results, they also require samples to be sent to a central laboratory to complete testing. In addition to transportation time, these methods require at least overnight (12-16 hr) incubation and trained laboratory personnel to execute the procedure and analyze results.[9]

Alternative methods for detecting AMR bacteria have also been developed. Card et al. introduced the use of expanded microarrays for accurately and simultaneously testing gram-negative bacteria against 75 different antibiotics.[10] Although this method tests for a breadth of antibiotic susceptibility, it requires an extensive procedure,

including overnight culturing, cell lysing, and DNA extraction, which increases both detection time and expense. Microfluidic devices fabricated with poly-dimethysiloxane (PDMS) have also been developed for determining the minimum inhibitory concentration (MIC) of different antibiotics against a specific bacteria strain.[11] Among these PDMS devices, Choi et al developed an assay that is capable of determining MIC using a single bacterium within 3-4 hr.[12] While this is a promising system, it required constant monitoring via a microscope, necessitating the use of a laboratory and trained personnel, and as a result, makes it more suitable for clinical settings. Similar to traditional disk diffusion methods, Deiss et al published a paper-based portable culture device specifically designed for in-field diagnostics.[13] Using similar concepts to antibiotic susceptibility testing, the device requires an autoclave for sterilization and 18 hr of incubation in a 37 °C incubator. While this method uses paper over conventional materials, which decreases costs, reagent consumption, and waste generation, it still requires the use of additional instrumentation and lengthy analysis time. To monitor AMR bacteria in the field and diagnose AMR infections at the point-of-care, a rapid, disposable, and inexpensive device that does not require instrumentation or trained laboratory personnel for analysis is still needed.

Paper-based analytical devices (PADs) have shown significant promise as an alternative platform for performing diagnostics, having grown in popularity with over 1000 papers published since 2007.[14,15] PADs have been developed for a variety of applications, including point-of-care (POC) diagnostics and environmental monitoring. Because AMR displays current and emerging concerns for both developed and developing countries, the WHO specifically mentions in their *Global Action Plan for*

Antimicrobial Resistance that these diagnostic tools should be portable and inexpensive.[16] PADs offer a cost effective platform for global use because the starting substrate materials are inexpensive (often less than $0.01US), the manufacturing techniques rely largely on everyday office equipment, and the reagents (the most expensive part) are deposited in small amounts (µg-ng).[17] Additionally, PADs are easy to transport due to their small size, simple to manufacture, and easy to dispose. Many diagnostic motifs have been developed for PADs, yet few have been developed to detect naturally-produced enzymes. Our group previously published two papers utilizing colorimetric assays to detect different bacteria from food and water sources based on the enzymes they produce.[18,19] This same detection motif can be used to detect different forms of AMR, as some of these antimicrobial properties can be traced back to bacterial enzymes responsible for deactivating antibiotics.[20,21]

β-lactam antibiotics are the most widely used class of antibiotics, however, bacterial resistance to these antibiotics are also the most commonly acquired resistance and is classified as a serious threat by the CDC.[22] Resistance is a result of bacterial expression of β-lactamase enzymes,[23,24] which inactivates penicillins by hydrolyzing the β-lactam ring in the antibiotic, rendering it useless in controlling infection.[21] β-lactamase production has been studied in many species of bacteria, including, but not limited to *Salmonella enterica*,[25] *Myobacterium tuberculosis*,[26] *Klebsiella pneumoniae*, and *Escherichia coli*.[27] There are several ways to detect β-lactamase activity,[28] but the most user-friendly and sensitive way is to react a bacterial solution with nitrocefin, a chromogenic cephalosporin.[29] The reaction results in the hydrolysis of the carbon-nitrogen bond in the β-lactam ring, as seen in antibiotic inactivation, causing a distinct

color change from yellow to red (Scheme 3.1). Using this straight-forward detection method, we have developed a paper-based test that can detect β-lactamase-expressing bacteria in real-world samples as demonstrated by the successful analysis of urban sewage water, as well as β-lactam-resistant bacteria from various species isolated from environmental samples. The platform is inexpensive, costing ~$0.20US per test, compared to $10-22US for antibiotic susceptibility testing.[9]

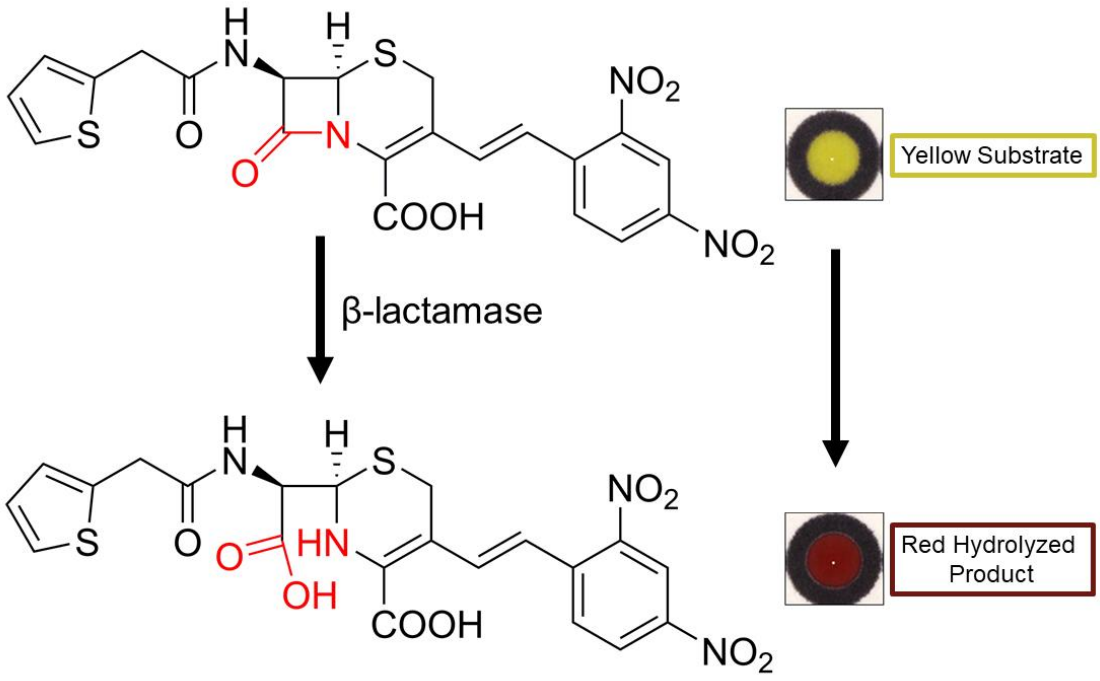

Scheme 3.1 | Reaction overview of β-lactamase and nitrocefin. Hydrolysis of the β-lactam ring in nitrocefin, mediated by β-lactamase, results in a distinct color change from yellow to red, making a visually detectable and user-friendly test.

Materials and Methods

Device Fabrication and Data Analysis. The devices were fabricated with Whatman chromatography paper grade 4 [GE Healthcare Life Sciences], using a simple design of black circles on a 7 by 12 grid designed with CorelDraw X4. Whatman 4 was

selected based on separate enzyme kinetics experiments. It was determined in this separate project that Whatman 4, due to its larger pores, therefore less surface area, has less nonspecific adsorption, results in a higher colorimetric signal. Each device circle was designed with a 4 pt line and measured 8 x 8 mm. To define the device's hydrophobic barriers, a ColorQube 8870 [Xerox] wax printer was used to dispense wax on the surface. An IsoTemp [Fisher Scientific] hot plate was set to 150 °C with two metal plates and wax-printed paper was placed between the hot plate and a metal plate for 1 min to allow wax to melt through the pores. Scotch Shipping Heavy Duty packing tape was then taped on the back of the paper to prevent sample leakage (Figure 3.1).

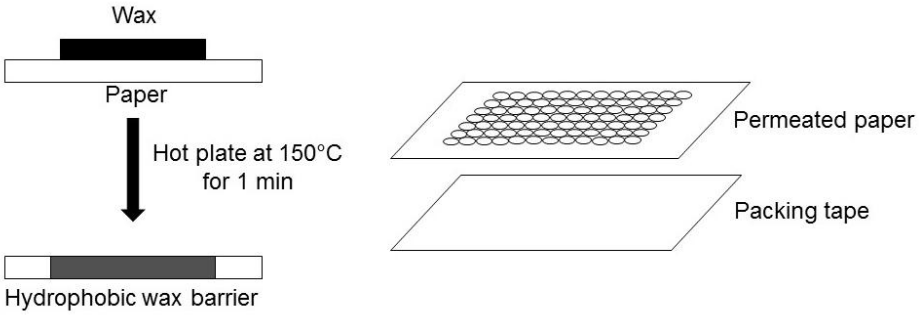

Figure 3.1 | Devices were developed by printing wax on Whatman chromatography grade 4 paper, then heated on a hot plate to melt the wax through the pores, creating a defined hydrophobic barrier. The back of the device sheet was then covered in packing tape to prevent sample leakage.

To make devices with nitrocefin dried into the paper before reaction, 5 µL of nitrocefin solution was dried into the chromatography paper before taping the back with packing tape. Devices were dried at 4 °C because it was determined that drying at lower temperatures away from light resulted in more efficient reactions with samples.
For quantifying colorimetric products, a "light box" and the camera of an iPhone 5C or 5S were used to capture images and send to computer for image analysis (Figure 3.2).

The resolution on an iPhone 5C and 5S are reported to be 8 megapixels with a resolution of 3264 x 2448. Using this method, we could obtain kinetic results as opposed to simply endpoint results that would be obtained using an office scanner.[30] Pictures were taken within the box (measured 16 x 16 x 16 cm) designed to encompass the entire paper analytic device and to limit any outside light. To capture the image, a slit measured 2 x 5 cm was cut out of the top to allow a view inside the box for the camera phone and flash. The box interior was lined with standard white copy paper to best disperse light from the camera's flash. For each experiment, three samples of each reaction were placed in every other column of circles. Water was placed in the columns on each side of the samples to act as a "light control." Due to the imperfect flash intensity across the paper, the light controls were used to normalize the intensity of each sample spot to give more precise results.

Images were sent to a computer and analyzed using NIH ImageJ software. The image was split into its color channels and the green color channel was selected and inverted. The green channel was selected because it is the complimentary color of red, the reaction's endpoint color. The color intensity of each sample spot was quantified, then normalized by subtracting the mean intensity of the water spots on each side of the sample spot. Normalized values were input into Microsoft Excel where the mean and standard deviation of samples were obtained. Standard deviation was represented in statistical graphs as error bars.

Characterization of β-lactamase and nitrocefin reaction. Nitrocefin [VWR International], a chromogenic cephalosporin, was used for detection of β-lactamase because of the distinct color change from yellow to red in the presence of the enzyme,

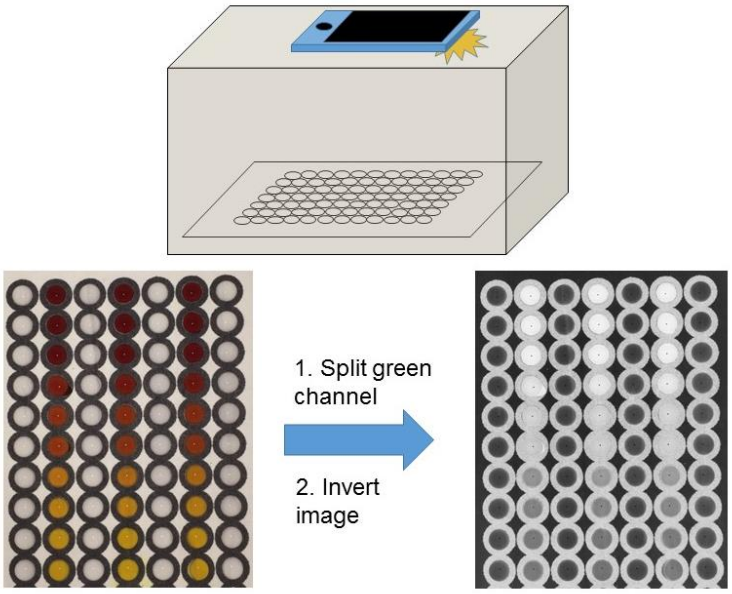

Figure 3.2 | Devices were imaged using a cardboard box lined with copy paper and a hole on the top that allows for a camera to view and image the devices. These images were then wirelessly sent to a computer to analyze using ImageJ software.

making it a user-friendly platform. 5 mg of nitrocefin was initially dissolved in 1 mL dimethylsulfoxide (DMSO), because the substrate is insoluble in water. Aliquots of 9.68 mM nitrocefin was frozen at -20 °C in amber microcentrifuge tubes [VWR International]. These tubes were used to minimize degradation from UV exposure. Aliquots were taken out and allowed to thaw and warm to room temperature. Nitrocefin was further diluted with pH 7.4 phosphate buffered saline (PBS) [1.37 M NaCl, 0.027 M of KCl, 0.1 M Na_2HPO_4, and 0.018 M KH_2PO_4] to a concentration of 0.5 mM for each experiment (except for nitrocefin concentration optimization where 0.5 mM was selected). During pH optimization experiments, nitrocefin was diluted in pH buffers ranging from pH 6 to pH 9. Recombinant β-lactamase was purchased at a concentration of 1,500 U/mg [Abcam] and was initially dissolved in dH_2O and aliquoted and frozen. It was diluted with PBS before optimization experiments. For each reaction, 20 µL of nitrocefin would react

with 20 µL of β-lactamase. Images were obtained at 2 hr, to ensure reaction completion. For determining the limit of detection of β-lactamase, the image was taken at 4 hr.

β-lactamase kinetics. To quantify the concentration of nitrocefin that was hydrolyzed every minute, a calibration curve was generated by quantifying the red product after the reaction had completed, and plotting green light intensity *vs*. product concentration. The linear regression equation of this line was used to calculate the product concentration in the solution at each time point. The slope of the line of red intensity between 3 and 5 min was used to calculate the reaction rate. Eight different concentrations of nitrocefin was used to obtain a kinetic curve (0.1, 0.2, 0.3, 0.4, 0.5, 0.6, and 0.7 mM). To obtain V_{max} and K_m, a Lineweaver-Burk plot was generated by plotting 1/[S] *vs.* 1/v and the inverse x- and y-intercepts were obtained. The calculated V_{max} and K_m values were carried out in the Michaelis-Menten equation to obtain a theoretical kinetic curve to compare to data points.

Live Bacteria Detection. DH5α *E. coli* cells [New England Biolabs] were used for both control and experimental bacteria in initial laboratory bacterial analysis. The control *E. coli* did not express β-lactamase, while the experimental bacteria expressed a previously published plasmid, pBG143, which encodes β-lactamase.[31] The pBG143 plasmid was transformed into DH5α cells and the bacteria were incubated in Luria broth (LB) media containing 50 µg/mL ampicillin to select bacteria exclusively expressing β-lactamase. For subsequent experiments, bacteria were cultured in LB media overnight (~12-16 hr) before each experiment. To determine our limit of detection, bacteria concentration was calculated using serial dilution and plating 50 µL of 10^{-6} and 10^{-7} dilutions on LB Agar plates containing no antibiotics and allowed to grow for 24 hr. The

colonies were counted on each plate, calculated back to the original concentration, and the average was taken to obtain an estimate of the original bacteria concentration. To determine whether cell lysis was necessary for β-lactamase detection, the cells were sonicated for 20 sec using a XL-2000 Series probe sonicator set at 5 W, 22 kHz. The sonication settings and time was selected due to previously published data on sonicating *E. coli* cells.[18] Similar to optimizing the reaction with pure enzyme, 20 µL of bacterial culture was reacted with 20 µL of 0.5 mM nitrocefin and images were obtained after 2 hr of reaction. For all experiments involving bacteria, devices were placed in a petri dish to help prevent outside contamination and evaporation during the reaction time.

To detect bacteria using UV-vis spectrophotometry, a PerkinElmer Victor X5 multilabel plate reader was used to measure the change in absorbance in a microtiter plate. 100 µL of nitrocefin was mixed with 100 µL of bacteria sample and allowed to react for 2 hr when the absorbance was taken at 490 nm. The microtiter plate was covered with a plate lid to prevent evaporation during reaction.

Detecting β-lactamase in Sewage Samples. Waste water samples were collected from the Drake Water Reclamation Facility located in Fort Collins, Colorado, United States [Collected on 09/07/2016 at approximately 10 a.m.]. Influent samples were collected using a Hawk Composite Sampler, and effluent samples were collected as a grab sample post SO_2 treatment. After collection, influent and effluent samples were put directly on ice away from light for transportation back to the laboratory. 1 mL of sample was mixed with 3 mL of LB media and incubated in a 37 °C shaker. Three samples were taken of each the influent and effluent. Sample solution was taken out of

the incubator every 2 hr to test for the presence of β-lactamase activity by reacting 20 µL of sample with 20 µL of 0.5 mM nitrocefin for 2 hr, when a picture would be obtained and analyzed. 0 hr samples were not mixed with media, but were reacted directly with nitrocefin.

Results were confirmed by membrane [0.45µm mixed cellulose esters millipore membrane, MilliporeSigma™] filtration techniques on Orientation plates and extended-spectrum-β-lactamase (ESBL) selecting plates [CHROMagar™]. Influent sewage samples were diluted through 10-fold dilutions, and the 10^{-6}, 10^{-5}, and 10^{-4} dilutions were plated on ESBL and Orientation plates and allowed to grow at 37 °C for 24 hr. The colony forming units were counted and calculated to CFUs/100 mL. Relative percentage of resistant bacteria was calculated with Orientation (non-selective) as the denominator and ESBL (selective) as the numerator from the same source.

Obtaining and Testing Bacterial Isolates from Sewage and Environmental Samples. Bacterial isolates were obtained from grab samples in the field, except for influent. Field samples include influent, effluent, surface water from a river and sewage samples from city sewers. All samples were plated by pipetting 50-100 µL on various clinical agars [CHROMagar™ Orientation, CHROMagar™ ESBL, and CHROMagar™ KPC]. Bacterial isolates were purified by selecting a single colony with an inoculating loop and spreading the colony on the same kind of agar the colony was selected from, or was spread onto a MacConkey agar plate [Difco]. To remove potential inhibitors before any testing, they were further subcultured onto non selective agar [Tryptic Soy Agar, Thermo Scientific™ Remel™] and then grown in a nutrient broth [Tryptic Soy Broth, Thermo Scientific™ Remel™, Soybean Casein Digest] at 37 °C and 2% CO_2.

After replenishing the nutrient broth, all bacterial isolates were grown using a shaker for 12-18 hr depending on bacteria growth rate. They were also re-plated on ESBL plates to confirm resistance mechanisms. The isolates were given to the tester blind for accurate, unbiased results. Bacteria were not lysed before reacting 20 µL of bacteria solution with 20 µL of 0.5 mM nitrocefin. Images were obtained after 2 hr of reaction.

Matrix-assisted laser desorption ionization time of flight mass spectrophotometry (MALDI-TOF) was used for speciation of isolates. Isolated bacterial cultures purified from selective media were sent to the Colorado State University Veterinary Teaching Hospital-Diagnostic Medical Center (Vet-DMC) to be analyzed. These samples were grown on blood agar plates and analyzed to identify species [VITEK-MS™ *Biomerieux*, USA]. Samples that could not be confidently identified at 99.9% or above by MALDI-TOF analysis were identified by 16-S-PCR of the variable 4 region.

To determine antibiotic susceptibility of *Chromobacterium violaceum* and the 32 *E. coli* isolates, each isolate was subjected to antibiotic susceptibility testing [VITEK 2™ *Biomerieux*, USA] using microdilution and photometric determination of growth at the Colorado State University Veterinary Diagnostic Laboratory located in Fort Collins, CO, US. Minimum Inhibitory Concentration's (MICs) were reported in µg/mL, and results were interpreted per the Clinical Laboratory Standard Institute (CLSI). The antibiotics that were tested against *C. violaceum* included amikacin, amoxicillin-clavulanate, ampicillin, cefazolin, cefpodoxime, ceftazidime, cephalothin, imipenem, ticarcillin, and ticarcillin-clavulanate. Antibiotics tested against each *E. coli* isolate included amoxicillin, ampicillin, cefalexin, cefovecin, cefpodoxime, ceftiofur, piperacillin, ceftazidime, cefotaxime, and imipenem.

Polymerase chain reaction (PCR) was also performed by the Colorado State University Veterinary Diagnostic Laboratory. These diagnostic tests were used to determine whether the bacterial isolates' genome contained ESBL genes blaTEM and/or blaCTX-M. PCR was performed using the diagnostic lab's standard procedure as follows. The following are the primer sequences used for the amplification of the isolated DNA[32]: CTX-M (F: ATG TGC AGY ACC AGT AAR GTK ATG GC, R: TGG GTR AAR TAR GTS ACC AGA AYC AGC GG, 593 bp) and TEM (F: CGC CGC ATA CAC TAT TCT CAG AAT GA, R: ACG CTC ACC GGC TCC AGA TTT AT, 445 bp). 32 *E. coli* isolates from ChromAgar™ ESBL and ChromAgar™ Orientation were lysed in 100 µL of water per sample at 100 °C for 1 hr using BIO-RAD T100™ Thermocycler [Bio-Rad Laboratories, Inc, California]. Amplification was carried out by 2 µL DNA, 10 pmol of each primer, and 12.5 µl Emerald Amp® GT PCR Master Mix [Takara Bio Inc., Clontech, Japan] under conditions described by Amaya 2011.[33] The PCR conditions were as followed: 15 minutes of denaturation at 95 °C (1 cycle), 30 seconds of denaturation at 94°C, 90 seconds of annealing at 62 °C, and 1 minute of polymeration at 72 °C (34 cycles), with a final extension at 72 °C for 10 minutes. PCR products were analyzed on a 1.5% agarose gel [BioRad] and visualized using Ethidium Bromide (item). Single reaction PCR confirmed the presence or absence of each gene.

Results and Discussion

Optimizing β-lactamase Detection. Reaction optimization was performed using arrays of 8-mm-diameter paper wells fabricated with Whatman #4 chromatography paper. In all studies, assays were kept at room temperature (~22 °C) to best mimic field

conditions. The devices were photographed, then analyzed with NIH ImageJ software. To determine the optimal assay pH, β-lactamase and nitrocefin were reacted in phosphate buffered saline (PBS) solutions between pH 6 and pH 9 (Figure 3.3A). PBS pH 6.0 and 7.5 displayed the highest reaction efficiency. Why there was a dip reaction efficiency between pH 6 and 7.5 is unknown. Future trials were performed at pH 7.4 (pH 7.0 for enzyme limit-of-detection) to best mimic blood pH for possible point-of-care diagnostic applications.

Optimal substrate concentration was determined using a constant concentration of β-lactamase (100 U/mL for prompt results) incubated with varying concentrations of nitrocefin. 1 mM nitrocefin provided the highest final color intensity, whereas 0.25 to 0.5 mM nitrocefin produced the largest color intensity change of 85-83% compared to a 64% intensity change observed with 1 mM nitrocefin (Figure 3.3B). Using nitrocefin at a concentration above 1 mM results in a very dark starting sample solution, making changes in the reaction color difficult to measure. Hence, lower concentrations of nitrocefin are optimal for generating the widest dynamic range for detection of β-lactamase.

To find the limit of β-lactamase enzyme detection, the minimum concentration of β-lactamase present that could react with nitrocefin to give a measurable color change was established. 0.5 mM nitrocefin was reacted with decreasing concentrations of recombinant β-lactamase for 4 hr and imaged. The enzyme showed little difference in light intensity at lower concentrations (Figure 3.3C). Any concentration of β-lactamase lower than 10 mU mL^{-1}, does not show enough color intensity to be detected accurately. The optimal nitrocefin concentration to dry into the paper was determined by drying 5 µL

of different concentrations of nitrocefin on chromatography paper and observing the change in color intensity before and after adding 1 U/mL of β-lactamase for 30 min. Similar to nitrocefin in solution, too high of concentrations of nitrocefin resulted in too dark of a starting spot, thus 1 mM was determined to be the optimal concentration to dry on paper with a color intensity change of 71% (Figure 3.3D).

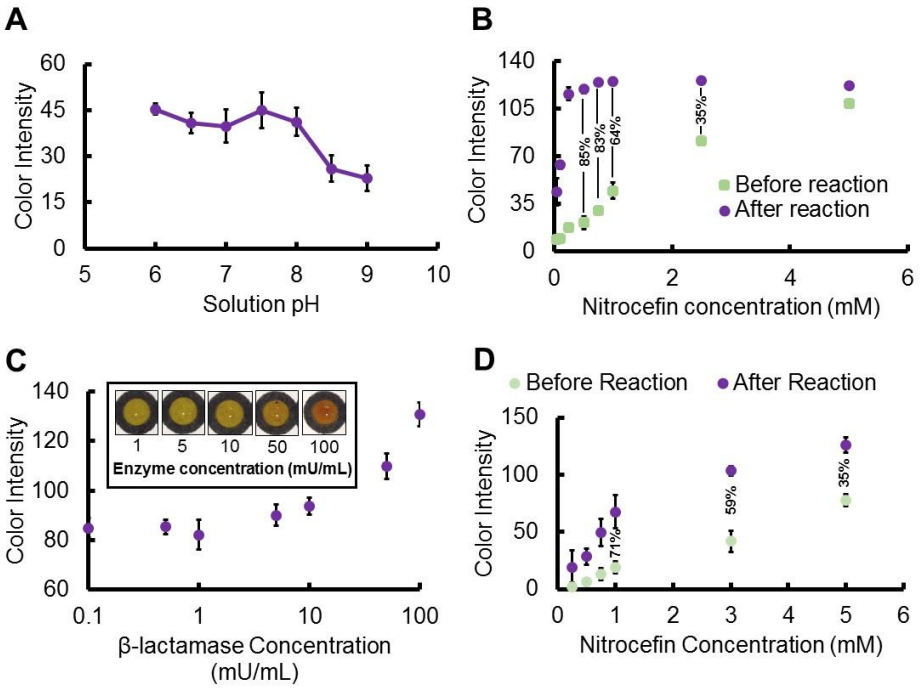

Figure 3.3 | Nitrocefin and β-lactamase reaction optimization on paper. **(A)** β-lactamase enzyme was reacted with nitrocefin using different pH buffers to determine the optimal reaction pH. **(B)** Optimal nitrocefin concentration was determined using change in signal from starting color intensity of nitrocefin alone (before reaction) and increase in color intensity (after reaction). **(C)** Determining the β-lactamase enzyme LOD. **(D)** Optimal nitrocefin concentration to dry in paper. Error bars denote s.d. where n = 3.

The Michaelis-Menten kinetics of β-lactamase and nitrocefin were calculated for reactions on paper at ~22 °C. Using a Lineweaver-Burk plot, the calculated V_{max} was 0.0285 ± 0.0012 mM/min and K_m was 0.293 ± 0.013 mM (Figure 3.4). Literature searches have not generated published Michaelis-Menten values for β-lactamase

reacting with nitrocefin, but were similar to other reported values for β-lactamase.[34] This similarity in Michaelis-Menten values exhibits promise for the paper-based assays.

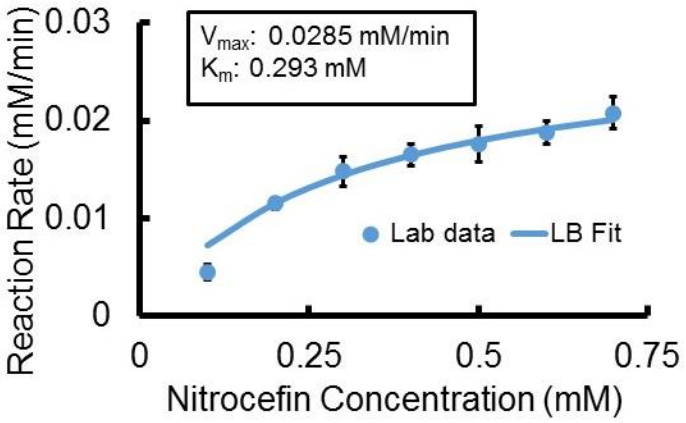

Figure 3.4 | The paper-based devices were used to determine kinetic values by reacting 1 U/mL of β-lactamase with nitrocefin between 0.1 and 0.7 mM. Error bars denote s.d. where n = 3.

Optimizing Bacteria Detection. To demonstrate detection of β-lactamase in live bacteria, the optimized reaction conditions were used to analyze *E. coli* without culturing. Serial dilutions of β-lactamase-expressing *E. coli* and control *E. coli* were reacted with 0.5 mM nitrocefin at room temperature directly on the paper devices. No color change was observed unless the bacteria expressed β-lactamase (Figure 3.5A). The color change in the assay occurred with more than 3.8×10^6 CFU/mL bacteria, but not with lower concentrations. To determine whether non-β-lactamase producing bacteria would interfere with the detection of β-lactamase-producing *E. coli*, different ratios of β-lactamase-expressing bacteria to control bacteria were analyzed. The color intensities were the same with or without non-β-lactamase producing bacteria present in the sample (Figure 3.5B). *E. coli* that do not express β-lactamase do not interfere with the reaction as similar color intensities were observed in pure or mixed cultures.

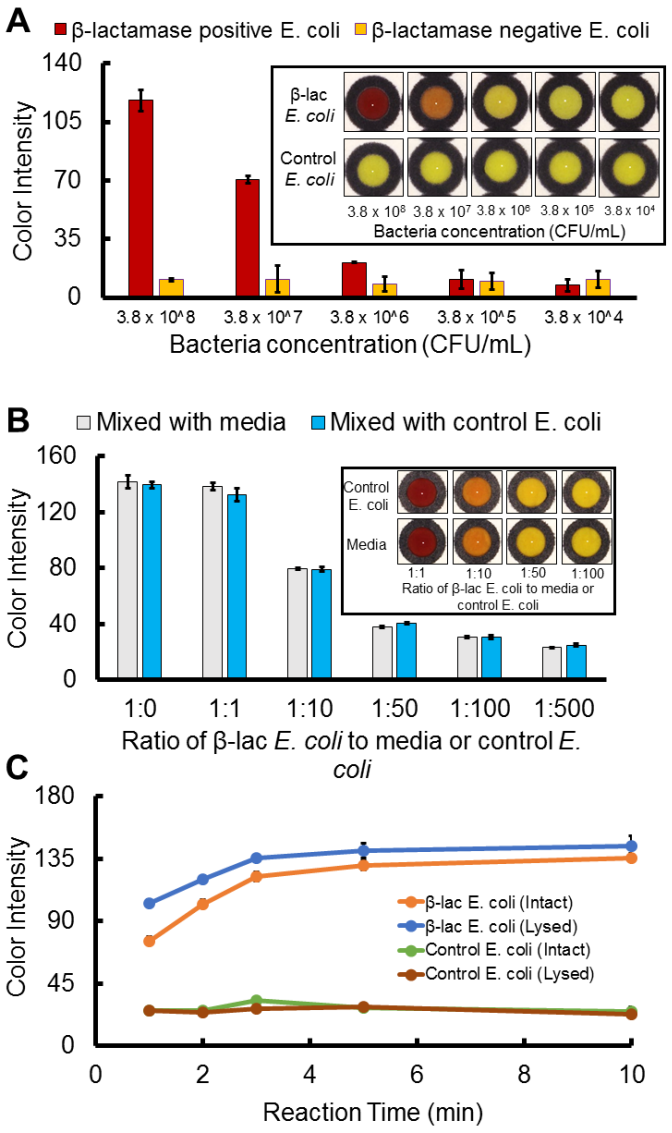

Figure 3.5 | **(A)** The paper-based tests were used for serial dilutions of bacteria that were positive and negative for β-lactamase expression. **(B)** β-lactamase-expressing bacteria were mixed with either non-β-lactamase-expressing bacteria or pure media to determine if other bacteria interfered with the reaction. **(C)** Determining if bacteria lysis would result in more sensitive detection. Error bars denote s.d. (n=3).

β-lactamase is produced within bacteria, so to attempt increasing sensitivity, we repeated the assay with lysing. For DH5α *E. coli* cells expressing β-lactamase, lysing the cells using probe sonication helped obtain a faster and more intense signal, but only marginally compared to no lysing (Figure 3.5C). After 10 min of reaction, the color

intensity of lysed cells was approximately 5% higher than intact cells. These results indicate the cells either secrete β-lactamase or nitrocefin is cell permeable. Several studies support bacteria translocating β-lactamase from the cytoplasm across the bacteria's inner membrane into the periplasm, but not outside the cell entirely, supporting the latter hypothesis.[35-37]

Because nitrocefin is a colorimetric substrate, it has been speculated whether using UV-visible spectrophotometry would result in more sensitive bacteria detection. Serial dilutions of laboratory *E. coli* expressing β-lactamase were reacted in a microtiter plate with nitrocefin and the absorbance was measured using a plate reader. Using a microtiter plate and plate reader compared to a PAD and smartphone did not yield a lower LOD (Figure 3.6A). This demonstrates that using a PAD and smartphone is a cost-effective way to detect bacteria using nitrocefin, without the need for expensive instrumentation. Because the goal of point-of-need devices is to have a final product that can be taken into the field with minimal supplies for testing, it was also investigated whether nitrocefin could be dried in the paper beforehand. It was determined that the ideal concentration to dry into paper was 5 µL of 1 mM nitrocefin as mentioned above. Adding 40 µL of bacteria sample to the PAD test with dried nitrocefin was compared to PAD tests that held 20 µL of 0.5 mM nitrocefin solution and 20 µL of bacteria sample. Drying nitrocefin onto the paper before adding the sample showed slightly more sensitive results compared to nitrocefin solution (Figure 3.6B). This is likely because nitrocefin did not need to be added to the total solution volume, therefore more sample could be added. Nitrocefin's long-term stability on paper is unknown, but will be the subject of future studies.

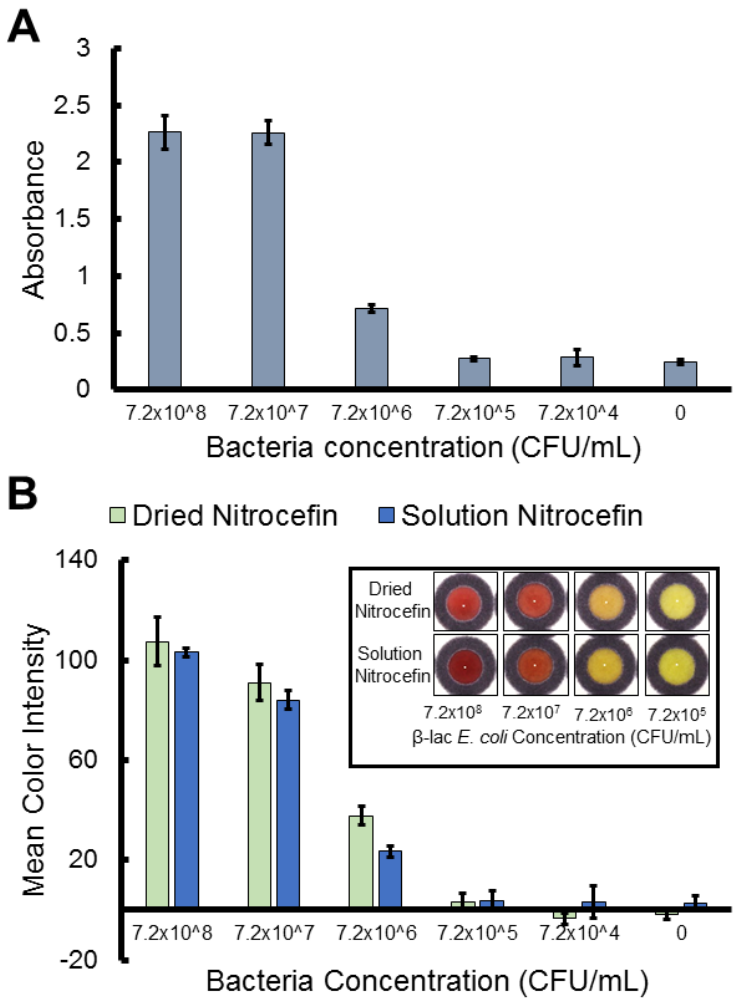

Figure 3.6 | **(A)** Detecting color change using UV/vis spectrophotometry in a plate reader yielded the same limit of detection of 106 CFUmL@1 as observed on paper. **(B)** Drying nitrocefin on paper before adding sample yielded similar or slightly more sensitive results compared to adding nitrocefin solution to the bacterial sample on paper. Error bars denote s.d. (n=3).

Detecting AMR in Sewage Samples. To confirm the new method would work with real-world samples, influent and effluent water was obtained from the Drake Water Reclamation Facility located in Fort Collins, Colorado, United States. In the influent, β-lactamase was detected after only 2 hr of sample incubation in media. The signal continually increased until reaching a maximum at ~10 hr of incubation (Figure 3.7).

Similar results could be obtained with a microtiter plate but at much higher costs. The effluent, which should contain less bacteria, did not show a signal until 8 hr of incubation. These results were confirmed using dilution and plating methods, which gave a concentration of 4.50×10^6 CFU/mL of total bacteria in the influent, and 5.08×10^3 CFU/mL of total bacteria in the effluent. AMR bacteria were confirmed using commercially available extended-spectrum-β-lactamase (ESBL) plates from CHROMagar™. On these plates, there were 4.96×10^4 CFU/mL of total ESBL-containing bacteria in the influent and 1.30×10^1 CFU/mL in the effluent. This correlates to 1.1% and 0.257% ESBL bacteria in the influent and effluent respectively. Why such a high signal was obtained in the influent sample, considering a 1:99 ratio of β-lactam-resistant bacteria to non-resistant bacteria, could be due to several factors. First, bacteria

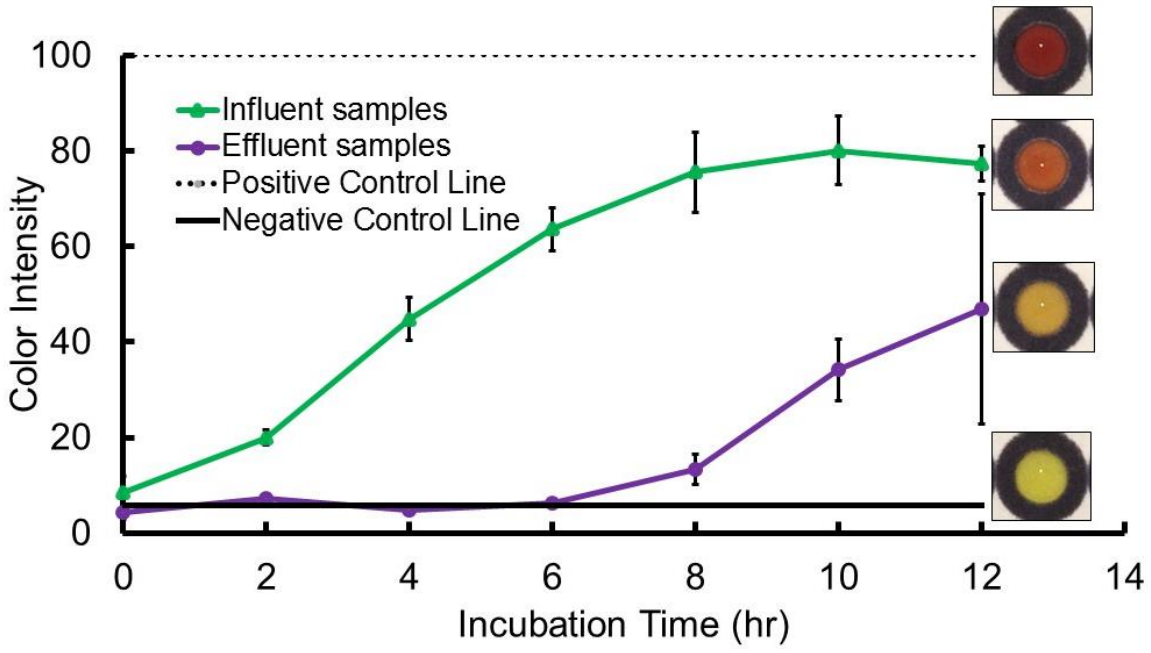

Figure 3.7 | Detecting β-lactam resistance in urban sewage water. Samples of influent and effluent water were obtained and incubated in media for 12 h. Samples were obtained every 2 h for testing and both the influent and effluent tested positive for β-lactam resistance, which was confirmed by traditional culture methods. Error bars denote s.d. (n=3).

resistant to β-lactam antibiotics could be growing at a faster rate compared to non-resistant bacteria, therefore occupying more of the sample once it was concentrated enough to detect resistance. This variance in growth rate was also observed in the effluent between samples as demonstrated by the large error bars at 12 hr. The sewage sample bacteria also had to react for over an hour with nitrocefin to obtain a detectable signal, compared to 2-5 min of reaction for samples that were entirely resistant bacteria. However, this slower reaction rate could also be due to chemicals in the sewage water interfering with the enzymatic reaction.

Identifying Resistance in Different Species. To determine how many different bacterial species were detected in the sewage samples, several bacteria species were isolated and cultured from the original sewage and other environmental samples. The bacteria cultures were given to the tester blind to ensure no biases when using the paper-based tests. Of 10 different bacteria isolates tested from a variety of species and environmental sources, there were no false positives and one false negative (Figure 3.8). Bacteria solutions were kept intact and not lysed for consistency. When using the paper-based test on intact bacteria, results indicate that the assay could also quantify resistivity for different bacteria species. The “slightly positive” paper tests corresponded to “weak positives” that were confirmed via CHROMagar™ ESBL plates. “Slightly positive” was defined as having a color intensity change of 20%-80% compared the positive control laboratory *E. coli*, and “weak positive” was defined as reduced bacteria growth on ESBL plates compared to a non-antibiotic plate.

One bacterial isolate, *Chromobacterium violaceum,* tested negative using the paper-based test but tested positive using a CHROMagar™ ESBL plate. This same

species did not grow on an ampicillin-containing agar plate, indicating that it is likely susceptible to penicillins. To confirm which test was correct, the minimum inhibitory concentration (MIC) of different β-lactam antibiotics was tested. The isolate was resistant to cephalosporins like cefazolin and cephalothin, but was susceptible to penicillins, such as amoxicillin and ticarcillin. The bacteria were also susceptible to imipenem, a carbapenem β-lactam antibiotic that is used as a last resort in clinical cases. Overall, this resistance profile is inconclusive, but similar to a previously published profile on resistance to cephalosporins, but sensitive to penicillins.[38] Why nitrocefin would not react with *C. violaceum*'s β-lactamase is unknown. Nitrocefin is defined as a chromogenic cephalosporin, so in theory should be reactive with a β-lactamase that protects the cell against cephalosporin antibiotics.

Nitrocefin Test	Bacteria Species	ESBL Status	Isolation Source	Nitrocefin Test	Bacteria Species	ESBL Status	Isolation Source
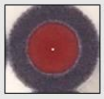	**Positive Control** *Escherichia coli*	(+)	New England Biolabs (DH5α cells)	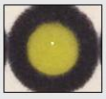	**Negative Control** *Escherichia coli*	(-)	New England Biolabs (DH5α cells)
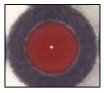	*Enterobacter (cloacae/ absurdium)*	(+)	Effluent	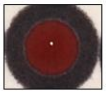	*Citrobacter werkmanii*	(+)	City Sewage
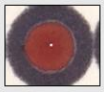	*Chryseobacterium gleum*	(+)	Effluent		*Serratia liquefaciens*	(+) (weak)	Effluent
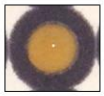	*Pseudomonas alcaligenes*	(+) (weak)	Effluent	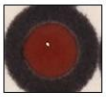	*Pseudomonas putida*	(+)	City Sewage
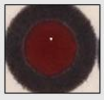	*Escherichia coli*	(+)	Influent	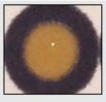	*Escherichia coli*	(+) (weak)	River Water
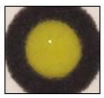	*Chromobacterium violaceum*	(+)	Influent	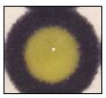	*Serratia fonticola*	(-)	River Water

Figure 3.8 | Detecting b-lactam resistance in bacterial isolates. Different bacterial species were isolated from environmental samples and tested for individual resistance using the paper-based test. There have been no false positives and one false negative (Chromobacterium violaceum isolated from the influent of urban sewage water).

While ESBL-selecting plates are a common method to determine β-lactamase expression, it is more common in medicine to subject bacteria to antibiotic susceptibility testing. To compare the PAD to this method, 32 different environmental *E. coli* isolates were subjected to antibiotic susceptibility testing of different β-lactam antibiotics as well as plating the isolates on ESBL-selecting plates. The PAD test was compared to these methods for accuracy, and no false negatives were observed (Figure 3.9). When comparing the PAD test to ESBL-selecting plates, two false positives occurred (isolate #7 and #20). However, when comparing to antibiotic susceptibility testing, these isolates were resistant to at least two penicillin antibiotics. When comparing the PAD test to antibiotic susceptibility testing, the tests were negative when the bacteria were susceptible to all tested antibiotics, and were positive when resistant to any of the tested antibiotics. As further confirmation, the *E. coli* isolates were also tested for the presence of ESBL genes blaTEM and blaCTX-M using polymerase chain reaction (PCR). Isolates #7 and #20 had the blaTEM gene present in their genome, also corresponding to the PAD results (Figure 3.9). With 42 tested isolates and one true false negative, this test has so far shown 97.6% accuracy.

Conclusions

A straightforward and accurate paper-based colorimetric assay to detect bacteria resistant to β-lactam antibiotics has been developed that costs ~$0.20 per test but gives similar sensitivity to more expensive microtiter plate methods. We have also optimized the enzymatic reaction between nitrocefin and β-lactamase on paper, and demonstrated that non-AMR bacteria do not interfere with the assay performance and cell lysis is not

E. Coli #	Source	PAD	ESBL (agar plate)	bla-TEM	bla-CTX-M	Amoxicillin	Ampicillin	Cefalexin	Cefovecin	Cefpodoxime	Ceftiofur	Piperacillin	Ceftazidime	Cefotaxime	Imipenem
1	Effluent		+	NA	NA	R	R	R	R	R	R	R	-	-	R
2	Sewage		+	+	-	R	R	-	R	-	R	-	-	-	-
3	Sewage		+	+	+	R	R	R	R	R	R	R	-	-	R
4	Sewage		+	+	+	R	R	R	R	R	R	R	-	-	R
5	Influent		+	+	-	R	R	R	R	R	R	R	-	-	R
6	Influent		+	-	-	R	R	R	R	R	R	R	-	-	R
7	Influent		-	-	+	I	R	S	S	S	S	R	S	S	S
8	Influent		-	-	-	S	S	S	S	S	S	S	S	S	S
9	Surface Water		-	-	-	S	S	S	S	S	S	S	S	S	S
10	Surface Water		-	-	-	S	S	S	S	S	S	S	S	S	S
11	Influent		+	+	-	R	R	R	R	R	R	R	R	R	R
12	Influent		+	+	-	R	R	R	R	R	R	R	R	R	R
13	Influent		-	-	-	S	S	S	S	S	S	S	S	S	S
14	Influent		-	-	-	S	S	S	S	S	S	S	S	S	S
15	Influent		-	-	-	S	S	S	S	S	S	S	S	S	S
16	Influent		-	-	-	S	S	S	S	S	S	S	S	S	S
17	Sewage		-	-	-	S	S	S	S	S	S	S	S	S	S
18	Sewage		+	+	-	R	R	R	R	R	I	R	-	-	R
19	Sewage		-	-	-	S	S	S	S	S	S	S	S	S	S
20	Sewage		-	-	+	S	R	S	S	S	R	S	S	S	S
21	Sewage		-	-	-	S	S	S	S	S	S	S	S	S	S
22	Sewage		-	-	-	S	S	S	S	S	S	S	S	S	S
23	Sewage		-	-	-	S	S	S	S	S	S	S	S	S	S
24	Sewage		-	-	-	S	S	S	S	S	S	S	S	S	S
25	Sewage		-	-	-	S	S	S	S	S	S	S	S	S	S
26	Sewage		-	-	-	S	S	S	S	S	S	S	S	S	S
27	Sewage		-	-	-	S	S	S	S	S	S	S	S	S	S
28	Sewage		+	+	-	S	R	R	R	R	I	R	R	R	S
29	Sewage		-	-	+	S	S	S	S	S	S	S	S	S	S
30	Surface Water		-	-	-	S	S	S	S	S	S	S	S	S	S
31	Surface Water		-	-	-	S	S	S	S	S	S	S	S	S	S
32	Surface Water		-	NA	NA	S	S	S	S	S	S	S	S	S	S

Figure 3.9 | Comparing the PAD test to an ESBL-selecting plate, antibiotic susceptibility testing, and PCR gene analysis.

required. Detecting β-lactamase-expressing bacteria in community sewage water and identifying resistance in various species of bacterial isolates has demonstrated the practicality of this method. All tests were confirmed and compared to traditional culturing methods, antibiotic susceptibility testing, and PCR gene analysis. Although a laboratory was necessary to concentrate the sewage samples, this method still reduced the laboratory process by 14-20 hr. This test is also possible to ultimately integrate into a field-ready module by creating a more sensitive test or concentrating samples in the field. Bacterial samples were shown to react with nitrocefin whether in solution or dried into the paper, also demonstrating its potential for a field-ready module. It was confirmed that using a paper-based test and a camera phone for quantification yielded the same LOD as using an expensive and non-transportable plate reader and microtiter plate. While traditional methods are also quantitative of resistance, our paper-based method would be a rapid, cost-effective surveillance tool with a yes/no informed decision outcome prior to establishing a need for additional testing.

REFERENCES

(1) Boehle, K. E.; Gilliand, J.; Wheeldon, C. R.; Holder, A.; Adkins, J. A.; Geiss, B. J.; Ryan, E. P.; Henry, C. S. *Angew. Chem. Int. Ed. Engl.* **2017**, *56*, 6886-6890.
(2) Levy, S. B.; Marshall, B. *Nat. Med.* **2004**, *10*, S122-129.
(3) Antimicrobial Resistance: Global Report on Surveillance, World Health Organization, **2014**.
(4) Lupo, A.; Coyne, S.; Berendonk, T. U. *Front. Microbiol.* **2012**, *3*, 116-128.
(5) Novo, A.; Andre, S.; Viana, P.; Nunes, O. C.; Manaia, C. M. *Water Res.* **2013**, *47*, 1875-1887.
(6) Holvoet, K.; Sampers, I.; Callens, B.; Dewulf, J.; Uyttendaele, M. *Appl. Environ. Microbiol.* **2013**, *79*, 6677-6683.
(7) Jiang, L.; Hu, X.; Xu, T.; Zhang, H.; Sheng, D.; Yin, D. *Sci. Total Environ.* **2013**, *458-460*, 267-272.
(8) Baquero, F.; Martinez, J. L.; Canton, R. *Curr. Opin. Biotechnol.* **2008**, *19*, 260-265.
(9) Jorgensen, J. H.; Ferraro, M. J. *Clin. Infect. Dis.* **2009**, *49*, 1749-1755.
(10) Card, R.; Zhang, J.; Das, P.; Cook, C.; Woodford, N.; Anjum, M. F. *Antimicrob. Agents Chemother.* **2013**, *57*, 458-465.
(11) Kim, K. P.; Kim, Y. G.; Choi, C. H.; Kim, H. E.; Lee, S. H.; Chang, W. S.; Lee, C. S. *Lab Chip* **2010**, *10*, 3296-3299.
(12) Choi, J.; Jung, Y. G.; Kim, J.; Kim, S.; Jung, Y.; Na, H.; Kwon, S. *Lab Chip* **2013**, *13*, 280-287.
(13) Deiss, F.; Funes-Huacca, M. E.; Bal, J.; Tjhung, K. F.; Derda, R. *Lab Chip* **2014**, *14*, 167-171.
(14) Cate, D. M.; Adkins, J. A.; Mettakoonpitak, J.; Henry, C. S. *Anal. Chem.* **2015**, *87*, 19-41.
(15) Martinez, A. W.; Phillips, S. T.; Butte, M. J.; Whitesides, G. M. *Angew. Chem. Int. Ed. Engl.* **2007**, *46*, 1318-1320.
(16) Global Action Plan on Antimicrobial Resistance, World Health Organization, **2015**.
(17) Akram, M. S.; Daly, R.; da Cruz Vasconcellos, F.; Yetisen, A. K.; Hutchings, I.; Hall, E. A. H. In *Lab-on-a-Chip Devices and Micro-Total Analysis Systems*, Castillo-Leon, J.; Svendson, W. E., Eds.; Springer International Publishing Switzerland, 2015, pp 161-195.
(18) Jokerst, J. C.; Adkins, J. A.; Bisha, B.; Mentele, M. M.; Goodridge, L. D.; Henry, C. S. *Anal. Chem.* **2012**, *84*, 2900-2907.
(19) Bisha, B.; Adkins, J. A.; Jokerst, J. C.; Chandler, J. C.; Perez-Mendez, A.; Coleman, S. M.; Sbodio, A. O.; Suslow, T. V.; Danyluk, M. D.; Henry, C. S.; Goodridge, L. D. *J. Vis. Exp.* **2014**, *88*.
(20) Shi, K.; Caldwell, S. J.; Fong, D. H.; Berghuis, A. M. *Front. Cell Infect. Microbiol.* **2013**, *3*, 22.
(21) Murray, B. E.; Mederski-Samaroj, B. *J. Clin. Invest.* **1983**, *72*, 1168-1171.
(22) *Center for Disease Control and Prevention,* **2013**.
(23) Zeng, X.; Lin, J. *Front. Microbiol.* **2013**, *4*, 128.

(24) Lin, J.; Nishino, K.; Roberts, M. C.; Tolmasky, M.; Aminov, R. I.; Zhang, L. *Front. Microbiol.* **2015**, *6*, 34.
(25) Chuma, T.; Miyasako, D.; Dahshan, H.; Takayama, T.; Nakamoto, Y.; Shahada, F.; Akiba, M.; Okamoto, K. *Front. Microbiol.* **2013**, *4*, 113.
(26) Green, K. D.; Garneau-Tsodikova, S. *Front. Microbiol.* **2013**, *4*, 208.
(27) Watkins, R. R.; Papp-Wallace, K. M.; Drawz, S. M.; Bonomo, R. A. *Front. Microbiol.* **2013**, *4*, 392.
(28) Livermore, D. M.; Brown, D. F. J. *J. Antimicrob. Chemother.* **2001**, *48*, 59-64.
(29) O'Callaghan, C. H.; Morris, A.; Kirby, S. M.; Chingler, A. H. *Antimicrob. Agents Chemother.* **1972**, *1*, 283-288.
(30) Christodouleas, D. C.; Nemiroski, A.; Kumar, A. A.; Whitesides, G. M. *Anal. Chem.* **2015**, *87*, 9170-9178.
(31) Geiss, B. J.; Thompson, A. A.; Andrews, A. J.; Sons, R. L.; Gari, H. H.; Keenan, S. M.; Peerson, O. B. *J. Mol. Biol.* **2009**, *385*, 1643-1654.
(32) Fang, H.; Ataker, F.; Hedin, G.; Dornbusch, K. *J. Clin. Microbiol.* **2008**, *46*, 707-712.
(33) Amaya, E.; Reyes, D.; Vilchez, S.; Paniagua, M.; Mollby, R.; Nord, C. E.; Weintraub, A. *J. Med. Microbiol.* **2011**, *60*, 216-222.
(34) Labia, R.; Andrillon, J.; Le Goffic, F. *FEBS Letters* **1973**, *33*, 42-44.
(35) Koshland, D.; Botstein, D. *Cell* **1980**, *20*, 749-760.
(36) Koshland, D.; Botstein, D. *Cell* **1982**, *30*, 893-902.
(37) Minsky, A.; Summers, R. G.; Knowles, J. R. *Proc. Natl. Acad. Sci.* **1986**, *83*, 4180-4184.
(38) Aldridge, K. E.; Valainis, G. T.; Sanders, C. V. *Diagn. Microbiol. Infect. Dis.* **1988**, *10*, 31-39.

CHAPTER 4. MICROFLUIDIC PAPER-BASED DEVICE FOR DETECTING ANTIMICROBIAL RESISTANT BACTERIA THROUGH ANTIBIOTIC HYDROLYSIS

While many different antimicrobial resistant (AMR) bacteria pose a significant worldwide threat, it has been acknowledged that Carbapenem-resistant *Enterobacteriaceae* are one of the world's top AMR bacteria threats as identified by the Center for Disease Control and Prevention. This chapter describes a new device that further expands our first paper-based device for AMR bacteria detection (Chapter 3) by detecting bacteria resistant against specific β-lactam antibiotics through monitoring a change in pH caused by antibiotic hydrolysis. A 3-layered microfluidic device was designed and developed for detection that allows bacteria to react with a specific antibiotic, then a valve is opened for the resulting solution to travel to three different pH indicators. If the bacteria express an enzyme that hydrolyzes the antibiotic, this will result in a pH decrease, and display a positive result. If the bacteria do not express an enzyme that hydrolyzes the antibiotic, then there will not be a decrease in pH, resulting in a negative result. The device has been optimized and demonstrated for detecting bacteria resistant to specific penicillin and cephalosporin antibiotics, expanding the specificity of our β-lactamase paper-based device. This new device has not been successful in detecting bacteria resistant to carbapenem antibiotics yet, but this is likely due to the initial bacterial samples that were used to test the system, and will therefore be the subject of future study.

Introduction

The emergence of antimicrobial resistant (AMR) bacteria is a prevalent and growing problem around the world that threatens to be the number one cause of death worldwide by 2050.[1] The Center for Disease Control and Prevention (CDC) released a report on the top AMR threats in the United States where they identified specific classes of resistance that were classified as either urgent, serious, or concerning threats.[2] Of these threats, they identified 12 serious threats, but only three urgent threats, including hospital-acquired *Clostridium difficile* infections and drug-resistant *Neisseria gonorrhoeae*. The third urgent threat was carbapenem-resistant *Enterobacteriaceae* (CRE), which are considered one of the top threats of AMR bacteria worldwide.[3,4] These gram-negative bacteria are resistant against a class of last resort antibiotics used in clinical cases, the carbapenems. CRE bacteria are currently estimated to cause 9,000 drug resistant infections per year that result in around 600 deaths.[2] CRE can be especially deadly in sepsis infections as the mortality rate in CRE-associated infections is almost 50%.[2] Similar to many other resistance mechanisms used in bacteria,[5,6] the most common resistance pathway used in CRE is through the expression of carbapenemase, a broad spectrum β-lactamase enzyme.[7,8] While the spread of AMR and CRE bacteria cannot be entirely prevented, many steps can be taken to slow their emergence, including developing new antibiotics, decreasing the use of current antibiotics, and developing new detection methods and diagnostic tests to study the spread of AMR and accurately prescribe antibiotics.[9]

Although detecting and studying AMR bacteria in the field is important, commonly used methods for detection still require a central laboratory.[10] Antibiotic susceptibility

testing is considered the gold standard in hospitals as it accurately detects and quantifies susceptibility against specific drugs;[11] however, the procedure is time-consuming as it can take up to 2-3 days to obtain a result. As one study identified, every hour that a patient does not receive appropriate treatment is critical, especially in the case of sepsis patients where every hour without treatment can lead to a 7% increase in mortality risk.[12] Polymerase chain reaction (PCR) has also been proposed as a faster alternative that is based on amplifying specific genes associated with antimicrobial resistance.[13] However, PCR is susceptible to inhibition effects and detects only known resistance genes. It is unknown whether these genes are expressed, and cannot detect emerging mechanisms of resistance.

Many alternative methods have been proposed for AMR and CPE detection including mass spectrometry based methods.[14,15] Rapid antibiotic susceptibility testing has also been proposed in polymer-based microfluidic devices using a resazurin-based assay that can determine whether bacteria are dead or alive and can therefore determine the effectiveness of specific antibiotics.[16,17] Isothermal nucleic acid amplification techniques have also been applied to microfluidic devices for more portable and user-friendly detection of AMR-associated genes, including those associated with carbapenem-resistance.[18] The Carba-NP test is a popular test to directly test for resistance against specific carbapenem antibiotics by observing a color change from red/orange to yellow when the test is positive.[19,20] This is completed through reacting the bacteria sample with imipenem, a carbapenem antibiotic, and seeing if the color changes through a change in pH that is observed during antibiotic hydrolysis. Although these methods are accurate, they suffer from the need for trained

personnel, a central laboratory, or expensive equipment, and therefore are not conducive to field settings for applications such as environmental monitoring or point-of-care diagnostics.

Microfluidic paper-based analytical devices (μPADs) are a growing field of analytical tests based on a paper platform.[21] Paper-based devices provide many advantages for user-friendly testing including its inexpensive material, natural fluid-wicking properties through capillary action, reagent-storage capabilities, and the ability to apply many different user-friendly detection motifs, such as colorimetry.[22] Because of these properties, many μPADs have been developed specifically for point-of-care and environmental applications for field testing without the need for training the users or expensive equipment.[23] Several μPADs have been developed to detect bacteria using antibodies,[24-26] nucleic acid amplification,[27] and through detecting bacteria based on unique and naturally produced bacterial enzymes.[28-31] As seen in the previous chapter, we have developed a paper-based device to detect bacteria resistant against β-lactam antibiotics based on their expression of β-lactamase.[32]

In this new work, we have expanded this paper-based test for detecting bacteria resistant against specific antibiotics, not just detecting resistance against all β-lactam antibiotics. Using a similar concept to the Carba-NP test, we have designed a μPAD where a bacteria sample reacts with an antibiotic, then a valve is opened for the resulting reaction solution to go to three different pH indicators. By using three different indicators, phenol red, chlorophenol red, and bromothymol blue, we can expand our pH range to allow us to see slight changes in pH over a broader range, increasing the sensitivity of our device (Scheme 4.1). This new device has been demonstrated for

detecting bacteria resistant against specific antibiotics, such as ampicillin and cefazolin. The final goal of this assay is to detect bacteria resistant against imipenem, a commonly used carbapenem antibiotic, however, this has not been demonstrated yet. While the assay with imipenem has been attempted, the assay was not successful, which is likely due to the level of resistance of the bacteria we were detecting.

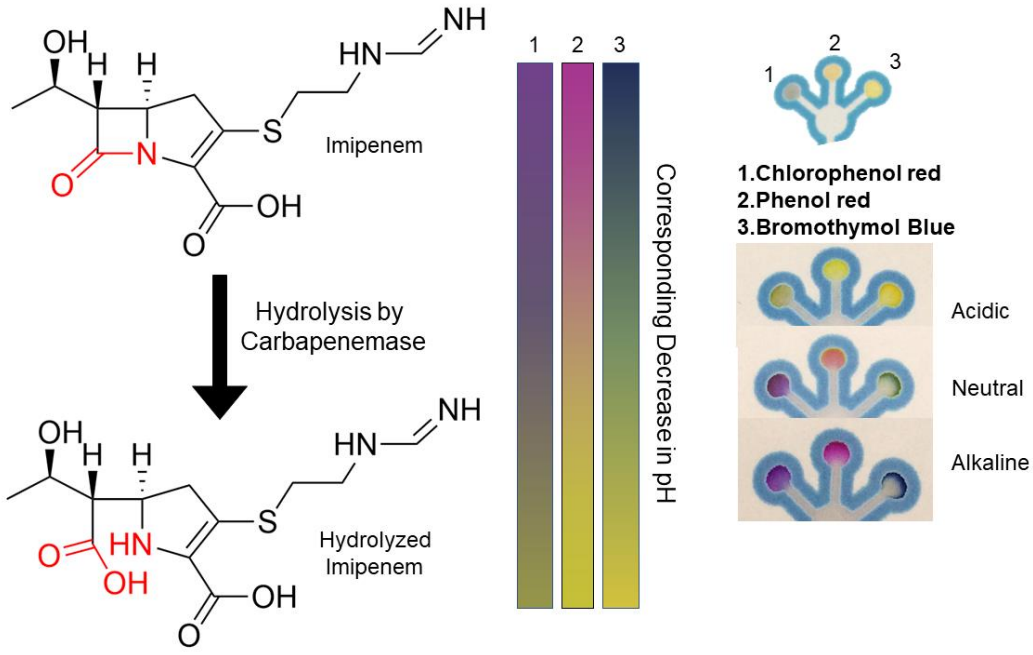

Scheme 4.1 | Detection scheme for the assay to detect bacteria resistant against specific antibiotics by monitoring a pH change through chemical hydrolysis.

Methods

μPAD Design and Fabrication. Devices were designed with Whatman grade 4 chromatography paper [GE Healthcare Sciences] and transparency sheets, and were designed using CorelDRAW. This material was chosen because initial optimization experiments showed no significant difference in color change of the pH indicators, but Whatman 4 showed faster and more consistent flow to the pH indicators compared to Whatman grade 1 chromatography paper. The device consists of three layers, the top

and bottom layers are wax-printed Whatman 4 chromatography paper, while the middle layer is wax-printed transparency sheet.

The bottom layer (pH indicator layer) was designed with an 8 mm diameter circle that leads to three separate pH indicator arms; each arm is a 3 mm by 4.5 mm channel leading to a 5 mm diameter pH detection zone for each selected pH indicator. The top layer, where antibiotic is dried, is a single 8 mm diameter circle surrounded by solid wax. Both top and bottom layers were wax-printed using a ColorQube 8870 [Xerox] wax printer. To define the hydrophobic barriers, an IsoTemp [Fisher Scientific] hot plate was set to 165 °C with two metal plates. The wax-printed paper was placed between the hot plate and a metal plate for 2 min to allow wax to melt through the pores completely. The top layer was then modified with 4 µL of varying concentration of a select antibiotic and allowed to dry at room temperature. The bottom layer was modified with three different pH indicators: one application of 0.35 µL of chlorophenol red; two applications of 0.35 µL of phenol red; and one application or 0.35 µL of bromothymol blue. Following chemical modification, Scotch Shipping Heavy Duty packing tape was used to tape the back of the bottom layer to prevent sample leakage. Because the top layer is supposed to open to the bottom layer, no packing tape was used on this layer.

The middle layer is a wax-printed transparency sheet to act as a “valve” or barrier between the top and bottom layers. To increase hydrophobicity and prevent sample leakage before the intended time, black wax was printed on the sheet, but the hot plate step was omitted. Following wax printing, the transparency sheet was cut into 9.5 mm by 20 mm rectangles using an Epilog Zing Laser Cutter (30 Watt) set to 195% speed, 5% power, and 200 Hz frequency. Following laser-cutting, the tip of one end of the

transparency sheet was folded up to create an accessible tab to enable users to easily move the transparency sheet between the top and bottom layers. All three layers were tightly taped down onto copy paper using transparent Scotch Magic™ tape.

Images were captured using an iPhone 5S and “light box” that was described in the previous two chapters. The images were analyzed qualitatively because a quantitative procedure has not yet been established.

Optimizing pH Indicators. The pH indicators chlorophenol red [Alfa Aesar] and phenol red [Fluka Analytical] have been previously optimized on paper in our lab, therefore the same concentrations and volumes were used for this device.[33] Bromothymol blue [Sigma Aldrich] was optimized by drying different concentrations and volumes onto 5 mm circles. The ideal concentration and volume was chosen by adding 1 µL of different pHed buffers and qualitatively comparing the pH indicator range, between pH 6 and 9. Different concentrations of bromothymol blue include 0.5 mM, 1 mM, 1.5 mM, and 3 mM.

Enzymatic Reaction Optimization. To demonstrate that hydrolysis would result in a pH decrease, the system was first demonstrated using lyophilized β-lactamase [Abcam, ab67672] and ampicillin sodium salt [Ward’s Science]. For initial experiments, the entire device was not used, only the bottom pH indicator layer. Varying concentrations of ampicillin were mixed equal parts with varying concentrations of β-lactamase and allowed to react for 10 min in a microcentrifuge tube before adding to the pH indicator layer of the device and capturing an image.

Bacteria Detection Optimization. DH5α *Escherichia coli* cells [New England Biolabs] were used for both control and experimental bacteria in initial laboratory

bacterial analysis. The control *E. coli* did not express β-lactamase, while the experimental bacteria expressed a previously published plasmid, pBG167, which encodes β-lactamase.[34] The pBG167 plasmid was transformed into DH5α cells and the bacteria were grown on Luria Broth (LB) agar plates containing 50 μg mL^{-1} ampicillin to select bacteria expressing β-lactamase. For subsequent experiments, bacteria were cultured in LB media overnight (~16-18 hr) before each experiment. To determine our limit of detection, bacteria concentration was calculated using serial dilution and plating 50 μL of 10^{-5}, 10^{-6}, and 10^{-7} dilutions on ampicillin-containing LB Agar plates and grown for 24 hr. The colonies were counted on each plate, calculated back to the original concentration, and the average was taken to obtain an estimate of the original bacteria concentration. For lysing the cells during optimization, the cells were sonicated for 15 s using a XL-2000 Series probe sonicator set at 5 W, 22 kHz. These settings were chosen based on past experimental data for bacteria detection based on enzyme expression.[30]

Bacteria solutions were reacted with ampicillin for 10 min until it was determined that 30 min was the optimal reaction time. Initial experiments were completed using only the bottom layer of the device and reacting equal parts bacteria sample with ampicillin in a microcentrifuge tube before adding 12 μL to the pH indicator layer to assess pH change. Once the entire 3-layer device was finished, 40 μL of bacteria sample was added to the top layer of the device and reacted for 30 min. Following reaction, the center part of the device, the wax-printed transparency layer, was removed, allowing the reacted mixture to flow from the top layer to the bottom layer, and to each individual pH indicator (Figure 4.4).

To determine if chemical lysing was adequate for enzyme detection, SolyLyse™ was used. Different volumes and reaction times were added to the final device as previous experimentation with the liquid revealed that too high of volumes (>20% total solution volume) used of the solution leads to the sample bleeding through the wax. For 200 µL of bacteria sample, 10, 20, and 30 µL of SoluLyse™ were added and allowed to incubate for 10 min. After determining the ideal SoluLyse™ volume, incubation times were varied for 10, 20, and 30 min before adding the bacteria solution to the device to incubate for 30 min as previously optimized.

Detecting Resistance Against Other Antibiotics. To determine what antibiotics the DH5α cells were resistant against, 20 µL of 50 mg mL^{-1} penicillin V potassium salt [Acros Organics], amoxicillin sodium salt [Alfa Aesar], and cefazolin sodium salt [Chem Impex Int'l Inc.], were spread across LB agar plates containing no antibiotics. After allowing the antibiotic to dry on the surface, 50 µL of the 10^{-4} dilution of the bacteria was plated and incubated at 37 °C for 24 hr. If the bacteria grew on the plate, it was considered resistant against the antibiotic and should theoretically hydrolyze the antibiotic in the µPAD test. Because antibiotics have varying starting pH compared to ampicillin, penicillin V and cefazolin were dissolved in pH 8.5 Tris buffered saline as opposed to dH_2O, like ampicillin and amoxicillin. 4 µL of 125 mM antibiotic was dried onto the top layer of the device at room temperature. The sample addition and reading procedures were the same as described above for ampicillin resistance.

Detecting Carbapenem-Resistant Bacteria. To test this system on carbapenem-resistant bacteria, different *E. coli* environmental isolates were obtained from different environmental samples, such as river or sewage water. These isolates

were obtained and maintained by the Elizabeth P. Ryan laboratory in Environmental Health and Radiological Sciences department, the same collaborators as in Chapter 3. The isolates were grown overnight in Tryptic Soy broth. Instead of using the final device, the isolate was reacted in a microcentrifuge tube with 3 mg mL^{-1} imipenem or ertapenem dissolved in 0.1 mM $ZnSO_4$ for 30 and 120 min. Following these reaction times, 12 µL was deposited onto the pH indicator layer of the device and imaged. To increase bacteria concentration, 1 mL of bacteria solution was resuspended in 0.5 mL of media. 1 mL of bacteria solution was centrifuged at 10,000 RPM for 5 min, then the supernatant was carefully removed, before resuspending the solution in fresh bacteria media.

Determining Carbapenem Resistance of Environmentally Isolated Bacteria. To confirm resistance against imipenem and ertapenem, the minimum inhibitory concentration (MIC) was determined using 200 µL of diluted bacteria mixed with 20 µL of different concentrations of ertapenem or imipenem. The antibiotic concentrations started at 500 µg mL^{-1} and were serially diluted by half until 244 ng mL^{-1}. Because the antibiotics were diluted in bacteria 10-fold, the actual concentration range was 50 µg mL^{-1} to 24.4 ng mL^{-1}. Once the bacteria and antibiotic were mixed, the microtiter plate was incubated in a 37 °C shaker overnight. The MIC was determined by selecting the lowest concentration of antibiotic where the bacteria did not grow.

Results and Discussion

Optimizing Initial Device. This pH indicator device is based off a previously optimized µPAD that was developed in the Henry Laboratory for saliva diagnostics.[33]

For that device, chlorophenol red, phenol red, and phenolphthalein were chosen to indicate saliva pH to the device operator as an indication of specific health ailments. During initial proof-of-concept experiments for a device that detects antimicrobial resistant bacteria using a pH change of antibiotic hydrolysis, it was determined that the ideal quantitative range for pH was between 6 and 8. Because phenolphthalein changes color at around a pH of 9, this indicator was replaced with bromothymol blue, which has a quantitative range between 6 and 7.6. For determining the ideal concentration and volume application of bromothymol blue, the indicator was dried on the device through one or two applications of 0.3 µL and compared 0.5 mM, 1 mM, 1.5 mM, and 3 mM concentrations. Two applications of 1.5 mM bromothymol blue were found to provide the most visually quantitative results between different buffer pHs. Following this optimization, a calibration chart was developed of the final pH indicator device with all three pH indicators (Figure 4.1).

Once the pH indicators were optimized for different buffers, the next step was to establish whether the device could be used to detect a change in pH as a result of hydrolysis by an enzyme to an antibiotic. Because carbapenemase is not available to buy as an isolated enzyme, the system was demonstrated with β-lactamase hydrolyzing ampicillin. Equal parts ampicillin and enzyme of varying concentrations were mixed in microcentrifuge to react for 10 min before adding 10 µL of reaction sample to the pH indicator device to see if a pH change occurs that is noticeable via color change. When reacting ampicillin from concentrations of 10 mM to 150 mM with variable concentrations of β-lactamase, it was determined that 25 or 50 mM ampicillin would be most ideal. While 50 mM was more sensitive to different concentrations of β-lactamase,

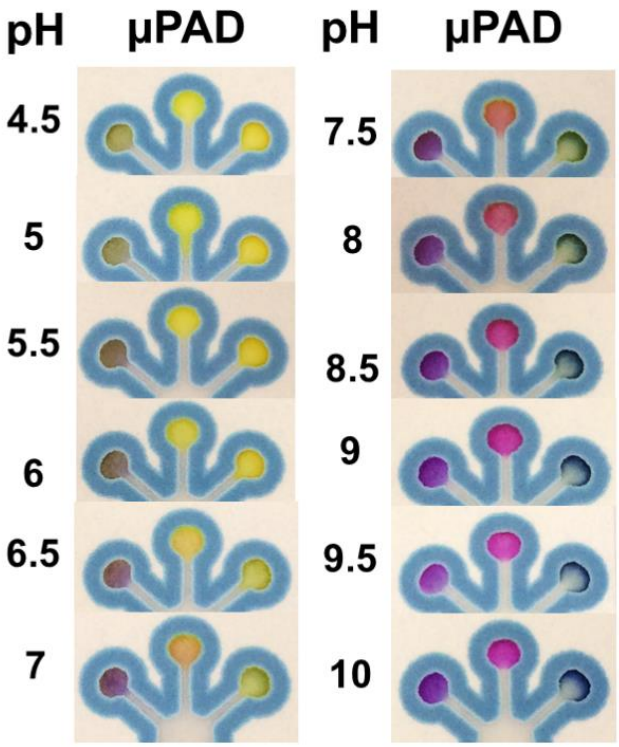

Figure 4.1 | Calibration chart of chosen pH indicators at a variety of pHs to demonstrate quantifiability of the assay.

25 mM did provide a lower detection limit. Using a lower concentration of ampicillin did not allow enough antibiotic hydrolysis for a noticeable change in pH. On the other hand, too high of a concentration of antibiotic leads to higher detection limits, because there is too much antibiotic to hydrolyze for lower concentrations of enzymes to result in a noticeable color change (Figure 4.2).

Following initial optimization of the system using pure β-lactamase, the system was tested on laboratory bacteria. When 25 mM and 50 mM ampicillin were first reacted with bacteria, there was very little color change. But when the bacteria were lysed using mechanical sonication, a noticeable color change occurred with concentrated bacteria solution (Figure 4.3). However, despite the addition of cell lysing, the detection limit of

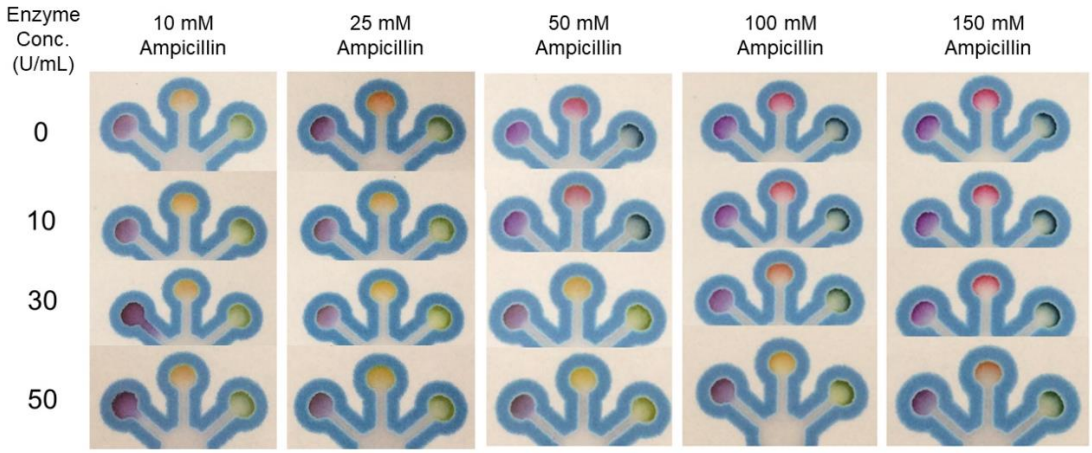

Figure 4.2 | Initial optimization of antibiotic concentration reacting pure β-lactamase and ampicillin in a microcentrifuge tube before putting on pH indicator layer of paper-based device.

the assay was 10^8 CFU mL^{-1}, two orders of magnitude higher than observed when using nitrocefin for β-lactamase detection (Chapter 3). During initial optimization experiments, the enzyme sample and antibiotic reacted for 10 min, which was adequate for detection, but longer reaction times could improve detection limits. The pH of the reaction was taken at 10, 20, and 30 min of reaction for *E. coli* reacting with 25 mM and 50 mM ampicillin. For 50 mM ampicillin, reacting the solution for 30 min did not change the pH

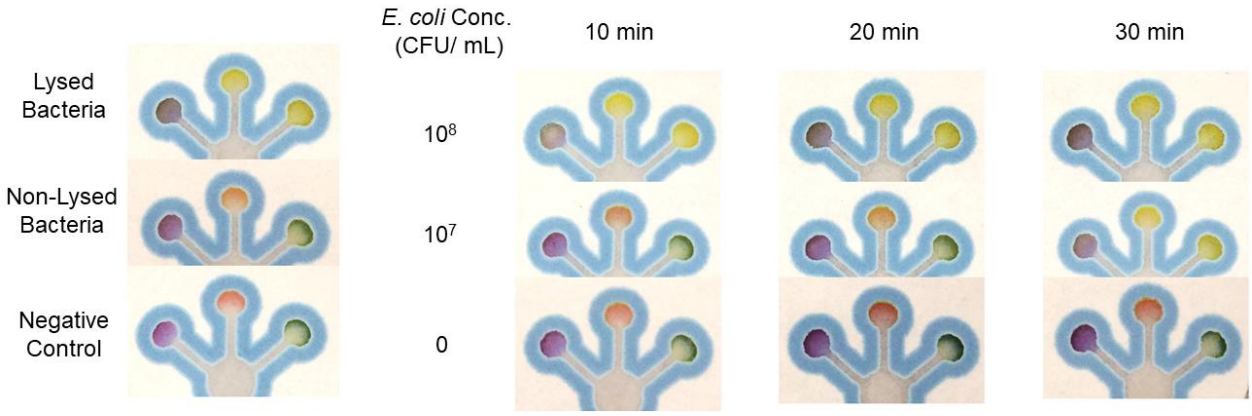

Figure 4.3 | Initial optimization of bacteria detection to determine ideal bacteria preparation and reaction time for sensitive detection.

significantly from 10 min of reaction. However, 25 mM ampicillin did result in a noticeable pH change at 30 min of reaction, therefore, this concentration and reaction time were chosen for the final device (Figure 4.3).

Developing a 3-Layer Device for AMR Detection. Up until this point, all detection of β-lactamase or β-lactamase-producing bacteria was completed by first reacting the sample in a microcentrifuge tube, followed by adding the reacted sample to the pH indicator microfluidic device. However, this reaction setup is not conducive to field settings. The ideal device simply requires the user to add sample to one device without the need to bring multiple solutions and tools into the field. It was originally theorized that simply drying antibiotic in the sample addition zone of the pH indicator device for bacteria to react with before going to the pH indicator zones. However, as previously optimized, the ideal reaction time for the bacteria sample with antibiotic is at least 30 min. Therefore, the device requires a reaction zone where the sample can be stored for 30 min, then travel to the pH indicators following reaction. Several devices have been fabricated that control flow to specific sections of a device for applications such as environmental monitoring and biomedical testing.[35,36] Using a similar concept, a device composed of three layers was developed. When all three layers are taped together, the user simply needs to add a bacteria sample, wait 30 min, then pull the middle layer valve, wax printed transparency sheet to prevent sample leaking. Pulling the valve allows the reacted sample to flow to the bottom pH indicator layer. If the bottom layer indicates an alkaline pH, the bacteria did not hydrolyze the antibiotic, indicating a negative result. If the pH is acidic, then the antibiotic was hydrolyzed, displaying a positive result (Figure 4.4).

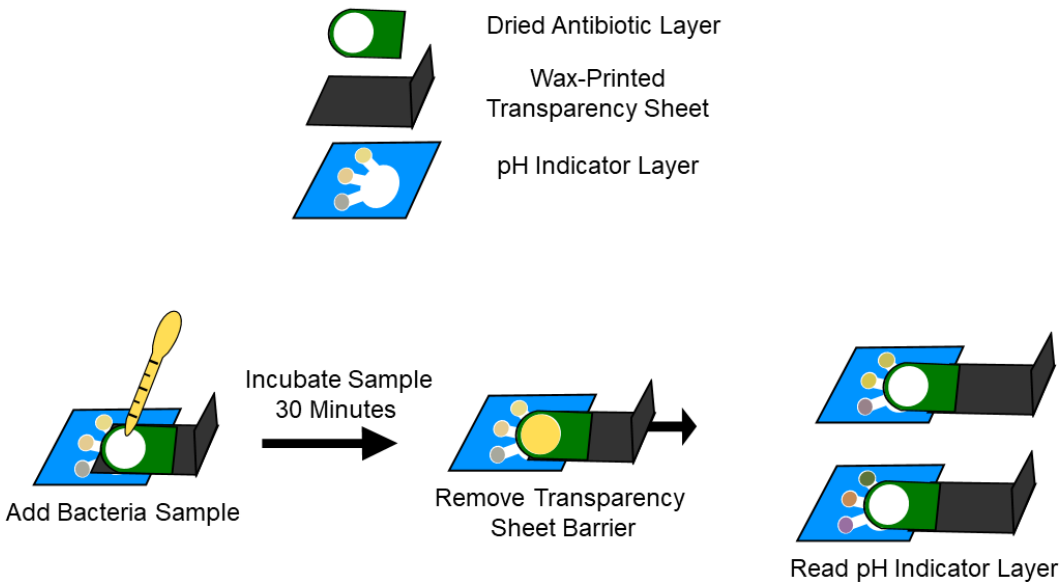

Figure 4.4 | Designing a µPAD that allows the user to add sample to a reaction layer (top layer with dried antibiotic) for 30 min, then pull a valve (the middle layer, a wax-printed transparency sheet), which allows the reacted solution to travel to the bottom detection layer (pH indicator layer) for the user to read for whether the sample is positive or negative for bacteria resistant against that specific antibiotic.

Optimizing 3-Layer Device for Bacteria Detection. While initially optimizing the 3-layer device, it was made apparent that regular transparency film was not hydrophobic enough to hold the sample in one place for 30 min. Over time, the sample would diffuse to the edges of the film and eventually leak from the device. Because wax is used as a hydrophobic barrier in paper-based devices, wax was printed onto the transparency film before cutting into individual valves. This enabled the device to hold samples for the necessary 30 min required for the reaction to take place before opening the valve and allowing the sample to flow to the pH indicators. Similarly, while the pH indicator only requires 12 µL of sample to saturate the device, the addition of the valve and top reaction layer with dried antibiotic, resulted in increasing the sample size to 40 µL. Because some sample is lost to the top layer and evaporation over 30 min of

reaction, volumes lower than 40 µL would not result in enough sample to saturate the pH indicators.

When drying antibiotic into the top layer of the device, the reaction layer, the concentration would need to be reoptimized to account for increased sample volume and assuming antibiotic is lost to the paper. Concentrations ranging from 10 to 150 mM were dried into the top layer of the device. Choosing the ideal concentration was determined qualitatively by comparing the detection of 10^8, 10^7, and 0 CFU mL^{-1}. The ideal concentration could detect at least 10^7 CFU mL^{-1}, but adequately distinguish this concentration from when no antibiotic is hydrolyzed. Similar to optimizing the antibiotic concentration in solution, lower concentrations of antibiotic yielded indistinguishable changes in pH across different bacteria concentrations (Figure 4.5). The pH difference

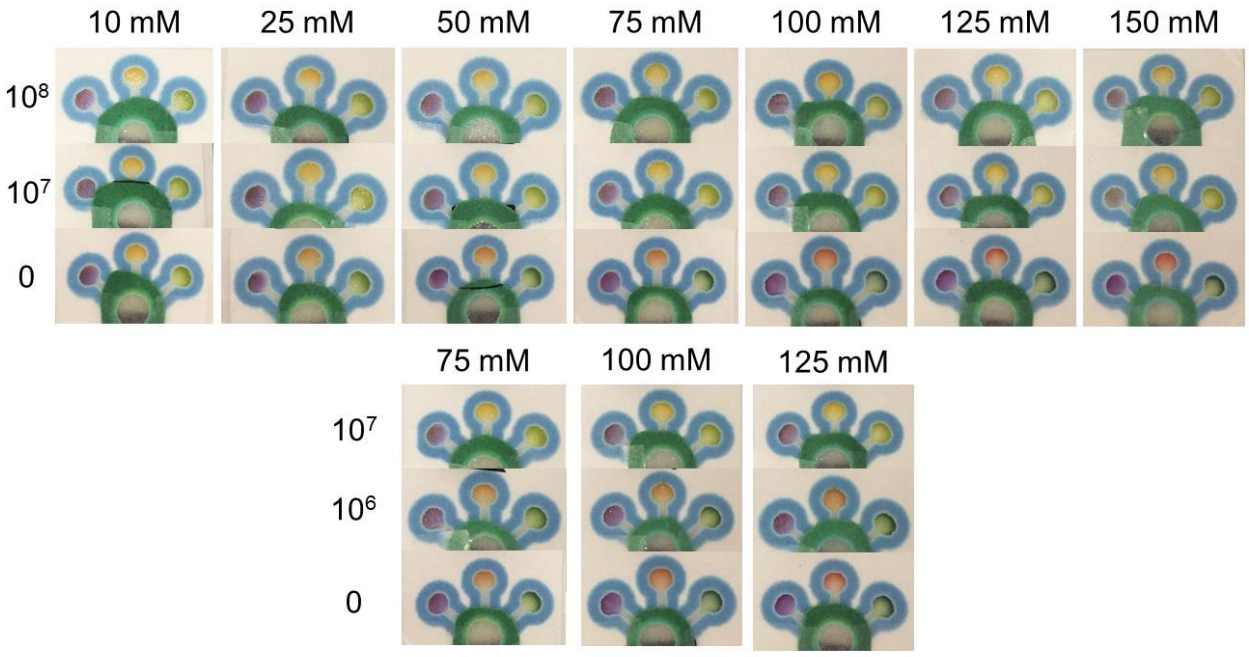

Figure 4.5 | Optimizing antibiotic concentration to store in the top layer of the device for optimal bacteria detection.

between no bacteria and higher bacteria concentrations continually increase until 125 mM. Higher concentrations were not tested as it was assumed that concentrations higher than 150 mM would lead to an increase in the detection limit as what was observed with the solution assay.

Based on these initial optimizations, it appeared 125 mM would provide the most sensitive results. However, as previously demonstrated, lower concentrations often provide better detection limits. Therefore, 75 mM, 100 mM, and 125 mM were chosen to react with 10^6 and 10^7 CFU mL^{-1} bacteria to determine whether a lower detection limit was achievable. As seen in the bottom portion of Figure 4.5, there was a slight pH change with 10^6 CFU mL^{-1}. This pH change was most noticeable with 125 mM ampicillin, and it was therefore selected for subsequent experiments.

Detecting Bacteria Resistant to Specific Antibiotics. Following optimization, a calibration chart was generated for β-lactamase-producing *E. coli*. As seen in Figure 4.6, the device detected bacteria resistant to ampicillin only when the bacteria were resistant, as confirmed by growing the bacteria an ampicillin resistant selective plate.

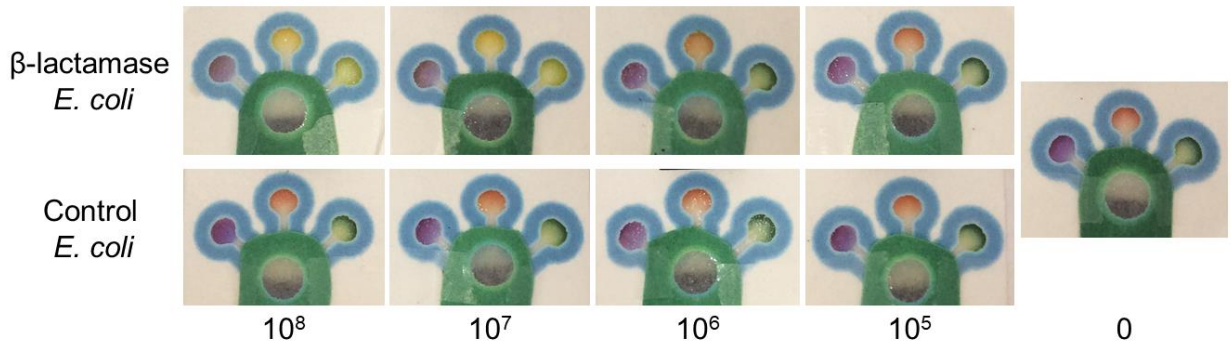

Figure 4.6 | Demonstrating the sensitivity and specificity of the device by generating a calibration chart of *E. coli* both resistant and not resistant to ampicillin.

One of the advantages of this device over the device described in Chapter 3 that detects AMR bacteria based on nitrocefin hydrolysis is the ability to detect resistance against specific antibiotics. Nitrocefin detects β-lactamase activity, which indicates to the user that the bacteria are likely resistant against any β-lactam antibiotic. However, as also discussed in Chapter 3, bacteria that express β-lactamase can be resistant against some β-lactam antibiotics, but not others. By drying different antibiotics on the reaction layer of the device, the user can test for resistance against specific antibiotics for a more precise resistance profile. In addition to testing resistance against ampicillin, we tested the laboratory *E. coli* for resistance against amoxicillin, penicillin V, and cefazolin, a cephalosporin β-lactam antibiotic (Figure 4.7). The caveat of using this device to detect resistance against several antibiotics is the starting pH of each antibiotic. Amoxicillin's starting pH is more alkaline compared to ampicillin, and therefore there is not as significant of a pH change when reacted with the same concentration of bacteria. The opposite is seen in penicillin V and cefazolin as their starting pH's are more acidic than when the device stops being quantifiable. Despite dissolving penicillin V and cefazolin in pH 8.5 Tris buffered saline, the starting pH was lower than ampicillin, also making the device less quantifiable. The pH of naturally acidic antibiotics can be adjusted by dissolving the chemicals in alkaline buffers. However, as what will be discussed in more detail in Chapter 5, alkaline solutions cause speedier degradation of β-lactam antibiotics. The hypothesis as to why this happens is because of hydroxyl groups present in alkaline solutions hydrolyzing the β-lactam ring at an increased rate compared to neutral or acidic solutions.

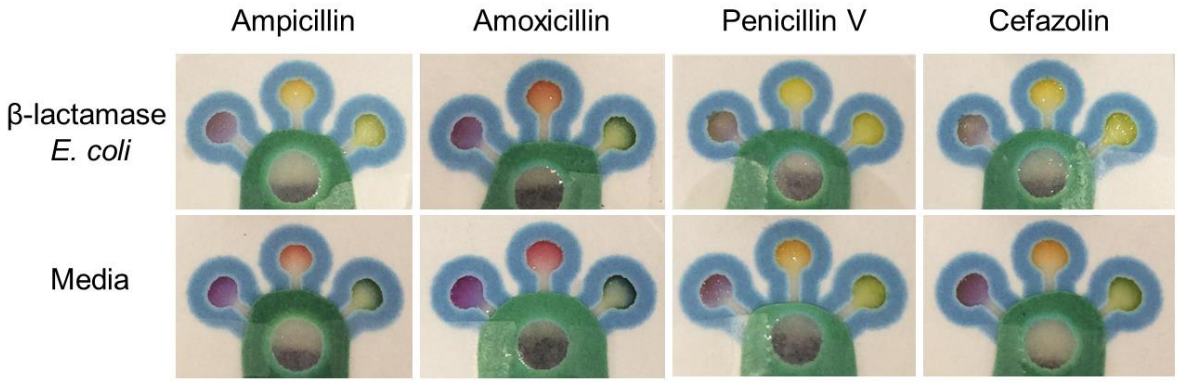

Figure 4.7 | Detecting resistance against other β-lactam antibiotics.

Adapting the Assay for Detecting Carbapenem-Resistant Bacteria. The final goal of this assay is to detect bacteria resistant against different classes of β-lactam antibiotics, including last resort antibiotics, the carbapenems. For testing the system of β-lactam-resistant bacteria, laboratory *E. coli* DH5α was transformed with a plasmid that expresses β-lactamase. Unfortunately, a plasmid is not available to express carbapenemase, therefore bacteria species that have been isolated from environmental samples were used. These isolates were identified as carbapenemase-producing bacteria based on selective plates, a commonly used traditional method. Because carbapenem-resistant bacteria that have been isolated from the environment are going to have different resistance profiles compared to transformed laboratory bacteria, we did not use our optimized reaction conditions. Instead, we followed a procedure like the Carba-NP test, and only used the pH indicator layer of the device. Unlike detecting traditional β-lactamase activity, many carbapenemases are metalloenzymes, meaning they require a metal to facilitate the reaction. The creators of the Carba-NP test were successful when using 10 mM imipenem dissolved in 0.1 mM $ZnSO_4$, therefore these conditions were used.[37]

When testing these reaction conditions in distinguishing environmentally isolated bacteria that do and do not grow on carbapenemase-selecting plates, the test was not successful (Figure 4.8). Isolates #1 and #2 grew on these selective plates, while isolates #3 and #4 did not grow, however, all bacteria isolates are indistinguishable using this device. Several different preparation techniques were attempted, including extending the reaction time to 2 hr instead of the optimized 30 min. Similar to what was demonstrated for bacteria detection in Chapter 2, we resuspended the bacteria in a lower volume of buffer than the original sample, concentrating the sample. Neither of these procedures were effective. As seen in Figure 4.8, all bacteria isolates are decreasing the pH compared to the media control sample. Therefore, either all bacterial species are hydrolyzing imipenem, or another bacterial property is causing the decrease in pH.

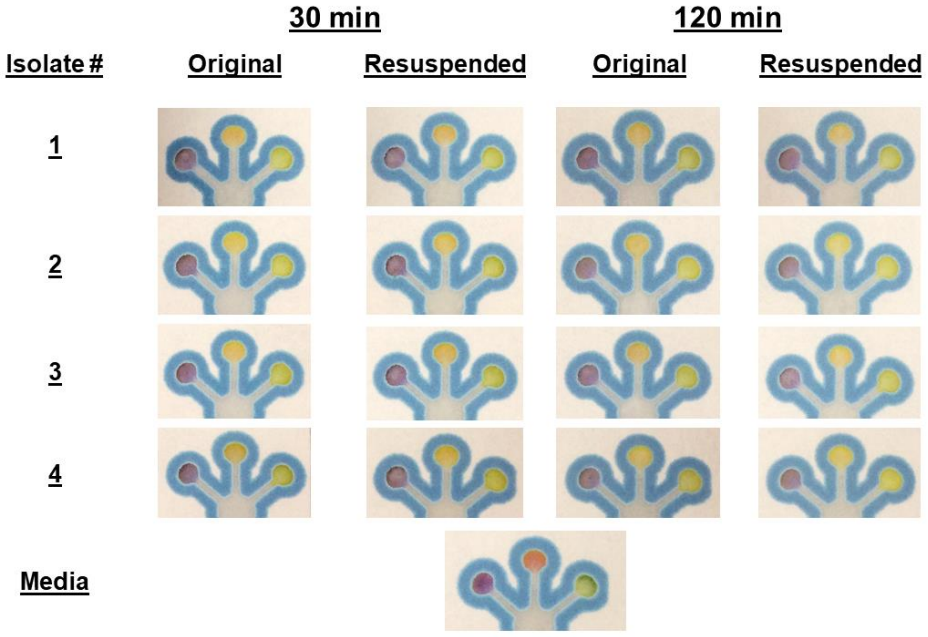

Figure 4.8 | Detecting resistance of environmentally isolated bacteria against imipenem, a carbapenem antibiotic. Using traditional methods, bacteria isolates #1 and #2 tested positive for resistance against imipenem while isolates #3 and #4 tested negative for resistance.

To confirm whether these bacteria were resistant or susceptible to imipenem and ertapenem (another carbapenem antibiotic), a minimum inhibitory concentration (MIC) assay was performed using serial dilutions of these antibiotics. Whether or not the bacteria would grow in the presence of a specific concentration of antibiotic determined whether bacteria were resistant to the antibiotic at that concentration. Using this traditional technique, we determined that all four isolates had similar resistance against imipenem with isolates #1-3 having an MIC of 0.78 μg mL^{-1} and isolate #4 with an MIC of 0.39 μg mL^{-1} (Table 4.1). All isolates were more resistant against imipenem when compared to ertapenem, therefore would likely be a better antibiotic to test for initial carbapenem-resistance. All isolates display similar MICs for imipenem, suggesting that our results show all bacterial species hydrolyzing imipenem. However, when using this system to detect resistance in β-lactamase-producing DH5α cells, these laboratory bacteria were growing in the presence of much higher concentrations of antibiotics. At 50 μg mL^{-1}, the DH5α cells were approximately 64x more resistant than these environmental isolates, therefore are likely to hydrolyze much less antibiotic for a noticeable color change in the pH indicators.

Table 4.1 | Calculated minimum inhibitory concentration (MIC) of the tested environmental isolates. N/A designates the bacteria did not grow in the presence of the lowest tested antibiotic.

Bacteria Isolate #	Imipenem MIC (μg mL^{-1})	Ertapenem MIC (μg mL^{-1})
1	0.78	0.195
2	0.78	0.39
3	0.78	N/A
4	0.39	N/A

Conclusions and Future Directions

A device has been designed and partly optimized for detecting bacteria resistant against different classes of β-lactam antibiotics. The device has been optimized for detecting bacteria resistant against ampicillin, but will need further optimization for other antibiotics such as amoxicillin, penicillin V, and cefazolin for maximum pH and color change. The system should eventually work for detecting bacteria resistant against carbapenem antibiotics, however, this will involve verifying the MIC of multiple additional environmental isolates before selecting a few isolates for optimization. Another option would be to customize a new plasmid for DH5α cells that encodes carbapenemase for optimization experiments before demonstrating the device with bacteria isolated from environmental samples. Another issue to note is that the media used to grow bacteria is most likely acting as a pH buffer. Hence, we will also be testing whether centrifuging the bacteria and resuspending in deionized water will yield more sensitive results. Once the final device has been optimized, it will eventually be verified for clinical applications using inoculated plasma or serum samples.

REFERENCES

(1) Tackling Drug-Resistant Infections Globally: Final Report and Recommendations Welcome Trust, United Kingdom Government, **2016**.
(2) Antibiotic Resistance Threats in the United States, Center for Disease Control and Prevention, **2013**.
(3) Nordmann, P.; Dortet, L.; Poirel, L. *Trends Mol. Med.* **2012**, *18*, 263-272.
(4) Nordmann, P.; Naas, T.; Poirel, L. *Emerg. Infect. Dis.* **2011**, *17*, 1791-1798.
(5) Lin, J.; Nishino, K.; Roberts, M. C.; Tolmasky, M.; Aminov, R. I.; Zhang, L. *Front. Microbiol.* **2015**, *6*, 34.
(6) Murray, B. E.; Mederski-Samaroj, B. *J. Clin. Invest.* **1983**, *72*, 1168-1171.
(7) Rodriguez-Martinez, J. M.; Poirel, L.; Nordmann, P. *Antimicrob. Agents Chemother.* **2009**, *53*, 4783-4788.
(8) Poirel, L.; Nordmann, P. *Clin. Microbiol. Infect.* **2006**, *12*, 826-836.
(9) Global Action Plan on Antimicrobial Resistance; World Health Organization, **2015**.
(10) Jorgensen, J. H.; Ferraro, M. J. *Clin. Infect. Dis.* **2009**, *49*, 1749-1755.
(11) Bauer, A. W.; Kirby, W. M.; Sherris, J. C.; Turck, M. *Am. J. Clin. Pathol.* **1966**, *45*, 493-496.
(12) Kumar, A.; Roberts, D.; Wood, K. E.; Light, B.; Parrillo, J. E.; Sharma, S.; Suppes, R.; Feinstein, D.; Zanotti, S.; Taiberg, L.; Gurka, D.; Kumar, A.; Cheang, M. *Crit. Care Med.* **2006**, *34*, 1589-1596.
(13) Woodford, N.; Ellington, M. J.; Coelho, J. M.; Turton, J. F.; Ward, M. E.; Brown, S.; Amyes, S. G.; Livermore, D. M. *Int. J. Antimicrob. Agents.* **2006**, *27*, 351-353.
(14) Burckhardt, I.; Zimmermann, S. *J. Clin. Microbiol.* **2011**, *49*, 3321-3324.
(15) Alvarez-Buylla, A.; Picazo, J. J.; Culebras, E. *J. Clin. Microbiol.* **2013**, *51*, 1589-1592.
(16) Kaushik, A. M.; Hsieh, K.; Chen, L.; Shin, D. J.; Liao, J. C.; Wang, T. H. *Biosens. Bioelectron.* **2017**, *97*, 260-266.
(17) Elavarasan, T.; Chhina, S. K.; Parameswaran, M.; Sankaran, K. *Sens. Actuators B Chem.* **2013**, *176*, 174-180.
(18) Kalsi, S.; Sellars, S.; Turner, C.; Sutton, J.; Morgan, H. *Micromachines* **2017**, *8*, 111.
(19) Osterblad, M.; Hakanen, A. J.; Jalava, J. *Antimicrob. Agents Chemother.* **2014**, *58*, 7553-7556.
(20) Dortet, L.; Poirel, L.; Errera, C.; Nordmann, P. *J. Clin. Microbiol.* **2014**, *52*, 2359-2364.
(21) Yang, Y.; Noviana, E.; Nguyen, M. P.; Geiss, B. J.; Dandy, D. S.; Henry, C. S. *Anal. Chem*. **2017**, *89*, 71-91.
(22) Cate, D. M.; Adkins, J. A.; Mettakoonpitak, J.; Henry, C. S. *Anal. Chem.* **2015**, *87*, 19-41.
(23) Hu, J.; Wang, S.; Wang, L.; Li, F.; Pingguan-Murphy, B.; Lu, T. J.; Xu, F. *Biosens. Bioelectron.* **2014**, *54*, 585-597.
(24) Srisa-Art, M.; Boehle, K. E.; Geiss, B. J.; Henry, C. S. *Anal. Chem.* **2018**, *90*, 1035-1043.

(25) Khan, M. S.; Pande, T.; van de Ven, T. G. *Colloids Surf. B Biointerfaces* **2015**, *132*, 264-270.
(26) Li, C.-z.; Vandenberg, K.; Prabhulkar, S.; Zhu, X.; Schneper, L.; Methee, K.; Rosser, C. J.; Almeide, E. *Biosens. Bioelectron.* **2011**, *26*, 4342-4348.
(27) Lafleur, L. K.; Bishop, J. D.; Heiniger, E. K.; Gallagher, R. P.; Wheeler, M. D.; Kauffman, P.; Zhang, X.; Kline, E. C.; Buser, J. R.; Kumar, S.; Byrnes, S. A.; Vermeulen, N. M.; Scarr, N. K.; Belousov, Y.; Mahoney, W.; Toley, B. J.; Ladd, P. D.; Lutz, B. R.; Yager, P. *Lab Chip* **2016**, *16*, 3777-3787.
(28) Zakir Hossain, S. M.; Ozimok, C.; Sicard, C.; Aguirre, S. D.; Monsur Ali, M.; Li, Y.; Brennan, J. D. *Anal. Bioanal. Chem.* **2012**, *403*, 1567-1576.
(29) Bisha, B.; Adkins, J. A.; Jokerst, J. C.; Chandler, J. C.; Perez-Mendez, A.; Coleman, S. M.; Sbodio, A. O.; Suslow, T. V.; Danyluk, M. D.; Henry, C. S.; Goodridge, L. D. *J. Vis. Exp.* **2014**, 88, e51414.
(30) Jokerst, J. C.; Adkins, J. A.; Bisha, B.; Mentele, M. M.; Goodridge, L. D.; Henry, C. S. *Anal. Chem.* **2012**, *84*, 2900-2907.
(31) Adkins, J. A.; Boehle, K.; Friend, C.; Chamberlain, B.; Bisha, B.; Henry, C. S. *Anal. Chem.* **2017**, *89*, 3613-3621.
(32) Boehle, K. E.; Gilliland, J.; Wheeldon, C. R.; Holder, A.; Adkins, J. A.; Geiss, B. J.; Ryan, E. P.; Henry, C. S. *Angew. Chem. Int. Ed. Engl.* **2017**, *56*, 6886-6890.
(33) Noiphung, J.; Nguyen, M. P.; Punyadeera, C.; Wan, Y.; Laiwattanapaisal, W.; Henry, C. S. *Theranostics* **2018**, *In Press*.
(34) Steel, J. J.; Franz, A. W.; Sanchez-Vargas, I.; Olson, K. E.; Geiss, B. J. *PLoS One* **2013**, *8*, e84930.
(35) Verma, M. S.; Tsaloglou, M. N.; Sisley, T.; Christodouleas, D.; Chen, A.; Milette, J.; Whitesides, G. M. *Biosens. Bioelectron.* **2018**, *99*, 77-84.
(36) Dungchai, W.; Sameenoi, Y.; Chailapakul, O.; Volckens, J.; Henry, C. S. *Analyst* **2013**, *138*, 6766-6773.
(37) Nordmann, P.; Poirel, L.; Dortet, L. *Emerg. Infect. Dis.* **2012**, *18*, 1503-1507.

CHAPTER 5. PAPER-BASED ENZYME COMPETITION ASSAY FOR DETECTING FALSIFIED ANTIBIOTCS

Falsified and substandard antibiotics are a growing worldwide problem that leads to increased patient mortality, decreased trust in healthcare, and contributes to antimicrobial resistance. Monitoring falsified antibiotics is difficult because most falsified pharmaceuticals are found in developing countries, where detecting the active ingredient is difficult due to lack of access to complex instrumentation. Herein, we describe the development and optimization of a microfluidic paper-based analytical device (μPAD) to detect the active ingredient in the most falsified class of antibiotics, β-lactams. The assay is based on enzyme competition, making it the first demonstrated competitive enzyme assay reported in paper-based devices. The assay uses nitrocefin, a chromogenic substrate, to compete with β-lactam antibiotics in a reaction with β-lactamase. A yellow color indicates legitimate drugs, while a color change from yellow to red indicates falsified drugs. In addition to testing for the active ingredient, another section of the device was added to test the sample pH to further verify results and identify common falsified ingredients like aspirin or baking soda. Calibration curves for four different antibiotics, including cefazolin, have been generated making it the first paper-based device capable of detecting the purity of both cephalosporin and penicillin antibiotics. The μPAD has also been tested with common falsified ingredients and Augmentin antibiotics in tablet form, demonstrating its potential for in-field falsified antibiotic testing.

This work was accepted for publication in *ACS Sensors*.[1]

Introduction

The field of medicine was transformed with the advent of antibiotics in the early 20th century when doctors could start efficiently treating bacterial infections. However, antibiotics are only helpful to the patient if they are legitimate. Substandard and falsified drugs have become a serious worldwide problem recognized by the World Health Organization (WHO) and the International Police Organization (INTERPOL).[2-4] Despite serious efforts by these groups, per the Pharmaceutical Security Institute, the number of reported cases of drug counterfeiting increased over 10-times between the years 2002 and 2010.[5] Although this increase could be due to heightened awareness and monitoring efforts, it is impossible to know how many falsified drugs go undetected. While falsified drug sales are still prevalent in developed countries due to sales from online pharmacies, sales are the highest in developing countries, making the drugs difficult to track and detect.[6] The WHO estimates that up to 10% of drugs worldwide could be falsified, with 50% of these involving antimicrobials.[7] Falsified and substandard antibiotics often lead to treatment failure, increasing the chances of patient mortality.[8] In addition to increasing mortality, treatment failure also results in more patients receiving unnecessary broad-spectrum antibiotics, thereby contributing to the growing worldwide problem of antimicrobial resistance.[7] It is estimated that 5% of the global antibiotics market are falsifieded.[9] Of these antibiotics, β-lactams are the most commonly falsifieded, making up half of the falsified antibiotics in the world.[7]

The standard procedure to determine drug purity is via mass spectroscopy (MS) or high-performance liquid chromatography (HPLC).[10,11] However, it is difficult to test for drug purity in developing countries due to lack of access to these expensive

instruments. Consequently, drug efficacy is often determined by looking at the quality of packaging and labeling in resource-limited settings. Although legitimate pharmaceutical companies are putting more effort into their labeling to distinguish from falsified sellers, it is possible for counterfeiters to replace antibiotics in legitimate packaging.[12] To help combat this problem, the Global Pharma Health Fund manufactures the GPHF-Minilab® for in-field pharmaceutical ingredient analysis using thin-layer chromatography.[13] While a robust system that tests the authenticity of dozens of antibiotics and antimalarial drugs, it still requires an initial investment cost and trained personnel to operate, and is therefore not a system that could be used by laypersons.[14] Consequently, there is still a need for inexpensive and portable tests that can be used by untrained individuals for determining the purity of active pharmaceutical ingredients in antibiotics.

Microfluidic paper-based analytical devices (μPADs) have gained significant traction in the field of point-of-need diagnostics and detection methods for developing countries.[15] Paper is an attractive platform for point-of-need detection over other materials because of paper's natural ability to store reagents, fluid-wicking properties, and cost.[16] Because of these properties, there have been thousands of publications over the last decade demonstrating paper-based detection of metals, biomolecules, bacteria, and viruses in a large range of complex biological and environmental sample matricies.[17]

In 2013, Weaver et al. developed a μPAD for screening β-lactam antibiotics and antituberculosis pharmaceuticals to ensure purity.[18] While a promising system and an important step toward inexpensive in-field pharmaceutical analysis, the device is qualitative and primarily focuses on detecting common substitute pharmaceutical

ingredients and unapproved excipients. To test for the active ingredient of ampicillin and amoxicillin, the authors describe using copper (II) as a qualitative colorimetric indicator. This chemistry was also studied by Fernandez et al. for ampicillin and amoxicillin detection, but not for other β-lactam antibiotics.[19,20] Additionally, although 60% of falsified drugs contain no active ingredient, the remaining 40% involve variable amounts of active ingredient, rendering qualitative detection methods insufficient.[21] In 2014, Koesdjojo et al. reported a μPAD for detection of artesunate anti-malarial drugs that detected the active ingredient through the reaction of the active ingredient using fast red.[22] While this method provides excellent results for artesunate anti-malarials, it cannot be extended to common β-lactam antibiotics. Therefore, an inexpensive and portable device that can test for the universal purity of all β-lactam antibiotics in a quantitative capacity is still needed.

Nitrocefin is a chromogenic cephalosporin first reported in 1972 as a novel and straight-forward substrate used to detect bacteria resistant to β-lactam antibiotics.[23] Nitrocefin is hydrolyzed in the presence of β-lactamase, a bacterial enzyme that facilitates resistance against β-lactam antibiotics by hydrolyzing the β-lactam ring, deactivating the antibiotic. A distinct color change from yellow to red occurs after nitrocefin is hydrolyzed by β-lactamase, allowing for detection of the enzyme (Scheme 5.1). Nitrocefin was utilized in Chapter 3 of this document in the detection of antimicrobial resistant bacteria in environmental bacterial isolates and sewage water.

Applying the nitrocefin-β-lactamase reaction, we have developed a paper-based device that detects the presence of β-lactam antibiotics using an enzymatic competition assay. By dissolving the antibiotic in water and adding it to the device, the solution will

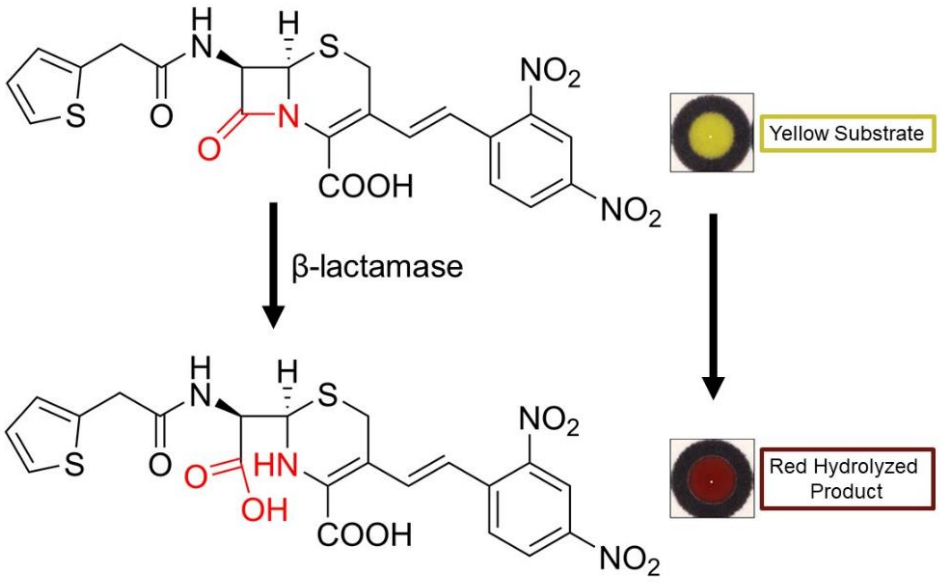

Scheme 5.1 | Reaction scheme for β-lactamase and nitrocefin, a chromogenic cephalosporin that turns from yellow to red upon hydrolysis.

rehydrate dried nitrocefin and travel to the detection zone containing deposited β-lactamase. If the antibiotics are present, they will compete in a concentration dependent manner for the β-lactamase active site with the dilute nitrocefin, resulting in little to no color change through the course of the measurement. If the antibiotics are falsified, the β-lactamase will react more quickly with nitrocefin as there will be no competition for the active site, turning the device red as an indication of falsified drugs (Scheme 5.2). To add further verification of the results, a second channel in the μPAD is used to determine pH, as some falsified agents strongly affect the resulting solution pH. This μPAD demonstrates the capability to distinguish between falsified and legitimate antibiotics using four different β-lactam antibiotics, including both penicillin and cephalosporin antibiotics. The detection motif has also been tested using Augmentin antibiotics in tablet form and six different common excipients and active ingredient

replacements found in falsified drugs. To the best of our knowledge, this is the first demonstration of an enzyme competition assay as a viable detection method in µPADs.

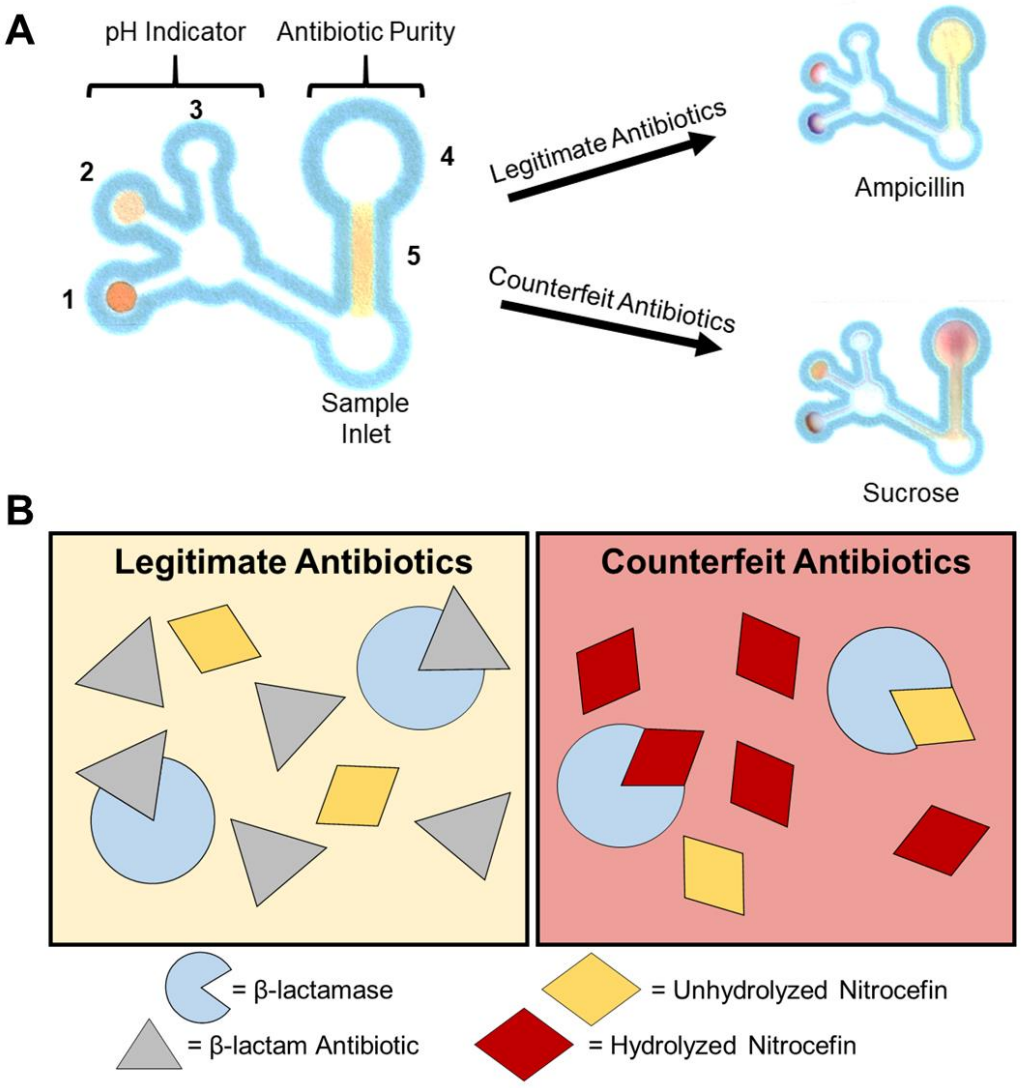

Scheme 5.2 | Falsified antibiotic detection method. **(A)** Final optimized antibiotic purity device with a pH Indicator region and Antibiotic Purity region. The pH indicator region contains bromophenol blue (1), phenol red (2), and phenolphthalein (3). The antibiotic purity region contains a detection zone with β-lactamase (4) and nitrocefin substrate (5). **(B)** Using enzyme competition as a detection motif. When antibiotics are legitimate, ampicillin will be present in the detection zone at a higher concentration compared to nitrocefin, therefore the device will stay yellow. When antibiotics are falsified, more nitrocefin will be present in the detection zone to react with β-lactamase, leading to a color change from yellow to red.

Materials and Methods

Proof of Concept Using Absorbance. Different ratios of ampicillin sodium salt [Ward's Science, >98% purity] and a constant concentration of nitrocefin [VWR International] were reacted with β-lactamase [Abcam, ab67672] in a 96-well plate and read using a Biotek Synergy 2 Plate Reader at 510 nm. 50 µL of 1 mM nitrocefin was mixed with 50 µL of ampicillin at concentrations 0.01, 0.1, 1, 10, and 100 mM. 100 µL of 1 Unit mL^{-1} β-lactamase was added to the mixture and allowed to react for 20 min, obtaining the absorbance every minute for kinetic results. The final graph (Figure 5.1) was developed using absorbances at 15 min into the assay reaction.

Paper-Based Device Fabrication and Data Analysis. The devices were designed using 3 point blue lines in CorelDRAW X4 with the following dimensions: a 8 mm diameter circle for the sample inlet; a 4 mm wide by 10 mm long rectangular channel and a 10 mm diameter circle for the detection zone of the antibiotic purity section; for the pH indicator section of the device, a 3.5 mm wide by 10 mm long channel leading to an 8 mm diameter circle that leads to each pH indicator arm; each arm is a 3 mm by 4.5 mm channel leading to a 5 mm diameter pH detection zone (Scheme 5.1A). Following design, the devices were printed on either Whatman chromatography paper grade 1 or grade 4 [GE Healthcare Sciences] using a ColorQube 8870 [Xerox] wax printer. To define hydrophobic barriers and direct sample flow, the devices were placed on an IsoTemp [Fisher Scientific] hot plate and covered with a metal plate at 165 °C for 90 s to allow the wax to melt through the paper pores. To prevent sample leakage, the back of the device was taped with Scotch Shipping Heavy

Duty packing tape. For “covered” devices, an additional packing tape layer was used to cover the entire device except for the sample inlet.

Before taping the µPADs, sections of the device were modified with different chemicals to enable different aspects of the assay (Scheme 5.1). For the antibiotic purity section, the channel was modified with 2 µL of nitrocefin solution and the detection zone was modified with 2.5 µL of β-lactamase solution. In the pH indicator section, the first detection zone was modified with 0.45 µL of bromophenol blue [EM Science]; the second detection zone was modified with two deposits of 0.35 µL of phenol red [Fluka Analytical]; and the third detection zone was modified with 0.40 µL of phenolphthalein [Flinn Scientific Inc.]. Why each pH indicator was selected is further explained in the discussion.

For using the devices, 35 µL of sample (deionized H_2O or varying concentrations of antibiotics) was added to the sample inlet and allowed to saturate and react with the device. 15 min following sample addition, devices were scanned as Tagged Image File Format (TIFF) documents using a Xerox Documate 3220 scanner. The images were analyzed using ImageJ [NIH] software by splitting the file into red, green, and blue color channels. The green channel was selected and inverted for analysis by using the circle tool to measure the color intensity of the detection zone in the antibiotic purity section of the device. The pH segment of the device was analyzed qualitatively by the user.

Paper-Based Device Optimization. Optimization experiments were carried out by adding 35 µL of sample (either dH_2O or 50 mg mL^{-1} ampicillin) and allowing the devices to react for 15 min before scanning and image analysis. Before paper

optimization, all substrate optimization experiments were carried out on covered Whatman 4 filter paper.

For β-lactamase concentration optimization, concentrations of 1, 5, 10, 25, 50, 75, and 100 U mL^{-1} was dried onto circular paper sample spots like the detection zone in the final antibiotic purity device, but without a channel and sample inlet. The β-lactamase solution was dried on paper either at room temperature (~22 °C) in the light, room temperature in the dark, or in a dark refrigerator at 4 °C. 40 µL of 0.5 mM nitrocefin in solution was added to the sample spot and allowed to react for 30 min before capturing an image. 30 min was chosen for maximum color response, because it is not time-dependent like the competition reaction. Because the devices were not covered, the image was captured using an Apple iPhone 5S Smartphone camera and a cardboard "light box" that has been described previously.[24] Image analysis was carried out as described above.

To determine ideal nitrocefin concentration, our final antibiotic purity device was used with 75 U mL^{-1} β-lactamase in the detection zone. 2 µL of nitrocefin at concentrations of 0.5, 0.75, 1, 2, 3, 5, and 7.5 mM were dried onto the channel of the microfluidic device. Both dH_2O and 50 mg mL^{-1} ampicillin were added to the device and reacted for 15 min. The color intensity between the two "samples" was compared.
For paper optimization, devices were made using both Whatman 1 and Whatman 4 chromatography paper. Whether the device should be covered with tape was also investigated by comparing devices with only the back taped to devices where both the back and top were taped except for the sample inlet. The devices were fabricated using

what was concluded to be the ideal concentrations of β-lactamase and nitrocefin, 75 U mL^{-1} and 3 mM respectively.

The pH range of the final optimized device was determined by adding buffers ranging from pH 4.5 to pH 10 in increments of 0.5 pH units and analyzing the color intensity of the detection zone. Phenol red and phenolphthalein in the pH indicator section of the device has been previously optimized and described by our lab (Ref). Bromophenol blue had not been previously optimized, but 0.45 µL of 1% solution deposited and dried at room temperature proved to provide ideal results.

Antibiotic Testing. In addition to ampicillin, calibration curves were also generated for amoxicillin sodium salt [Alfa Aesar, >88% purity), penicillin V potassium salt [Acros Organics, >99% purity], and cefazolin sodium salt [Chem Impex Int'l Inc., >93% purity] Calibration curves for four different antibiotics were generated using the final optimized device. For ampicillin, amoxicillin [Alfa Aesar], and penicillin V [Acros Organics], concentrations of 0.1, 0.2, 0.4, 0.6, 0.8, 1, 2, 4, 6, 8, and 10 mg mL^{-1} were used. Concentrations used for the calibration curve of cefazolin were 0.5, 1, 2, 4, 6, 10, 20, 30, 40, 50, 60, 80, and 100 mg mL^{-1}. All antibiotic solutions were dissolved in dH_2O to best mimic field conditions where buffer will not always be available. 35 µL of each antibiotic sample was added to the sample inlet of the device. Images were captured of the devices via scanner at 7.5 and 15 min after sample addition and analyzed as previously described. Images of the devices (Figure 5.10) with common antibiotics were generated by adding 50 mg mL^{-1} of antibiotic to the device and capturing the device image 15 min after sample deposition. All calibration curves used the units mg mL^{-1} instead of molarity because when testing real samples the user will not know how many

moles of antibiotic are supposed to be present, but the mass of active ingredient in milligrams is available.

Augmentin, a commonly prescribed pharmaceutical drug that contains amoxicillin and clavulanic acid, a β-lactamase inhibitor, was also tested. Because this antibiotic was in tablet form, the pill was crushed using a mortar and pestle until it was a fine powder. A solution of 10 mg mL^{-1} was made using the powder and vortexed, though not all the tablet's contents would completely dissolve in dH_2O. 35 µL of sample was deposited into the device and an image was captured after 15 min.

Stability of Nitrocefin and β-lactamase on Paper. Storage testing of β-lactamase and nitrocefin was performed on paper well plates. To create the wells, 7 mm diameter wax circles were printed onto either Whatman 1 or 4 paper. The paper well plates had 7 wells in each row, three sample wells and four blank wells to account for inconsistences in lighting across the row as previously described.[24] β-lactamase and Nitrocefin were dried onto each well in varying concentrations and volumes and stored in Ziploc bags at different temperature, lighting, and humidity's to optimize storage conditions. Stabilizing agents used for β-lactamase storage include, bovine serum albumin (BSA), sucrose, trehalose, dextrose, chitosan, poly(vinylsulfonic Acid sodium salt), and poly(diallyldimethylammonium chloride). Stabilizing agents used for nitrocefin include an acidic citric acid-disodium phosphate buffer ranging from pH 3 to 6 (0.1 M Citric Acid and 0.2 M Na_2PO_4 in varying volumetric ratios), benzene, acetone, acetonitrile, ethanol, and methanol.

To determine the enzymatic activity after a certain storage time, 20 µL of 0.5 mM nitrocefin was added to each well containing β-lactamase. To quantify the color change,

pictures of the well plate were taken 30 min after nitrocefin addition. All pictures were taken with a Samsung Galaxy S7 Smartphone using the phone's flash and a light-box to remove ambient light. Images were processed using ImageJ as previously described with mean color intensity used to quantify β-lactamase activity. All enzyme activity experiments were performed at room temperature. To determine the viability of nitrocefin dried on paper, 20 U/mL β-lactamase was added to each well containing dried nitrocefin and the same process described above was followed to ascertain the stability of the substrate after storage. For the nitrocefin study only, an additional picture was taken before the β-lactamase was added to observe any degradation of nitrocefin over time. Different storage conditions included room temperature constantly exposed to light, room temperature in the dark, 37 °C in the dark, and storage in a dark 4 °C refrigerator.

Testing Common Drug Replacements. Selected falsified ingredients included gelatin [Ward's Science], sodium bicarbonate [Ward's Science], acetylsalicylic acid [Sigma Aldrich], sucrose [Fisher Scientific], D-(+)-lactose [J. T. Baker Chemical Co.], and calcium carbonate [Fisher Scientific]. 50 mg mL^{-1} solutions were made of each falsified replacement and dissolved (to varying degrees) in dH_2O. As previously described with antibiotic samples, 35 µL of sample was deposited onto the device and an image was captured 15 min later. The image underwent the same image analysis as previously described.

Blind Testing. Someone unfamiliar with the devices was selected to analyze six blinded 10 mg mL^{-1} samples. The user was provided with an image key for what the device should look like if the samples were legitimate or falsified (Figures 5.10 and 5.11)

and a pH indicator key of how several common drug replacements would show up on the pH indicator (Figure 5.12). The user was told which antibiotic each sample was supposed to represent and was given instructions on pipetting and reading the device. After 15 min, the user identified each sample as either legitimate or falsified.

Results and Discussion

Enzyme Competition: Proof of Concept. Before designing the μPAD, an enzyme competition assay in solution was studied to determine if it was a viable detection motif for β-lactam antibiotics. To confirm this idea, concentrations of ampicillin, a commonly falsifieded β-lactam antibiotic,[7] ranging from 0.01 to 100 mM was mixed with a constant concentration of nitrocefin. This mixture of nitrocefin and ampicillin was reacted with β-lactamase in a 96-well plate and the results were analyzed with a plate reader at an absorbance of 510 nm after 15 min of reaction. Molar ratios ranged from 1:100 to 100:1 of ampicillin to nitrocefin, and the absorbance at the λ_{max} of the red hydrolyzed nitrocefin decreased as the concentration of ampicillin increased (Figure 5.1), demonstrating enzyme competition as a viable method for antibiotic detection.

Paper-Based Microfluidic Device Optimization. While using a plate reader for absorbance is a reliable and quantifiable method for determining ampicillin concentration relative to nitrocefin, it requires the use of expensive and non-portable instrumentation. There are inexpensive, portable spectrophotometers available, however, these instruments can exceed $3000 USD and require multiple solutions to complete the test.[25] The ideal detection system could be used by someone with little training and without any external instruments or solutions beyond the sample. Using a

μPAD format, these requirements can be achieved. Using paper's ability to store reagents and natural fluid-wicking properties,[26] a device was conceived where the user would simply add sample and wait 15 min to see if a color change occurs (Scheme 5.1A). Nitrocefin was stored in the channel of the antibiotic purity section of the device, which leads to a detection zone where β-lactamase is stored. Thus, when the user adds sample, the fluid wicks down the channel, rehydrating and transporting the stored nitrocefin to the detection zone to react with β-lactamase. If the user's sample contains antibiotic, it should be present at a higher concentration relative to nitrocefin, therefore β-lactamase will react with the antibiotic and the device will stay yellow. However, if the user's sample is falsified and does not contain the active antimicrobial ingredient, nitrocefin will be the dominant substrate in the system for β-lactamase to hydrolyze, resulting in a distinct color change from yellow to red (Scheme 5.1B).

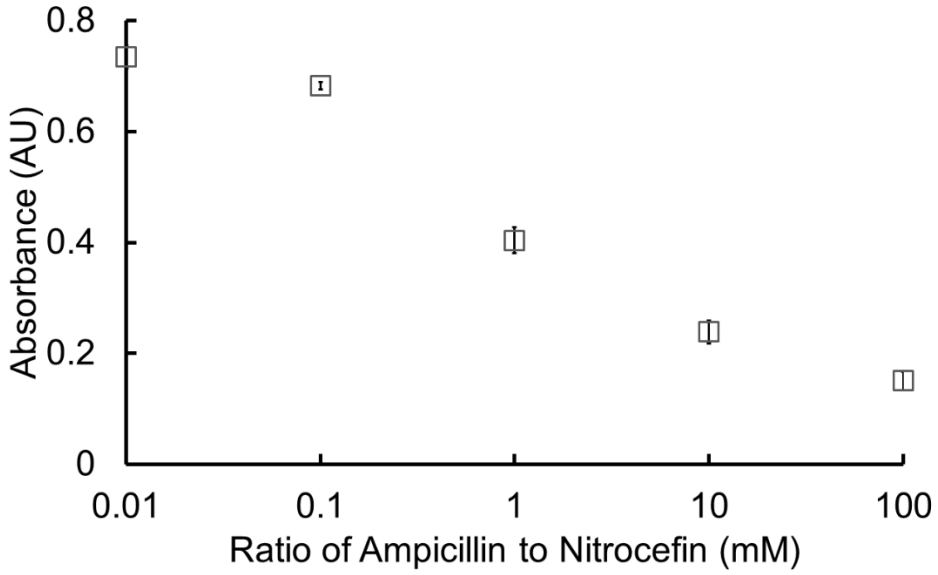

Figure 5.1 | Using spectrophotometry as a proof-of-concept to demonstrate when more ampicillin is present compared to nitrocefin, β-lactamase will choose to react with ampicillin more often, leading to less hydrolysis of nitrocefin, therefore less color change. (n =3)

Several aspects of the device were optimized, including β-lactamase and nitrocefin concentration (Figure 5.2). To optimize β-lactamase on the device, concentrations varying from 1-100 U mL^{-1} were dried onto simple circular devices in various conditions (Figure 5.2A). Concentrations lower than 75 U mL^{-1} did not give as intense of a color change, and higher concentrations did not increase color intensity. Drying the enzyme on paper at 4 °C gave the best results compared to drying at room temperature (~22 °C), likely due to enzymes being more stable at lower temperatures while in solution. Nitrocefin concentration was optimized using the antibiotic purity section of the device by drying nitrocefin of varying concentrations (0.5-7.5 mM) in the channel (Figure 5.2B). Unlike β-lactamase optimization, the color intensity was measured for no antibiotic (representing falsified antibiotics) and a high concentration of ampicillin (representing legitimate antibiotics). The difference between the color intensity of the falsified and legitimate samples was calculated to determine the concentration of nitrocefin that could most effectively distinguish between the two samples. As observed in Figure 5.2B, the contrast between legitimate and falsified antibiotics increased until 3 mM when the gap started to close again. Although the color intensity was high for falsified antibiotics using higher concentrations of nitrocefin, the color intensity increased for legitimate antibiotics after 3 mM (Figure 5.2B). This discrepancy could be due to two different reasons. As we have previously reported, higher concentrations of non-hydrolyzed nitrocefin tend to appear more red than a diluted sample before hydrolysis,[27] which likely leads to more red in the detection zone when using a high concentration of nitrocefin. Secondly, because this is an enzyme competition assay, increasing nitrocefin concentration leads to more competition with antibiotic present in

the sample, hence β-lactamase will statistically react with nitrocefin more often than with a lower concentration of nitrocefin.

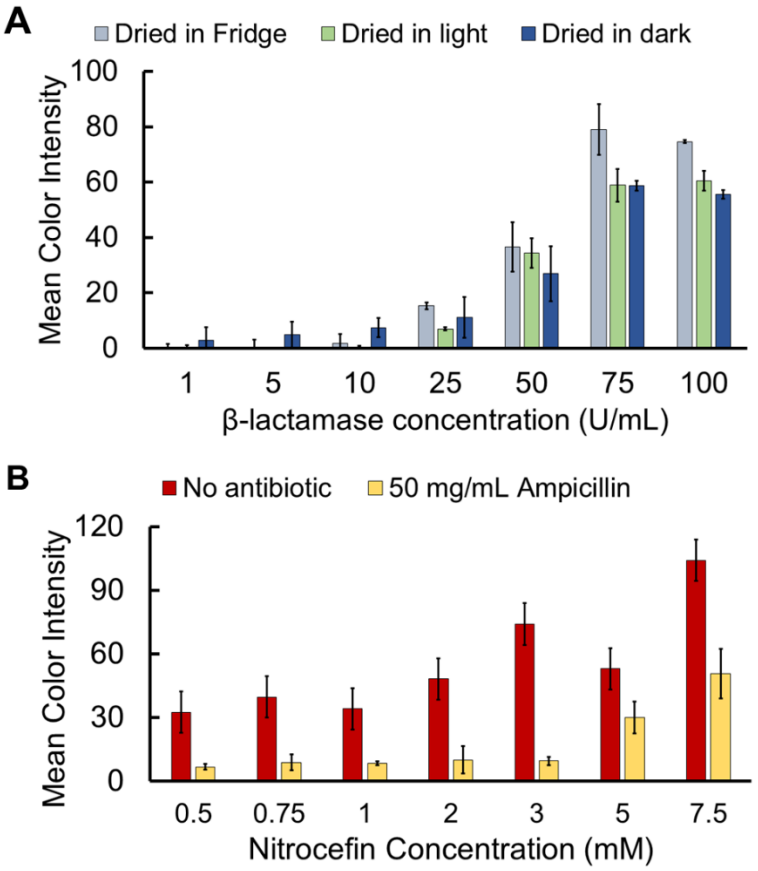

Figure 5.2 | Optimization of substrates for the µPAD. **(A)** Optimization of concentration and drying method for β-lactamase, the detection enzyme. **(B)** Nitrocefin concentration optimization based on net color change between a no antibiotic and a high concentration of antibiotic. (n = 3)

In addition to optimizing reagent concentrations and drying conditions, there are several kinds of paper that can be used for µPADs (Figure 5.3A). Because of their widespread use and inexpensive materials, we limited this study to Whatman chromatography paper grade 1 and grade 4. Additionally, paper-based devices can be open to the environment or taped or laminated to protect the reagents present on the device. Because this device includes enzymes deposited on the paper, lamination was

eliminated due to the potential for high temperatures to denature the enzymes. Devices fabricated with Whatman 1 paper and taped on both the bottom and top delivered the best reaction and were used for the final device (Figure 5.3A). Devices that were taped on the top and bottom of the device likely performed better due to decreased sample evaporation, along with slower and more controlled flow. Whatman 1, which has smaller pores relative to Whatman 4, also performed better, supporting the hypothesis that slower flow increases reaction efficiency. Slow and controlled flow likely allows the sample to rehydrate more nitrocefin to react with β-lactamase in the detection zone, resulting in a more noticeable color change when falsified antibiotics are detected.

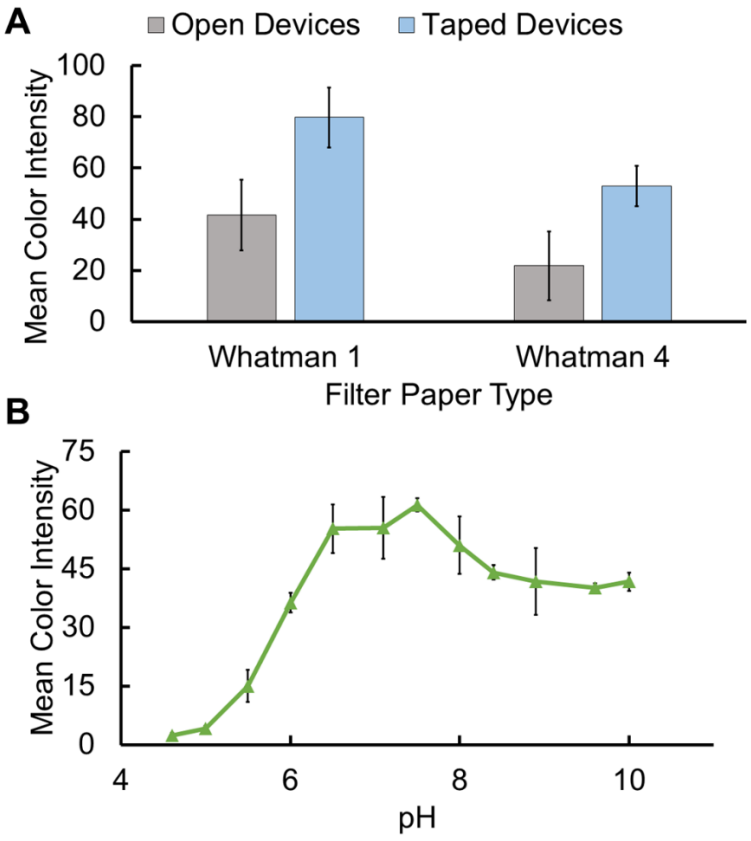

Figure 5.3 | Additional optimization of µPAD. **(A)** Determining ideal paper to use and whether the device should be taped on bottom only or top and bottom. **(B)** Working pH range of final optimized device. (n = 3)

Because the enzymatic reaction between nitrocefin and β-lactamase is pH dependent,[27] it is important to verify the pH range at which this device can operate. Therefore, we added buffers to the device ranging in pH between 4.5 and 10 (Figure 5.3B and 5.4A). The device works optimally between pH 6.5 and pH 8, and does not work at acidic pHs. Although the device does not work as well at a pH above 8, it does not entirely stop working like it does in acidic pH conditions. In basic conditions the hydrolysis of nitrocefin can still take place with a hydroxide ion rather than a water molecule. In fact, the hydrolysis is more favorable in basic conditions because hydroxide is more nucleophilic than water (Figure 5.4B). The increased rate of hydrolysis in alkaline solutions offsets the decrease in enzyme activity expected at high pH's. The opposite is true in acidic solutions, which is why we observe lower signals.

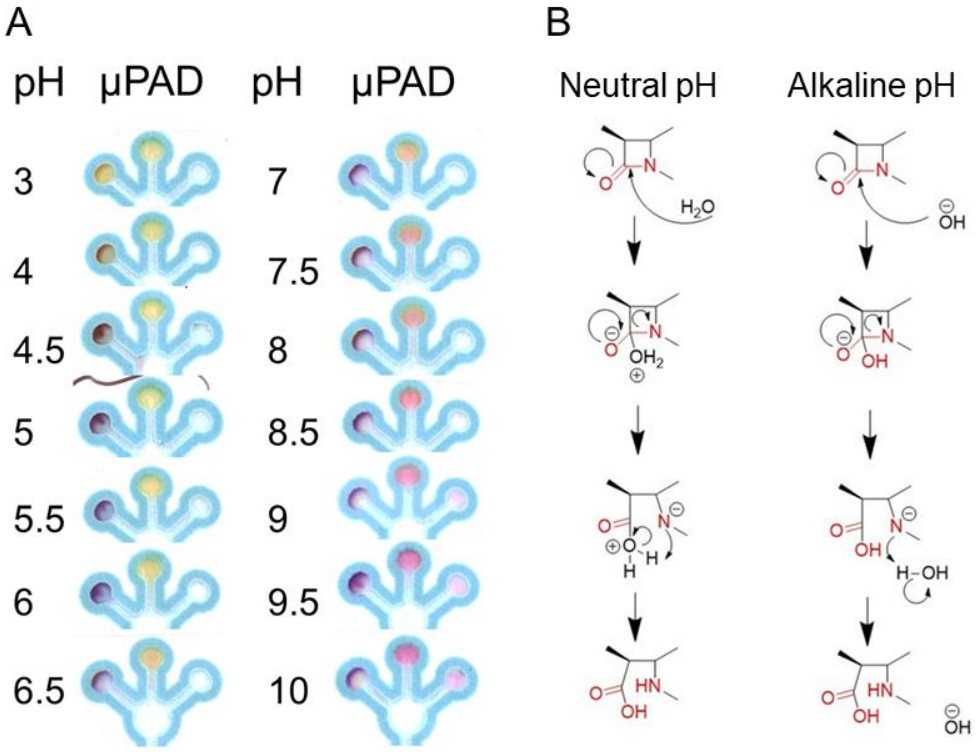

Figure 5.4 | **(A)** Proposed mechanism for hydrolysis of nitrocefin via H_2O or OH^-. **(B)** The pH indicator region of the μPAD at different pH buffers.

Stability of Nitrocefin and β-lactamase on Paper. Most falsified antibiotics are found in resource-limited settings where storage options are limited.[5] Therefore, it is important to determine the most effective way to store the device without reagent degradation. A study by Nery et al. examined 33 different stabilizing agents used to increase shelf-life of glucose oxidase stored on paper.[28] We chose five of the most successful and facile stabilizing methods from this paper for use with β-lactamase and found that BSA blocking of the paper had the most significant impact on storage ability (Figure 5.5).

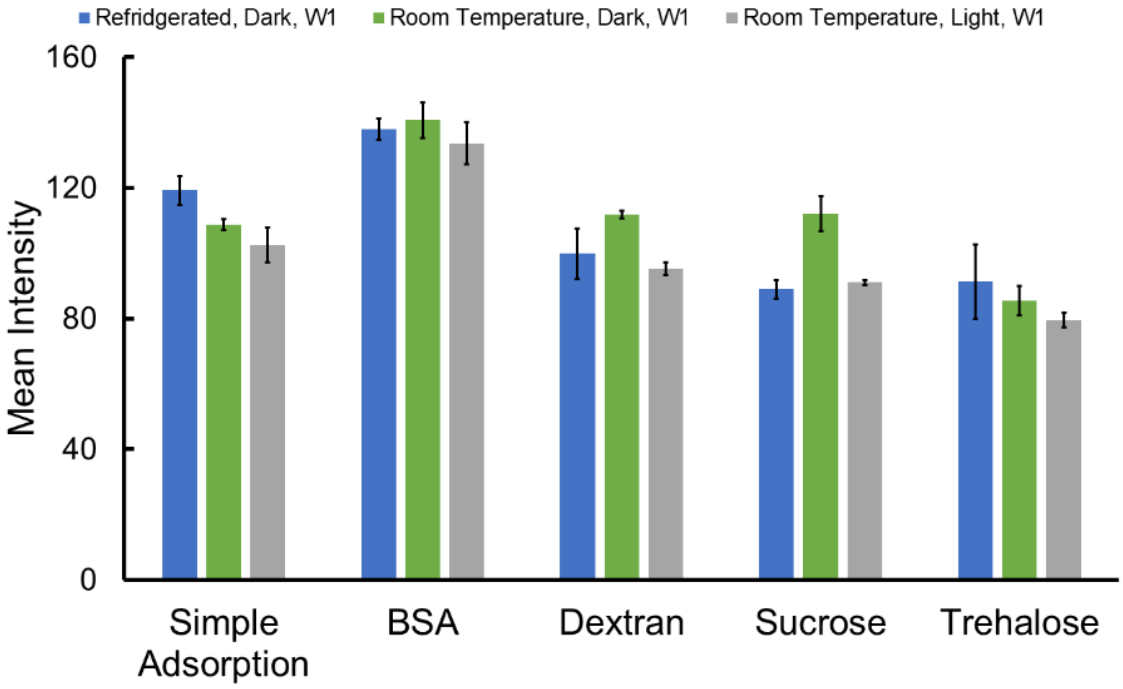

Figure 5.5 | Five different stabilizing methods and/or reagents were used to store β-lactamase on Whatman 1 filter paper in three different storage conditions. All samples were stored in their respective storage conditions for two weeks.

As previously theorized by Ramachandran et al. and others, we believe the BSA binds to the paper thereby decreasing the loss of enzyme to adsorption in an inactive

form.[29] We also theorize that the BSA forms a protective coating that shields the β-lactamase from agents that can affect activity. In addition to selecting a stabilizing agent, we also optimized the paper used as a substrate for storage. We found that Whatman 1 filter paper increased shelf-life of β-lactamase over Whatman 4, nitrocellulose, and polyethersulfone. When BSA was used to stabilize β-lactamase on Whatman 1 filter paper, the enzyme showed no decrease in activity over three months at room temperature and retained >80% of its activity after one year of storage (Figure 5.6).

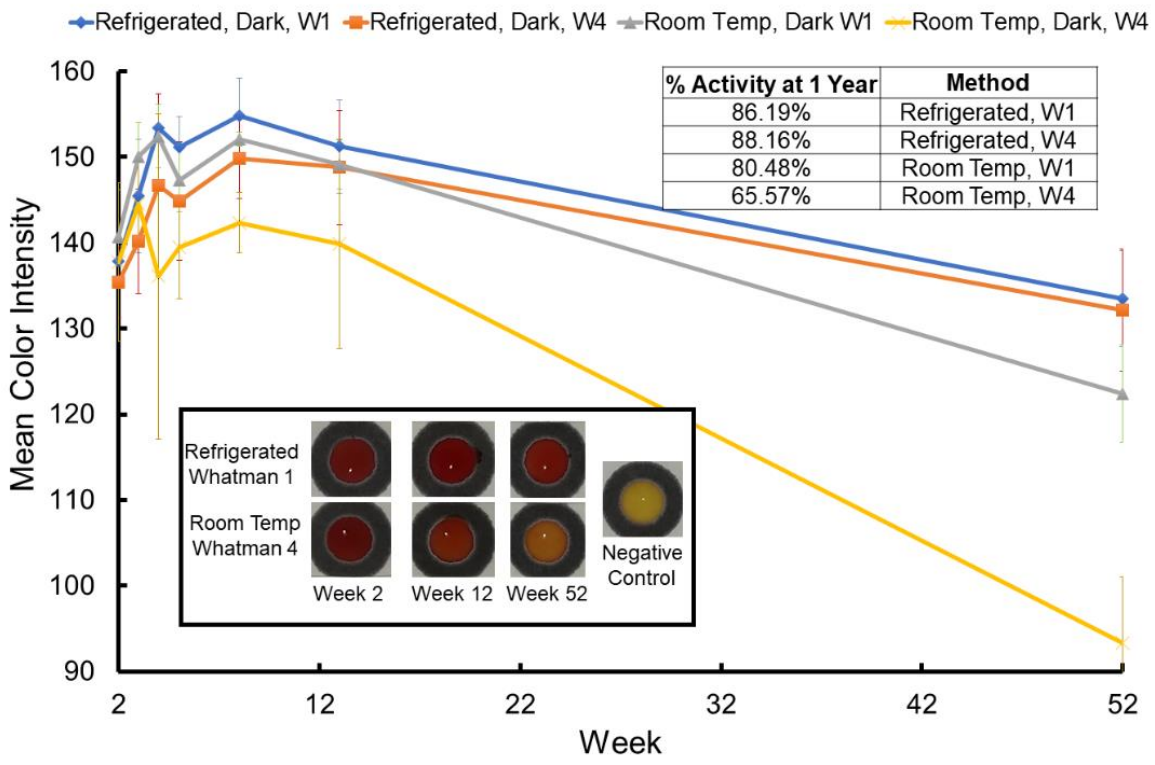

Figure 5.6 | Activity of β-lactamase over 52 weeks in four different storage conditions. Variable results in weeks 2 – 4 are the result of old nitrocefin and inconsistencies in photographic methods.

Nitrocefin proved more difficult to stabilize. At room temperature, nitrocefin degraded to its red hydrolyzed form in two days, rendering it useless for the assay. As the degradation mechanism is a hydrolysis, we attempted to keep the device water-free by drying the paper, diluting the nitrocefin in organic solvents, vacuum sealing the device, and storing with desiccant. Unfortunately, these efforts only increased the effective shelf life of nitrocefin on paper to roughly one week. To store nitrocefin for more than one week, the device must be stored in a refrigerator to slow or stop the degradation through hydrolysis. When stored at 4 °C, the nitrocefin was stable for at least 4 weeks (Figure 5.7).

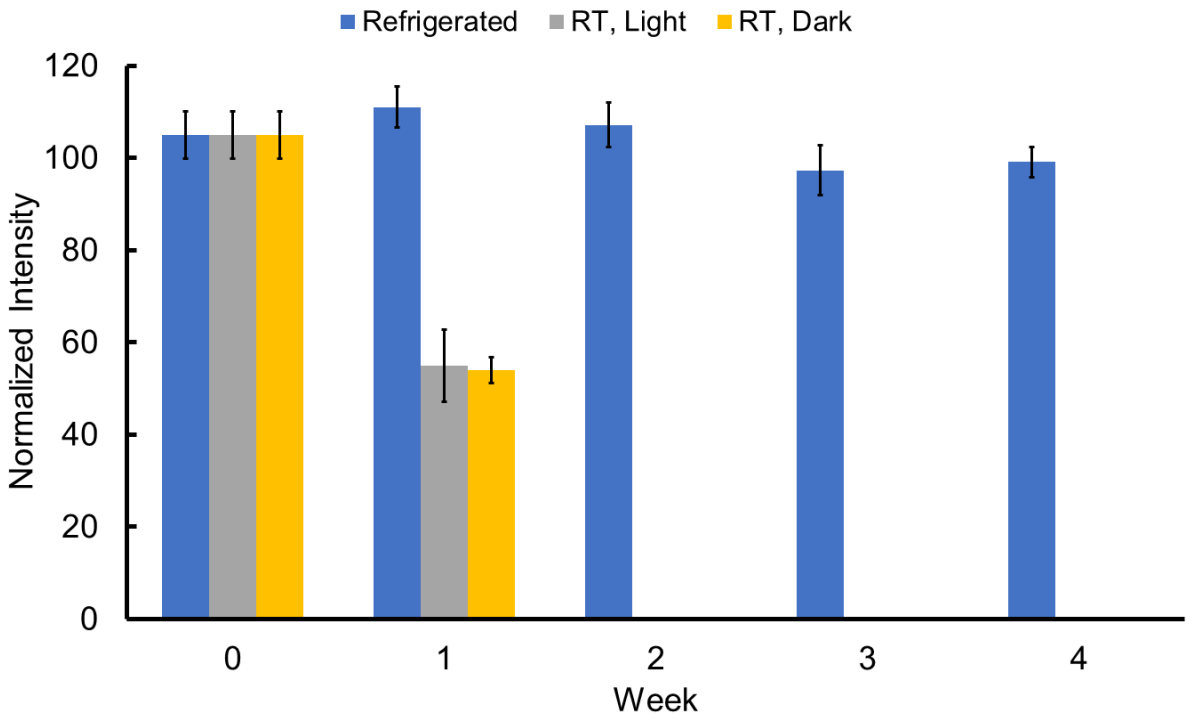

Figure 5.7 | Activity of nitrocefin over 4 weeks in different storage conditions. Nitrocefin should not be stored outside the refrigerator or it will degrade to it's red, hydrolyzed form less than three days.

µPAD for Testing Antibiotic Purity. As previously mentioned, β-lactam antibiotics are one of the most falsifieded drugs on the market. Of the β-lactam antibiotics, ampicillin and amoxicillin are two of the most common targets of falsified drug manufacturers. However, it is important to establish whether this method can be used universally across many β-lactam drugs. In addition to amoxicillin and ampicillin, the device was tested with penicillin V and cefazolin (Figure 5.8). Although not in the class of penicillin drugs, cefazolin is still a β-lactam antibiotic in the class of cephalosporins.

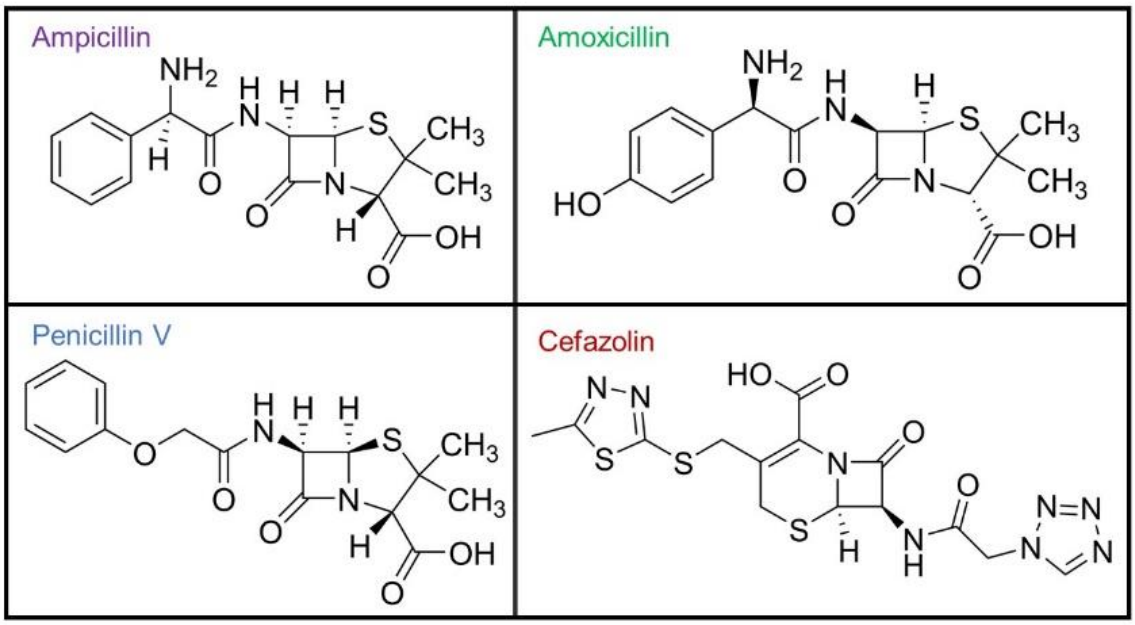

Figure 5.8 | Structures of four different β-lactam antibiotics used to demonstrate µPAD.

When completing the enzyme competition assay in the 96-well plate and measuring the absorbance, a linear trend between color intensity and antibiotic concentration was observed, indicating that the system could be quantifiable. Calibration curves were established for all tested antibiotics using the completed µPAD (Figures 5.9 and 5.10)

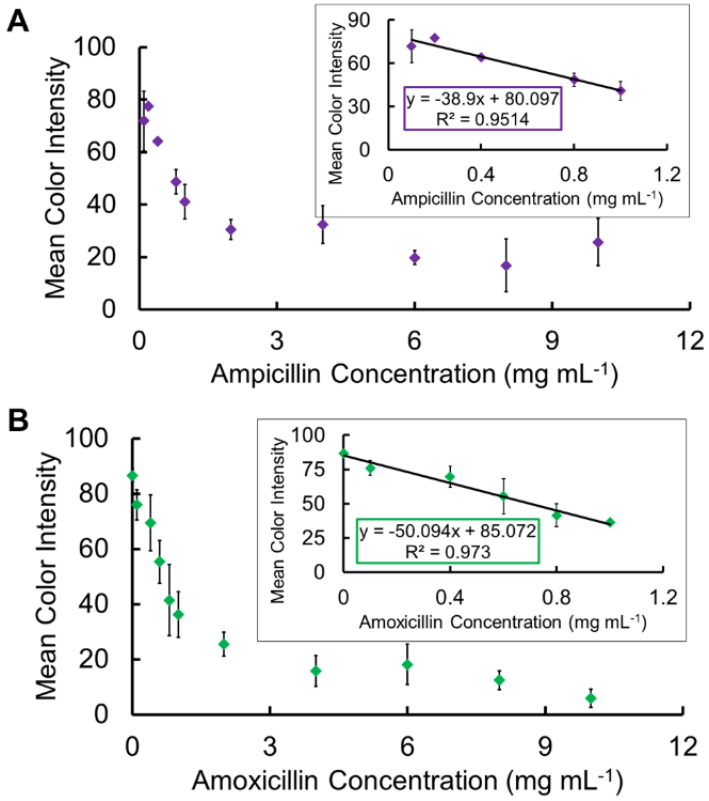

Figure 5.9 | Calibration curves of common antibiotics including **(A)** Ampicillin (m error = 4.75, b error = 2.64) **(B)** Amoxicillin (m error = 4.17, b error = 2.51)

All four antibiotics showed the general trend of a linear region that levels off at higher antibiotic concentrations (2 mg mL^{-1} for penicillin antibiotics and 20 mg mL^{-1} for cefazolin). The curves show a negative trend because we are measuring the red intensity of nitrocefin hydrolyzation. The more antibiotic present, the less nitrocefin will hydrolyze, resulting in lower red intensity. Amoxicillin showed the greatest sensitivity with a slope of -50 mL mg^{-1}, while ampicillin and penicillin V showed similar sensitivities with slopes of -39 and -40 mL mg^{-1} respectively (Figure 5.9 and 5.10A). Although cefazolin did eventually quench the reaction of nitrocefin and β-lactamase, it showed an order of magnitude less sensitivity compared to penicillin antibiotics with a slope of -4.0 mL mg^{-1} (Figure 5.10B).

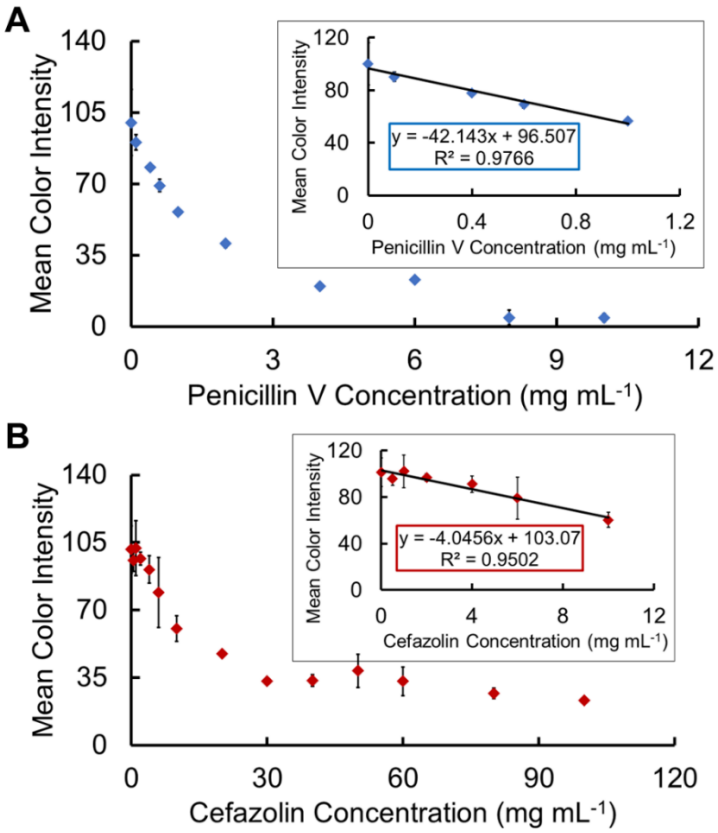

Figure 5.10 | Calibration curves of common antibiotics including **(A)** Penicillin V (m error = 3.77, b error = 2.08) and **(B)** Cefazolin (m error = 0.41, b error = 1.96). (n = 3)

This decrease in sensitivity could be due to β-lactamase having a decreased sensitivity with cephalosporin antibiotics compared to penicillin antibiotics. To the best of our knowledge, direct evidence of β-lactamase displaying lower sensitivity to cephalosporins compared to penicillin antibiotics has not been published. However, varying enzyme coefficients for different substrates has been reported,[30] suggesting that enzymes can have different sensitivities for different substrates. Not only can nitrocefin be used to colorimetrically detect the purity of different antibiotics, but we could also calculate Michaelis-Menten kinetics colorimetrically. This will be completed in future work to confirm our hypothesis of our selected β-lactamase having lower sensitivity toward cephalosporin antibiotics as compared to penicillin antibiotics. Additionally,

cefazolin has a molecular weight of 454.5 g mol^{-1} compared to amoxicillin and penicillin which have lower molecular weights at 365.4 and 334.4 g mol^{-1} respectively. The difference in size equates to fewer moles of cefazolin in the same mg mL^{-1} antibiotic concentration, thus a lower molar ratio relative to nitrocefin. Larger molecular size could also lead to steric hindrance when reacting with β-lactamase, leading to decreased kinetics. Despite decreased sensitivity, the μPAD can still be used to detect falsified cephalosporin β-lactam antibiotics. The user would simply need to dissolve more sample in water compared to penicillin antibiotics.

To determine if these calibration curves can identify substandard antibiotics, we used the error of the slope and the Y-intercept of the calculated linear regression. Assuming the user dissolves 1 mg mL^{-1} of ampicillin, amoxicillin, and penicillin V, and 10 mg mL^{-1} of cefazolin, these devices are capable of distinguishing between 70% API (or 65% for ampicillin) and 100% API. Although the ideal system could confidently distinguish between 90% API and 100% API, this still offers better quantitative abilities than any other inexpensive field test currently available. The confidence could likely be increased by implementing reagent printers to eliminate device-to-device variability that is likely currently in place due to fabricating the devices by hand. Decreasing the error associated with the linear regression line will be the subject of future work and optimization. The μPAD was also used to determine the purity of an antibiotic in tablet form. Antibiotic tablets never contain 100% antibiotic as there are always some form of pharmaceutical excipients present. Excipients, which are defined as any non-active ingredient present in the tablet, are added for a variety of reasons including to stabilize and/or preserve the active ingredient.[31] Therefore, it is important to confirm this method

works even when the antibiotic is in the presence of pharmaceutical excipients. The device was tested with Augmentin, a commonly prescribed antibiotic that contains amoxicillin and clavulanic acid. At a concentration of 10 mg mL^{-1}, the device verified the antibiotic as pure (Figure 5.11), although this was not confirmed by conventional methods. A concern for this method is the use of an enzymatic reaction using β-lactamase, which can be inhibited by clavulanic acid, a well-known β-lactamase inhibitor. However, we do not believe this should be a concern for this device as clavulanic acid is not a common falsifieding ingredient. Common falsified ingredients tend to be cheap and accessible, and clavulanic acid is neither. Additionally, clavulanic acid is an acid and should therefore be detected using the pH indicators in the second portion of the device.

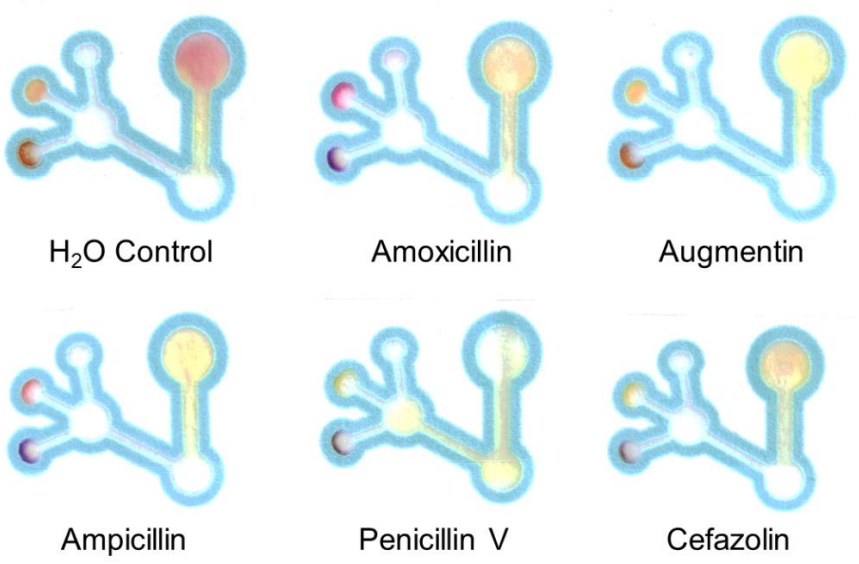

Figure 5.11 | Comparing full microfluidic device reacted with a dH_2O control and 50 mg mL^{-1} of amoxicillin, ampicillin, penicillin V, and cefazolin; and 10 mg mL^{-1} of Augmentin.

Testing Common Drug Replacements. Many ingredients are used as replacements for active ingredients in falsified drugs and it is important to verify the

method still works with a variety of the most common replacement ingredients. An extensive list of materials can be used in place of the active ingredient, which makes it impossible to test for all falsified ingredients. For this study, we have limited our tested falsifieds to ingredients that are more common in falsified drugs, such as chalk and sugar, and ingredients we believe would interfere with the assay.[32,33]

As previously discussed, this assay is dependent on pH, so a pH indicator section was added to the device in addition to the antibiotic purity device component. The pH indication zone can alert the user when the assay is at an acidic or alkaline pH, suggesting the drug may be tampered. Three pH indicators were chosen, including bromophenol blue (Scheme 5.2A-1) to indicate an acidic pH (below pH 4.5), phenolphthalein to indicate an alkaline pH (Scheme 5.2A-3) above pH 8.5, and phenol red (Scheme 5.2A-2) was added to system for the user to indicate the pH between 6 and 8.

To determine whether antibiotics could be distinguished from falsified ingredients outside the working pH range, acidic and alkaline ingredients were tested. Acetylsalicylic acid (aspirin) and sodium bicarbonate (baking soda) were chosen because of their extreme pH values as well as their use in falsified drugs.[34,35] As expected, using aspirin in the device resulted in a false positive (no color change) due to its acidic pH (Figure 5.12). However, the pH indicators show an acidic pH with phenol red turning yellow, and bromophenol blue turning light brown on its way to yellow. The indicators suggest a pH around 4, which is below the device's working pH range and correctly identifies the antibiotic as falsified without the hydrolysis of nitrocefin. Baking soda on the other hand did show some color change in the detection zone indicating a

falsified drug while also indicating an alkaline pH as phenolphthalein turned pink. The only concern with the pH indicator method resides in the fact that antibiotics can also impact pH (Figure 5.12 and 5.13). However, pure amoxicillin displayed an alkaline-leaning pH, while its counterpart in tablet form, Augmentin, displayed a neutral/slightly acidic pH. This is likely due to clavulanic acid and pharmaceutical excipients, which can often act as pH stabilizers. To the best of our knowledge, pH variabilities in antibiotics in tablet form has not been published, therefore, this is an area that would need extensive optimization in future work.

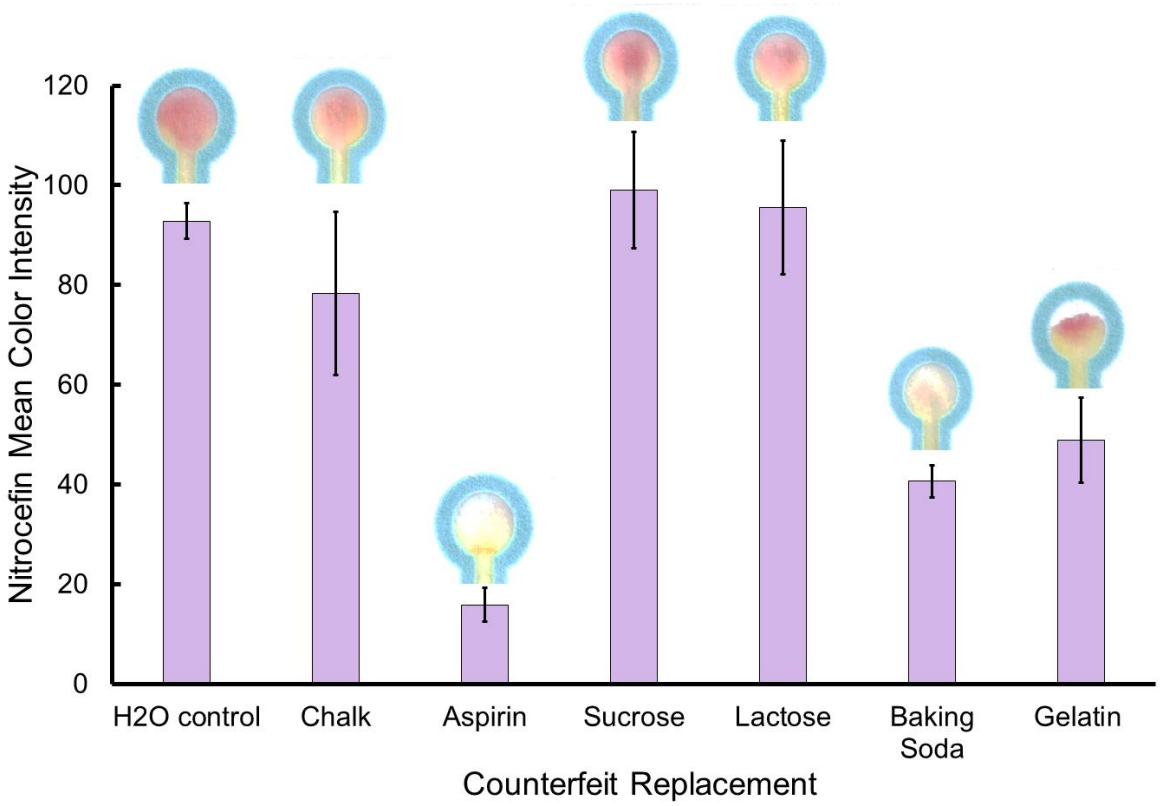

Figure 5.12 | To determine whether common drug replacements interfere with the µPAD, six different drug falsified ingredients were tested with the device.

In addition to baking soda and aspirin, other common replacements such as chalk, sugar (sucrose and lactose), and gelatin were also tested. Likely because of their

lack of solubility in water, chalk and gelatin tested falsified using the device. Gelatin created a viscous solution, so it did not completely saturate the device (Figure 5.12), but the section of the device it did saturate turned red, indicating falsified. Sucrose and lactose also tested falsified.

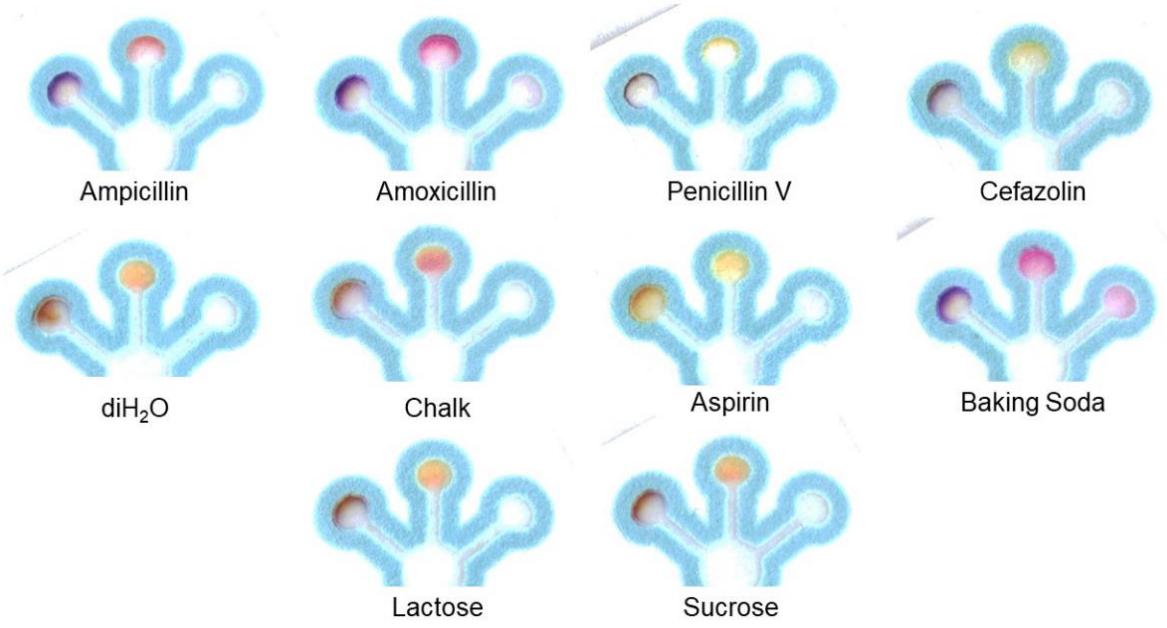

Figure 5.13 │ The pH of each antibiotic and different common excipients using the pH indicator portion of the µPAD.

Blind Testing. For this device to be used by the general population, it is important to confirm that it can be used by individuals who have not been trained and are not as familiar with µPADs. Six blind samples were given to a new user and labeled as the “supposed” antibiotic. The user was provided with Figures 5.11, 5.12, and 5.13 as a key for comparison of the completed test so the user could assess the assay results. The user then pipetted the samples into the device, waited 15 min, and concluded whether the sample contained legitimate or falsified antibiotics. Without bias,

the users correctly identified 29/32 blind samples (Figure 5.14), indicating an easy-to-read and user-friendly test to identify most falsified antibiotics. The primary blind sample that was most difficult to identify was acetylsalicylic acid when labeled as cefazolin, likely due to both having a similar initial pH and acetylsalicylic acid not turning as red as other counterfeit ingredients. Being able to accurately distinguish these two antibiotics will be the subject of future research and optimization.

Sample Name	Sample Contents	User Conclusion (Qualitative)	Test Image
Ampicillin "A"	100% Ampicillin	Legitimate	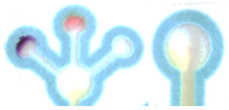
Ampicillin "B"	Lactose	Counterfeit	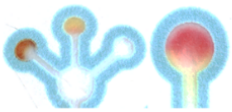
Amoxicillin "A"	Sodium Bicarbonate	Counterfeit	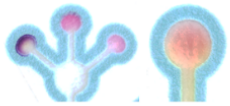
Amoxicillin "B"	100% Amoxicillin	Legitimate	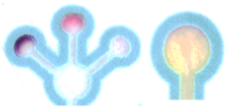
Penicillin "A"	Acetylsalicylic Acid	Counterfeit Legitimate	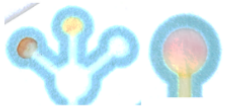
Penicillin "B"	100% Penicillin V	Legitimate	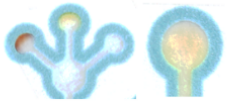
Cefazolin	100% Cefazolin	Legitimate	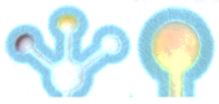

Figure 5.14 | Six different blind samples were given to a new user to test on the device and conclude whether the sample is legitimate or falsified. 6/6 samples were guessed correctly.

Conclusions

A μPAD that can distinguish between falsified and legitimate β-lactam antibiotics has been developed using an enzyme competition assay. The μPAD tested the quality of five different β-lactam antibiotics, including cephalosporins, something that has not been demonstrated on a paper-based device. The detection of antibiotics in tablet form demonstrates its potential for real-world analysis. This work is also the first demonstration of enzyme competition as a viable detection method for μPADs. The current approach detects falsified antibiotics qualitatively by visual inspection, which is very important for field detection as over half of falsified drugs contain no active ingredient. However, it has been reported that drug counterfeiters are manufacturing antibiotics with around 20% of the advertised active ingredient. Low quality antibiotics like these are likely to bypass some of the detection systems in place,[10] so a portable quantitative system that can distinguish low levels of active ingredient from no active ingredient would be an important tool for global monitoring efforts. The described μPAD has shown quantitative properties as demonstrated by the calibration curves generated for four different antibiotics. In future work, a portable system to quantify the color intensity of the device could be optimized, such as a cell phone application. When combining the μPAD with a portable system to quantify color, it has the potential to be an inexpensive and practical in-field device to detect both falsified and substandard antibiotics.

REFERENCES

(1) Boehle, K. E.; Carrell, C. S.; Caraway, J.; Henry, C. S. *ACS Sens* **2018**, *Just Accepted Manuscript*.
(2) Global Surveillance and Monitoring System for Substandard anf Falsified Medical Products, World Health Organization, **2017**.
(3) Pharmaceutical Crime and Organized Criminal Groups, INTERPOL, **2014**.
(4) Counterfeit Drugs: Guidlines For the Development of Measures to Combat Counterfeit Drugs, World Health Organization, **1999**.
(5) Degardin, K.; Roggo, Y.; Margot, P. *J. Pharm. Biomed. Anal.* **2014**, *87*, 167-175.
(6) Mackey, T. K.; Liang, B. A. *J. Pharm. Sci.* **2011**, *100*, 4571-4579.
(7) Kelesidis, T.; Falagas, M. E. *Clin. Microbiol. Rev.* **2015**, *28*, 443-464.
(8) A Study on the Public Health and Socioeconomic Impact of Substandard and Falsified Medical Products, World Health Organization, **2017**.
(9) Delepierre, A.; Gayot, A.; Carpentier, A. *Med. Mal. Infect.* **2012**, *42*, 247-255.
(10) Fernandez, F. M.; Cody, R. B.; Green, M. D.; Hampton, C. Y.; McGready, R.; Sengaloundeth, S.; White, N. J.; Newton, P. N. *ChemMedChem* **2006**, *1*, 702-705.
(11) Fadeyi, I.; Lalani, M.; Mailk, N.; Van Wyk, A.; Kaur, H. *Am. J. Trop. Med. Hyg.* **2015**, *92*, 87-94.
(12) Deisingh, A. K. *Analyst* **2005**, *130*, 271-279.
(13) Jahnke, R. W. O.; Kusters, G.; Fleischer, K. *Ther. Innov. Regul. Sci.* **2001**, *35*, 941-945.
(14) Bate, R.; Tren, R.; Hess, K.; Mooney, L.; Porter, K. *Afr. J. Pharm. Pharmacol.* **2009**, *3*, 165-170.
(15) Martinez, A. W.; Phillips, S. T.; Whitesides, G. M. *Anal. Chem.* **2010**, *82*, 3-10.
(16) Cate, D. M.; Adkins, J. A.; Mettakoonpitak, J.; Henry, C. S. *Anal. Chem.* **2015**, *87*, 19-41.
(17) Yang, Y.; Noviana, E.; Nguyen, M. P.; Geiss, B. J.; Dandy, D. S.; Henry, C. S. *Anal. Chem.* **2017**, *89*, 71-91.
(18) Weaver, A. A.; Reiser, H.; Barstis, T.; Benvenuti, M.; Ghosh, D.; Hunckler, M.; Joy, B.; Koenig, L.; Raddell, K.; Lieberman, M. *Anal. Chem.* **2013**, *85*, 6453-6460.
(19) Fernandez-Gonzalez, A.; Badia, R.; diaz-Garcia, M. E. *Anal. Chim. Acta* **2003**, *484*, 223-231.
(20) Fernandez-Gonzalez, A.; Badia, R.; diaz-Garcia, M. E. *Pharm. Biomed. Anal.* **2002**, *29*, 669-679.
(21) Wertheimer, A. I.; Norris, J. *Res. Social Adm. Pharm.* **2009**, *5*, 4-16.
(22) Koesdjojo, M. T.; Wu, Y.; Boonloed, A.; Dunfield, E. M.; Remcho, V. T. *Talanta* **2014**, *130*, 122-127.
(23) O'Callaghan, C. H.; Morris, A.; Kirby, S. M.; Chingler, A. H. *Antimicrob. Agents Chemother.* **1972**, *1*, 283-288.
(24) Boehle, K. E.; Gilliand, J.; Wheeldon, C. R.; Holder, A.; Adkins, J. A.; Geiss, B. J.; Ryan, E. P.; Henry, C. S. *Angew. Chem. Int. Ed. Engl.* **2017**, *56*, 6886-6890.
(25) Adkins, J. A.; Boehle, K.; Friend, C.; Chamberlain, B.; Bisha, B.; Henry, C. S. *Anal. Chem.* **2017**, *89*, 3613-3621.

(26) DR1900 Portable Spectrophotometer, 2018, Available at http://www.hach.com, Accessed May 9, 2018.
155
(27) Yang, Y.; Noviana, E.; Nguyen, M. P.; Geiss, B. J.; Dandy, D. S.; Henry, C. S. *Anal. Chem.* **2017**, *89*, 71-91.
(28) Nery, E. W.; Kubota, L. T. *J. Pharm. Biomed. Anal.* **2016**, *117*, 551-559.
(29) Ramachandran, S.; Fu, E.; Lutz, B.; Yager, P. *Analyst* **2014**, *139*, 1456-1462.
(30) Eustice, D. C.; Feldman, P. A.; Colberg-Poley, A. M.; Buckery, R. M.; Neubauer, R. H. *BioTechniques* **1991**, *11*, 739-742.
(31) *Amer. Acad. Pediat.,* **1997**, *99*, 268-278.
(32) Newton, P. N.; Fernandez, F. M.; Plancon, A.; Mildenhall, D. C.; Green, M. D.; Ziyong, L.; Christophel, E. M.; Phanouvong, S.; Howells, S.; McIntosh, E.; Laurin, P.; Blum, N.; Hampton, C. Y.; Faure, K.; Nyadong, L.; Soong, C. W.; Santoso, B.; Zhiguang, W.; Newton, J.; Palmer, K. *PLoS Med.* **2008**, *5*, e32.
(33) Kelesidis, T.; Kelesidis, I.; Rafailidis, P. I.; Falagas, M. E. *J. Antimicrob. Chemother.* **2007**, *60*, 214-236.
(34) Newton, P. N.; Green, M. D.; Fernández, F. M.; Day, N. P. J.; White, N. J. *Lancet Infect. Dis.* **2006**, *6*, 602-613.
(35) Tipke, M.; Diallo, S.; Coulibaly, B.; Storzinger, D.; Hoppe-Tichy, T.; Sie, A.; Muller, O. *Malar. J.* **2008**, *7*, 95.

CHAPTER 6. DEVELOPING A RASPBERRY PI SYSTEM TO QUANTIFY COLOR CHANGE AND CALCULATE ENZYME KINETICS ON PAPER-BASED DEVICES

Colorimetric detection, while a user-friendly and easily implemented method of analysis on paper-based devices, often suffers from subjectivity by the device user. In this chapter, we describe the development of two generations of a Raspberry Pi system to automatically analyze colored samples. With the implementation of an attached camera that obtains images every minute, we demonstrated that Michaelis-Menten enzyme kinetic values can be calculated directly from paper-based devices based on the change in color intensity over time. In our first-generation system, we demonstrated that just by obtaining one colored pixel per sample spot, we can generate enzyme kinetic values. A 3D-printed box was also designed and optimized with an independent light system that holds the paper-based devices and the Raspberry Pi board with attached camera. This box omits environmental light for consistent lighting and holds the camera in the same position between experiments for ideal image capture. Our second-generation system improves upon the limitations of the first generation including obtaining and averaging more pixels for more accurate analysis, and a new light box to improve the image quality. Preliminary analysis of enzyme kinetics on Whatman paper versus plastic-based transparency film devices shows that paper-based devices might inhibit enzyme activity, but this will be confirmed with further studies.

Introduction

The need to take advanced laboratory tests into resource-limited settings has sparked the field of portable lab-on-a-chip sensors where users can measure analytes without transporting samples to a central laboratory.[1-3] The desire for simple, inexpensive devices has driven the field of microfluidic paper-based analytical devices (μPADs), which have grown significantly in popularity since their inception in 2007.[4-6] Since then, paper-based devices have been developed for portable detection of environmental contaminants,[7,8] foodborne pathogens,[9,10] infectious diseases,[11,12] and other health ailments.[13,14]

Paper-based devices allow for many different detection motifs to be used including colorimetry, electrochemistry, fluorescence, or chemiluminescent detection.[15] Colorimetric detection provides one of the simplest options for in-field detection as it does not require external instrumentation. However, color-intensity-based measurements can suffer from subjective reading, causing inconsistent results between tests and users. To help combat this problem, colorimetric devices based on length of a colored band that forms during detection have been developed.[16,17] Like an analog temperature thermometer, the user simply measures the length of color to determine analyte concentration. However, an advantage of color-intensity-based spot tests is the ability to capture reaction kinetic information, not just end-point color formation. Distance-based devices also tend to have lengthy analysis times (typically 30 min) and the devices are not as easily fabricated. Additionally, not all analytes, such as cellular organisms like bacteria and fungi, are able to efficiently move through paper due to limited pore sizes.

Currently, most colorimetric devices using color intensity require images to be captured using either a digital camera or desktop scanner and then analyze the image using imaging software. While this setup works for laboratory settings, it is not as applicable to field settings where healthcare providers will have limited training. Whitesides and coworkers were the first to suggest the use of cellphones for offsite real-time diagnosis, where the healthcare provider would capture an image of a colorimetric device using a cellphone camera, then send the image offsite for image analysis and receive an official diagnosis.[18] With the rapid growth and deployment of smartphones worldwide, it is no longer necessary for images to be sent offsite for analysis. Smartphones are capable of storing and running complex applications for chemical analysis,[19] including image capture and automated analysis. Applications like these have been developed for paper-based devices for water quality monitoring[20] and *Salmonella* detection,[21] to name a few.[22] Smartphone applications and accessories have also been applied for infield fluorescent detection on paper-based devices, eliminating the need for a fluorescent microscope.[23] Although smartphones have opened the door for a variety of possibilities for portable medicine and environmental monitoring when combined with paper-based devices, there are drawbacks. The average cost of a smartphone is over $300 worldwide, a statistic that has not decreased significantly since 2011.[24] Additionally, smartphones are frequently updating with new software and these applications need to update with the software for compatibility. Programmers developing applications for point-of-care diagnostics also need to be concerned with the Health Insurance Portability and Accountability Act, a United States

legislation that was introduced to protect individual medical information, something that can be breached when using smartphones for sensitive medical information.

Raspberry Pi's are inexpensive, portable single-board computers that have become popular because they are easy to program for a variety of uses.[25] While a common application is for automation of household appliances such as temperature, lights and home security,[26,27] Raspberry Pi computers can also be programmed for automating scientific analysis.[28,29] Furthermore, specialized cameras have been commercialized for direct attachment to a Raspberry Pi board and can be controlled through programming.[30] A Raspberry Pi system has been created for automatic color analysis in colorimetric assays, but this system is for analyzing color in solution, not on paper-based devices.[31] In addition to programming the Raspberry Pi to automatically analyze images after capture,[32] these images can be captured at specific times points, enabling kinetic analysis.

One of the most common detection motifs used in μPADs are enzymatic reactions, including the first μPAD that was developed.[6] Enzymes are an attractive detection motif because of their selectivity, specificity, and catalytic abilities to amplify a product, yielding lower detection limits. Since the first μPAD, demonstrating glucose detection has become a common application for demonstrating new devices as a proof-of-concept, such as electrochemical detection and three-dimensional devices.[33-35] The most common way to detect glucose is using a bienzyme system of glucose oxidase and horseradish peroxidase.[35] Beyond glucose detection, enzymes have been used in the detection of urine creatine, uric acid, cholesterol, and pesticides, to name a few.[13,36-38] In addition to using enzymes to detect specific substrates, enzyme detection can be

used for clinical diagnostics[39-41] and measuring pathogens.[42,43] Because of the common employment of enzymes in paper-based devices, it is important to understand how different papers can affect an enzymatic reaction. Studies have demonstrated the impact of paper substrate on the color intensity of an enzyme reaction, and how different papers affect nucleic acid amplification.[44,45] To the best of our knowledge, however, there has not been a study completed that directly analyzes changes in enzyme kinetic parameters depending on the device substrate.

Herein, we describe the development of two different Raspberry Pi systems for the automatic calculation of Michaelis-Menten enzyme kinetic parameters on different microfluidic device substrates. The first system was developed as a proof-of-concept and was compared to manual analysis for the enzyme kinetics on Whatman 1 and Whatman 4 chromatography paper. Because of the variable difference in manual and Raspberry Pi analysis, a second-generation system was created to improve short-comings of the first-generation system. In the second-generation system, we have improved the device holder for better quality images. Additionally, the program was improved for more precise and accurate analysis, giving rise to the first system of its kind. Using the second-generation system, we have investigated how enzyme kinetics are affected whether the devices are fabricated with paper or transparency film. While this analysis system was specifically programmed for obtaining and analyzing colorimetric images, then automatically calculating Michaelis-Menten values, the program could be modified for other applications on paper-based devices and to eliminate subjectivity in colorimetric devices.

Materials and Methods

Materials. For the Raspberry Pi setup, a Raspberry Pi 2 Model B was used along with a Wide Angle FOV160° Raspberry Pi camera [SainSmart], which is attached to the computer board with a 15-pin ribbon cable. The camera contains a Omnivision 5647 sensor in a fixed focus module with 5-megapixel resolution. The Raspberry Pi board was enclosed in a transparent case that allowed access to all ports [SB Components].

The enzyme kinetic experiments were carried out with two enzyme/substrate pairs, β-lactamase [Abcam] and nitrocefin [VWR International] and β-glucuronidase [Sigma] and p-nitrophenol-β-d-glucuronide [Sigma].

Paper-Based Device Fabrication. Paper used for testing included Whatman 1 and Whatman 4 chromatography papers [GE Healthcare Sciences] and clear plastic transparency film [Apollo]. A simple 9 by 8 grid design of 7 mm black circles was designed with CorelDRAW. To define hydrophobic barriers, a ColorQube 8870 [Xerox] wax printer was used to dispense wax on the paper or plastic's surface and an IsoTemp [Fisher Scientific] hot plate was set to 150 °C with two metal plates on it. Wax-printed paper was placed between the hot plate and a metal plate for 60 sec, for the wax to melt through the pores. This step was omitted for transparency film. After cooling, Scotch Shipping Heavy Duty packing tape was used to cover the back of the paper to prevent sample leakage. The paper-based devices were laser-cut to be 9.4 x 9.4 cm with four 3 mm holes located one each at each corner for the paper-based devices to fit onto the pegs designed into the PAD holder. The laser cutter used was an Epilog Zing Laser Cutter (30 Watt) set to 100% speed, 9% power, and 2500 Hz frequency.

Designing and Fabricating the Raspberry Pi Holders. The holder for both the Raspberry Pi computer board/camera and the paper-based devices were designed using computer-assisted design software and 3D printing. All components were 3D printed using clear resin and the Form 2: Stereolithography 3D Printer [Formlabs]. The bottom component of the holder, which holds the paper-based devices, was designed using SketchUp [Microsoft]. This component (Figure 6.2A) measures 10.4 x 10.4 cm with a 3 mm lip that allows for the top component (that holds the Raspberry Pi card and camera) to consistently sit in a set position. There are 3 mm pegs in the floor of the holder to place the paper-based device in the same location every experiment. The PADs had 3 mm holes cut in the exact locations of the pegs located in the holder. The walls of the holder are 5 mm thick to compensate for the 3 mm lip, and the floor of the holder is 3 mm thick.

Generation 1 Raspberry Pi Holder. The first Raspberry Pi holder was designed using Autodesk Inventor software. The holder (Figure 6.2B and 6.2C) measures 5 cm in diameter at the top of the holder and 10 cm in diameter at the bottom of the holder, and is overall 10 cm tall, not including the pegs on top of the holder. Pegs on top of the device were used to hold the Raspberry Pi camera in the same position between experiments. Pegs were also added on the side of the device for the option of using a rubber band to hold the camera down for more consistent placement between experiments (seen in use in Figure 6.2C). Pegs were used on another side of the holder and measured 4 mm at the base and 6 mm at the top. The pegs were used to hold the Raspberry Pi board which is housed in a plastic case. This holder contains notches that the pegs were specifically designed to hold for the Raspberry Pi board case to snap into

place. The interior of the Raspberry Pi holder was spray painted with matte-white spray paint to help reflect light for optimal images. The lighting system to illuminate the inside of the holder was a standard light circuit where the bulbs were designed to be in parallel. A 9V battery was wired first to a toggle switch, then to the light bulbs in parallel, then to the resistor, back to the negative input of the battery. 3 white LEDs and an 820 Ω resistor were used. The wires, bulbs, and resistor were soldered together on a breadboard using a soldering iron for optimal electrical connection. Holes were drilled into the side of the holder using a 15/64 inch drill bit for the LEDs to insert into the device. The breadboard was taped to the side of the holder using electrical tape to hold the lighting system in place.

Generation 2 Raspberry Pi Holder. The second Raspberry Pi holder was designed using Onshape, a cloud-based CAD software. The holder measures 10 x 10 x 10 cm. The pegs on the side to hold the Raspberry Pi board plastic case are the same dimensions as described above. The lid of the holder also measures 10 x 10 cm and is 3 cm deep, making the entire holder 13 cm tall. The lid was attached to the body of the holder by attaching metal hinges to both the lid and the body using Epoxy glue. The walls of the holder, both the lid and body, were 3 mm wide. To hold the camera, the user lifts the lid and places the camera on similar pegs to the first Raspberry Pi holder. The camera is placed in the center of the holder through a 15 mm diameter circle on pegs the same size and distance apart as the first holder. The camera holder was held in the center of the device using 3 mm diameter supports leaving most of the device open for the light to illuminate the paper-based device. A light diffuser was generated to sit on the camera holder supports. The light diffuser was made with clear poly(methyl

methacrylate) (PMMA) and cut to be 9.4 x 9.4 cm with a 2.5 x 2.9 cm square cut out of the center for the Raspberry Pi camera to lay flat. To give the PMMA a frosted texture, sandpaper and water was used to lightly scratch the surface of the plastic. The light circuit was designed to fit into the lid of the Raspberry Pi holder so the lighting was placed behind the Raspberry Pi camera. 16 LEDs were arranged in a circle by laser-cutting two 3 mm holes in white PMMA for each LED to be placed in a circle orientation. The wires from each LED were inserted into the 3 mm holes and were wired in parallel. All anodes and cathodes of each LED were each soldered to a circular copper wire ring to eliminate the need for 32 separate wires. One wire was soldered to each the “anode ring” and the “cathode ring” and a light circuit was generated the same as previously described, but with a 100 Ω resistor. Hot glue was dried over the wiring to insulate the electrical connections. The light circuit in the PMMA board was glued in the lid of the Raspberry Pi holder also using Epoxy.

Determining the Best Lighting System (Generation 2). A paper-based device without any samples was placed in the bottom of the device holder and several different lighting conditions were tested. This includes whether the light diffuser was necessary; if the frosted side of the diffuser should face up or down; whether lining the side of the holder with copy paper would help diffuse light (with and without the first light diffuser); and covering the entire device with a dark cover to further limit exterior light. Images were captured using the Raspberry Pi camera and analyzed using ImageJ by measuring the light intensity of each sample spot after selecting the green color channel, without inverting the image. The ideal lighting system was selected by calculating the standard deviation from each row and column and averaging all standard

deviations. The most consistent lighting had the smallest average standard deviation across all sample spots. A heat map was generated in Microsoft Excel for a visual demonstration of light distribution across the sample spots on the paper-based device.

Kinetic Experiments and Analysis. For reactions between nitrocefin and β-lactamase, 5 mg of nitrocefin was initially dissolved in 1 mL dimethylsulfoxide (DMSO), because the substrate is insoluble in water. Aliquots of 9.68 mM nitrocefin was frozen at -20 °C in amber microcentrifuge tubes [VWR International]. These tubes were used to minimize degradation from UV exposure. Aliquots were taken out and allowed to thaw and warm to room temperature. Nitrocefin was further diluted with pH 7.4 phosphate buffered saline (PBS) [1.37 M NaCl, 0.027 M of KCl, 0.1 M Na_2HPO_4, and 0.018 M KH_2PO_4] to the following concentrations for enzyme kinetic experiments: 0.05, 0.1, 0.25, 0.4, 0.5, 0.6, 0.7, and 0.9 mM were used to generate a kinetic curve. For reactions between β-glucuronidase and p-nitrophenol-β-d-glucuronide (PNP-glucr), the substrate and enzyme were each dissolved in pH 7.4 phosphate buffered saline. The same concentrations were used to obtain a kinetic curve as nitrocefin. 6 U mL^{-1} and 300 U mL^{-1} concentrations were used for β-lactamase and β-glucuronidase respectively. To generate a calibration curve for nitrocefin, concentrations of 0.01, 0.025, 0.05, 0.075, 0.1, 0.15, 0.2, and 0.25 mM were used. For p-nitrophenol, concentrations of 0.05, 0.1, 0.2, 0.3, 0.4, 0.5, 0.6, and 0.7 mM were used.

For each experiment, three samples of each reaction were placed in every other column of circles. The columns on each side of the samples were used for water to act as a “light control.” This concept and a schematic of the setup are further described in Chapters 2 and 3. For manual analysis, the images were analyzed using NIH ImageJ

software. The image was split into its color channels and the green (β-lactamase) or blue (β-glucuronidase) color channel was selected and inverted. The intensity of each color spot was quantified, then normalized by subtracting the average brightness of the water spots on each side of the sample spot. After normalization, color intensity was converted to product concentration using a calibration curve. To eliminate the need to input a different calibration curve for each experiment, a calibration curve was implemented into the paper-based device in the eighth column. The calibration curve was generated by plotting color intensity *vs.* known product concentration (either hydrolyzed nitrocefin or p-nitrophenol as products) and generating a linear regression line. Color intensity was converted to product concentration by inputting color intensity into the “Y” variable, and calculating “X”, the product concentration.

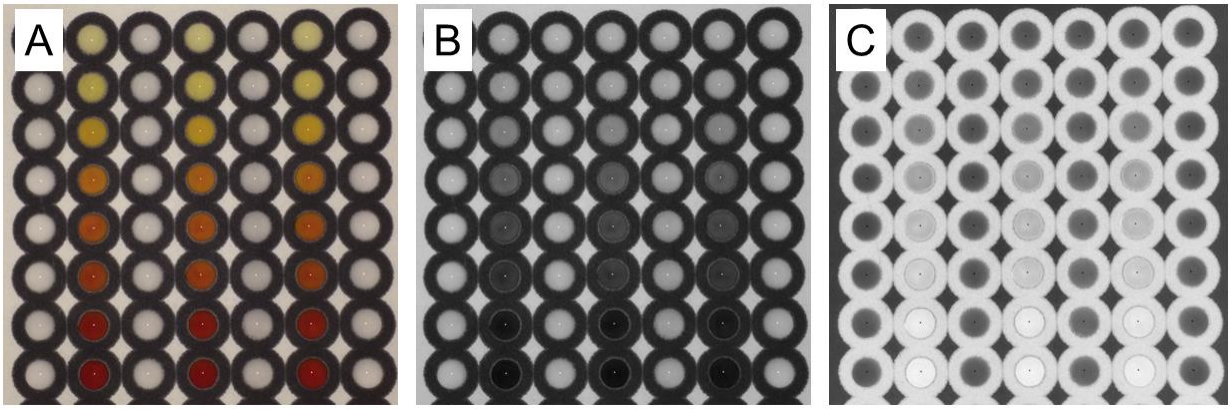

Figure 6.1 | Analyzing images in NIH ImageJ (beta-lactamase and nitrocefin). **(A)** Original image. **(B)** The green channel was selected after splitting the original image into red, blue, and green color channels. **(C)** Inverting the image for light intensity to be a positive trend as chemical concentration increases.

To obtain Michaelis-Menten parameters, images were captured at minutes 1, 2, and 3, to represent reaction progression. To calculate the reaction rate, the product formed (calculated using the linear regression equation as described) at each time point

was calculated and plotted on a graph of product formed *vs*. reaction time. The slope of the linear regression was determined to be the reaction rate in units of mM min^{-1}. The rate of eight different concentrations of each substrate were used to obtain a kinetic curve. V_{max} and K_m values were calculated for each enzyme and substrate pair by generating a Lineweaver-Burk plot. 1/[S] was plotted *vs.* 1/v and the inverse x- and y-intercepts were obtained. The calculated V_{max} and K_m values were carried out in the Michaelis-Menten equation to obtain a theoretical kinetic curve to compare to the data points and verify the accuracy of V_{max} and K_m.

Using the Raspberry Pi. Generation 1: Programming the Raspberry Pi was completed by a collaborative computer science student, Sadie Henry. The Raspberry Pi was programmed to obtain images every minute for three minutes and analyze the color intensity by selecting a specific pixel from each sample spot in the image. The specific pixel was selected by the user before each experiment to accommodate any inconsistent camera placement. The kinetics are analyzed as previously described for manual analysis for obtaining Michaelis-Menten parameters.

Generation 2: Programming was completed by another collaborative computer science student, Erin Doan. This generation was programmed using a flood fill algorithm that also selects an initial specific pixel (again chosen by the user for each experiment), but then continues to analyze the pixels surrounding it, eventually filling the entire sample spot. Once pixels have been selected, the program averages the color intensity of all pixels, like manual data analysis. The kinetics are analyzed as previously described for manual analysis for obtaining V_{max} and K_m.

Results and Discussion

Designing a Raspberry Pi and PAD Holder. In addition to programming the Raspberry Pi, one of the first steps of this project was to design a holder to house the paper-based devices and hold the Raspberry Pi board with attached camera. This holder was designed to make the system more portable and user-friendly, and for consistent placement of the PADs and Raspberry Pi camera. Additionally, one of the recognized pitfalls of using computer programs for objective analysis are variable lighting conditions found in field settings.[46] Creating a holder with an independent lighting system should eliminate this pitfall by not relying on natural light. The final holder was composed of two different parts (Figure 6.2). The bottom component of the holder was designed to hold the PADs in the same location between experiments. 3 mm pegs were used in the bottom component, and 3 mm holes were designed into the PADs via laser cutting for the 3 mm holes to be in the same location as the holder's pegs for consistent device placement (Figure 6.2A). The top component of the holder secures the Raspberry Pi computer board and places the attached camera in the same location between experiments using pegs, like the PAD. The Raspberry Pi board was housed in a plastic case with notches that were designed for wall-mounting, so pegs were designed into the side of the holder for the Raspberry Pi to have a secure fitting. The camera, which is attached to the board through a ribbon, is placed at the top of the holder where pegs can hold the camera over a window for the camera to image the paper-based device (Figure 6.2B and 6.2C). Additional pegs were placed on either side of the camera for the option of securing the camera using a rubber band. The holder is 10 x 10 cm on the bottom of the holder, but decreases to 5 x 5 cm at the top of the

holder where the camera is held, similar to a pyramid. This design was initially chosen instead of a square device to enhance the system's portability, along with generating an overall cheaper holder by using less materials. To illuminate the inside of the holder, a light circuit was fabricated using a toggle switch, three white LEDs, an 820 Ω resistor, and a 9V battery. Although it was calculated that only a 75 Ω resistor was necessary, using a larger resistor dimmed the LEDs to an appropriate brightness as to not "wash out" the devices. The inside of the holder was also spray-painted with matte-white paint to defuse light more evenly across the device. Finally, a dark cloth covered the entire holder during experiments due to natural light affecting the photos through the camera's viewing window on top of the holder.

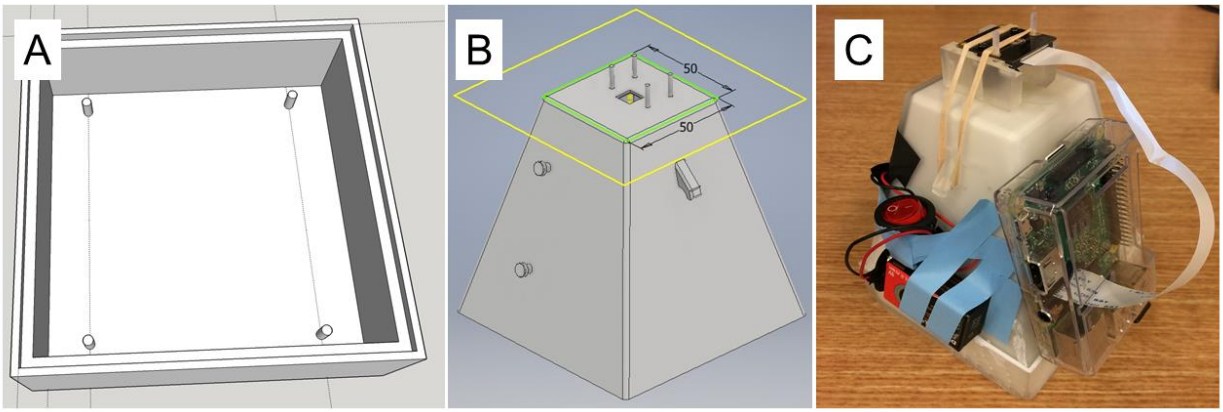

Figure 6.2 | The holder for the Generation 1 Raspberry Pi. **(A)** CAD image of the bottom component that houses the paper-based devices. **(B)** CAD image of the top component that holds the Raspberry Pi and attached camera. **(C)** How the Raspberry Pi and attached camera fit onto the entire holder put together.

Kinetic Experiments and Analysis. For the first Raspberry Pi system, we compared Raspberry Pi photo analysis to manual photo analysis using β-lactamase and nitrocefin on Whatman grade 1 and Whatman grade 4 chromatography papers. The Raspberry Pi camera obtained images at minutes 1, 2, and 3 throughout the reaction

once the program was initialized (Figure 6.3). The same images were analyzed whether it was the Raspberry Pi program or manual analysis (detailed photo analysis can be found in the materials and methods). For manual analysis, NIH ImageJ was used to measure the mean color intensity of each sample spot using the circle tool to encompass the entire spot, around 1000 pixels. When the Raspberry Pi analyzed the images, one specific pixel from each sample spot was chosen to measure the light intensity instead of averaging the color intensity of all pixels within the sample spot. The obtained color intensity pixel values, whether manual or Raspberry Pi analysis, both used the same data analysis process to calculate V_{max} and K_m as explained in detail in the materials and methods section.

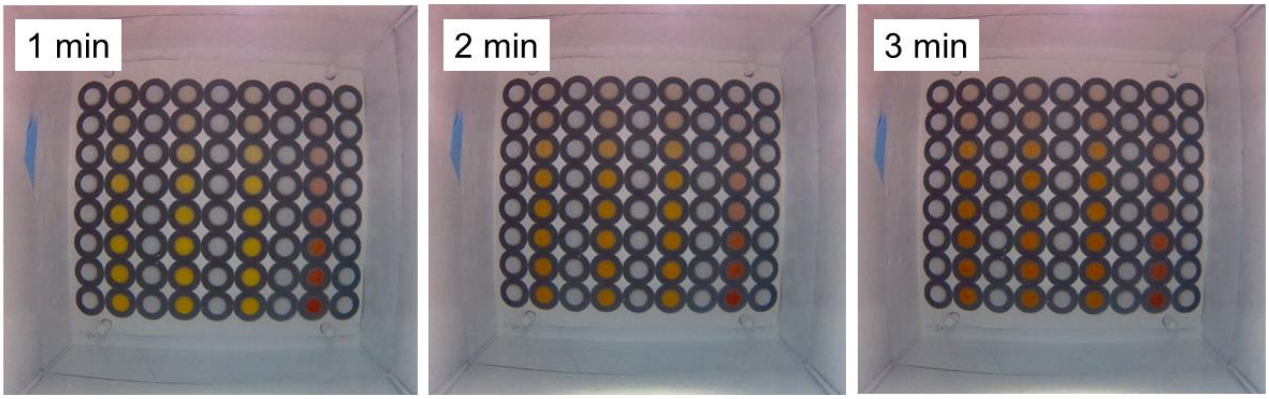

Figure 6.3 | Images obtained from the Raspberry Pi during a kinetic experiment.

Manual vs. Raspberry Pi Analysis. The goal of this project was to design a program that obtains similar values of color intensity and Michaelis-Menten values whether it is a person or a Raspberry Pi program analyzing the images. Michaelis-Menten constants, V_{max} and K_m, were calculated through Raspberry Pi and manual analysis, then compared for overall average. As seen in Figure 6.4, the average V_{max} and K_m calculated using the Raspberry Pi program were similar to values obtained

through manual analysis, especially for Whatman 1 paper. In Whatman 4 paper, the averages were similar value, but the error was much larger at 30-50% relative standard deviation compared to 2% in manual analysis. This only occurred for Whatman 4, therefore this error could be indicative of inconsistent color formation across each sample spot. In manual analysis, the color intensity values are based off an average of 1000 pixels across the sample, *vs*. Raspberry Pi analysis, the color intensity is based off one pixel.

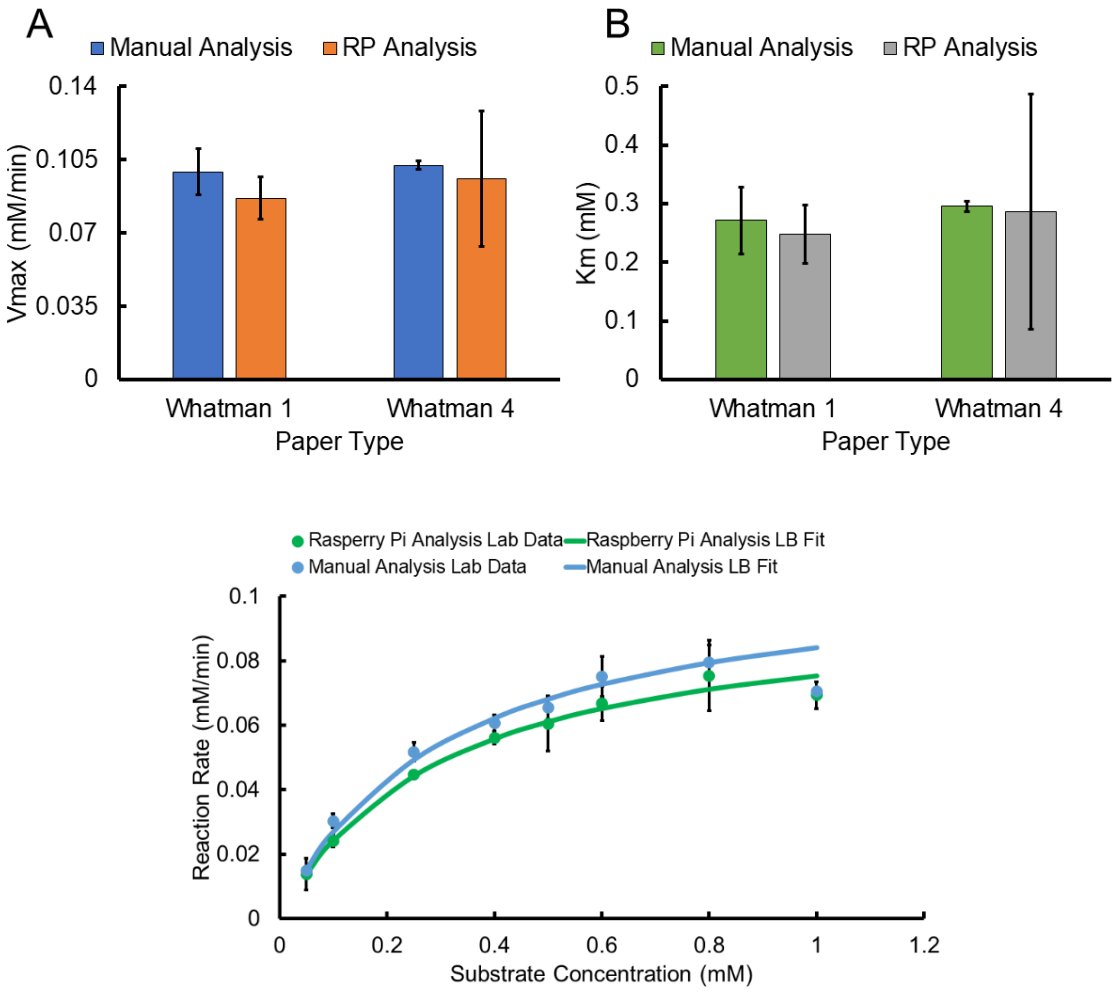

Figure 6.4 | Comparing **(A)** V_{max} and **(B)** K_m of β-lactamase and nitrocefin on Whatman 1 and Whatman 4 papers as calculated via manual analysis or Raspberry Pi (RP) analysis. **(C)** A sample Michaelis-Menten kinetic curve comparing manual analysis and Raspberry Pi computer analysis.

If color formation across the sample spot is consistent, obtaining color intensity based on one pixel is satisfactory. However, if color intensity is inconsistent, using one pixel could lead to significant error. When comparing Whatman 1 and Whatman 4, whether manual or Raspberry Pi analysis, there is no statistically significant difference in either V_{max} or K_m. Whatman 4 appears to be more consistent across experiments, but only when averaging all 1000 pixels across the sample spot. This implies that although color formation rate is consistent between experiments, it is not consistent across the sample spot.

Generation 2: Raspberry Pi Holder Design. While the first generation of the Raspberry Pi program was an excellent proof-of-concept, there are many areas that could be improved to create a better system. The images currently do not have consistent lighting across the device, necessitating a new light box system. For the updated lightbox, we used CAD and 3D printing to create a new holder for the Raspberry Pi. Because the paper-based devices are the same, the bottom component from the first-generation holder was maintained, and only a new holder for the Raspberry Pi board and camera was designed. The first-generation holder contained three white LEDs that were placed in the wall of the device. While this illuminated the inside of the holder, it did not disperse light evenly across the paper-based device. For this second-generation holder, we changed the lighting system to be placed behind the camera with light diffusers to increase light distribution. This was accomplished by making the holder square, instead of pyramidal like the first holder, and implementing a lid (Figure 6.5). A circular ring of 16 LEDs was glued into the lid (Figure 6.5B) for the lid

to close over the camera that was situated in the center of the holder like the first-generation system (Figure 6.5C). Frosted clear PMMA was used as a light diffuser.

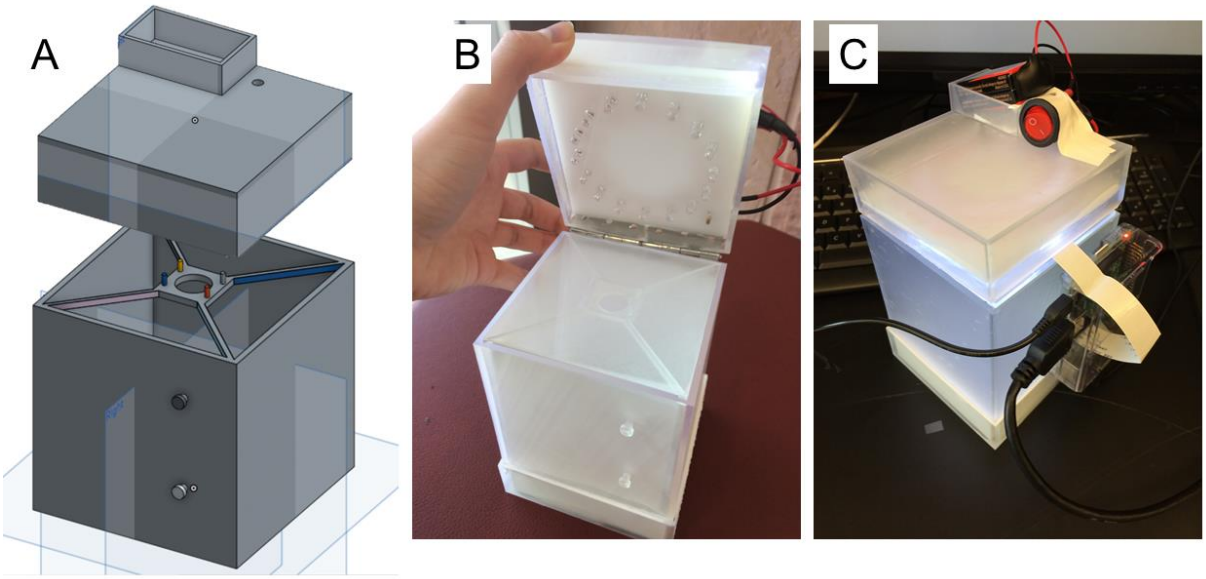

Figure 6.5 | The second generation Raspberry Pi holder composed of a main component and a lid to hold the lighting system. **(A)** CAD drawing of Raspberry Pi holder. **(B)** Lifting the lid of the final 3D-printed holder with lighting system enclosed in the lid. **(C)** Final system with Raspberry Pi held in place on the side of the holder.

Optimizing Lighting in the Raspberry Pi Holder. To generate the best lighting system, we compared light distribution using one or several light diffusing methods. Light distribution was compared by measuring the light intensity of each sample spot on a clean paper-based device. The standard deviation of light intensity in each row and column of the PAD were calculated, then all standard deviations were averaged. The smaller the average standard deviation, the more evenly distributed the light. For a visual comparison, heat maps were generated in Excel to demonstrate where on the paper-based devices there was uneven light distribution. In addition to testing whether the frosted plastic light diffuser was necessary, we also investigated the position of the frosted plastic diffuser in the holder, the use of white copy paper inside the holder, and

putting a dark cloth over the entire holder to limit exterior light. The best distribution of light was accomplished with the frosted diffuser, with the frosted side facing the PAD, lining the holder with white copy paper, and without a dark cover over the holder. The average standard deviation of light intensity across the PAD was 4.85 (highlighted in Figure 6.6A), which was much lower than the average light intensity SD of 15.20 seen in the worst light distribution in Figure 6.6B.

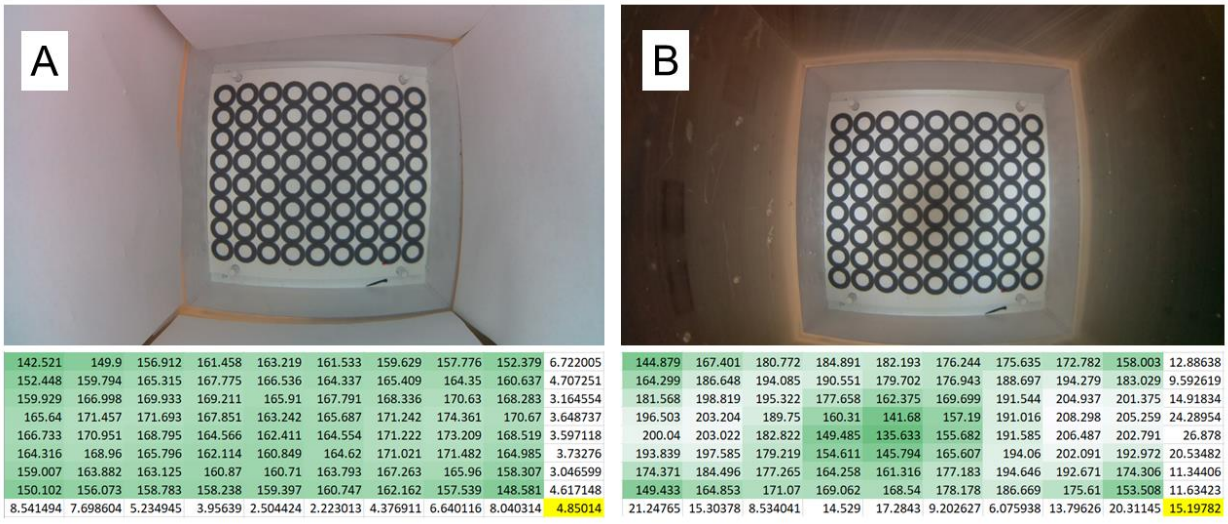

142.521	149.9	156.912	161.458	163.219	161.533	159.629	157.776	152.379	6.722005
152.448	159.794	165.315	167.775	166.536	164.337	165.409	164.35	160.637	4.707251
159.929	166.998	169.933	169.211	165.91	167.791	168.336	170.63	168.283	3.164554
165.64	171.457	171.693	167.851	163.242	165.687	171.242	174.361	170.67	3.648737
166.733	170.951	168.795	164.566	162.411	164.554	171.222	173.209	168.519	3.597118
164.316	168.96	165.796	162.114	160.849	164.62	171.021	171.482	164.985	3.73276
159.007	163.882	163.125	160.87	160.71	163.793	167.263	165.96	158.307	3.046599
150.102	156.073	158.783	158.238	159.397	160.747	162.162	157.539	148.581	4.617148
8.541494	7.698604	5.234945	3.95639	2.504424	2.223013	4.376911	6.640116	8.040314	4.85014

144.879	167.401	180.772	184.891	182.193	176.244	175.635	172.782	158.003	12.88638
164.299	186.648	194.085	190.551	179.702	176.943	188.697	194.279	183.029	9.592619
181.568	198.819	195.322	177.658	162.375	169.699	191.544	204.937	201.375	14.91834
196.503	203.204	189.75	160.31	141.68	157.19	191.016	208.298	205.259	24.28954
200.04	203.022	182.822	149.485	135.633	155.682	191.585	206.487	202.791	26.878
193.839	197.585	179.219	154.611	145.794	165.607	194.06	202.091	192.972	20.53482
174.371	184.496	177.265	164.258	161.316	177.183	194.646	192.671	174.306	11.34406
149.433	164.853	171.07	169.062	168.54	178.178	186.669	175.61	153.508	11.63423
21.24765	15.30378	8.534041	14.529	17.2843	9.202627	6.075938	13.79626	20.31145	15.19782

Figure 6.6 | Comparison of the best and worst distributions of light. **(A)** The best distribution of light was to line the holder with copy paper, have the plastic light diffuser with frosted side facing the paper-based device, and without a dark cover over the entire holder. **(B)** The worst distribution of light was no frosted plastic diffuser, no copy paper lining the sides, and with a dark cover over the entire holder.

The use of a dark cover over the holder consistently resulted in less light distribution across all experiments. This is surprising considering a dark cover was necessary in the first-generation Raspberry Pi holder. The difference is likely because the new holder encloses the camera with the paper-based device, unlike the first-generation holder where the camera sat on top of the holder and viewed the PAD through a viewing window. By sitting on top of the holder, environmental light easily

affected image capture. Because the second-generation holder is fabricated with clear resin, exterior light can still penetrate the inside the holder. Lining the interior of the holder with copy paper likely assisted with limiting exterior light, plus these experiments were completed indoors with consistent environmental lighting. Therefore, this is an aspect that could change when the system is used outdoors. For example, exterior light can affect the interior of the holder differently whether it is the middle of the day where the sun is directly above the user, *vs*. earlier or later in the day when the sun is closer to the horizon. Once the Raspberry Pi system is more portable, the use of an external cover will be re-investigated.

Overall, the image quality significantly improved between the first-generation and second-generation Raspberry Pi holders (Figure 6.7). The paper-based devices are noticeably better illuminated with better light distribution across the PAD. Additionally, by having the camera inside the holder, this allows the camera to be closer to the device, averaging more pixels per sample spot, and eliminates the “vignette” seen in the first-generation photo (Figure 6.7A).

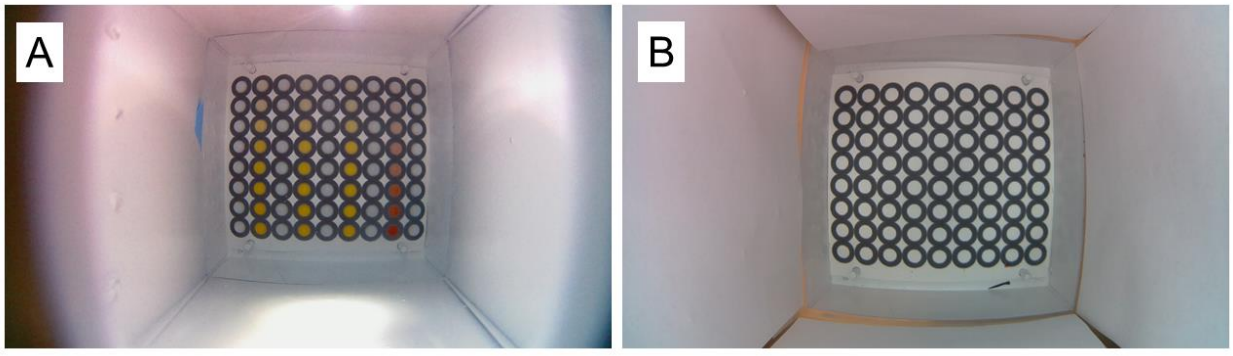

Figure 6.7 | Comparison of the images capture by the Raspberry Pi in the first-generation holder **(A)** vs. second-generation holder **(B)**.

Modifying the Raspberry Pi Program. Once the image quality was improved, the program to analyze the images was modified for more accurate and consistent kinetic analysis. The primary pitfall of the first Raspberry Pi program lied in the analysis of one pixel vs. averaging 1000+ pixels in manual analysis. If the selected pixel was not representative of the entire sample zone, this could cause significant error. In the updated Raspberry Pi program, the same pixel is selected as the first program, but then the program analyzes the color intensity of the pixels surrounding the first pixel using an algorithm called “flood fill.” If the color intensity of each pixel analyzed is a similar color intensity (within a selected threshold), then the pixel is included in the overall average. Once included in the overall average, then the pixels around that pixel are also analyzed. If a pixel is not within the color intensity threshold, the pixel is omitted. One of the many advantages of this code is if the camera is off-center and the starting pixel is toward the edge of the sample zone, then it should stop growing in one direction faster than growing in the opposite direction. This code would most likely provide more accurate results compared to manual analysis for reasons including customizable sample zones and eliminating subjectivity. For example, a single oval shape is created to encompass the entire sample zone during manual analysis, then the same oval is used throughout analysis for consistency and analysis speed. However, using a wide-angle fisheye lens for the Raspberry Pi system has caused inconsistent sample spots, which is visible when comparing Figure 6.1 (obtained with a camera phone) and Figure 6.3 (obtained with the Raspberry Pi camera). Using the flood-fill algorithm enables customizable sample zones and avoiding areas in the sample with inconsistent lighting, which will be discussed later.

Generation 2: Enzyme Kinetics Analysis. To verify the second generation Raspberry Pi system, we compared manual and Raspberry Pi kinetics analysis of two different enzymes and on two different kinds of devices. We used β-lactamase and nitrocefin again, along with β-glucuronidase with p-nitrophenol-β-d-glucuronide, which turns from clear to yellow to verify other colors could be analyzed. We compared manual analysis to Raspberry Pi analysis on Whatman 1 filter paper, and compared kinetics on paper to devices fabricated with transparency film.

The second-generation Raspberry Pi kinetics analysis displayed little error when comparing to manual analysis. Values of V_{max} ranged from 1% off to 11% off from manual analysis (Figure 6.8A), compared to 10% to 43% off when using Generation 1. Values of K_m displayed larger error, which varied from 2% to 17% off (Figure 6.8B), however, this is still down from the first-generation code, which could be off by 44%.

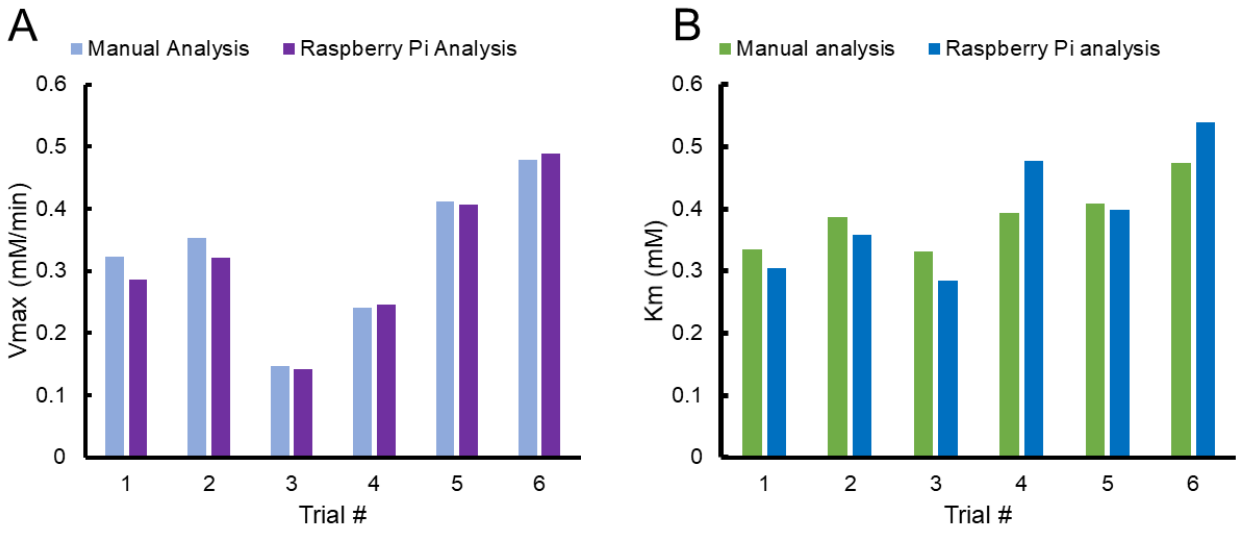

Figure 6.8 | Comparison of **(A)** V_{max} and **(B)** K_m through manual and Raspberry Pi image analysis using the second generation Raspberry Pi system.

The largest discrepancy between manual and Raspberry Pi analysis was calculating V_{max} for a reaction taking place on a transparency sheet. While the Raspberry Pi program was consistently obtaining slightly lower values compared to manual analysis, the V_{max} obtained for a β-lactamase reaction on transparency sheet was 70% higher at 0.51 mM min^{-1} compared to 0.16 mM min^{-1}. However, this is likely due to error by manual analysis, not the Raspberry Pi program. Due to the reflectiveness of plastic, error was introduced into the sample spots by the ring of lights (Figure 6.9). Whatman filter paper is matte white, therefore helped to disperse light. Despite placing copy paper under the transparency sheet, plastic still reflects the light in a more specific, rather than dispersive, manner. In the transparency sheet kinetics images, one can see the reflection of the light ring in the sample spots. When the specific channel is obtained and inverted, this light ring reflection turns into

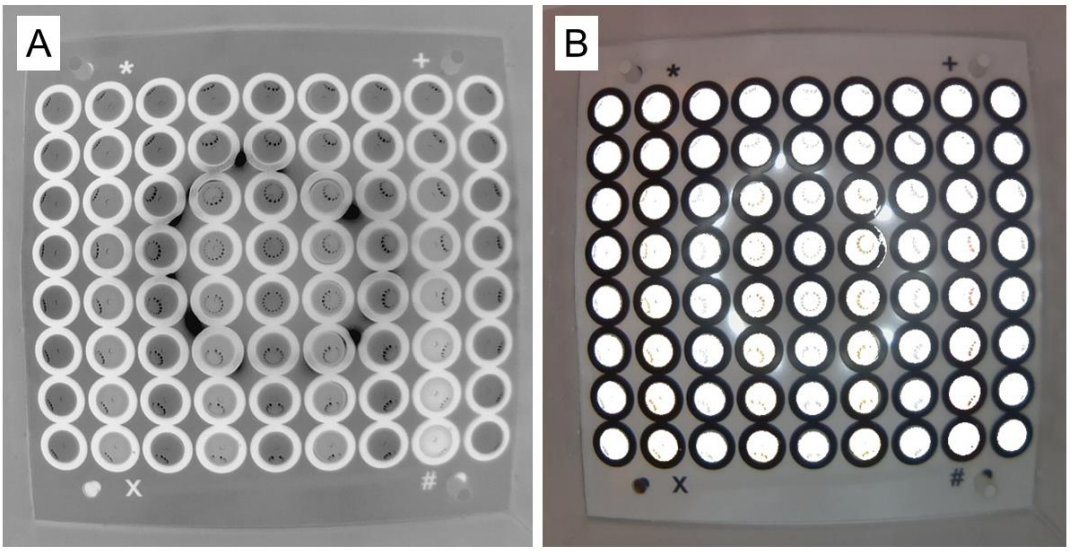

Figure 6.9 | Analyzing kinetic data on transparency sheets. **(A)** Kinetic experiment image that has been inverted to demonstrate that light ring reflection can affect data analysis. **(B)** Raspberry pi program using flood fill algorithm to avoid these light reflections.

black spots, and can therefore affect the color intensity when averaging the entire sample spot (Figure 6.9A). However, the flood-fill algorithm can avoid these light spots because the pixel values are not within the program's threshold. These light spots are eliminated from the overall average (Figure 6.9B), which would not be possible in manual analysis.

Kinetics on Different Platforms. When comparing enzyme kinetics from paper-based devices to plastic-based devices, we used the values obtained by the updated Raspberry Pi program. Because of the program's ability to avoid reflections from the light source, the program likely obtains more accurate results compared to manual analysis. Preliminary results show that kinetic values for β-lactamase and β-glucuronidase on transparency film are higher compared to kinetics on Whatman paper (Figure 6.10A), but not statistically significantly higher for β-glucuronidase. Although more experiments will need to be completed before this conclusion can be drawn, a hypothesis can be made as to why enzyme kinetics could be affected by the device material. When Linnes et al were determining which paper substrates affect nucleic acid amplification the least, the authors hypothesized that enzymes involved in replication were nonspecifically binding to the paper substrate, decreasing amplification efficiency.[45] This could be happening during colorimetric enzyme kinetics as well. Although it is unlikely that enzymes are completely inhibited when they nonspecifically bind to paper, this would likely decrease the amount of substrate that is turned over, therefore decreasing the observed V_{max}. However, if this hypothesis is true, then K_m would likely increase as it would theoretically require more substrate to reach the enzyme's V_{max}. With experiments thus far, K_m has consistently been lower on paper

compared to transparency film, except for one experiment which was higher. Completing more enzyme kinetic experiments across different paper and plastic substrates and paper modifications will be the subject of future research to further explore this hypothesis.

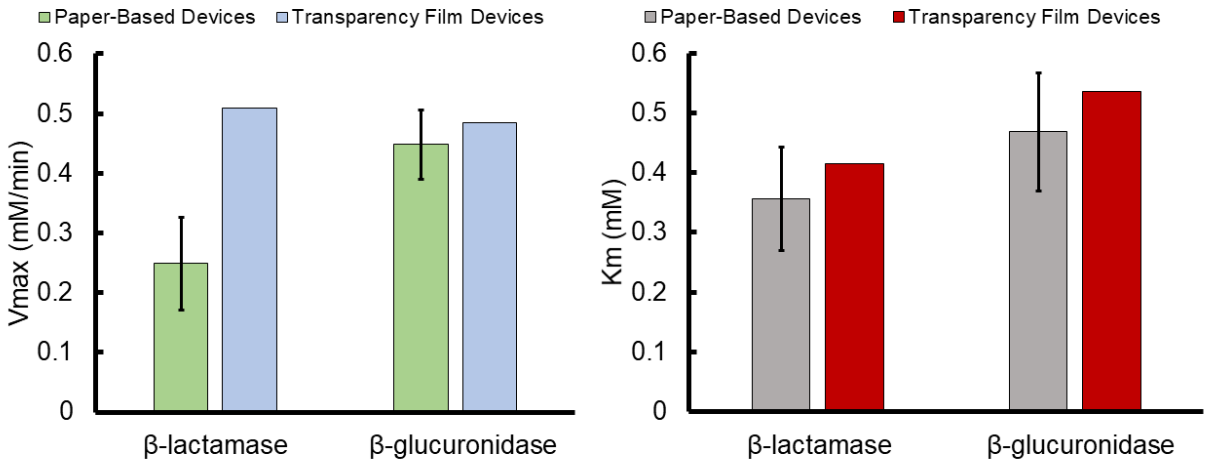

Figure 6.10 | Comparing kinetic data on different substrates. **(A)** Vmax and **(B)** Km of enzymes on paper-based devices first transparency sheet devices.

Conclusions and Future Directions

A new and accurate Raspberry Pi program has been developed for automatically calculating enzyme kinetics on different device substrates based on color change. The first-generation program was an excellent step in the right direction and obtained relatively accurate kinetic values despite obtaining one pixel vs. averaging 1000+ pixels. However, the second-generation system has been demonstrated in obtaining what is most likely more accurate values compared to manual analysis with a new code that averages most pixels present in a single sample spot. A new 3D-printed Raspberry Pi holder with better light dispersion has also been developed for obtaining better images for analysis compared to our first-generation holder, further improving our results. Data

obtained using the program so far has suggested that transparency film as a device substrate inhibits enzyme kinetics less compared to paper substrates, but more data will be needed across several enzymes and substrates to confirm this hypothesis.

To verify whether nonspecific enzyme adsorption to the paper is what is causing decreased enzyme activity on paper-based devices, we will test additional paper substrates and paper modifications. For example, bovine serum albumin and non-fat dry milk solutions are used to prevent proteins from nonspecifically binding to paper and other substrates. Theoretically, these modifications to paper could be used to increase enzyme activity on devices. Other polymer-based materials could also be tested for enzyme kinetics such as PMMA or polydimethylsiloxane (PDMS) to help confirm whether plastic-based materials used in devices inhibit enzyme activity less compared to paper substrates.

While we demonstrated this system to obtain enzyme kinetic values, the program could be modified for other colorimetric device applications. Because the program does not analyze a set number of pixels, but continues to analyze pixels until the device's edge, it is not limited by device shape. The program currently obtains an average color intensity, then calculates the product formed over three minutes to calculate V_{max} and K_m of a specific enzyme. The program could be modified to relate the average color intensity back to a specific calibration curve and output a concentration that relates to the analyte being detected, whether metals, pathogens, or biomarkers. Additionally, the program is currently measuring color intensity, but the program could be modified to count specifically colored pixels within a color intensity, enabling objective distance-based measurements. With minor revisions to the code, this technology could be

applicable for a large variety of colorimetric detection applications to eliminate the subjectivity currently seen in colorimetric paper-based devices.

REFERENCES

(1) Srinivasan, B.; Tung, S. *J. Lab. Autom.* **2015**, *20*, 365-389.
(2) Meredith, N. A.; Quinn, C.; Cate, D. M.; Reilly, T. H., 3rd; Volckens, J.; Henry, C. S. *Analyst* **2016**, *141*, 1874-1887.
(3) Jokerst, J. C.; Emory, J. M.; Henry, C. S. *Analyst* **2012**, *137*, 24-34.
(4) Yang, Y.; Noviana, E.; Nguyen, M. P.; Geiss, B. J.; Dandy, D. S.; Henry, C. S. *Anal. Chem.* **2017**, *89*, 71-91.
(5) Yamada, K.; Shibata, H.; Suzuki, K.; Citterio, D. *Lab Chip* **2017**, *17*, 1206-1249.
(6) Martinez, A. W.; Phillips, S. T.; Butte, M. J.; Whitesides, G. M. *Angew. Chem. Int. Ed. Engl.* **2007**, *46*, 1318-1320.
(7) Mentele, M. M.; Cunningham, J.; Koehler, K.; Volckens, J.; Henry, C. S. *Anal. Chem.* **2012**, *84*, 4474-4480.
(8) Gomes, H. I.; Sales, M. G. *Biosens. Bioelectron.* **2015**, *65*, 54-61.
(9) Jokerst, J. C.; Adkins, J. A.; Bisha, B.; Mentele, M. M.; Goodridge, L. D.; Henry, C. S. *Anal. Chem.* **2012**, *84*, 2900-2907.
(10) Hossain, S. M.; Ozimok, C.; Sicard, C.; Aguirre, S. D.; Ali, M. M.; Li, Y.; Brennan, J. D. *Anal. Bioanal. Chem.* **2012**, *403*, 1567-1576.
(11) Rodriguez, N. M.; Linnes, J. C.; Fan, A.; Ellenson, C. K.; Pollock, N. R.; Klapperich, C. M. *Anal. Chem.* **2015**, *87*, 7872-7879.
(12) Teengam, P.; Siangproh, W.; Tuantranont, A.; Henry, C. S.; Vilaivan, T.; Chailapakul, O. *Anal. Chim. Acta* **2017**, *952*, 32-40.
(13) Talalak, K.; Noiphung, J.; Songjaroen, T.; Chailapakul, O.; Laiwattanapaisal, W. *Talanta* **2015**, *144*, 915-921.
(14) Yildiz, U. H.; Alagappan, P.; Liedberg, B. *Anal. Chem.* **2013**, *85*, 820-824.
(15) Cate, D. M.; Adkins, J. A.; Mettakoonpitak, J.; Henry, C. S. *Anal. Chem.* **2015**, *87*, 19-41.
(16) Cate, D. M.; Dungchai, W.; Cunningham, J. C.; Volckens, J.; Henry, C. S. *Lab Chip* **2013**, *13*, 2397-2404.
(17) Cate, D. M.; Noblitt, S. D.; Volckens, J.; Henry, C. S. *Lab Chip* **2015**, *15*, 2808-2818.
(18) Martinez, A. W.; Phillips, S. T.; Carrilho, E.; Thomas, S. W.; Sindi, H.; Whitesides, G. M. *Anal. Chem.* **2008**, *80*, 3699-3707.
(19) Trojanowicz, M. *Mod. Chem. Applic.* **2017**, *05*.
(20) Sicard, C.; Glen, C.; Aubie, B.; Wallace, D.; Jahanshahi-Anbuhi, S.; Pennings, K.; Daigger, G. T.; Pelton, R.; Brennan, J. D.; Filipe, C. D. *Water Res.* **2015**, *70*, 360-369.
(21) Park, T. S.; Li, W.; McCracken, K. E.; Yoon, J. Y. *Lab Chip* **2013**, *13*, 4832-4840.
(22) Gong, M. M.; Sinton, D. *Chem. Rev.* **2017**, *117*, 8447-8480.
(23) Thom, N. K.; Lewis, G. G.; Yeung, K.; Phillips, S. T. *RSC Adv.* **2014**, *4*, 1334-1340.
(24) Average selling price of smartphones worldwide from 2011 to 2017 (in U.S. dollars), Statistica, 2017, Available at https://www.statista.com/statistics/510668/smartphone-average-selling-price-worldwide/, Accessed May 10, 2018.

(25) Robinson, A.; Cook, M.; Evans, J.; McManus, S. *Raspberry Pi Projects*; Wiley: Hoboken, NJ, 2014.
(26) Jain, S.; Vaibhav, A.; Goyal, L. **2014**, 277-280.
(27) Chowdhury, M.; Nooman, S.; Sarker, S. *IJSER* **2013**, *4*, 550-558.
(28) Ferdoush, S.; Li, X. *Procedia Comput. Sci.* **2014**, *34*, 103-110.
(29) Bougot-Robin, K.; Paget, J.; Atkins, S. C.; Edel, J. B. *J. Chem. Educ.* **2016**, *93*, 1232-1240.
(30) Senthilkumar, G.; Gopalakrishnan, K.; Sathish Kumar, V. *IJETTCS* **2014**, *3*, 213-215.
(31) Luka, G. S.; Nowak, E.; Kawchuk, J.; Hoorfar, M.; Najjaran, H. *R. Soc. Open Sci.* **2017**, *4*, 171025.
(32) K S, S.; H, L.; Shivkumar, H. *Ijarcce* **2015**, *4*, 199-202.
(33) Dungchai, W.; Chailapakul, O.; Henry, C. S. *Anal. Chem.* **2009**, *81*, 5821-5826.
(34) Sechi, D.; Greer, B.; Johnson, J.; Hashemi, N. *Anal. Chem.* **2013**, *85*, 10733-10737.
(35) Liu, S.; Su, W.; Ding, X. *Sensors* **2016**, *16*.
(36) Yu, J.; Ge, L.; Huang, J.; Wang, S.; Ge, S. *Lab Chip* **2011**, *11*, 1286-1291.
(37) Nantaphol, S.; Chailapakul, O.; Siangproh, W. *Anal. Chim. Acta* **2015**, *891*, 136-143.
(38) Zakir Hossain, S. M.; Luckham, R. E.; McFadden, M. J.; Brennan, J. D. *Anal. Chem.* **2009**, *81*, 9055-9064.
(39) Nosrati, R.; Gong, M. M.; San Gabriel, M. C.; Pedraza, C. E.; Zini, A.; Sinton, D. *Clin. Chem.* **2016**, *62*, 458-465.
(40) Yen, T. H.; Chen, K. H.; Hsu, M. Y.; Fan, S. T.; Huang, Y. F.; Chang, C. L.; Wang, Y. P.; Cheng, C. M. *Talanta* **2015**, *145*, 66-72.
(41) Kannan, B.; Jahanshahi-Anbuhi, S.; Pelton, R. H.; Li, Y.; Filipe, C. D.; Brennan, J. D. *Anal. Chem.* **2015**, *87*, 9288-9293.
(42) Zakir Hossain, S. M.; Ozimok, C.; Sicard, C.; Aguirre, S. D.; Monsur Ali, M.; Li, Y.; Brennan, J. D. *Anal. Bioanal. Chem.* **2012**, *403*, 1567-1576.
(43) Bisha, B.; Adkins, J. A.; Jokerst, J. C.; Chandler, J. C.; rez, M.; ndez, A.; Coleman, S. M.; Sbodio, A. O.; Suslow, T. V.; Danyluk, M. D.; Henry, C. S.; Goodridge, L. D. **2014**, e51414.
(44) Evans, E.; Gabriel, E. F.; Coltro, W. K.; Garcia, C. D. *Analyst* **2014**, *139*, 2127-2132.
(45) Linnes, J. C.; Rodriguez, N. M.; Liu, L.; Klapperich, C. M. *Biomed. Microdevices* **2016**, *18*, 30.
(46) Teles, F. S. *Anal. Chim. Acta* **2011**, *687*, 28-42.

CHAPTER 7. CONCLUSIONS AND FUTURE DIRECTIONS

Bacterial contamination of food and water is a major concern worldwide as a single foodborne illness outbreak can result in many hospitalizations and deaths, and cost the industry tens to hundreds of millions of US dollars.[1,2] For example, the recent multistate *E. coli* outbreak in romaine lettuce from Yuma, Arizona, has caused infections in over half of the United States with almost 150 reported serious illnesses.[3] Because the outbreak and its investigation is still ongoing, it is unknown how the lettuce was contaminated and the total cost of the outbreak. It is currently too expensive and time consuming to test for bacterial contamination in all food products or irrigation water, therefore, contamination is not made apparent until a consumer contracts an illness after all contaminated products have been distributed. The work presented at the beginning of this dissertation offers cheaper and faster alternatives to traditional methods for the detection of common bacteria indicative of bacterial contamination, and specific and sensitive detection of *Salmonella typhimurium* as a model organism.[4,5] These methods were successfully demonstrated in real-world samples such as contaminated alfalfa sprouts and inoculated irrigation water, and even bird fecal samples. Although it is difficult to prevent foodborne illness outbreaks entirely, generating inexpensive field-ready tests for detection of common foodborne pathogens is an important step in the right direction.

While bacteria identification is important, classifying whether bacteria are susceptibility to specific antibiotics is another critical component to bacteria detection. To help slow the emergence of antimicrobial resistant (AMR) bacteria, scientists need to

understand the epidemiology and spread of resistant bacteria in the environment, and doctors must be able to identify AMR bacteria during diagnosis to help prevent unnecessary antibiotic use. Inexpensive and user-friendly alternatives to AMR bacteria detection to help satisfy these needs have also been successful demonstrated by detecting AMR bacteria based on enzymes that facilitate resistance. These paper-based devices are the first of their kind as no other paper-based detection method for AMR bacteria has been proposed since the publication of the dissertation. The first device, based on colorimetric detection from yellow to red, was successful in detecting AMR in different bacterial species isolated from environmental samples, and in detection of AMR in uninoculated sewage water. All results were validated by traditional methods, but the results were obtained using our tests at a fraction of the time and cost.[6] To further advance this method, we developed a 3-layer device that can test for resistance against specific β-lactam antibiotics based on a change in pH when enzymes react with antibiotics. Although it has not been demonstrated yet, this method should be able to confirm bacterial resistance against specific classes of β-lactam antibiotics, including carbapenem antibiotics, which are considered a major health threat.[7]

While all these methods to detect bacteria and their resistance to antibiotics are excellent improvements over traditional methods, they still have drawbacks that need to be addressed. When detecting bacteria based on enzymatic expression, the detection limit is much higher than what is necessary in the field. Improving the detection limit in colorimetric detection could be done through paper modifications that either enhance the reaction efficiency, or enhance color formation. For example, silica nanoparticles and chitosan have been used to improve color formation in glucose detection.[8,9] Or, as

observed in Chapter 5 for antibiotic purity, carbohydrates such as sucrose and lactose appears to enhance color formation of the nitrocefin and β-lactamase reaction. Modifying paper with both nitrocefin and sucrose or lactose could improve the detection limit seen in AMR bacteria detection, and will be the subject of future studies. Furthermore, an infield bacterial concentration system could also be implemented, such as syringe filters or an in-field incubator. For example, chemical hand warmers and Styrofoam cups have been optimized as an inexpensive incubator for isothermal amplification.[10] A similar system could be optimized for bacteria incubation in the field, eliminating the need for a bulky and expensive shaking incubator currently used to enumerate bacteria to a detectable concentration.

We improved upon the detection limit by using immunomagnetic separation (IMS) coupled with an enzymatic sandwich immunoassay for specific and sensitive detection of *S. typhimurium* in milk and feces samples. However, with this improvement in detection came the drawback of an extensive and complicated procedure that generate excessive waste. An important aspect of field-ready tests is their user-friendliness, and the procedure associated with *S. typhimurium* detection requires training personnel. To improve upon the drawbacks of the conventional procedure, our lab has designed and is currently optimizing a 3D-printed rotational manifold to semi-automate all these steps for a user-friendly procedure. In preliminary studies, the manifold successfully completes all the steps of the procedure and has a detection limit of 10^4 CFU mL^{-1}. Although the detection limit is higher than the original procedure completed in a microcentrifuge tube, this is still an excellent step for the goal of true in-field bacteria detection and will continue to be improved.

Beyond bacteria detection, this dissertation has also presented research that advances detection of falsified and sub-standard antibiotics and improving colorimetric analysis. While the current gold standard for quantitatively determining antibiotic purity are high performance liquid chromatography and mass spectrometry, our demonstrated device has the potential to give quantitative results in the field without a central laboratory.[11] Further optimization will be needed, such as creating a calibration curve for percentage of active pharmaceutical ingredient, instead of mg mL^{-1}. The assay will also need to be tested with more antibiotics in tablet form to assess the concern of pH affecting the ability to determine the difference between legitimate and falsified antibiotics. Quantitative capabilities in the field could be taken a step further by implementing a system similar to the Raspberry Pi program and device holder that has already been developed and optimized. Developing the Raspberry Pi program and device holder for determining enzyme kinetics on paper is just the tip of the iceberg of what can be completed with this system. At this point, the Raspberry Pi needs to be connected to a monitor, mouse, and keyboard, plus the device user needs to input commands into a command center. However, small touchscreens have been developed that can control a Raspberry Pi, further advancing this system for field settings. To improve user-friendliness of the Raspberry Pi, graphical user interfaces, or GUIs, can be programmed into the device. By implementing GUIs, this eliminates the need for a user to be trained on how to input commands into a command center on the Raspberry Pi and analyze results. In summary, with further programming and optimizations, a user would simply need to push an icon on a touch screen to run a program and output user results. In combination with our inexpensive and user-friendly paper-based tests, we

can develop a truly portable and user-friendly system for objective colorimetric detection of a variety of pathogens for food safety, environmental, and biomedical applications.

REFERENCES

(1) Minor, T.; Lasher, A.; Klontz, K.; Brown, B.; Nardinelli, C.; Zorn, D. *Risk Anal.* **2015**, *35*, 1125-1139.
(2) Hoffman, S.; Batz, M.; Morris, J. G. *J. Food Prot.* **2012**, *75*, 1291-1302.
(3) In *2018 Outbreaks*; Center for Diseason Control and Prevention: ww.cdc.gov, 2018.
(4) Adkins, J. A.; Boehle, K.; Friend, C.; Chamberlain, B.; Bisha, B.; Henry, C. S. *Anal. Chem.* **2017**, *89*, 3613-3621.
(5) Srisa-Art, M.; Boehle, K. E.; Geiss, B. J.; Henry, C. S. *Anal. Chem.* **2018**, *90*, 1035-1043.
(6) Boehle, K. E.; Gilliand, J.; Wheeldon, C. R.; Holder, A.; Adkins, J. A.; Geiss, B. J.; Ryan, E. P.; Henry, C. S. *Angew. Chem. Int. Ed. Engl.* **2017**, *56*, 6886-6890.
(7) Antibiotic Resistance Threats in the United States, Center for Disease Control and Prevention, **2013**.
(8) Gabriel, E. F.; Garcia, P. T.; Cardoso, T. M.; Lopes, F. M.; Martins, F. T.; Coltro, W. K. *Analyst* **2016**, *141*, 4749-4756.
(9) Evans, E.; Gabriel, E. F.; Benavidez, T. E.; Tomazelli Coltro, W. K.; Garcia, C. D. *Analyst* **2014**, *139*, 5560-5567.
(10) Huang, S.; Do, J.; Mahalanabis, M.; Fan, A.; Zhao, L.; Jepeal, L.; Singh, S. K.; Klapperich, C. M. *PLoS One* **2013**, *8*, e60059.
(11) Boehle, K. E.; Carrell, C. S.; Caraway, J.; Henry, C. S. *ACS Sens.* **2018**, *Under Review*.

APPENDIX I. DIAGNOSING FUNGAL INFECTIONS USING A 3D-PRINTED MANIFOLD AND PAPER-BASED MICROLFUIDICS

Summary and Specific Aims

The goal of this project is to develop a fast, user-friendly, point-of-care diagnostic test to detect the presence of *Candida albicans* in blood samples from sepsis patients, commonly referred to as invasive candidiasis or candidemia. Invasive candidiasis is responsible for around 9% of all nosocomial infections, making it the 4th most common bloodstream infection in the world. Of all the species that cause invasive candidiasis, *Candida albicans* is the most prevalent, and is associated with almost 70% of *Candida*-associated infections. Candidemia is also associated with a mortality rate that exceeds 40%, which can be decreased with early diagnosis and treatment. This high mortality rate is due to candidemia presenting symptoms similar to bacterial infections, leading to more than 95% of patients often receiving two or more antibiotics before medical personnel determine that bacteria are not causing the infection. The medical field currently employs empirical diagnoses, meaning that many health care providers assume what is causing the infection and prescribes treatment without proper diagnostic tests. The current gold standard for medical diagnostics are blood cultures, which take around two days for bacterial infections and upwards of five days for fungal infections. Thus, doctors often take the risk of empirical diagnoses because, especially in the case of sepsis, waiting 2-5 days for a diagnosis can mean life or death for the patient. With fungal infections being more common than realized, many initiatives have spurred to increase fungal infection awareness including the Center for Disease Control

and Prevention's (CDC) Fungal Disease Awareness Week in mid-August. Likewise, the Global Action Fund for Fungal Infections (GAFFI) is actively working to implement their 95-95 by 2025 Roadmap whose goal is for 95% of fungal infections diagnosed, therefore 95% of patients receiving treatment for the best outcome possible. Consequently, effective and rapid diagnosis of fungal infections is a current and pressing public health need.

While awareness is the first step in fighting fungal infection prevalence, designing and implementing new fungal diagnostic tools is key to decreasing high mortality rates caused by fungal infections. Because fungal infections are prevalent in developing countries, the ideal diagnostic platform is not only rapid, but low cost while not requiring a central laboratory. Polymerase chain reaction (PCR) and β-glucan tests have been demonstrated as faster alternatives to traditional culture techniques for diagnosing candidiasis, but still require trained personnel and expensive laboratory equipment. Paper-based microfluidic devices (μPADs) provide an attractive platform for these requirements because of paper's ability to store reagents, natural fluid wicking capabilities, and inexpensive materials. μPADs were first introduced in 2007 and have since gained popularity with thousands of publications, demonstrating many different diagnostic techniques in an inexpensive and user-friendly format. *Despite the importance of fast and portable detection of candidemia, no true point-of-care diagnostic test has been proposed for diagnosing invasive candidiasis at the point-of-care.* In this project, we will develop the first paper-based assay to detect candidemia at the point-of-care using an inexpensive and user-friendly format that does not require trained personnel or a central laboratory.

Aim 1: Optimize an in-solution assay for the detection of *C. albicans* using immunomagnetic separation (IMS) and an enzymatic sandwich immunoassay. IMS can be used to separate analytes of interest from complex sample matrices using antibodies covalently attached to magnetic beads. Coupled with an enzyme-based sandwich immunoassay, this detection scheme can provide fast and sensitive detection. We have established this technique in the detection of *Salmonella typhimurium* and *Escherichia coli* in complex sample matrices including bird feces and milk. This system will be optimized for the detection of candidemia using *C. albicans*-specific antibodies for rapid and sensitive detection in whole blood samples.

Aim 2: Adapt the IMS/immunoassay to a user-friendly rotational manifold for use in resource-limited settings without trained personnel. While IMS coupled with an immunoassay is a fast and sensitive method for detecting pathogens, the traditional assay still requires trained personnel and an exhaustive procedure. We have recently developed a reusable rotational manifold where all the steps of IMS and the immunoassay were performed on disposable paper-based devices that are inserted into the manifold. All assay reagents are dried in the paper beforehand and the user simply rotates a device through several steps to complete the assay and read the sample layer for color change to determine whether the pathogen is present in their sample. Moving the entire assay to our unique rotational manifold will allow rapid and consistent performance of *C. albicans* detection in a format that can be automated and used by untrained personnel in the field. These devices will then be demonstrated for field settings using *C. albicans*-inoculated and non-inoculated serum and whole blood

samples. Our final assay and device will be compared to traditional diagnostic tests for total assay time, sensitivity, specificity, and accuracy.

The outcome of this project will be a fast, accurate, and user-friendly diagnostic test that can be used at the point-of-care to diagnose candidemia in patient samples, providing rapid actionable information for health care providers and resulting in the best outcome for patients with invasive candidiasis.

Significance

Despite 1.5 million annual deaths, fungal infections still go largely undiagnosed and untreated around the world. Despite the high mortality rate associated with invasive fungal infections, there is still a lack of public health awareness of the prevalence of fungal infections worldwide. *There are over 11.5 million invasive fungal infections each year, which results in around 1.5 million annual deaths globally, more than either tuberculosis or malaria.*[1] While there are over 600 species of fungi that cause invasive infections in humans every year, infections associated with *Candida spp.* are especially common with over 400,000 life-threatening infections per year worldwide with a 46-75% mortality rate.[2] Approximately 93% of candidemia infections are acquired in healthcare facilities, and because these infections display symptoms like bacterial infections, patients are often placed on broad-spectrum antibiotics.[3] One study found >95% of candidemia patients received two or more antibiotics before receiving the correct treatment.[4] Delaying treatment in candidemia patients significantly increases patient mortality from 10% to over 40% by the third day without treatment.[5,6] In addition to increasing patient mortality, this unnecessary use of antibiotics in fungal infections

are contributing to the worldwide problem of antimicrobial resistant bacteria and increases patient risk for *Clostridium difficile* infections.[7-10] Although many *Candida* species can cause infections, the most prevalent and pathogenic species is *Candida albicans*, which is responsible for 68% of all *Candida*-associated sepsis infections.[11] To help increase awareness of fungal infections, the CDC launched Fungal Disease Awareness Week, emphasizing the importance of recognizing fungal infections to increase patient outcome with early treatment.[12] Awareness is also the goal of the Global Action Fund for Fungal Infections (GAFFI), who created a 10-year action plan entitled “95/95 by 2025” roadmap.[13] This roadmap’s goal is for diagnosing 95% of fungal infections so 95% of patients receive antifungal treatment to decrease morbidity and mortality by fungal infections.

Improving fungal infection outcome is not possible without improving current diagnostics. When most patients develop sepsis, doctors will likely complete an empirical diagnosis, which is when a diagnosis is made based on previous experience instead of a diagnostic test.[14] This is because the current gold standard for sepsis diagnosis are blood cultures, which can take anywhere from 2-5 days to complete based on individual pathogen growth rates.[15] In addition to being time-consuming, blood culture tests are frequently inaccurate with 50% of patients with candidemia receiving false negatives.[16] Because of these extensive wait times and inaccuracy, it is safer for a doctor to make an empirical diagnosis, because waiting for a diagnostic test leads to increased mortality rates for patients as several studies have shown.[5,6,14] Alternatives to fungal cultures have been proposed including polymerase chain reaction (PCR) and β-glucan assays. While these are promising methods that are

faster and more accurate than culture, each assay still has drawbacks. PCR has been demonstrated to have high sensitivity and specificity, and is much faster than culturing.[17] However, this method is still considered a research tool due to lack of standardization.[16] The β-glucan assay detects fungi based on the presence of β-glucan as a major cell wall component in most fungal species.[18] The assay displays high sensitivity and specificity to β-glucan, but is not species-specific and is prone to false positives.[16,19] Other drawbacks of these established methods include requiring trained personnel, a central laboratory, and expensive equipment. Because fungal infections are prevalent worldwide, the ideal fungal diagnostic test is not only accurate and fast, but user-friendly, inexpensive, and portable.

We recently developed an assay using immunomagnetic separation (IMS) coupled with a sandwich immunoassay for sensitive detection of *Salmonella typhimurium* in complex sample matrices including milk and bird feces.[20] IMS is a method that has been used for separation of target analytes in complex matrices by covalently attaching antibodies to magnetic particles and separating the beads from the sample using a magnet. This is a well-established method that has been demonstrated in the detection of many bacteria and viruses,[21-24] as well as one example in the detection of *Candida* spp.[25] While IMS with an immunoassay is a specific, sensitive, and fast method that can be used in many different sample matrices, traditional IMS still requires trained personnel to execute multiple pipetting steps, resulting in a laborious procedure and excessive waste. In unpublished work, we recently combined this method with microfluidic paper-based analytical devices (μPADs) for a user-friendly device that semi-automates all IMS steps for untrained personnel to detect pathogens

without an extensive procedure. Many detection motifs have been used in µPADs,[26] however, using paper-based devices to automate IMS has not been previously described. Furthermore, despite µPADs use to detect many analytes including viruses and bacteria,[27] there has yet to be a µPAD developed for the detection of fungi. Using a reusable rotational manifold and disposable paper-based sample and reagent cards, we will establish the first point-of-care test for diagnosing candidemia infection in patients. This device will be inexpensive, user-friendly, and fast, enabling health care providers to provide the correct treatment to their patients as soon as possible and help decrease the high mortality rates associated with fungal infections.

Innovation

A fast and sensitive diagnostic tool to detect C. alibicans in patient samples. The primary pitfall of current fungal diagnostics is the speed at which it detects fungi, which is currently 2-5 days. This test will detect the presence of *C. albicans* in patient blood in <1 hr, providing health care officials with fast answers enabling them to accurately treat patients for the best outcome.

User-friendly semi-automation of IMS coupled with an immunoassay. While IMS coupled with an immunoassay is a sensitive and selective procedure, it is a labor-intensive assay associated with excessive waste. By drying reagents into paper-based devices and employing a reusable rotational manifold to semi-automate the devices and hold buffer, we have eliminated most of the waste and labor associated with the procedure. Once established, this assay can easily be applied to other pathogens by simply changing the antibodies on the magnetic bead and the biotinylated antibodies.

The first point-of-care (POC) test for diagnosing candidemia. In addition to this assay being accurate and providing fast results, it will also be inexpensive (~$1-2 USD), user-friendly, and portable, making it the first true POC test for candidemia. This will enable organizations like Doctors Without Borders in resource-limited settings to use this diagnostic test as it does not require trained personnel or a central diagnostic laboratory. This will also be the first µPAD for the diagnosis of any fungal infection.

Approach Aim 1: Optimize an in-solution assay for the detection of *C. albicans* using immunomagnetic separation (IMS) and an enzymatic sandwich immunoassay.

When choosing a scheme for detecting candidemia, immunomagnetic separation (IMS) coupled with an enzymatic sandwich immunoassay was chosen for several reasons. IMS was developed to separate targets of interest from complex sample matrices by covalently attaching specific antibodies to magnetic beads. After allowing antibody-conjugated magnetic beads to incubate in a sample, a magnet is used to separate the magnetic beads and any bound analytes from the rest of the sample. This isolates the pathogen from any possible interferences for the final immuno- and enzymatic assay. Following sample removal, the beads are resuspended in buffer, presumably with your analyte of interest attached. Because the beads can be resuspended in a smaller volume of buffer than the original sample, this method can also be used for concentrating the pathogen as an alternative to culture and other enumeration techniques. Following IMS, the analyte recovered from the sample can be detected using a variety of techniques including microscopy, PCR, culture enrichment,

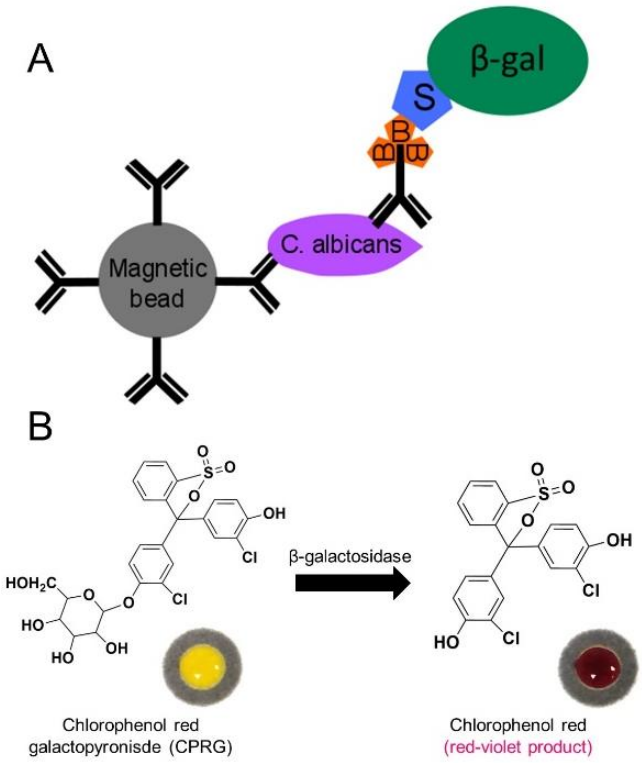

Figure A1.1 | Proposed detection scheme of *C. albicans* **(A)** Schematic of selected immunoassay approach for detecting *C. albicans* **(B)** Detecting analytes based on the enzymatic reaction between β-galactosidase and CPRG, resulting in chlorophenyl red as a red-violet product.

and immunoassays. Because we want a technique that is rapid and completed without electricity or trained personnel, we opted against PCR, microscopy, or culturing due to equipment and time requirements. An immunoassay detection format has been selected for our detection motif of the captured species because it can easily be applied to a μPAD format in a POC setting. Like enzyme-linked immunosorbent assays, the pathogen is detected by first adding a biotinylated antibody specific to the pathogen. After removing unattached antibody through washing, the sample is incubated with a streptavidin-conjugated enzyme that can link with the biotin attached to the antibody. After proper washing, a substrate specific to the enzyme can be added to the solution

for a detectable product. If no pathogen is present in the sample, then no product should be observed as any excess enzyme or biotinylated antibody should have been removed during washing steps. For the first part of this project, we will optimize an IMS system for the detection of *C. albicans* in media and spiked whole blood. We will use β-galactosidase (β-gal) and chlorophenol red galactopyranoside (CPRG) as the enzyme and chromogenic substrate pair for the sandwich immunoassay (Figure A1.1).

Feasibility. We have previously optimized IMS coupled with an immunoassay for the detection of bacteria in complex sample matrices. In collaboration with Dr. Geiss' laboratory (CSU Microbiology), we recently published a paper for the detection of *S. typhimurium* in bird feces and milk using an IMS assay.[20] Before detecting bacteria in complex matrices, we optimized the system in culture media with highly sensitive and specific results. Our limit of detection was 10^2 CFU/mL for *S. typhimurium* with no cross-reaction with other bacteria species using the same assay (Figure A1.2A). When detecting *C. albicans* in patient samples, it is not only imperative that the method is sensitive, but very specific to our pathogen because we want to distinguish fungal infections from bacterial infections. When determining the assay's specificity to *S. typhimurium* in the presence of other bacteria, we performed the assay with excess *E. coli* in the sample. Even when *E. coli* was present in the sample at 1000x higher concentration than *S. typhimurium*, the assay sensitivity and selectivity was not compromised (Figure A1.2B).

Experimental Approach. The first aim of this proposal will be focused on adapting this IMS/sandwich immunoassay format to detect *C. albicans* in media. We have learned from optimizing IMS for *E. coli* and *S. typhimurium* detection that each

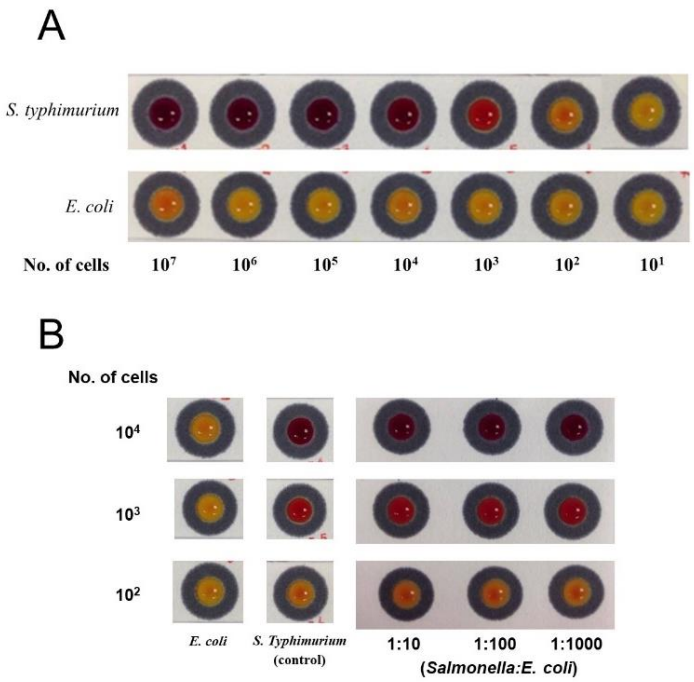

Figure A1.2 | IMS assay limit of detection and sensitivity for *S. typhimurium*. (A) Assay limit of detection in media as compared to same concentrations of *E. coli*. (B) Sensitivity of assay to *S. typhimurium* in the presence of excess *E. coli*.

IMS/immunoassay system is unique and requires its own individual optimizations. For IMS, there are several antibodies to select for the assay. In addition to selecting the optimal antibodies for the assay, volume and concentration of each reagent will need to be optimized, along with incubation times of each reagent.

Optimize IMS procedure for C. albicans detection. Using IMS to detect *C. albicans* has been successfully demonstrated in the detection of general *Candida* species in whole blood samples, with capture efficiencies varying from 11-43% depending on the species of *Candida* and used culturing as their detection method.[25] While IMS shortened the culturing procedure by 24 h, we will take this concept and improve the assay time further by adding a sandwich immunoassay to detect *C. albicans* in under an hour without enrichment. This will require two different antibodies

that pair well together in the same assay (there are several *C. albicans* antibodies available from AbCam and Fisher Scientific), and optimizing concentrations and incubation times for each of the assay components. One aspect to consider when finding the correct pair of antibodies is to ensure that each antibody is specific to a different component of the pathogen's cell wall to eliminate competition between the two antibodies. It is also important to verify that these targets are abundant on the cell wall to increase capture efficiency. To optimize the IMS assay in solution, the volume of beads will be optimized. Although using more beads will increase capture efficiency in the sample, too many beads could lead to more nonspecific binding from other assay reagents and the beads are naturally a red color, both of which can cause background for the assay. The concentration of biotinylated antibody and streptavidin-conjugated enzyme will need to be determined. After concentration optimization, the substrate incubation time of each step, including bacteria capture, will be optimized. Like substrate concentrations, increasing the incubation time can decrease the assay LOD up to a certain time point. This point will be determined for the assay to be as short, but as sensitive, as possible. Once the procedure has been optimized for detecting *C. albicans*, specificity will be tested in the presence of other yeast genus' along with different bacteria species that are common in sepsis patients, such as *E. coli*, *Staphylococcus aureus*, or *Klebsiella pneumoniae*.[28] Because the primary purpose of this assay is to distinguish between yeast and bacterial sepsis infections, it is crucial that this method is specific to *C. albicans* and not any bacteria species, resulting in a false positive and incorrect patient treatment.

Detecting C. albicans in whole blood and different morphologies. Part of the reason *C. albicans* is more pathogenic compared to other *Candida* species is because of its ability to morph from its original yeast form into a filamentous hyphae form.[29] Hence, when it infects its host, it takes on this hyphae form, and it is essential that this method can detect *C. albicans* in this morphology. Once the device has been optimized in the detection of C. albicans in yeast form, we will test this method in the detection of *C. albicans* in hyphae and pseudohyphae form. Once the LOD has been determined for all forms of *C. albicans*, we will confirm that we can detect the pathogen in plasma and whole blood samples and an LOD will be established.

Potential Pitfalls. The primary concern with any new diagnostic test is whether it will be as sensitive and specific as necessary for diagnosing infections. Concentrations in patients with confirmed candidemia can be as low as 5 CFU/mL.[30] With our IMS system to detect *Salmonella*, the LOD was at 100 CFU/mL. This detection limit will detect some fungal infections, but for the best patient outcome, the LOD needs to be as low as possible. The LOD can be dictated by the antibodies selected for the assay, therefore it is likely that we will purchase and test many different antibodies to find the ideal pair for optimal detection. Once the optimal antibody pair is selected, we can also investigate the use of other enzyme and substrate pairs. We chose β-gal and CPRG as our enzyme-substrate pair in *Salmonella* detection because it is a user-friendly and noticeable color change from yellow to red. While this pair was successful, if necessary, we can also investigate the use of poly-horseradish peroxidase (poly-HRP) and 3,5,3’5’-trimethylbenzidene (TMB) as an alternative enzyme and substrate pair as it could increase our assay speed and sensitivity.

Expected Outcomes. Upon completing Aim 1, we will have demonstrated rapid and sensitive detection of *C. albicans* using IMS and a sandwich immunoassay in media and blood samples for fast and sensitive diagnosis of candidemia.

Approach Aim 2: Adapt the optimized IMS/immunoassay to a user-friendly rotational manifold for use in resource-limited settings without trained personnel.

While IMS coupled with an immunoassay for *C. albicans* in solution would enhance clinician's ability to diagnose candidemia in infected patients, this method will still require trained personnel and reagent refrigeration. For infections occurring in resource-limited settings, a diagnostic test that is also robust, user-friendly, and portable is required. The focus of Aim 2 is to develop such a test for candidemia diagnosis. Once the assay has been demonstrated in a paper-based format using the rotational manifold, it will need to be verified that this new diagnostic motif can be applied in real-world settings and will demonstrate the final device with whole blood samples and plasma.

A user-friendly and reusable device for diagnosing candidemia. We are currently optimizing an inexpensive 3D-printed rotational manifold that has been developed to semi-automate all the steps of IMS coupled with an immunoassay. This manifold completes the entire procedure on paper so the user only needs to add buffer and rotate the device through each step. All the reagents are stored and stabilized on paper, therefore no refrigeration is required to store reagent solutions, increasing device robustness and portability. As seen in Figure A1.3A, the reusable manifold consists of three main plastic parts, the manifold top, center, and bottom pieces. Each of these

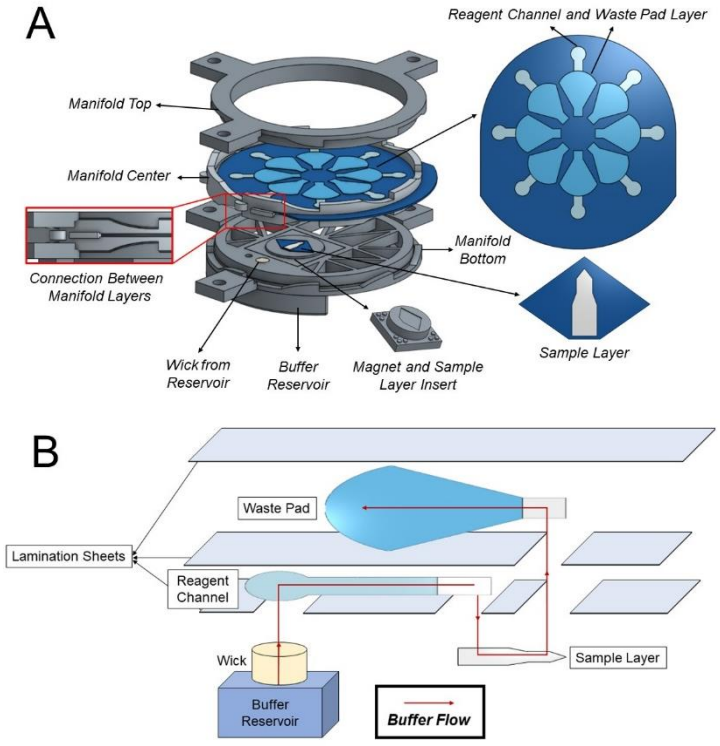

Figure A1.3 | 3D representation of reusable rotational manifold and fluid flow. **(A)** CAD drawing of the 3D-printed rotational manifold and each of the manifold components. Grey indicates plastic-based reusable components while blue designates disposable and paper-based devices. **(B)** Fluid flow of buffer from the buffer reservoir to the reagent channel, sample layer, and finally the waste pad.

components is held together using bolts, springs, and wingnuts to hold the components together tightly under constant pressure, yet allow the user to rotate the center of the manifold to complete each sequential step of the assay. The connection between the manifold layers are wedges to allow the manifold to rotate 45°, then snap into place, like the mechanism of a retractable pen. The manifold is reusable, but the sample and reagent/waste layers are disposable and interchangeable. The user will not need to pipette a set volume of buffer for each step because a wick will transport buffer from the reservoir to the manifold using capillary action. Buffer will be transported from the regent channel to the sample layer and waste pad using the natural fluid-wicking properties of

paper (Figure A1.3B). Once the waste pad is completely saturated, buffer flow will stop and the user can rotate the manifold to initiate the next step, allowing fine control of the assay to provide reproducible results. To keep the immunomagnetic beads in place during the assay, a magnet is located underneath the sample layer in the sample layer insert. To perform the test, the user will deposit a sample onto the sample layer, where immunomagnetic beads are stored, and allow the sample to incubate for 10 minutes. After incubation, the user will place the sample layer onto the sample layer insert and magnet and place the insert in the manifold. Next, the user will insert a reagent and waste card into the slot of the manifold center, then fill the buffer reservoir. Once the manifold is set up, the user can start with the first reagent channel, then rotate the manifold after each step is completed. As described in detail in Figure A1.4, each channel of the device will distribute a different reagent used in the original immunoassay procedure, including wash steps. The user will rotate the manifold after each step is complete, delivering a new reagent to the sample layer, which is stationary during the entire assay. After each step has been completed, the user will rotate the manifold one more time to dispense CPRG onto the sample layer and wait 30 minutes for a result. If the sample layer stays yellow, the test is negative, and if the sample layer turns red, the test is positive.

Feasibility. One of the many advantages of using paper-based devices is the simplicity of their fabrication. The Henry lab has been developing µPADs since close to their introduction, as we were the first lab to integrate electrochemical detection into paper-based devices in 2009,[31] and have since published 50 manuscripts in the field. Therefore, our lab is equipped with all the technology and resources to create and

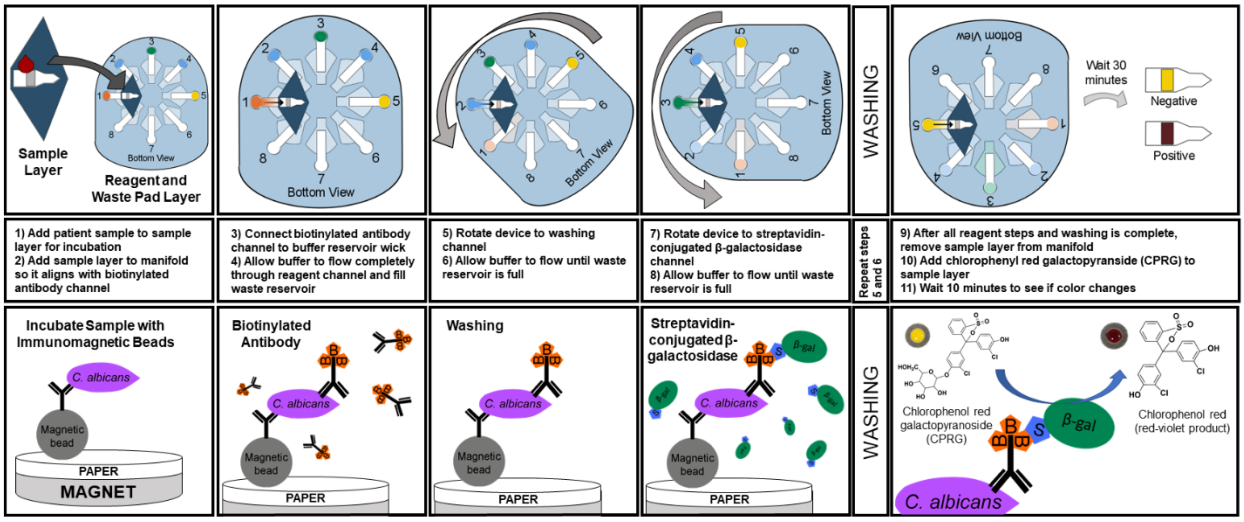

Figure A1.4 | Detailed step-by-step instructions and illustration of the mechanism to detect *C. albicans* in patient samples using IMS in a 3D-printed rotational manifold at the user level (top) and molecular level (bottom).

optimize this device for the detection of *C. albicans*, including a 3D printer for the reusable rotational manifold. IMS has been demonstrated in whole blood multiple times including for the detection of bacteria, cancer cells, and neutrophils, to name a few.[32-35] We have previously collaborated with an environmental and health sciences lab at Colorado State University for the acquisition of different environmental and human samples, including human blood plasma. Additionally, whole human blood can be purchased from Lee Biologicals.

Experimental Approach. Like optimizing IMS in solution, the rotational manifold reagent and waste layer will need to be optimized for detection of *C. albicans* on paper, as different concentrations and buffer volumes will likely be required compared to *S. typhimurium*.

Optimizing the rotational manifold for C. albicans detection. With the combination of optimizing the manifold for *S. typhimurium* detection, and optimizing *C. albicans*

detection in solution, optimizing *C. albicans* detection in the rotational manifold on a paper-based format should be straight-forward. Reagents and buffer volumes will need to be optimized, as well as number of assay steps. As seen in Figure A1.4, we are currently planning to use five of the eight channels designed into the device. This is purposeful, as the addition of other steps could be necessary. In addition to number of steps that can be optimized, we can also control the volume of buffer used for each step by changing the size of paper used in the waste pad, making the paper-based device customizable for each step and assay. When optimizing the manifold, we will perform several experiments for determining the best concentration of each reagent to deposit onto the paper. For most optimizations, as you increase reagent concentration, the final signal will increase up to a certain point, where the signal levels off. Once the reagent concentration is optimized, then the optimal buffer volume will be determined for each step by investigating several waste pad sizes.

Distance-based detection of C. albicans. Our current rotational manifold quantifies pathogens by analyzing the color intensity of the sample layer using ImageJ software. While a practical method for quantifying color change in a sample, this requires the use of a camera and image software to complete, tools that are not as available in resource-limited settings. Therefore, we are going to implement distance-based detection of chlorophenol red, the product of the reaction, for this project. Distance based detection has been demonstrated before in our lab using a chemometer format for the detection of metals and biomolecules.[36,37] Unfortunately, yeast and magnetic beads are both too large to move efficiently through paper, so the traditional chemometer format will not be applicable. However, chlorophenol red can move through

paper and has a -2 charge that will be attracted to cations.[20] We propose that modifying paper with poly(diallyldimethyl-ammonium chloride), chlorophenol red can move through paper and saturate modified regions of the paper that are shaped as bars, which can be completed using reagent printing.[38] This motif could be applied to a reaction of β-galactosidase and CPRG, which gives chlorophenol red as a product. The product will then travel through an additional channel in the manifold to modified paper, and the user will simply need to count the number of bars to quantify the concentration of *C. albicans* present in the sample.

Modifying the manifold for whole blood samples. While the manifold and paper-based devices will have been optimized, these optimizations were completed using pathogens in media. When adding a more complicated matrix like whole blood, additional optimizations will likely be necessary. For example, we designed the device to have eight channels even though only five are currently being used. After allowing the sample to incubate with immunomagnetic beads, additional wash steps will likely be necessary to wash the sample before completing the rest of the assay. We will start with the least complicated form of blood, serum, then move on to more complicated samples like plasma and whole blood to confirm whether different blood components will affect the assay LOD. Previous results from our lab saw an increase in LOD as the assay samples grew more complicated with whole milk and bird feces.[20] The final goal of the assay is to detect *C. albicans* in whole blood for the user to have minimal sample preparation.

Comparing to traditional diagnostic methods. Once the device has been optimized for whole blood samples, our diagnostic technique will be compared to

traditional diagnostic methods. We will compare our device to culturing, PCR, and the β-glucan assay for total detection time, accuracy, sensitivity, and user-friendliness.[16]

Potential Pitfalls. Like optimizing the assay in solution, one of the biggest concerns for the assay is the LOD. Several papers have been published on increasing sensitivity of biological assays on paper by modifying with surface with different chemicals, such as chitosan modification to increase color formation of an enzymatic reaction.[39] One of the many positive aspects of paper is its ability to store and stabilize reagents, however, this can also disadvantageous when applying immunoassays to paper. Antibodies and enzymes will often nonspecifically bind to the paper during immunoassays and are not removed during wash steps, causing background.[40] We have already determined that the best paper to use is Fusion 5 paper (GE Healthcare Sciences), which results in the least nonspecific adsorption of reagents to the paper. If additional nonspecific binding issues arise, we can modify the paper with different reagents used in other immunoassays including Tween 20 and bovine serum albumin (BSA). Modifying the manifold for real-world sample could also prove difficult, such as blood's natural red color creating background. Because whole blood is a different density and viscosity compared to media, different paper modifications or material may need to be optimized for preparing and washing the sample. If we see this same increase in the LOD in whole blood, we will investigate sample preparation and device modifications to increase sensitivity of the device. For example, whole blood samples will contain clotting factors, therefore clotting will be a concern for real patient samples as viscosity will increase and could affect the immunomagnetic beads' capture efficiency. To prevent clotting, we can investigate different anti-coagulants (such as

EDTA) to modify the sample layer to maintain a less viscous sample. Although the ideal system would allow the user to add the sample to the manifold's sample layer and proceed with the assay, if necessary, we can investigate sample preparation in a microcentrifuge tube before adding the sample to the sample layer. This would also allow the user to use a larger volume of sample, up to 1 mL, as compared to the current system that uses 20 µL of sample.

Summary. At the end of this project we will have developed, optimized, and demonstrated the first paper-based POC diagnostic motif for the detection of *C. albicans* in blood samples. If developed, this device could revolutionize the field of fungal diagnostics for being inexpensive, fast, user-friendly, and most importantly, accurate. This assay would give health care providers confidence in prescribing antifungals or antimicrobials to patients with sepsis without the compromise of waiting 2-5 days for culture results, therefore decreasing the high mortality rate associated with candidemia and improving patient outcome.

REFERENCES

(1) Tudela, J. L. R.; Denning, D. W. *Lancet Infect. Dis.* **2017**, *17*, 1111-1113.
(2) Brown, G. D.; Denning, D. W.; Gow, N. A. R.; Levitz, S. M.; Netea, M. G.; White, T. C. *Sci. Transl. Med.* **2012**, *4*, 1-9.
(3) Chen, S.; Slavin, M.; Ngyuen, Q.; Marriott, D.; Playford, G.; Ellis, D.; Sorrell, T. C. *Emerg. Infect. Dis.* **2006**, *12*, 1508-1516.
(4) Chakrabarti, A.; Sood, P.; Rudramurthy, S. M.; Chen, S.; Kaur, H.; Capoor, M.; al., e. *Intensive Care Med.* **2015**, *41*, 285-295.
(5) Garey, K. W.; Rege, M.; Pai, M. P.; Mingo, D. E.; Suda, K. J.; Turpin, R. S.; Bearden, D. T. *Clin. Infect. Dis.* **2006**, *43*, 25-31.
(6) Arnold, H. M.; Micek, S. T.; Shorr, A. F.; Zilberberg, M. D.; Labelle, A. J.; Kothari, S.; Hollef, M. H. *Pharmacotherapy* **2010**, *30*, 361-368.
(7) Denning, D. W.; Perlin, D. S.; Muldoon, E. G.; Colombo, A. L.; Chakrabarti, A.; Richardson, M. D.; Sorrell, T. C. *Emerg. Infect. Dis.* **2017**, *23*, 177-183.
(8) Antimicrobial Resistance: Global Report on Surveillance, World Health Organization, **2014**.
(9) Global Action Plan on Antimicrobial Resistance, World Health Organization, **2015**.
(10) Fridkin, S.; Baggs, J.; Fagan, R.; Magill, S.; Pollack, L. A.; Malpiedi, P.; Slayton, R.; Khader, K.; Rubin, M. A.; Jones, M.; Samore, M. H.; Dumyati, G.; Dodds-Ashley, E.; Meek, J.; Yousey-Hindes, K.; Jernigan, J.; Shehab, N.; Herrera, R.; McDonald, L. C.; Schneider, A.; Srinivasan, A. *Morb. Mortal. Wkly. Rep.* **2014**, *63*, 194-200.
(11) Morgan, J. *Curr. Inf. Dis. Rep.* **2005**, *7*, 429-439.
(12) In *Fungal Diseases*; Center for Disease Control and Prevention, **2017**.
(13) Improving Outcomes for Patients with Fungal Infections Across the World: A Road Map for the Next Decade, Global Action Fund for Fungal Infections, **2015**.
(14) Morrell, M.; Fraser, V. J.; Kollef, M. H. *Antimicrob. Agents Chemother.* **2005**, *49*, 3640-3645.
(15) Mylonakis, E.; Clancy, C. J.; Ostrosky-Zeichner, L.; Garey, K. W.; Alangaden, G. J.; Vazquez, J. A.; Groeger, J. S.; Judson, M. A.; Vinagre, Y. M.; Heard, S. O.; Zervou, F. N.; Zacharioudakis, I. M.; Kontoyiannis, D. P.; Pappas, P. G. *Clin. Infect. Dis.* **2015**, *60*, 892-899.
(16) Perfect, J. R. *Curr. Med. Res. Opin.* **2013**, *29 Suppl 4*, 3-11.
(17) Arvanitis, M.; Anagnostou, T.; Fuchs, B. B.; Caliendo, A. M.; Mylonakis, E. *Clin. Microbiol. Rev.* **2014**, *27*, 490-526.
(18) Theel, E. S.; Doern, C. D. *J. Clin. Microbiol*. **2013**, *51*, 3478-3483.
(19) Onishi, A.; Sugiyama, D.; Kogata, Y.; Saegusa, J.; Sugimoto, T.; Kawano, S.; Morinobu, A.; Nishimura, K.; Kumagai, S. *J. Clin. Microbiol.* **2012**, *50*, 7-15.
(20) Srisa-Art, M.; Boehle, K. E.; Geiss, B. J.; Henry, C. S. *Anal. Chem.* **2018**, *90*, 1035-1043.
(21) Monceyron, C.; Grinde, B. *J. Virol. Methods* **1994**, *46*, 157-166.
(22) Bakkali Kassimi, L.; Gonzague, M.; Boutrouille, A.; Cruciere, C. *J. Virol. Methods* **2002**, *101*, 197-206.
(23) LeJeune, J. T.; Hancock, D. D.; Besser, T. E. *J. Clin. Microbiol*. **2006**, *44*, 872-875.

(24) Skjerve, E.; Rorvik, L. M.; Olsvik, O. *Appl Environ Microbiol* **1990**, *56*, 3478-3481.
(25) Apaire-Marchais, V.; Kempf, M.; Lefrancois, C.; Marot, A.; Licznar, P.; Cottin, J.; Poulain, D.; Robert, R. *BMC Microbiol.* **2008**, *8*, 157.
(26) Cate, D. M.; Adkins, J. A.; Mettakoonpitak, J.; Henry, C. S. *Anal. Chem.* **2015**, *87*, 19-41.
(27) Yang, Y.; Noviana, E.; Nguyen, M. P.; Geiss, B. J.; Dandy, D. S.; Henry, C. S. *Anal. Chem.* **2017**, *89*, 71-91.
(28) MacVane, S. H.; Nolte, F. S. *J. Clin. Microbiol.* **2016**, *54*, 2455-2463.
(29) Moran, G.; Coleman, D.; Sullivan, D. In *Candida and Candidiasis*, Calderone, R. A.; Clancy, C. J., Eds.; ASM Press: Herndon, VA, 2012.
(30) Loeffler, J.; Henke, N.; Hebart, H.; Schmidt, D.; Hagmeyer, L.; Schumacher, U.; Einsele, H. *J. Clin. Microbiol.* **2000**, *38*, 586-590.
(31) Dungchai, W.; Chailapakul, O.; Henry, C. S. *Anal. Chem.* **2009**, *81*, 5821-5826.
(32) Aloni-Grinstein, R.; Schuster, O.; Yitzhaki, S.; Aftalion, M.; Maoz, S.; Steinberger-Levy, I.; Ber, R. *Front. Microbiol.* **2017**, *8*, 312.
(33) Wang, Y.; Sun, H.; Li, R.; Ke, P.; Zhu, H.; Guo, H.; Liu, M.; Sun, H. *Anal. Meth.* **2016**, *8*, 7324-7330.
(34) Cotter, M. J.; Norman, K. E.; Hellewell, P. G.; Ridger, V. C. *Am. J. Pathol.* **2001**, *159*, 473-481.
(35) Jin Kim, S.; Ikeda, N.; Shiba, E.; Tukamura, Y.; Noguchi, S. *Breast Cancer* **2001**, *8*, 63-69.
(36) Cate, D. M.; Dungchai, W.; Cunningham, J. C.; Volckens, J.; Henry, C. S. *Lab Chip* **2013**, *13*, 2397-2404.
(37) Cate, D. M.; Noblitt, S. D.; Volckens, J.; Henry, C. S. *Lab Chip* **2015**, *15*, 2808-2818.
(38) Yamada, K.; Suzuki, K.; Citterio, D. *ACS Sens.* **2017**, *2*, 1247-1254.
(39) Gabriel, E. F.; Garcia, P. T.; Cardoso, T. M.; Lopes, F. M.; Martins, F. T.; Coltro, W. K. *Analyst* **2016**, *141*, 4749-4756.
(40) Cheng, C. M.; Martinez, A. W.; Gong, J.; Mace, C. R.; Phillips, S. T.; Carrilho, E.; Mirica, K. A.; Whitesides, G. M. *Angew. Chem. Int. Ed. Engl.* **2010**, *49*, 4771-4774.